LEABHARLANN CHOLÁISTE NA TRÍONÓIDE, BAILE ÁTHA CLIATH | TRINITY COLLEGE LIBRARY DUBLIN
Ollscoil Átha Cliath | The University of Dublin

Terms and Conditions of Use of Digitised Theses from Trinity College Library Dublin

Copyright statement

All material supplied by Trinity College Library is protected by copyright (under the Copyright and Related Rights Act, 2000 as amended) and other relevant Intellectual Property Rights. By accessing and using a Digitised Thesis from Trinity College Library you acknowledge that all Intellectual Property Rights in any Works supplied are the sole and exclusive property of the copyright and/or other IPR holder. Specific copyright holders may not be explicitly identified. Use of materials from other sources within a thesis should not be construed as a claim over them.

A non-exclusive, non-transferable licence is hereby granted to those using or reproducing, in whole or in part, the material for valid purposes, providing the copyright owners are acknowledged using the normal conventions. Where specific permission to use material is required, this is identified and such permission must be sought from the copyright holder or agency cited.

Liability statement

By using a Digitised Thesis, I accept that Trinity College Dublin bears no legal responsibility for the accuracy, legality or comprehensiveness of materials contained within the thesis, and that Trinity College Dublin accepts no liability for indirect, consequential, or incidental, damages or losses arising from use of the thesis for whatever reason. Information located in a thesis may be subject to specific use constraints, details of which may not be explicitly described. It is the responsibility of potential and actual users to be aware of such constraints and to abide by them. By making use of material from a digitised thesis, you accept these copyright and disclaimer provisions. Where it is brought to the attention of Trinity College Library that there may be a breach of copyright or other restraint, it is the policy to withdraw or take down access to a thesis while the issue is being resolved.

Access Agreement

By using a Digitised Thesis from Trinity College Library you are bound by the following Terms & Conditions. Please read them carefully.

I have read and I understand the following statement: All material supplied via a Digitised Thesis from Trinity College Library is protected by copyright and other intellectual property rights, and duplication or sale of all or part of any of a thesis is not permitted, except that material may be duplicated by you for your research use or for educational purposes in electronic or print form providing the copyright owners are acknowledged using the normal conventions. You must obtain permission for any other use. Electronic or print copies may not be offered, whether for sale or otherwise to anyone. This copy has been supplied on the understanding that it is copyright material and that no quotation from the thesis may be published without proper acknowledgement.

Mechanisms linking obesity, genomic instability and the radioresponse in oesophageal adenocarcinoma

---



A dissertation submitted to the University of Dublin, Trinity College

for the degree of Doctor of Philosophy

Ann Marie Mongan

Scientific Supervisor:
Dr. Jacintha O'Sullivan

Clinical Supervisor:
Prof. John V. Reynolds

Department of Surgery

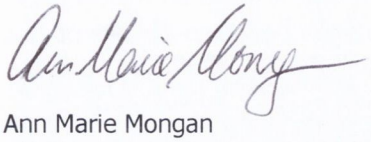
2014

TRINITY COLLEGE
5 JAN 2015
LIBRARY DUBLIN

Thesis 10789

Declaration

I hereby declare that this thesis has not been submitted as an exercise for a degree at this, or any other University and that it is entirely my own work, except where otherwise acknowledged. This thesis may be made available from the library for consultation or copying.



Ann Marie Mongan

2014

Thesis Abstract

The increasing incidence of oesophageal adenocarcinoma (OAC) parallels the rapidly rising incidence of obesity. OAC is an exemplar model of obesity-associated cancer, with an increasing focus on the role of visceral adipose tissue (VAT). OAC confers a poor prognosis with five year survival of 20-40% in locally advanced disease[1]. The current standard of care involves neoadjuvant chemoradiotherapy (NA-CRT). Tumour response to NA-CRT is the best predictor of survival, but resistance to therapy remains a significant clinical problem with only 15-30% of patients achieving a complete pathological response (pCR). The identification of biomarkers and molecular mechanisms of radioresistance would be of substantial clinical benefit, and is critical for improving the efficacy of treatment. Obesity is associated with the pathogenesis and progression of OAC, but the interaction between obesity and treatment response is unknown. Genomic instability is a hallmark of cancer associated with obesity. We hypothesised that genomic instability events are implicated in the interaction between obesity and the radioresponse in OAC.

We have shown that OAC patients treated with neoadjuvant chemoradiotherapy (NA CRT) who were overweight or obese, are more likely to have a lower pathological T stage at surgery compared to normal weight patients, despite having similar clinical T stages prior to treatment and these patients are more likely to achieve a good TRG response (TRG 1-3) compared to normal weight patients. Using radioresistant (OE33R) and radioresponsive (OE33P) oesophageal adenocarcinoma (OAC) cell lines, we demonstrated that adipose conditioned media (ACM) decreased radioresistance *in vitro*.

This interaction between adipose tissue and the isogenic model was characterised in terms of cell cycle distribution, adipokine receptor gene expression, and ACM metabolomics profile. OE33P cells treated with ACM had a lower proportion of cells in the more radioresistant S phase compared to cells treated with control media, while OE33R cells treated with ACM had a lower proportion of cells in the more radioresistant S phase but a higher proportion of cells in G_0/G_1 phase. These differences were small however, suggesting that other mechanisms must play a greater role in affecting radioresponse in OE33P and OE33R. Given that cell cycle distribution did not explain the alteration in radiosensitivity induced by ACM, we examined the role of adipokines in the ACM. We assessed the expression of a panel of four adipokine receptors in the two cell lines: adiponectin receptor 1 (AR1), adiponectin receptor 2 (AR2), leptin receptor (LepR) and neuropilin 1 (NRP1). We demonstrated that adipokine receptor expression differs between OE33P and OE33R; AR1 and AR2 expression was higher in OE33P compared to OE33R, while LepR and NRP1 expression was lower in OE33P compared to OE33R, and the same trend was observed in OAC patient pre-treatment biopsy samples from patients who achieved a good TRG (TRG 1-3) compared to patients who had a poor TRG (TRG 4-5). To further investigate how ACM exerts a radiosensitising effect on the cell lines, comprehensive analysis of a full metabolomic screen was

performed on ACM, which revealed the metabolites responsible for the separation of non-cancer and OAC ACM. The most discriminating metabolites included lactate, threonine, glucose, lysine and valine. Concentrations of lactate, threonine, lysine and valine were significantly higher in the ACM of OAC patients, whereas glucose was significantly higher in the ACM of non-cancer patients. Obesity status influenced the metabolomic profile of OAC patients; non-obese OAC patients demonstrated higher levels of lactate and lower levels of alanine and pyruvate compared to obese OAC patients.

Having shown that adipose tissue influences radiosensitivity in OAC; next we investigated if telomere dysfunction was implicated in the interaction between obesity and radioresponse. Our study demonstrated that ACM promotes telomere shortening and dysregulation of telomerase and the shelterin complex, and that obesity status influences TERT gene expression in OAC patients. TERT, TEP1, DKC1 and TINF2 expression, but not telomere length, were associated with radioresistance in the isogenic model. This study also revealed that adipose tissue drives the genomic instability events anaphase bridge formation and spindle assembly complex dysregulation; obese OAC patients demonstrate a significant increase in MAD2L2 expression compared to non-obese patients. Furthermore, anaphase bridge levels were higher in radioresistant compared to radioresponsive oesophageal cancer cells.

Our next goal was to screen and identify the chromosomal aberrations that distinguish OE33P from OE33R, and that may be correlated with clinicopathological characteristics of radioresponse in OAC patients using array comparative genomic hybridization (CGH). The results showed that a deletion located on chromosome 9 in OE33R (9p24.2-21.3) was a significant area of copy number variation between the two cell lines. Hence, detection of 9p deletion might be helpful in the prediction of clinical outcome of patients with OAC. Several targets from this chromosome were investigated in our isogenic model, and significance was detected for IL33, located at 9p24.1. A trend of increased IL33 expression in responder compared to non-responders was detected in patient samples; however, the differences in expression were not statistically significant. Increasing the number of patients analysed for more accurate prediction is necessary, in addition to extensive validation of predictive classifiers in prospective clinical trials.

This study highlights a potential link between visceral adiposity and the biology, in particular radioresistance, of OAC. This study demonstrated that adiposity influences radiosensitivity, and drives genomic instability events in OAC, particularly radioresistant OAC. Uncovering the mechanisms of interaction of visceral obesity, genomic instability and radioresistance could identify shared pathways as potential preventative and therapeutic targets, improving outcomes in patients suffering from this aggressive malignancy.

Acknowledgements

Foremost I would like to sincerely express my gratitude to my supervisor Dr. Jacintha O'Sullivan, for her dedication, encouragement, guidance and support throughout this project. Many thanks to Professor Reynolds for providing me with the opportunity to work in this department and for his unwavering support and direction. I feel truly privileged to have worked with two such inspiring mentors. I would also like to thank Dr. Graham Pidgeon for his enthusiasm, sound advice and timely interjections when help was needed. Many thanks to Dr. Niamh Lynam-Lennon, for her constant guidance, motivation and, above all, her unlimited patience and good humour. I am grateful to Dr. Joanne Lysaght for her invaluable help with flow analysis, and for always having a supportive word at just the right moment. I am very grateful for all the helpful supervision I have enjoyed over the last three years, I have always felt that I could approach anybody in the department and I would receive sage advice and encouragement.

I would like to thank everybody at the Department of Pathology in Salt Lake City: Mary Bronner who kindly facilitated my visit and was so welcoming to me, to Dr. Katherine Geiersbach for all her guidance, and Dr. Christian Paxton for his technical expertise. I would also like to thank Dr. Lorraine Brennan and Eibhlin Carr for all their work on the metabolomics analysis. Many thanks to the Thoracic Oncology Group for their help and advice, and to everybody in the Durkan lab. To Dr. Laure Marignol, thank you for all your help planning the irradiations. I wish to thank the research nurses, Jenny and Zieta, the database managers, Sinead and Erin, and of course Siobhan and Alma, all of whom were always helpful. This project would not have been possible were it not for funding from the Health Research Board and the C.R.O.S.S Charity, Prof. Ravi and the surgical team at St. James's Hospital, and the patients who selflessly participate in research and without whom none of this work would have been possible.

To everybody in the Department of Surgery, past and present, it has been a genuine pleasure to work with you all. To my fellow writer-uppers Suzanne and NOF, thank you so much for all the laughs, the I.T. support, for lifting me out of all my slumps, and your efficient examples. To Rory, thanks for paving the way for my project, for all your PCR and telomere expertise, and for not breaking my arms despite provocation-the place isn't the same without you! To the original postgrad reading room crew, Sarah McG, Claire, Aoife, NOF, Suzanne, NLL, Emma-you've been a constant distraction and inspiration and I will miss you all. And to the new kids on the block-Gillian, James, Katie, Maria, Melissa and Róisín—I hope you have even half the fun I've had, please reinstate sports day, you won't regret it. Thanks to the postdocs, Gary, Mary Clare, Ronan, and to those who have moved on; Andy, Jannie, Karen, Lydia, Sam, Sarah P and Stephen M. Thank you all for creating such a fun environment to work in, for all the Dice bar nights, morning teas and Daily Mail updates.

To all my friends, Áine, Cait, Irene, Maria, Olivia, Sinead, Aideen, Catherine, Dee, Lisa, Elaine C, Triona, Elaine N and Kevin; thanks for suffering through my indecipherable genomic instability and obesity chatter, and for always being there when I needed support. Thanks to Dom for your words of encouragement and all the cups of tea and whiskey. To Áine: thanks for knowing that I needed a final push, and not being afraid to give it to me!

Finally, last, but by no means least, thanks to all my family, Mam, Dad, and my two lovely sisters Deirdre and Bríd. Thanks Dee for your patience and your statistical expertise...thanks Bid for listening to me and rehousing me. You are both wonderful inspirational women, and I could not have completed this thesis without your support. To my parents, Mary and Stephen, thank you for everything you've done for me and continue to do for me. I am lucky to have such a wonderful family.

Dedication

This thesis is dedicated to: Mam, Dad, Dee and Bid.

Table of Contents

Declaration i

Summary ii

Acknowledgements iv

Dedication vi

List of Figures xi

List of Tables xiii

Abbreviations xv

Units xviii

Publications and Presentations xix

Chapter 1 General introduction 21

1.1 Oesophageal adenocarcinoma 22

1.1.1 Epidemiology 22

1.1.2 Multifactorial aetiology for OAC 24

1.1.3 Diagnosis and staging 27

1.1.4 Management options: surgery, chemotherapy, radiotherapy, targeted therapies, survival outcomes 29

1.1.5 Tumour response to neoadjuvant CRT 31

1.1.6 Radiation and chemotherapy interactions 33

1.2 Radiation 35

1.2.1 Radiotherapy 35

1.2.2 Radiation induced damage 35

1.2.3 DNA repair 36

1.2.4 Radiosensitivity 38

1.2.5 Biomarkers of response to radiation 40

1.3 Obesity 41

1.3.1 Epidemiology of obesity 41

1.3.2 Adipose tissue depots 44

1.3.3 Measuring obesity 46

1.3.4 Epidemiology of obesity and cancer 48

1.3.5 Epidemiology of obesity and oesophageal adenocarcinoma 48

1.3.6 Obesity and outcomes 50

1.3.7 Candidate molecular mechanisms linking obesity and cancer 52

1.4 Genomic instability and cancer 57

1.4.1 Genomic instability as an enabling characteristic of cancer 57
1.4.2 Telomeres and genomic instability 59
1.4.3 Anaphase bridge formation and genomic instability 64
1.4.4 Breakage-fusion-bridge cycle 64
1.4.5 Spindle assembly checkpoint 66
1.4.6 Obesity and genomic instability 68
1.4.7 Radiosensitivity and BFB events 69
1.5 Overall Hypothesis 70
Chapter 2 The interaction between obesity and the radioresponse in oesophageal adenocarcinoma 71
2.1 Introduction 72
2.2 Overall aim and specific objectives 75
2.3 Materials and methods 76
2.3.1 Retrospective analysis 76
2.3.2 Reagents 77
2.3.3 Cell culture 77
2.3.4 Oesophageal tumour and adipose tissue biobank 78
2.3.5 Investigation of gene expression 83
2.3.6 X-Ray irradiation 86
2.3.7 Propidium iodide cell cycle analysis 88
2.3.8 Metabolomic screen of ACM 88
2.3.9 Statistical analysis 89
2.4 Results 91
2.4.1 Impact of obesity on radioresponse in OAC patients treated with neoadjuvant chemoradiotherapy. 91
2.4.2 Radiosensitivities of oesophageal cancer cell lines and optimisation of radiation seeding densities 101
2.4.3 Treatment with ACM decreases radioresistance in OE33P and OE33R 104
2.4.4 ACM treatment alters cell cycle kinetics in OE33P and OE33R cells 108
2.4.5 ACM treatment alters AR1 and NRP1 expression 111
2.4.6 Adipokine receptor expression is influenced by radiosensitivity status 114
2.4.7 Adipokine receptor expression changed during the generation of the radioresistant OE33R line 114
2.4.8 Adipokine receptor expression in responder and non-responder patient cohort..119
2.4.9 Metabolomic profile of ACM from non-cancer compared to OAC patients 122
2.4.10 Metabolomic profile of ACM from obese compared to nonobese OAC patients 130
2.5 Discussion 134
Chapter 3 Obesity drives telomere dysfunction in oesophageal adenocarcinoma 140

3.1 Introduction 141
3.2 Overall aims and specific objectives 143
3.3 Materials and methods 144
3.3.1 Cell Culture 144
3.3.2 Telomere length measurement 144
3.3.3 Oesophageal tumour and adipose tissue biobank 145
3.3.4 Investigation of gene expression 145
3.3.5 Statistical analysis 146
3.4 Results 147
3.4.1 ACM drives telomere shortening in OE33P and OE33R 147
3.4.2 ACM drives dysregulation of telomerase gene expression in OE33P and OE33R 149
3.4.3 TERC gene expression in OE33R cells correlates with visceral obesity 152
3.4.4 ACM drives dysregulation of shelterin complex gene expression 155
3.4.5 TERF1, TPP1 and TINF2 gene expression in OE33R correlates with visceral obesity 159
3.4.6 Telomere gene expression in obese and non-obese oesophageal cancer patients 162
3.4.7 Radiosensitivity status influences telomerase and TINF2 expression, but not telomere shortening 165
3.4.8 Shelterin and telomerase gene expression in responder and non-responder patient cohort 169
3.5 Discussion 171
Chapter 4 Obesity stimulates anaphase bridge formation and spindle assembly checkpoint dysregulation in oesophageal adenocarcinoma 177
4.1 Introduction 178
4.2 Overall aim and specific objectives 180
4.3 Materials and methods 181
4.3.1 Cell Culture 181
4.3.2 Anaphase bridge enumeration 181
4.3.3 Oesophageal tumour and adipose tissue biobank 181
4.3.4 Investigation of gene expression 182
4.3.5 Statistical analysis 182
4.4 Results 183
4.4.1 ACM stimulates cell growth in OE33P and OE33R 183
4.4.2 ACM stimulates anaphase bridge formation in OE33P and OE33R and 185
4.4.3 Anaphase bridge levels in ACM treated OE33R cells correlate with visceral obesity. 188
4.4.4 Anaphase bridge levels correlate with TERC, TERT and DKC1 gene expression in ACM treated cells 190

4.4.5 ACM drives dysregulated spindle assembly checkpoint gene expression in OE33P and OE33R 194

4.4.6 SAC gene expression does not correlate with visceral obesity 199

4.4.7 MAD2L2 and BUB1b expression in obese and non-obese oesophageal cancer patients 200

4.4.8 Anaphase bridge levels correlate with CENPE and ESPL1 gene expression in OE33R 202

4.4.9 Radiosensitivity status influences MAD2L2, CENPE and ESPL1 expression in oesophageal cancer cells following ACM treatment 205

4.4.10 SAC expression in responder and non-responder OAC patients 207

4.5 Discussion 209

Chapter 5 Identification of novel genomic instability events in radioresistant oesophageal adenocarcinoma using array comparative genomic hybridization 213

5.1 Introduction 214

5.2 Overall aim and specific objectives 216

5.3 Materials and methods 217

5.3.1 Cell Culture 217

5.3.2 Karyotyping of OE33P and OE33R 217

5.3.3 Array CGH analysis of OE33P and OE33R 218

5.3.4 Investigation of gene expression 223

5.3.5 Statistical analysis 223

5.4 Results 224

5.4.1 OE33P and OE33R have a complex, near tetraploid karyotype 224

5.4.2 Array CGH analysis identifies alterations in OE33R compared to OE33P 227

5.4.3 Selection of targets and validation in cell lines 231

5.4.4. Target gene expression in OE33P and OE33R 235

5.4.5 Target gene expression in responder and non-responder patient cohorts 235

5.5 Discussion 238

Chapter 6 Concluding discussion 242

6.1 Concluding discussion 243

6.2 Future directions 253

Figure List

Figure 1.1. Oesophageal cancer incidence rates between 1994 and 2009 categorised by histological type, (A) females, (B) males 23
Figure 1.2. Features used to stage oesophageal carcinoma according to the 2009 TNM classification system 28
Figure 1.3. Five-year relative age-adjusted survival is shown for OAC, 1975 to 2004 30
Figure 1.4. Tumour regression grades (TRG) proposed by Mandard et al 32
Figure 1.5. Rationale for cooperation between chemotherapy and radiotherapy 34
Figure 1.6. Double strand break repair may be mediated by NHEJ or HR 37
Figure 1.7. The cell cycle and checkpoint activation 39
Figure 1.8. Percent of men and women with increased risk from cardiovascular disease 43
Figure 1.9. Major adipose depots in humans 45
Figure 1.10. Fat measurement by computed tomography of the abdomen 47
Figure 1.11. Summary of mortality from cancer according to BMI for (A) U.S. men and (B) U.S. women in the Cancer Prevention study II, 1982 through 1998 51
Figure 1.12. Hallmarks of cancer and potential role of visceral obesity in tumourigenesis 53
Figure 1.13. Systemic alterations in visceral adiposity which may contribute to a pro-tumourigenic microenvironment 56
Figure 1.14. Genomic instability is an emerging enabling hallmark of cancer 57
Figure 1.15. Telomere structure 60
Figure 1.16. Telomere shortening leads to chromosomal fusion and genomic instability. 61
Figure 1.17. Telomerase structure 63
Figure 1.18. Shelterin complex structure 63
Figure 1.19. Repeated breakage-fusion-bridge cycels results in rampant genomic instability. 65
Figure 1.20. The spindle assembly checkpoint (SAC) ensures correct chromosomal alignment prior to anaphase 67
Figure 2.1. Comparison of clinical and pathological T stage in normal and overweight/obese patient cohorts 95
Figure 2.2. Comparison of tumour regression grade following NA CRT in normal and overweight/obese patient cohorts 96
Figure 2.3. Operative outcomes in normal weight and overweight/obese patient cohorts 99
Figure 2.4. Disease specific survival of normal and overweight/obese patient cohorts 100
Figure 2.5. Clonogenic assay of OE33P and O33R cells 102
Figure 2.6. OE33P cells are more radioresponsive than OE33R cells 103
Figure 2.7. ACM treatment decreases radioresistance in OE33P and OE33R 106
Figure 2.8. Comparison of the effect of ACM from three patient cohorts on radiosensitivity of OE33P and OE33R 107
Figure 2.9. Cell cycle kinetics in OE33P following ACM treatment 109
Figure 2.10. Cell cycle kinetics in OE33R following ACM treatment 110
Figure 2.11. The effect of ACM on adipokine receptor expression 113
Figure 2.12. Adipokine receptor expression in OE33P compared to OE33R 116
Figure 2.13. LepR expression is greater in ACM treated OE33R compared to ACM treated OE33P cells 117
Figure 2.14. Expression of adipokine receptors across a sequence of increasing passage OE33 cell lines during generation of the radioresistant OE33R cell line 118
Figure 2.15. Validation of adipokine receptor expression in responder and non-responder OAC patients 121
Figure 2.16. Separation of patient cohorts on the basis of metabolomic profile 124

Figure 2.17. Non cancer and surgery only OAC patients are associated with different metabolomes 125
Figure 2.18. Non cancer and NA CRT patients express different metabolomic profiles 127
Figure 2.19. Metabolomic profiles of surgery only OAC and NA CRT OAC patient cohorts .. .129
Figure 2.20. Metabolomic profiles of non-obese and obese OAC patient cohorts 132
Figure 3.1. ACM drives telomere shortening in OE33P and OE33R 148
Figure 3.2. ACM alters TERC and TERT expression in OE33P and OE33R 150
Figure 3.3. ACM alters DKC1 and TEP1 expression 151
Figure 3.4. TERC expression correlates with visceral obesity 154
Figure 3.5. ACM upregulates shelterin complex gene expression in OE33P and OE33R 157
Figure 3.6. ACM upregulates TINF2 gene expression in OE33P and OE33R 158
Figure 3.7. Shelterin gene expression in ACM treated OE33R cells correlates with visceral obesity 161
Figure 3.8. Telomerase and shelterin gene expression in obese and non-obese patient cohorts 164
Figure 3.9. Telomere length did not differ in untreated OE33P compared to OE33R cells 166
Figure 3.10. TERT and TINF2 gene expression in responder and non-responder patient cohorts 170
Figure 4.1. ACM stimulated cell growth in OE33P and OE33R cells at 24 hours 184
Figure 4.2. Anaphase bridge formation in OE33P and OE33R cells 186
Figure 4.3. Anaphase bridge levels in OE33P and OE33R cells following ACM treatment 187
Figure 4.4. Anaphase bridge levels correlate with obesity status in OE33R cells following ACM treatment 189
Figure 4.5. Telomerase gene expression correlates with anaphase bridge levels in ACM treated OE33P and OE33R cells 192
Figure 4.6. ACM upregulates MAD2L2 and BUB1b expression in OE33P and OE33R 196
Figure 4.7. ACM alters CDC20 and CENPE expression in OE33P and OE33R 197
Figure 4.8. ESPL1 expression in OE33P cells was downregulated following 72 hours of ACM treatment 198
Figure 4.9. MAD2L2 and BUB1b expression in obese and non-obese oesophageal cancer patients 201
Figure 4.10. CENPE and ESPL1 expression in OE33R cells treated with ACM negatively correlates with anaphase bridge levels 204
Figure 4.11. SAC expression in responder and non-responder OAC patient cohorts 208
Figure 5.1. Gains and losses in OE33P compared to OE33R 228
Figure 5.2. Loss of heterozygosity in OE33P and OE33R 229
Figure 5.3. Copy number losses on chromosome 9 in OE33P compared to OE33R 232
Figure 5.4. The 9p deletion in OE33R cells as seen on ChAs software encompasses 9p24.2-21.3 233
Figure 5.5. Genes located at the 9p deletion as per the National Centre for Biotechnology Infomration (NCBI) Map viewer: 9 2,200K-25,600K (9p24.2-21.3) 234
Figure 5.6. IL33 expression is higher in OE33P compared to OE33R cells 236
Figure 5.7. IL33 expression in oesophageal cancer patients 237

List of Tables

Table 1.1. Classification of obesity by BMI 42
Table 1.2. Cancer risk and obesity 49
Table 2.1. Constituents of visceral compared to subcutaneous adiposeconditioned media 82
Table 2.2. Constituents of obese compared to non-obese adipose conditioned media 82
Table 2.3. Constituents of adipose conditioned media from OAC patients treated with surgery only compared to OAC patients treated with NA CRT 82
Table 2.4. Reagents and volumes used in cDNA synthesis 85
Table 2.5 Optimum clonogenic cell seeding densities 87
Table 2.6. Clinical details of normal and overweight/obese cohorts 92
Table 2.7. Pathological details for normal and overweight/obese patient cohorts. 94
Table 2.8. Surgical resection in normal and overweight/obese patient cohorts. 98
Table 2.9. Actuarial life table analysis 100
Table 2.10. Anthropometric data for patient ACM used in clonogenic assays 105
Table 2.11. Anthropometric data for patient ACM used in cell cycle analysis. 108
Table 2.12. Patient cohort details (ACM used in adipokine receptor gene expression and genomic instability *in vitro* experiments 112
Table 2.13. Adipokine receptor expression in OE33P compared to OE33R cells 115
Table 2.14. Characteristics of responder and non responder OAC patients 120
Table 2.15. Anthropometric details of non-cancer patients 123
Table 2.16. Anthropometric details of surgery only OAC patients 123
Table 2.17. Anthropometric details of NA CRT OAC patients 123
Table 2.18. Relative intensities and VIP values of the most discriminating metabolites generated from the PLS-DA for comparison of ACM from non-cancer *versus* surgery only OAC patients 126
Table 2.19. Relative intensities and VIP values of the most discriminating metabolites generated from the PLS-DA for comparison of ACM from non-cancer *versus* NA CRT OAC patients 128
Table 2.20. Anthropometric details of non-obese and obese OAC patients 131
Table 2.21. Relative intensities and VIP values of the most discriminating metabolites generated from the PLS-DA for comparison of ACM from non-obese versus obese OAC patients 133
Table 3.1. Telomerase gene expression correlates with visceral obesity 153
Table 3.2. ACM upregulates shelterin gene expression in OE33P and OE33R 156
Table 3.3. Shelterin gene expression correlates with visceral obesity 160
Table 3.4. OAC tumour patient characteristics (in which TERC, TERT and TINF2 gene expression was assessed) 163
Table 3.5. Comparison of telomerase gene expression in OE33P and OE33R cell lines at baseline and following ACM treatment 167
Table 3.6. Comparison of telomerase gene expression in OE33P and OE33R cell lines at baseline and following ACM treatment 168
Table 4.1. Levels of anaphase bridges in ACM treated OE33R cells correlates with visceral obesity 189
Table 4.2. TERC, TERT and DKC1 gene expression correlates with anaphase bridge levels in ACM treated OAC cells 191
Table 4.3. Shelterin gene expression does not correlate with anaphase bridge formation. 193
Table 4.4. SAC gene expression in OE33P and OE33R cells treated with ACM does not correlate with visceral obesity 199
Table 4.5. CENPE and ESPL1 gene expression correlates with anaphase bridge levels in ACM treated OE33R cells 203
Table 4.6. SAC gene expression in OE33P compared to OE33R cells 206
Table 5.1. Digestion master mix 219

Table 5.2. Ligation master mix 219
Table 5.3. PCR Dilution 220
Table 5.4. PCR Master mix 220
Table 5.5. Cytoscan PCR Program 221
Table 5.6. Fragmentation master mix 221
Table 5.7. Labelling master mix 222
Table 5.8. Hybridisation master mix 222
Table 5.9. Summary of abnormalities (copy number gains and losses) detected in both OE33P and OE33R cell lines 225
Table 5.10. Summary of abnormalities (loss of heterozygosity) detected in both OE33P and OE33R cell lines Anthropometric details of NA CRT OAC patients 226
Table 5.11. Summary of differences in OE33R compared to OE33P cells identified by array CGH 230

Abbreviations

ABL	Anaphase bridge levels
ANOVA	Analysis of Variance
AR	Adiponectin receptor
ATM	Ataxia telangiectasia mutated
BCP	1-Bromo-2 Chloropropane
BMI	Body Mass Index
BO	Barrett's Oesophagus
BUB1B	Budding uninhibited by benzimidazoles homolog beta 1
CDC20	Cell division cycle protein 20
CD274	CD 274 molecule
CDKN2A	CDK4 inhibitor p16-INK4
CDKN2B	Cyclin-dependent kinase inhibitor 2B
CDKN2B-AS1	CDKN2B antisense RNA 1
cDNA	Complementary deoxyribonucleic acid
CENPE	Centromere protein E
ChAs	Chromosome analysis suite
CI	Confidence Interval
Cisplatin	cis-diamminedichloroplatinum(II)
CRC	Colorectal Adenocarcinoma
CRP	C-Reactive Protein
cRPMI	Complete RPMI
CRT	Chemoradiotherapy
CT	Computed Tomography
Ct	Threshold cycle
DNA	Deoxyribonucleic acid
DNA-PK	DNA-dependent protein kinase
DSB	Double strand breaks
ESPL1	Extra spindle pole like 1
EZH2	Enhancer of zeste 2
dH_2O	Deionised H_2O
DKC1	Dyskerin
dNTPs	Deoxyribonucleotide Triphosphates
FACS	Fluorescence-Activated Cell Sorting
FBS	Foetal Bovine Serum
FISH	Fluorescence in situ hybridization
G_0	Gap 0 phase
G_1	Gap 1 phase
G_2	Gap 2 phase
gDNA	Genomic deoxyribonucleic acid
GLDC	Glycine dehydrogenase (decarboxylating)
GORD	Gastro-oesophageal reflux disease
HR	Homologous recombination
IR	Ionising radiation
IDF	International Diabetes Federation
IFNB1	Interferon, beta 1
IFNA21	Interferon, alpha 1
IFNA17	Interferon, alpha 17
IFNA13	Interferon, alpha 13

IFNA2	Interferon, alpha 2
IFNA8	Interferon, alpha 8
IFNA1	Interferon, alpha 1
IGF	Insulin-Like Growth Factor
IGF-1	Insulin-Like Growth Factor-1
IL	Interleukin
IL6	Interleukin 6
IL8	Interleukin 8
IL33	Interleukin 33
JAK2	Janus kinase 2
LepR	Leptin receptor
LIG4	Ligase IV
MCP-1	Monocyte Chemotactic Protein-1
MAD2L2	Mitotic arrest deficient-like 2
MetSyn	Metabolic Syndrome
M	Mitosis
miRNA	Microribonucleic acid
MMP	Matrix Metalloproteinase
MRI	Magnetic Resonance Imaging
mRNA	Messenger ribonucleic acid
Mir-101-2	microRNA 101-2
Mir-31	microRNA 31
MLANA	Melan-A
MLLT3	Myeloid/lymphoid or mixed-lineage leukaemia (trithorax homolog, Drosophila); translocated to, 3
MTAP	Methylthioadenosine phosphorylase
mTOR	Mechanistic target of rapamycin
Nbs1	Nijmegen breakage syndrome protein 1
NF-κβ	Nuclear Factor-κβ
NER	Nucleotide excision repair
NHEJ	Non-homologous end joining
NRP1	Neuropilin-1
NS	Not significant
OAC	Oesophageal Adenocarcinoma
OE33P	OE33 parent
OE33R	OE33 resistant
OR	Odds Ratio
p	Probability
PBMC	Peripheral Blood Mononuclear Cells
PBS	Phosphate Buffered Saline
pCR	Pathological complete response
PCR	Polymerase chain reaction
PDCD1LG2	Programmed cell death 1 ligand 2
PE	Plating efficiency
PI	Propidium iodide
PLIN2	Perilipin 2
POT1	Protection of telomere 1
PRDKC	Protein kinase DNA-activated catalytic
PSIP1	PC4 and SFRS1 interacting protein 1
PTGS2	Prostaglandin-endoperoxide synthase 2

PTPRD	Protein tyrosine phosphatase delta
qPCR	Quantitative Polymerase Chain Reaction
R0	Total resection
RLN1	Relaxin 1
RLN2	Relaxin 2
RNA	Ribonucleic acid
ROC	Receiver Operating Characteristics
ROS	Reactive oxygen species
RPMI	Roswell Park Memorial Institute
RR	Relative Risk
RQ	Relative quantification = $2^{-\Delta\Delta Ct}$
RT	Room Temperature
S	Synthesis phase
SAC	Spindle assembly checkpoint
SCC	Squamous cell carcinoma
SD	Standard Deviation
SEM	Standard Error of the Mean
SFA	Subcutaneous Fat Area
SH3GL2	SH3-domain GRB2-like 2
SLC1A1	Solute carrier family 1
SLC24A2	Solute carrier family 24
STAT	Signal transducer and activator of transcription
TAM	Tumour-Associated Macrophage
TERC	Telomerase RNA component
TERT	Telomerase reverse transcriptase
TEP1	Telomere associated protein 1
TINF2	TRF1 interacting nuclear factor 2
TPP1	Tripeptidyl peptidase 1
TERF1	Telomeric-repeat binding factor 1
TERF2	Telomeric-repeat binding factor 2
TRG	Tumour regression grade
TFA	Total Fat Area
TGF-β	Transforming Growth Factor- β
Th	T Helper
Tis	Carcinoma in situ
TNF-α	Tumour Necrosis Factor-α
TNM	Tumour-Node-Metastasis
TPP1	Telomerase associated protein 1
TS	Tumour Associated Stroma
TYRP	Tyrosinase related protein 1
VEGF	Vascular endothelial growth factor
VFA	Visceral Fat Area
VLDLR	Very low density lipoprotein receptor
WC	Waist Circumference
WHO	World Health Organization
XRCC4	X-ray repair cross-complementing protein 4

Units

bp	base pairs
°C	degrees Celsius
cm	centimetre
g	grams
Gy	gray
× g	acceleration due to gravity
h	hour
kb	kilobase
keV	kiloelectron-Volt
kV	kilovolt
M	molar
mA	milliamp
mg	milligram
min	minute
mL	millilitre
mM	millimolar
mm	millimetre
µg	microgram
µL	microlitre
µM	micromolar
ng	nanogram
nM	nanomolar
nm	nanometre
nt	nucleotide
pmol	picomole
s	seconds
U	units
V	volts
v/v	volume per volume
w/v	weight per volume
X	magnification

Publications and Presentations

Published

- JM Howard, **AM Mongan,** B Manning, P Byrne, P Lawler, N Ravi, JV Reynolds. Outcomes in Achalasia from a Surgical Unit where Pneumatic Dilatations is First-Line Therapy. *Dis Esophagus, 2010 Aug;23(6):465-72*
- **Mongan AM**, Malik V, Rowley S, Claxton Z, Muldoon C, O'Toole D, Ravi N, Reynolds JV. Presentation and Management of Gastrointestinal Stromal Tumours. *IMJ, 2013, June*
- Doyle SL, Bennett AM, Donohoe CL, **Mongan AM,** Howard JM, Lithander FE, Pidgeon GP, Reynolds JV, Lysaght J, Establishing computed tomography-defined visceral fat area thresholds for use in obesity-related cancer research. *Nutr Res, 2013, Mar;33(3):171-9*

In preparation

- **Mongan AM**, Lynam-Lennon N, Marignol L, Maher S, Reynolds JV, Pidgeon G, O'Sullivan J. Obesity influences the response to radiotherapy in oesophageal adenocarcinoma. In preparation for submission to *Br J Cancer*
- **Mongan AM**, Casey R, Lynam-Lennon N, Marignol L, Maher S, Reynolds JV, Pidgeon G, O'Sullivan J. Adiposity drives telomere dysfunction in oesophageal adenocarcinoma. In preparation for submission to *Cancer Lett*
- **Mongan AM**, Lynam-Lennon N, Marignol L, Maher S, Reynolds JV, Pidgeon G, O'Sullivan J. Anaphase bridge formation and spindle assembly checkpoint dysfunction in radioresistant oesophageal adenocarcinoma. In preparation for submission to *J Mol Med*
- **Mongan AM**, Geiersbach K, Paxton C, Lynam-Lennon N, Marignol L, Maher S, Bronner M, Reynolds JV, Pidgeon G, O'Sullivan J. Novel genomic instability events in radioresistant oesophageal adenocarcinoma identified using array comparative genomic hybridization. In preparation for submission to *Radiation Research*
- **Mongan AM**, King S, Ravi N, O'Byrne K, Reynolds JV. Perioperative Chemotherapy in the Management of Gastric and Junctional Cancer. Accepted by *IJMS*
- O'Farrell NJ & Donohoe CL, **Mongan AM**, King S, Ravi N, Reynolds JV. Can neoadjuvant chemoradiotherapy downstage node positive oesophageal cancer?
- O'Farrell NJ, O'Brien M, Picardo SL, **Mongan AM**, Feighery R, Muldoon C, O'Sullivan JN, Reynolds JV. The prognostic outcomes associated with a diagnosis of indefinite and low grade dysplasia of the oesophagus. Under review at *The Surgeon*

Oral Presentations

International Oral Presentations (presenting author)

- Digestive Disorders Federation Annual Conference, Liverpool, UK. July, 2012
- Society of Academic and Research Surgery (SARS) and the Section of Surgery of the Royal Society of Medicine (RSM) Joint Meeting, London, UK. January 2013
- 13th World Congress of the International Society for Diseases of the Esophagus, Venice. October 2012

National Oral Presentations (presenting author)

- Plenary prize session of the Sylvester O'Halloran Annual Meeting, Limerick. March 2013
- Oral poster presentation at the Irish Association for Cancer Research (IACR), Dublin. March 2013
- Shortlisted for oral presentation at the 10th St. Luke's Young Investigator Award, St. Luke's Hospital and Royal Academy of Medicine Meeting, Dublin. January 2013
- Sir Peter Freyer annual meeting, Galway. September 2012
- Plenary prize session of the Sylvester O'Halloran annual meeting, Limerick. March 2012
- Three papers at the Sir Peter Freyer annual meeting, Galway. September 2011
- Sir Peter Freyer annual meeting, Galway. September 2009

Poster Presentations

International Poster Presentations (presenting author)

- European Association for Cancer Research annual meeting, Barcelona, Spain. June 2012
- Two papers at the Association of Upper Gastrointestinal Surgeons of Great Britain and Ireland (AUGIS), Belfast, UK. September 2011

National Poster Presentations (presenting author)

- Sir Peter Freyer annual meeting, Galway. September 2012
- Association of Upper Gastrointestinal Surgeons of Great Britain and Ireland (AUGIS), Belfast, UK. September 2011

Chapter 1 General introduction

This introduction is divided into four sections. The first section comprises an overview of oesophageal adenocarcinoma and a description of the role of neoadjuvant chemoradiotherapy in the management of this malignancy. The second section discusses radiotherapy and biomarkers of radioresponse in cancer. The third discusses the link between obesity status and cancer, and the fourth section summarises the emerging role of genomic instability in cancer, in particular its association with obesity and radiotherapy.

1.1 Oesophageal adenocarcinoma

1.1.1 Epidemiology

Cancer of the oesophagus represents a significant and increasing health problem. Worldwide it is the eighth most common cancer and the sixth most common cause of death from cancer[2]. The vast majority of oesophageal cancers may be classified into two histological subtypes, squamous cell carcinoma (SCC) or adenocarcinoma (OAC)[3]. OAC is the fastest increasing cancer in Western countries[4]. Between 1994 and 2009 the incidence rate of OAC in Ireland increased by 2.2% annually in women and 3.0% in men (Figure 1.1)[5]. The rising incidence is occurring across all disease stages and all age groups, but the greatest increase (>600%) is documented in men over 65 years old[4]. There is a striking male to female preponderance of OAC with incidence in males six-fold higher than incidence in females[6]. Ethnicity plays a major role, and rates of OAC are five-fold higher in Caucasians compared to African Americans[7]. Age is associated with increased risk of OAC, and median age at diagnosis is 60 years[8].

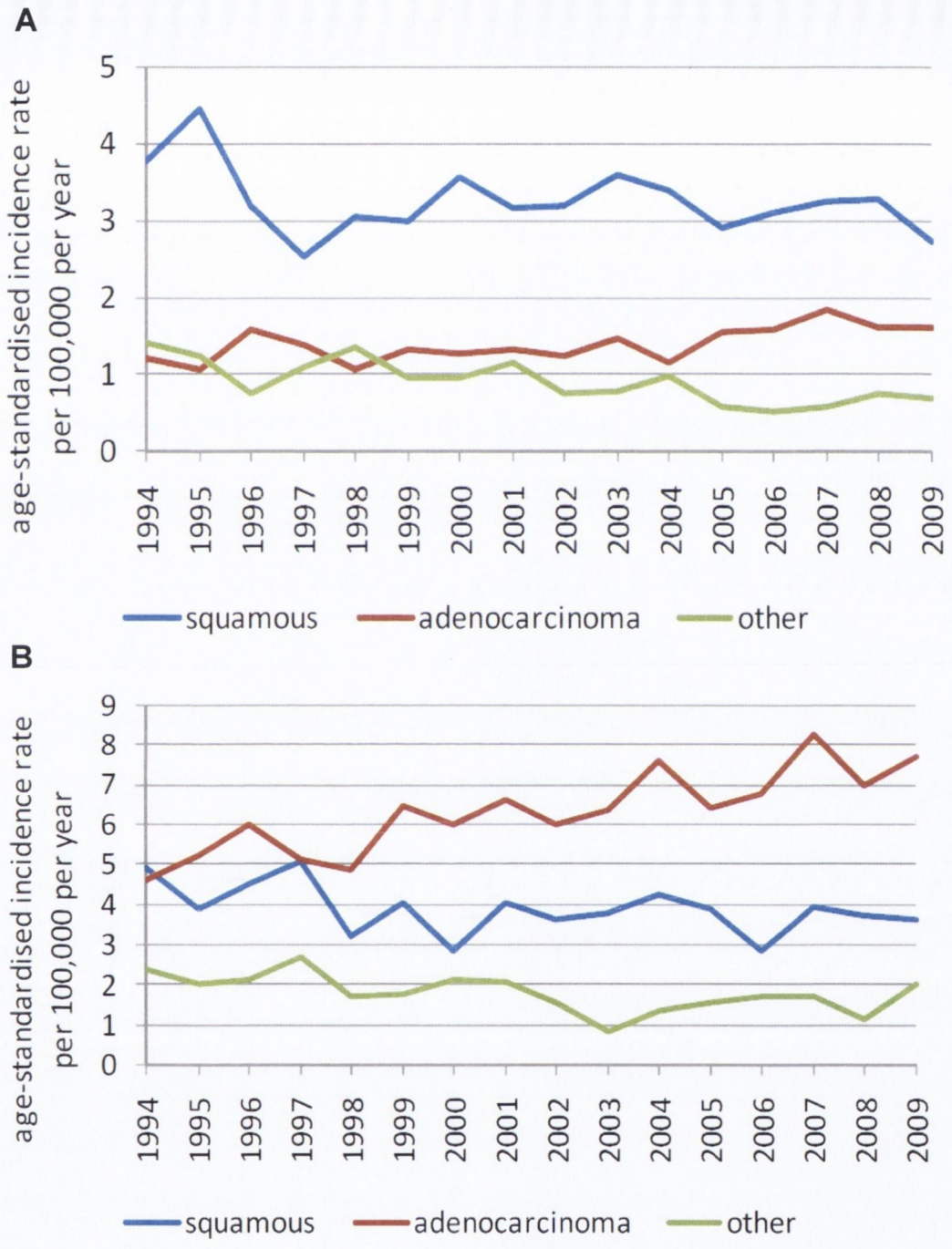


Figure 1.1. Oesophageal cancer incidence rates between 1994 and 2009 categorised by histological type, (A) females, (B) males

In Ireland, the incidence rate for squamous carcinoma of the oesophagus fell by 0.9% annually for females and 1.4% for males between 1994 and 2009 while the incidence rate for adenocarcinoma increased by 2.2% annually for women and 3.0% for men (reproduced with permission from 2011 National report of the National Cancer Registry[5]).

1.1.2 Multifactorial aetiology for OAC

Risk Factors for OAC

OAC has a multifactorial aetiology, but the established risk factors are Barrett's oesophagus (BO), gastro-oesophageal reflux, and obesity[8]. Chronic acid reflux leads to irritation of the distal oesophagus, and increases the risk of developing OAC by up to 8-fold[8]. BO occurs when the normal stratified squamous epithelium of the oesophagus transforms into columnar intestinal epithelium characteristic of the stomach lining[9,10]. Patients with BO have a 30-40-fold increased risk of developing OAC compared to the rest of the population[11,12]. However, up to 50% of individuals with OAC have no history of reflux disease while over 95% have no previous history of Barrett's[10,13,14].

Barrett's Oesophagus

Approximately 10-15% of people with GORD will go on to develop the premalignant condition Barrett's oesophagus[15]. Patients with BO have a 30-40-fold increased risk of developing OAC compared to the rest of the population[11,12]. BO occurs when the normal stratified squamous epithelium of the oesophagus transforms into columnar intestinal epithelium characteristic of the stomach lining[9,10]. Barrett's oesophagus develops as a defence mechanism to long term exposure to GORD. The exact aetiology for the metaplasia of the squamous cells to intestinal type epithelium has yet to be fully elucidated, but it may develop as a defence mechanism to long term exposure to GORD. It is hypothesized, that following insult from the components of the gastro-oesophageal reflux, stem cells of squamous mucosa undergo an altered differentiation during repair, and the cells begin to display traits atypical from mucosal gastric stem cells[16]. Although GORD appears to be crucial in the pathogenesis of Barrett's oesophagus and the subsequent progression to OAC[14], only 10-15% of long term GORD patients will actually develop Barrett's oesophagus, and in those patients that do, only a subset progress to OAC[15]. Up to 50% of individuals with OAC have no history of reflux disease while over 95% have no previous history of Barrett's[10,13,14].

Obesity

We and others have shown that obesity is strongly implicated in the pathogenesis of OAC[6,14,17–22]. The incidence of OAC in Ireland has increased by almost 50% in recent years, a trend mirrored across western industrialized nations, which parallels the sharp increase in the prevalence of obesity[23–25]. A recent meta-analysis indicated that a body mass index (BMI) $\geq$ 30 kg/m^2 is associated with a relative risk (RR) of 3.0 for developing OAC, a higher association than for any other cancer[26]. Our unit demonstrated a dose-dependent relationship between BMI and OAC risk; premorbid obesity was associated with an eleven fold increased risk of OAC in men[20]. The International Agency for Research on Cancer working group estimates that raised

bodyweight accounts for 39% of OACs[27]. Therefore, OAC may be considered an exemplar model of obesity-associated malignancy. BO is a recognized precursor to adenocarcinoma associated with a 30-40-fold increased risk of developing OAC[11]. A study from our department demonstrated that 46% of patients with BO display the metabolic syndrome, a constellation of conditions associated with visceral obesity, blood lipid disorders, insulin resistance and Type II Diabetes Mellitus[12,28]. Patients with BO are more likely to be obese and one possible mechanism for this association is that of increased acid reflux in patients with high levels of visceral adiposity[14,29]. Adipose tissue is principally accumulated in two compartments, subcutaneous and central or visceral. Visceral obesity promotes gastro-oesophageal reflux disease (GORD) and predisposes to BO, which may contribute to its association with OAC[30]. There is an association with visceral obesity, independent of BMI, with GORD, BO and OAC[12,15,29,31,32]. Obesity is a risk factor for OAC independent of GORD, suggesting that mechanisms other than reflux disease may contribute to disease risk in obese patients[14,20].

Molecular pathogenesis of oesophageal cancer

The progression of Barrett's oesophagus to OAC follows a distinct metaplasia-dysplasia-adenocarcinoma sequence, with an accumulation of molecular changes which occur along the pathway from normal squamous oesophagus to invasive cancer[16]. Unlike colon cancer, there does not seem to be a 'gatekeeper' gene which defines a predominant pathway for tumour progression. According to the hallmarks of cancer proposed by Hanahan and Weinberg, a normal cell must be able to undergo uncontrolled proliferation, become immortalized, resist apoptosis, resist antigrowth signals, promote angiogenesis and gain the ability to invade and metastasize to become cancerous[33]. Increased cell proliferation is an early step along the pathway towards development of oesophageal adenocarcinoma and is thought to be associated with increased EGF/EGFR expression[34], MAPK pathway upregulation[35,36], and increased ODC (ornithine decarboxylase) expression[37]. Immortalization in OAC and many other cancers, is facilitated by telomerase expression[38,39]. Subsequently, evasion of apoptosis is mediated in part by COX-2 stimulation[40,41], p53 deactivation[42,43] and reduced Fas expression[44]. Deregulation of cell cycle control is enabled by inactivation of the retinoblastoma gene (Rb), the activity of which is partially regulated by p16. Allelic loss of the p16 is common in OAC[45,46]. In addition, methylation of the p16 promoter (with or without p16 LOH) is a common mechanism of p16 inactivation in dysplasia and adenocarcinoma arising in Barrett's oesophagus[47,48]. Stimulation of angiogenesis is a key step in tumour progression. VEGF is a potent angiogenic factor. Increased expression of VEGF and its receptor VEGFR2 has been demonstrated in BO, and, to a greater degree, in OAC[49,50]. Loss of cell-cell adhesion is a necessary condition for malignant invasion and metastasis. In OAC, this is thought to be mediated via downregulation of the cell adhesion molecule E-cadherin,(138) and upregulation of the matrix metalloproteinases (MMPs) -1, -2 and -9[51]. Genomic instability appears to be associated with neoplastic progression, and OAC arising

from BO is no exception. The literature suggests that most cases of oesophageal adenocarcinoma arise in patients demonstrating a gain or loss of large portions of chromosomes (or indeed whole chromosomes)[52]. Spatial data from Barrett's biopsies have shown that loss of heterozygosity (LOH) at 9p is an early event in Barrett's oesophagus, followed by 17p LOH and the mutation of the P53 gene, along with DNA content aberrations[45,52,53]. A large number of molecular changes have been identified in the pathogenesis of OAC, however, there does not appear to be an obligate order of events and more work is required to fully elucidate genetic pathways in OAC.

1.1.3 Diagnosis and staging

Dysphagia is the most common symptom of oesophageal adenocarcinoma, although the number of asymptomatic patients in whom a diagnosis has been made by surveillance endoscopy has increased[54,55]. At late stage, the most common symptoms are dysphagia, weight loss, heartburn, odynophagia and shortness of breath[54]. Approximately 50% of patients have locally advanced disease at first diagnosis, which contributes to the high mortality rate[3]. An OAC diagnosis is confirmed by histological assessment of endoscopic biopsy. Over the course of this study, new diagnostic techniques became available, which potentially may be a source of stage migration-i.e., newer imaging techniques may demonstrate metastases that had formerly been silent and unidentified, resulting in a stage migration. Current staging methods include a computed tomography (CT) combined with ^{18}FDG-PET imaging (PET-CT) of the neck, thorax and abdomen, endoscopic ultrasound and bronchoscopy (for mid oesophageal or upper-oesophageal lesions[56]. From 1990 to 1995, evaluation was by oesophagoscopy, barium study, liver ultrasound, and occasional computed tomography (CT). Since 1995, all patients have had CT of the neck, thorax and abdomen. 18-F-deoxyglucose PET scans did not become available in this unit until mid-2003. Similarly, endoscopic ultrasound (EUS) was not freely available during this study period. Oesophageal tumours are staged according to the criteria of the American Joint Committee on Cancer tumour-node-metastasis (TNM) classification, which considers lymph node metastasis, distant metastasis and primary tumour (extent of invasion into oesophageal wall) characteristics[57,58]. The database was adapted and retrospectively classified in 2010 to include the new 7th edition AJCC Cancer Staging Manual N staging classification for oesophageal and junctional tumours[58]. However, both the radioresponder and nonresponder cohorts being compared in this study are equally at risk of stage migration, thus minimising the likelihood of misleading outcome statistics.

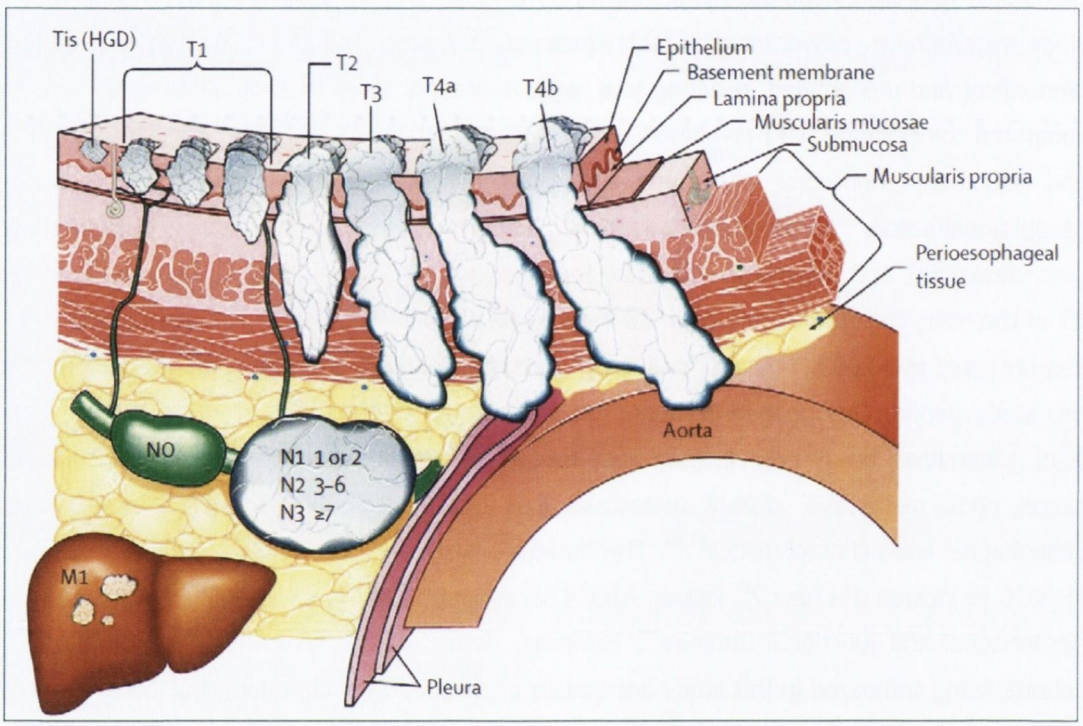


Figure 1.2. Features used to stage oesophageal carcinoma according to the 2009 TNM classification system

The TNM (tumour, node, and metastasis) staging system takes into account the depth of tumour invasion, the nodal status, and the presence or absence of metastatic disease. The stage determines whether the intent of the therapeutic approach will be curative or palliative. Precise clinical staging is critical for both the prognosis and management of the disease. The American Joint Committee on Cancer (AJCC) has designated staging by TNM classification to define cancer of the oesophagus and oesophagogastric junction.

Tis=Intraepithelial neoplasia HGD=High-grade dysplasia (reproduced with permission from Pennathur et al 2013[59]).

1.1.4 Management options: surgery, chemotherapy, radiotherapy, targeted therapies, survival outcomes

OAC carries a dismal prognosis, with five year survival rates of 15-25% (Figure 1.3)[25,60]. In patients treated with curative intent, five year survival increases to 35-50%[55,61–65]. Locally advanced disease, defined by the extent of the primary tumour and involvement of locoregional lymph nodes (higher than stage T2, node positive without distant metastases, or both), is generally treated with curative intent with a multimodal approach that includes surgery[59,61]. Multimodality approaches include both neoadjuvant and adjuvant treatment, with chemotherapy (CT), radiation therapy (RT) or a combination of both (CRT)[59].

Early studies of neoadjuvant CRT in oesophageal cancer demonstrated pathological complete response (pCR) rates which were higher than been expected from preoperative CT or RT when given alone[66–68]. These observations have led to randomised trials comparing preoperative CRT with surgery alone,[69–73] with conflicting results. Three meta-analyses of these trials (1116 patients) demonstrated that despite lower oesophageal resection rates, CRT resulted in improved overall survival[74–76]. This survival benefit was most pronounced when the CT and RT were administered concurrently rather than sequentially[74].

In St. James's hospital, a formal multidisciplinary team, including an advanced nurse specialist and defined lead clinicians in surgery, medical and radiation oncology, radiology, pathology, and gastroenterology, discuss the management of all patients diagnosed with an upper gastrointestinal malignancy. A weekly conference to discuss all new cases has been in place since 1999, and conference proceedings have been audited since 2004. Preoperative chemoradiotherapy (CRT) is the preferred multimodal approach for patients with predicted locally advanced oesophageal and gastro-oesophageal junction (GEJ) type I and II tumours, while patients with GEJ type III tumours have been considered for postoperative chemoradiation and more recently for pre and postoperative chemotherapy. Patients receiving neoadjuvant treatment are given CRT consisting of 40 Gy/15 fractions on days 1 to 5, 8 to 12 and 15 to 19, and synchronous CT of 5-fluorouracil (5-FU) on days 1 to 5 and cisplatin on day 7, with CT repeated on week 6[77].

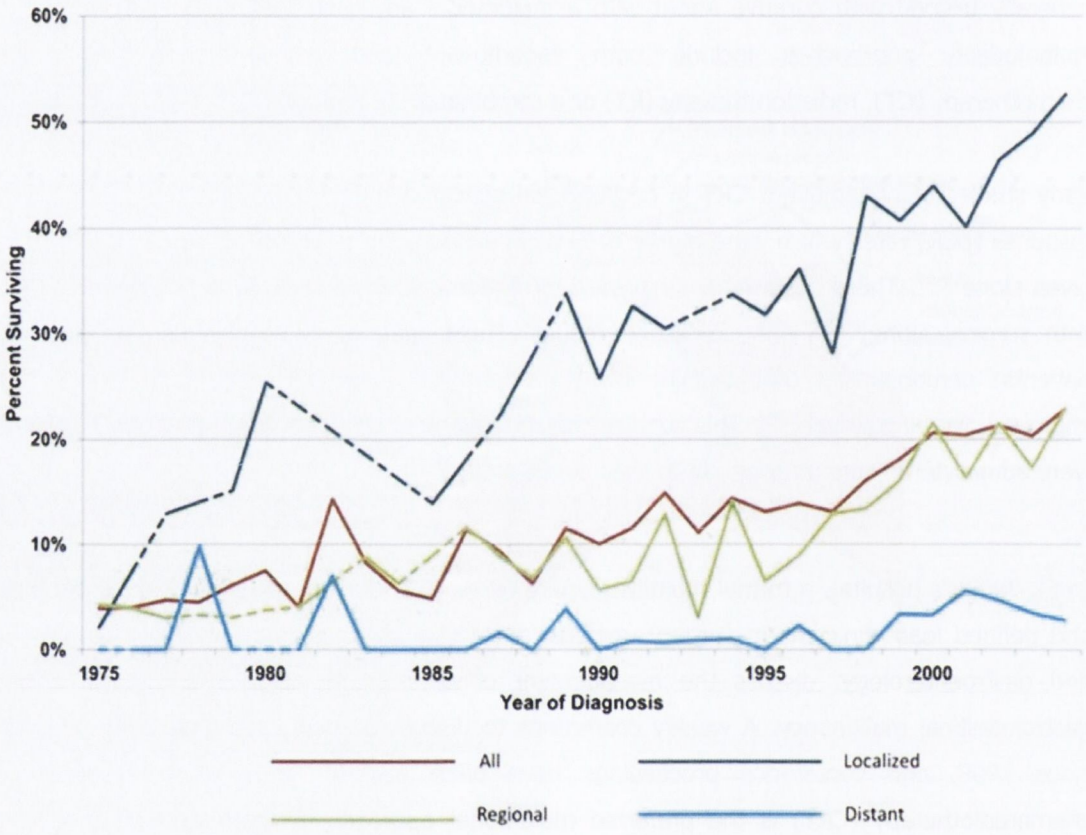


Figure 1.3. Five-year relative age-adjusted survival is shown for OAC, 1975 to 2004
Five-year survival rates have been improving since 1975, with greatest improvement in survival trends occurring in people diagnosed with localized disease. Dashed lines indicate imputed data points for those years for which values were not available (reproduced with permission from Hur et al, 2013[78]).

1.1.5 Tumour response to neoadjuvant CRT

Patients who do not respond to CRT are subject to toxicities without therapeutic gain and their prognosis may be worsened by the delay to surgery[79]. The identification of biomarkers capable of predicting those who will respond well to treatment is essential to improve survival rates. The patients who receive maximum benefit from neoadjuvant CRT are those who achieve a pCR, characterised by no residual cancer cells in the primary tumour or lymph nodes[79–83]. Five-year survival rates are increased to 60% for these patients, irrespective of treatment protocol, tumour histology or stage[79,80]. Patients achieving a pCR also appear to have a different pattern of relapse compared with those who do not attain a pCR, with recurrence predominantly systemic rather than locoregional. Higher pCR rates are achieved with CRT than with RT or CT alone, however, unfortunately only ~30% of patients achieve a pCR[71,79,84,85]. A further subdivision of histopathological response to neoadjuvant regimens was reported by Mandard et al in oesophageal cancer specimens (predominantly squamous cell carcinomas) following neoadjuvant CRT[86]. Tumour regression grade (TRG) analysis, as a marker of treatment response was undertaken in that study and scored from complete regression (TRG1) to absent regression (TRG5) (Figure 1.4). Tumour size, pathological lymph node status, TRG and oesophageal wall involvement correlated highly with disease-free survival but only TRG (TRG1–3 vs. TRG4–5) remained a significant predictor of disease-free survival on multivariate analysis[86]. The Mandard TRG classification has been used in this centre since 1997, and forms the basis for similar classification models[61,77]. Eight published measures of pathologic tumour response were validated in a large cohort of OAC tumour samples in this centre: no existing measure of histomorphologic regression in independently predicted outcome in the evaluation of this large cohort, thus supporting the lack of appropriateness of any for inclusion in current staging nomenclature (accepted, Annals of Surgery). A three-point variation of the Mandard TRG which separates complete (TRG 1), partial i.e. fibrosis predominates (TRG2/3) and minimal i.e. cancer outweighs fibrosis (TRG 4/5), responses was independently significant alongside the current AJCC staging system. Precise terminology of treatment response is increasingly required in cancer research, and these data suggest that this three-point system should be considered for validation across international consortia with robust data registries.

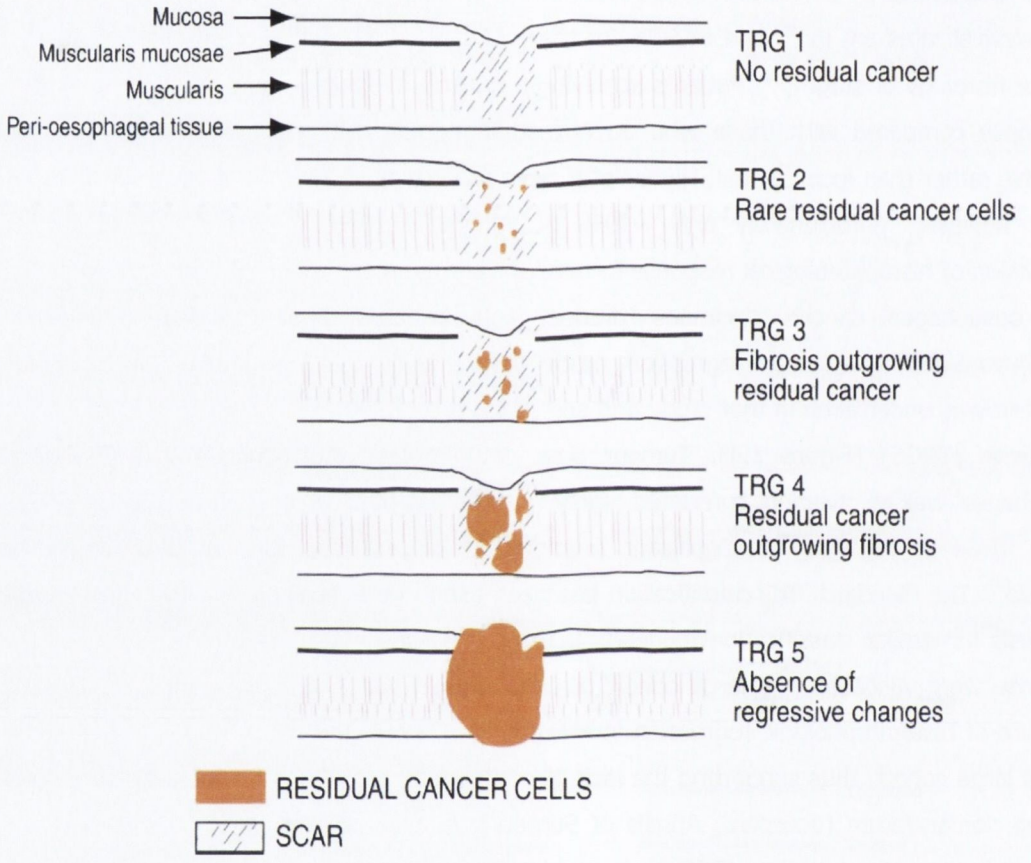


Figure 1.4. Tumour regression grades (TRG) proposed by Mandard et al
TRG 1 represents a complete response and is characterised by fibrosis within the oesophageal wall with no viable residual tumour cells. TRG 2 is characterised by rare residual tumour cells within the fibrosis. TRG 3 is characterised by predominant fibrosis with residual tumour cells. TRG 4 represents residual tumour cells outgrowing fibrosis, whilst TRG 5 represents a complete absence of regression change. A TRG of 1-3 was significantly associated with disease-free survival, when compared to TRG 4-5 (reproduced with permission from Gillham, 2007[87]).

1.1.6 Radiation and chemotherapy interactions

The aim of neoadjuvant RT is to facilitate increased local control by improving curative resection rates or reducing risk of recurrence or both[79,88,89]. Three clinical rationales support the use of CT delivered concurrently with RT[90]. First, concomitant CRT may be used to down-size tumours preoperatively[90]. Second, CT may act as a radiosensitiser, improving the probability of local control and, in some cases, survival, by aiding the destruction of radioresistant clones[90–92]. This interaction within the radiation field leads to increased killing of cells (cytotoxic activity) either to the same degree as (additive) or more than (supraadditive) using both modalities sequentially[90,93]. Finally, CT given as part of concurrent CRT may act systemically and potentially eradicate distant micro metastases[90]. The term spatial cooperation is used to describe the scenario whereby radiotherapy acts locoregionally, and chemotherapy acts against distant micro metastases, without interaction between the agents[90,93].

Cisplatin is one of the most commonly used drugs for concurrent CRT. Cisplatin integrates into DNA in close proximity to radiation-induced DNA breaks, acting synergistically to make the defect more difficult to repair[94–97]. In addition, cisplatin induces a G_2/M cell cycle arrest and programmed cell death.[98] Administration of cisplatin after RT produces the maximum supra-additive effect[99,100]. 5-FU is a pyrimidine nucleoside analogue that affects nucleoside and nucleotide metabolism and is a potent radiosensitiser[101–103]. Putative mechanisms for its radiosensitisation effects include the inappropriate progression through the S-phase of the cell cycle, redistribution of cells into radiosensitive phases of the cell cycle, and inhibition of repair of radiation-induced DNA damage[101–103].

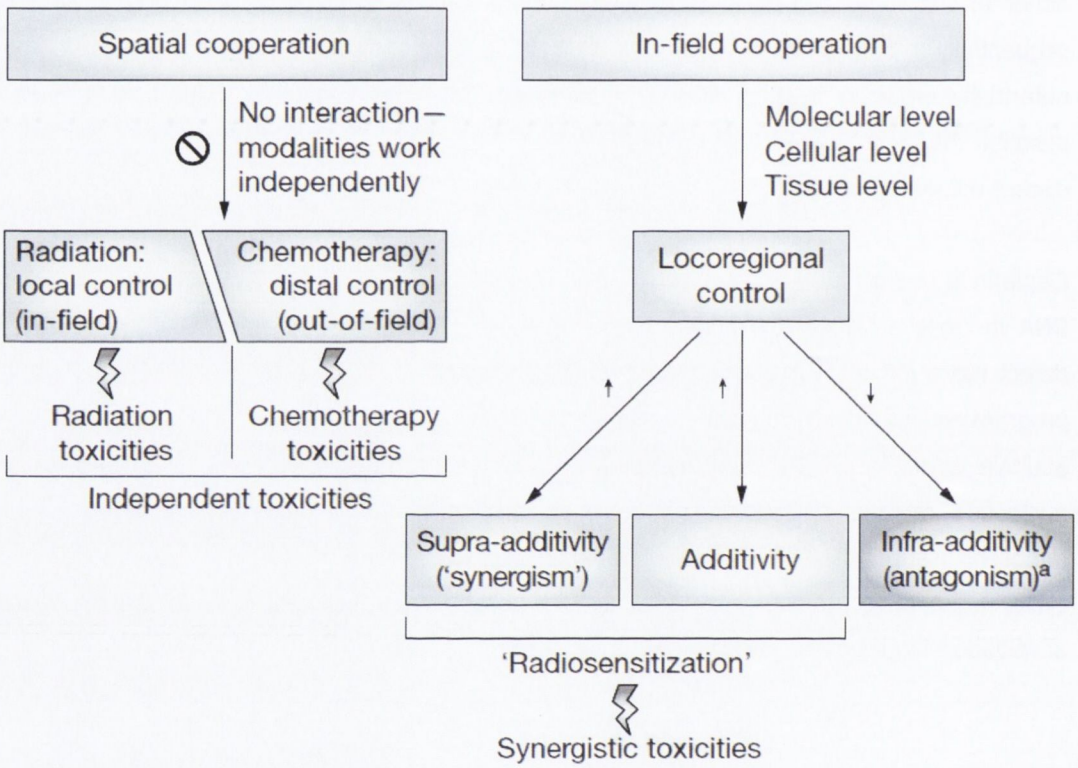


Figure 1.5. Rationale for cooperation between chemotherapy and radiotherapy
Spatial and in-field cooperation are the two idealized types of cooperation between radiation and chemotherapy. Both mechanisms can contribute synergistically to clinical benefit. a Usually not desirable as this could protect the tumour (reproduced with permission from Seiwert et al, 2007[90]).

1.2 Radiation

1.2.1 Radiotherapy

Radiotherapy (RT) is one of the major modalities of cancer treatment, used to treat almost all types of solid malignancies[104]. RT most commonly involves the use of low linear energy transfer ionising radiation (IR) such as X-rays and γ-rays[104]. The therapeutic mechanism for radiation is based on the differential repair capacities of slowly proliferating normal tissue cells and rapidly proliferating tumour cells and the ability of the radiation oncologist to take advantage of any geometric separation between malignant and non-malignant tissues[105,106]. The cytotoxicity of RT arises from the ability to produce DNA damage, however the exact mechanism of cell death is still an area of active investigation[107]. Radiation dose or exposure is measured in gray (Gy) which are units of absorbed radiation per unit of tissue (1Gy represents 1 J/kg tissue)[108]. The total radiation dose in OAC treatment is usually fractionated (spread out over time), the standard regimen consisting of 40 Gy/15 fractions on days 1 to 5, 8 to 12, and 15 to 19.

1.2.2 Radiation induced damage

Ionizing radiation (IR) therapy works by inducing a variety of DNA lesions, including oxidized base damage, abasic sites, single-strand breaks (SSBs) and double-strand breaks (DSBs)[109]. A one Gy dose can produce more than 2000 base damage, 1000 SSB, 40 DSB and 30 DNA cross-links[110]. These lesions, if unrepaired, ultimately result in cell death through mitotic catastrophe and apoptosis[109]. Double-stranded breaks (DSBs) of nuclear DNA are thought to be the most important cellular effect of radiation, but radiation also affects the processes of the cell cycle necessary for cell growth, cell senescence, and apoptosis[111–116]. Directly ionizing effects of radiation account for ~35% of radiation damage; however, 65% of radiation-induced DNA damage is indirectly ionizing via free-radical intermediaries formed from the radiolysis of cellular water[117]. DNA damage is detected by sensor proteins, which activate transducer proteins. The damage signal is amplified by transducer proteins to downstream effector proteins which mediate cell cycle checkpoint activation, and induce DNA repair or apoptosis. Effector proteins mediate the damage signal[118]. The activity of the DNA repair processes that deal with DNA damage can determine response to IR[109].

1.2.3 DNA repair

Various pathways are involved in the repair of IR-damaged DNA, depending on the type of DNA lesion. Alterations in these pathways modulate the cellular response to radiation[108]. DSB repair mechanisms include homologous recombination (HR) and non-homologous end joining (NHEJ) pathways (Figure 1.6)[119,120]. There is first a recognition of impaired DNA (ATM, ATR), followed by a cell-cycle arrest (CHK1, CHK2). NHEJ is the predominant DSB repair mechanism in humans. It functions by linking the extremities of broken DNA, without resynthesis of lost DNA and is active in all stages of the cell cycle[119,121]. Several proteins are involved in processing broken DNA ends, such as Ku70, DNA-PK, XRCC4 and LIG4[120,122]. Alterations in DNA-PK and XRCC4 expression and Ku end binding activity is associated with increased sensitivity to radiation[123–126]. The HR repair pathway restores damaged DNA using the homologous chromosome as a template during S and G2 phases of the cell-cycle[119]. Core proteins involved in HR include RPA, RAD51, RAD52, RAD5 and BRCA2. The attenuation of HR sensitises cells to ionizing radiation, and altered expression of core proteins such as RAD51 and BRCA2 is associated with decreased radiosensitivity[127–129]. NER plays a key role in repairing SSB and a variety of distorting lesions, notably platinum-induced DNA adducts and intrastrand cross-links[130–137]. The base excision repair (BER) pathway allows accurate removal of damaged bases as well as correction of SSB. Therefore, it is important in repairing both indirect ROS-mediated and direct actions of IR. Alterations in the components of the BER pathway have been demonstrated to modulate cellular radiosensitivity[138–142].

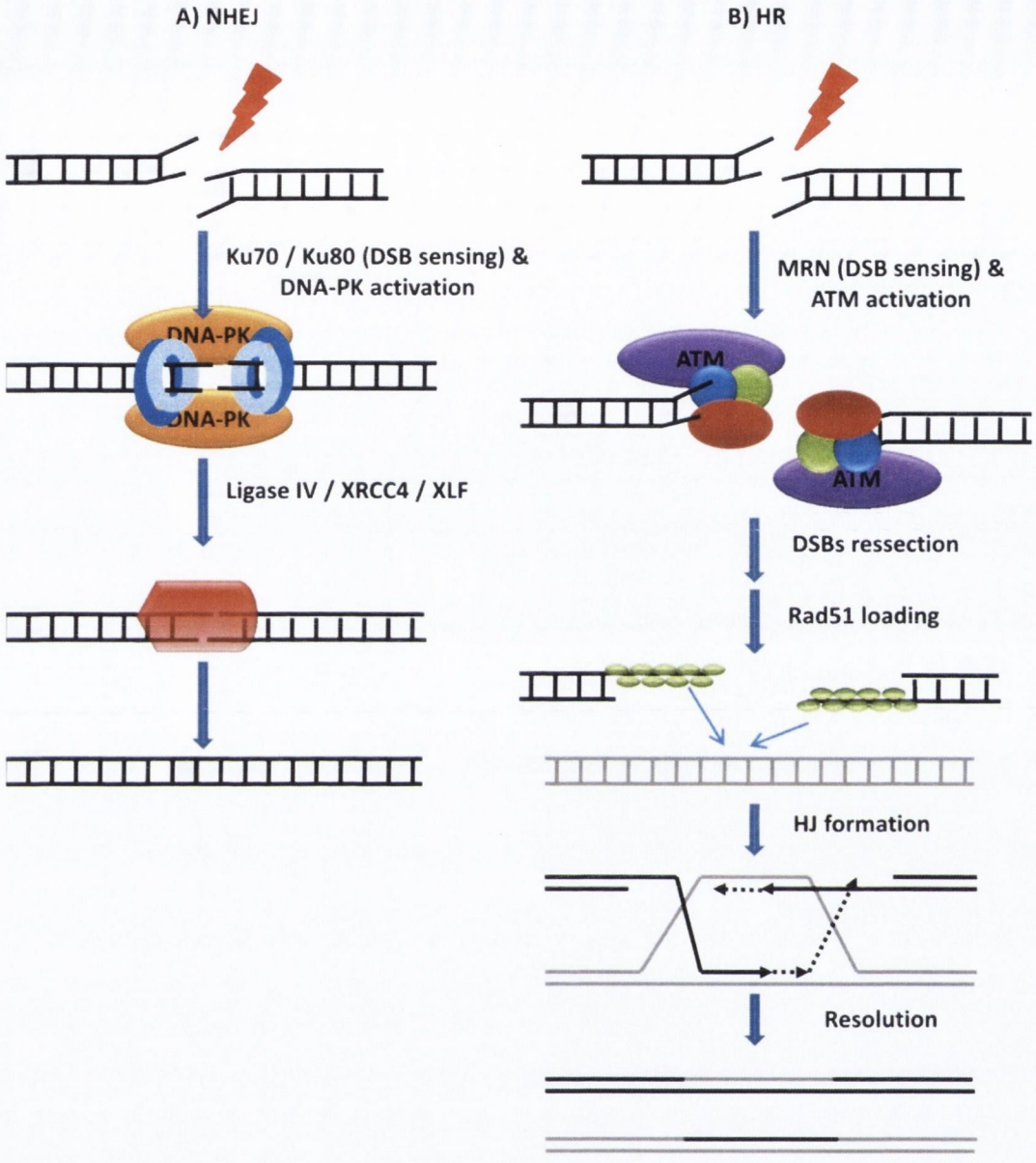


Figure 1.6. Double strand break repair may be mediated by NHEJ or HR
DSBs are repaired by two distinct but complimentary pathways: NHEJ and HR. **(A)** DSBs are sensed by the ring-shape heterodimer Ku70/Ku80 which then stabilizes the two DNA ends and recruits DNA-PK. DNA-PK phosphorylates and activates the NHEJ effector complex (ligase IV/XRC44/XLF) that finally religates the broken DNA. **(B)** The ATM kinase is recruited to DSB via an interaction with the MRN (Mre11-Rad50-Nbs1) complex. Once at the break, ATM becomes activated, phosphorylating multiple substrates. In a reaction that depends on multiple endo and exonuclease activities (including Mre11, Exo1 and CtIP) DSBs are resected forming ssDNA strands. These ssDNA regions attract Rad51 and other associated proteins. The Rad51-coated nucleoprotein filaments then invade the undamaged sister strands forming HJ structures. HR is completed by new DNA synthesis and still to be identified HJ "resolvase" enzymes (reproduced with permission from Lopez-Contreras and Fernandez-Capetillo, 2012[143]).

1.2.4 Radiosensitivity

The response of a cancer to radiation is described by its radiosensitivity. Besides being related to intrinsic cellular radiosensitivity, cell survival is also related to oxygen tension, the position of the cell in the mitotic cycle, activation of cell cycle checkpoints and dose rate[115,144]. Cell division in eukaryotic cells is subdivided into four distinct phases: the mitotic phase or M, the first gap phase or G_1, the DNA synthesis phase or S and the second gap phase or G_2, and one phase outside the cell cycle, G_0[145,146]. Cells in different phases exhibit different radiosensitivity and radiation can significantly affect cell cycle[147,148]. Cells in the M and G_2 phase are, in general, the most sensitive to radiation, cells with a long cycle time demonstrate another peak of resistance in early G_1 phase, whilst cells in S phase are most resistant[144,148]. It has been postulated that changes in DNA content throughout the cell cycle coupled with variation in DNA repair efficiency at different stages in the cell cycle may underpin this effect[108,119].

Cell cycle checkpoint and radiosensitivity

Checkpoints were originally identified as signalling pathways that delay mitosis in response to DNA damage or defects in chromosome replication[149,150]. Cells have several checkpoints that function at various phases of the cell cycle. Specifically, the G_1/S and intra-S checkpoints prevent inappropriate DNA replication, whereas the G_2/M checkpoint prevents cells with DNA damage from entering mitosis[151,152]. When these checkpoints detect DNA damage, they induce cell cycle arrest and make time for repair of DNA damage[151,152]. Alternatively, if the damage is irreparable, the checkpoints permanently prevent proliferation of severely damaged cells[151,152]. DNA repair and cell cycle checkpoints must cooperate closely to repair DNA damage and maintain genomic stability[151,152]. Defects in this network produce dysfunction in the repair of DNA damage induced by IR, which results in enhancement of the cytotoxic activity of radiation[153–156]. Thus, molecules involved in these mechanisms can be suitable targets for radiosensitisation. Abrogation of the G_2 checkpoint induces sensitivity to IR, while increased magnitude and duration of the late G_2 arrest is associated with increased resistance to radiation[153–156].

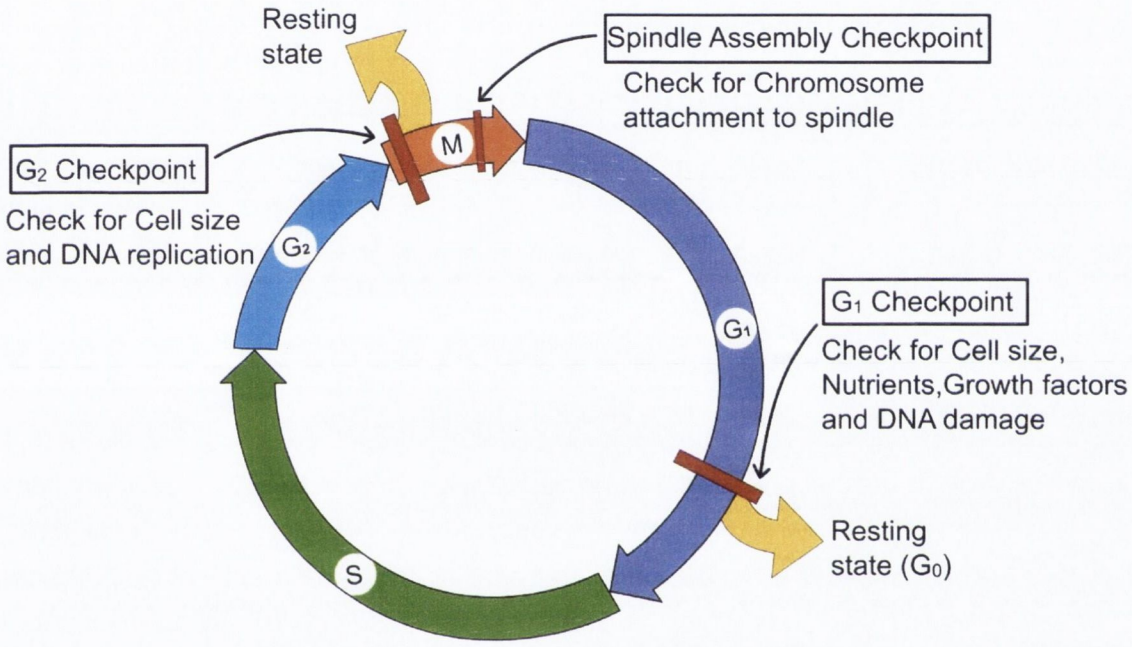


Figure 1.7. The cell cycle and checkpoint activation

Eukaryotic cells have four phases within the cell cycle: Gap 1 (G_1), synthesis (S), G_2, mitosis (M), and one phase outside the cell cycle G_0. Cell cycle checkpoints are control mechanisms that ensure the fidelity of cell division in eukaryotic cells. These checkpoints verify whether the processes at each phase of the cell cycle have been accurately completed before progression into the next phase (reproduced with permission from www.jpkc.scu.edu.cn[157]).

1.2.4 Biomarkers of response to radiation

Pre-treatment clinicopathological parameters and immunohistochemical studies do not reliably predict the response of oesophageal cancer to neoadjuvant chemoradiotherapy (CRT)[86,158,159]. Sequential metabolic imaging using fluorodeoxyglucose (FDG) imaging may have value for predicting pathologic response and outcome in locally advanced oesophageal cancer. Several studies corroborate these findings in regard to pathologic response and survival, but others conflict[160–171].

Altered expression of over 855 genes has been shown following short exposure to radiation[172]. The majority of genes relating to radioresponse are involved in DNA repair, signal transduction, cell cycle, cell adhesion, apoptosis and proliferation[173]. An isogenic radioresistant OAC cell line model was generated in our unit by exposing OE33 oesophageal adenocarcinoma cells to clinically relevant fractionated doses of radiation[174]. Enhanced DNA repair was implicated in the radioresistance of this radioresistant OAC model[174]. A study from our group also demonstrated that, in OAC tumour tissue, miR-31 expression is significantly reduced in patients demonstrating poor histomorphologic response to neoadjuvant CRT, whilst expression of the miR-31-regulated DNA repair genes is significantly increased[175]. Further studies from this unit identified an 8-gene signature in diagnostic oesophageal tumour tissue biopsies predicting the response to neoadjuvant CRT,[176] while serum proteomic profiling demonstrated that pre-treatment serum C4a and C3a levels were significantly higher in poor responders versus good responders[177]. Despite these advances, no consistent gene expression patterns associated with radioresponse are currently in clinical use in OAC patients. In addition, little is known about the impact of clinical parameters such as obesity status on the efficacy of chemoradiation in OAC.

1.3 Obesity

1.3.1 Epidemiology of obesity

The World Health Organisation defines obesity as an abnormal or excessive fat accumulation in adipose tissue, to the extent that health is impaired. The classification of obesity for epidemiological purposes defines overweight as body mass index (BMI) greater than 25 kg/m^2 and obesity as BMI greater than 30 kg/m^2 (Table 1.1)[178].

The obese state is increasingly more prevalent in Western society and in some countries is the most prevalent body composition accounting for 74% of males and 64% of females in the United States[179,180]. In Ireland, 39% of people are in the normal weight range, 37% are overweight and 24% are classified as obese[181]. The prevalence of obesity in 18-64 year old adults in Ireland has increased significantly between 1990 and 2011, from 8% to 26% in men, and from 13% to 21% in women, with the greatest increase observed in men aged 51-64 years[181]. Cut-off points established for waist circumference identify 23% of men and 27% of women as being associated with increased risk of cardiovascular disease[181]. This pattern shows no signs of abating as obesity rates are increasing among children,[182] and overweight children tend to become overweight adults[183].

Table 1.1. Classification of obesity by BMI

Classification	BMI ($kg/m^{2)}$
Underweight	<18.5
Normal weight	18.5-24.99
Overweight	25.00-29.99
Obese class I	30.00-34.99
Obese class II	35.00-39.99
Obese class III	≥40.00

(Adapted from the WHO Technical Report series 2000[178])

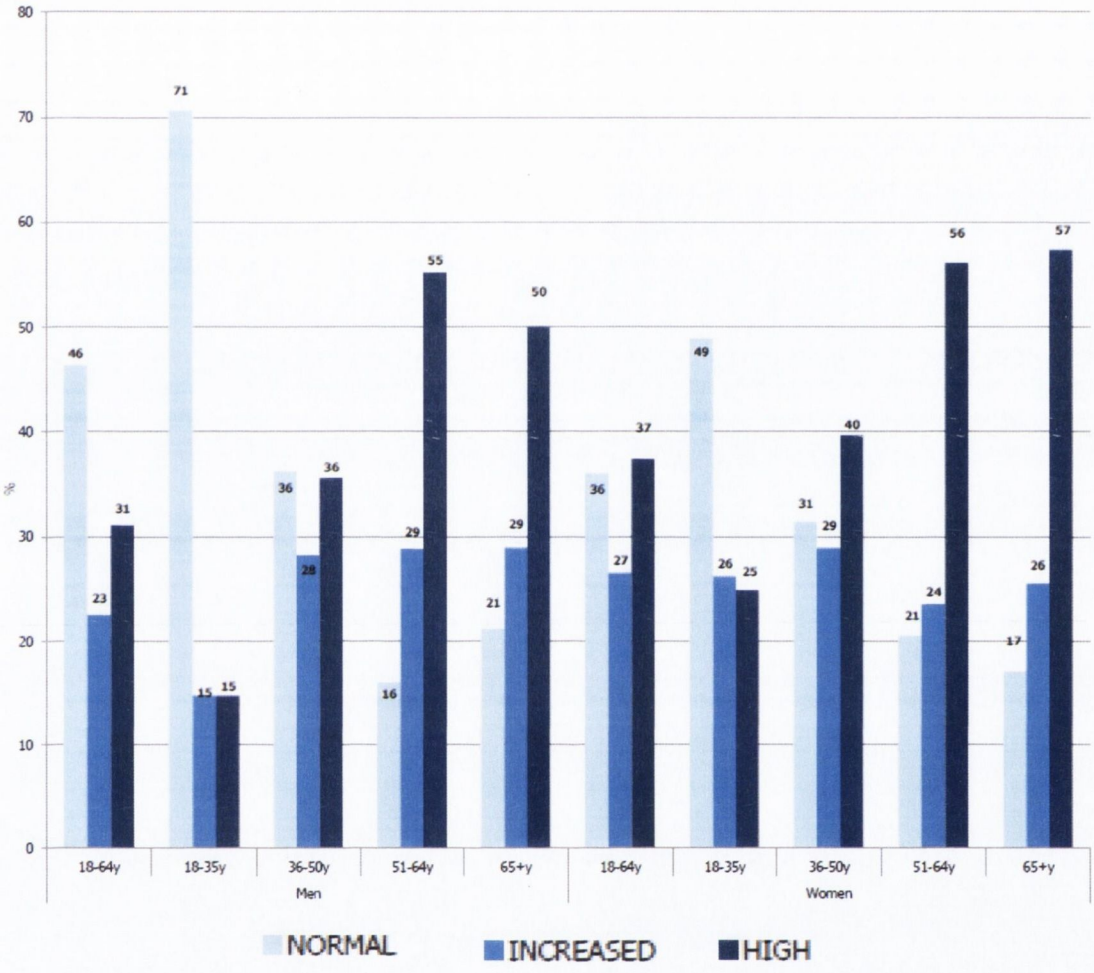


Figure 1.8. Percent of men and women with increased risk from cardiovascular disease identified by waist circumference.
Obesity is associated with increased risk of a number of chronic diseases, including cardiovascular disease (CVD). Body fat distribution is an important indicator of disease risk. In particular, increased levels of fat deposition in the central area of the body, measured by waist circumference, is associated with increased risk of CVD (reproduced with permission from Irish Universities Nutrition Alliance. National Adult Nutrition Survey 2011[181]).

1.3.2 Adipose tissue depots

Adipose tissue is principally deposited in two compartments; peripherally located subcutaneous fat and centrally located visceral fat. Centrally deposited or visceral adipose tissue is largely comprised of omental adipose tissue but also includes other intra-abdominal fat sources such as mesenteric fat[184]. Subcutaneous and visceral adipose tissue depots are pathologically and immunologically distinct, and visceral adipose tissue, compared to subcutaneous tissue, is more metabolically active, and is a rich source of adipokines and inflammatory cells[185–189]. We and others have shown that, for any given amount of total body fat, the subgroup of individuals with excess visceral fat (as opposed to subcutaneous fat) is at higher risk of developing insulin resistance and the metabolic syndrome[136,190]. Gender significantly influences fat distribution. Overall, men have twice as much visceral fat as women and demonstrate a high prevalence of the obesity-related metabolic diseases such as insulin resistance, cardiovascular disease, and the metabolic syndrome[191,192].

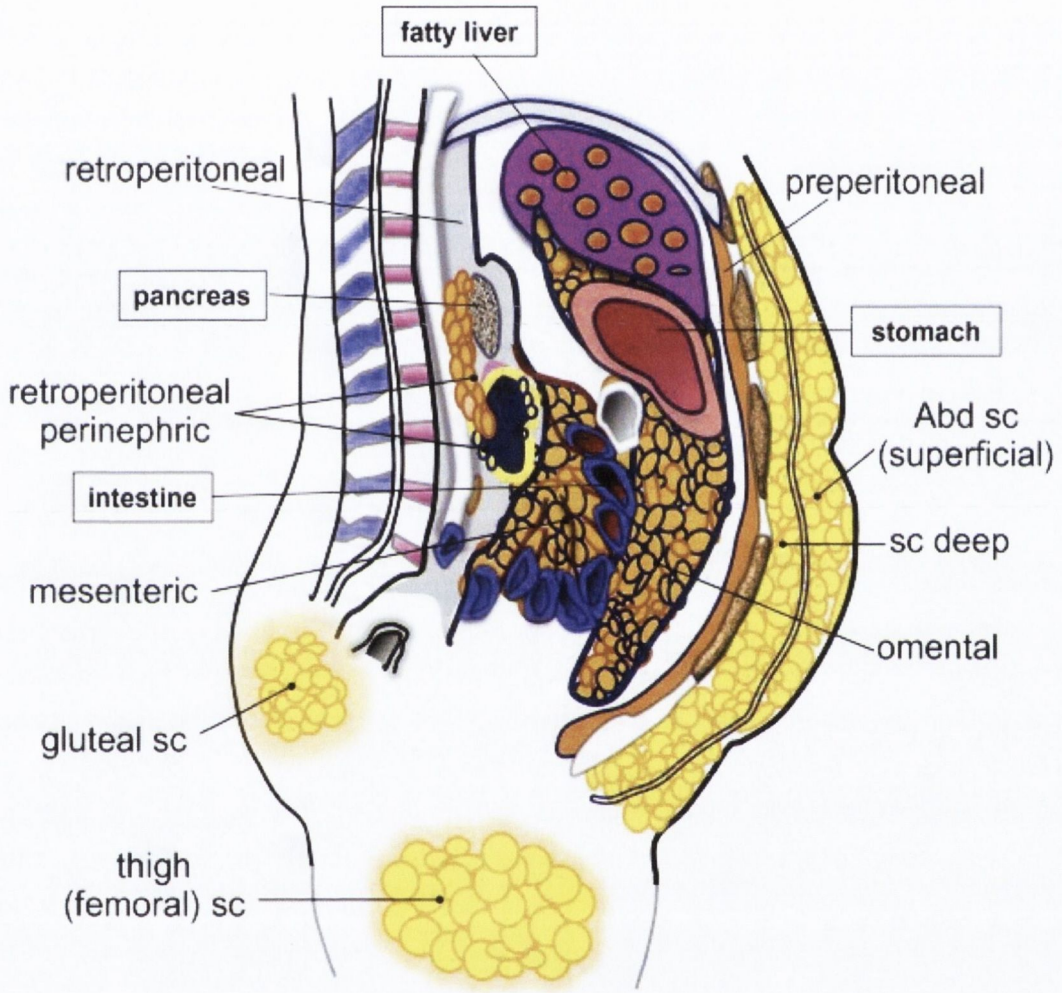


Figure 1.9. Major adipose depots in humans

Subcutaneous adipose tissues include abdominal and gluteal, as well as femoral. Visceral adipose tissues are associated with digestive organs. Omental is attached to the stomach and mesenteric and epiploic are associated with the intestine and colon respectively. Perinepheric fat surrounds the kidney and retroperitoneal fat is located in the retroperitoneal compartment (reproduced with permission from Lee et al 2013[193]).

1.3.3 Measuring obesity

BMI cut-off values to diagnose obesity have high specificity, but low sensitivity to identify adiposity, as they do not distinguish lean tissue mass from adipose tissue and do not reflect adipose tissue distribution[194–196]. The accuracy of BMI to diagnose obesity is limited, particularly for individuals in the intermediate BMI ranges[197]. While BMI has significant limitations, it is important to point out that the use of BMI is not without value. A BMI ≥ 30 kg/m^2 has an excellent specificity and positive predictive value for diagnosing obesity in both sexes, and the measurement of BMI requires no specialised equipment[197]. However, a more appropriate measure of central obesity is the gold standard computed tomography (CT) measurement of fat area, which enables accurate quantification of subcutaneous and visceral adipose tissue depots[198,199]. The cross sectional surface area of the visceral fat depot is measured by CT between lumbar vertebrae L3 and L4 to give visceral fat area (VFA) (cm^2) (Figure 1.10)[31]. Studies carried out in the 1990's determined that in both men and women, a VFA above 100 cm^2 was associated with moderate disturbances in the malignancy risk profile, whereas a VFA greater than 130 cm^2 was associated with a further deterioration of metabolic variables predictive of type 2 diabetes mellitus and cardiovascular disease[200,201]. However neither of these studies took into consideration the gender difference in adipose tissue distribution and dysmetabolism[202,203]. A recent study from this unit generated pathologically relevant CT derived VFA thresholds for Caucasian male and female gastrointestinal cancer patients[204]. A cut-off VFA of 163.8cm^2 in men and 80.1cm^2 in women is used to classify obesity status in cancer patients[204]. When the technology and expertise required to measure visceral fat area is not available, waist circumference is the next best proxy[205]. Waist circumference (WC) is an accurate predictor of visceral fat, directly reflecting total abdominal fat mass[206–210]. Gender and ethnic specific cut-offs can be used as reliable proxy values to predict an increased risk of the metabolic disease. The International Diabetes Federation waist circumference cut-offs for European patients may be used to determine obesity status by waist circumference, >80 cm for females and >94 cm for males[211].



Figure 1.10. Fat measurement by computed tomography of the abdomen
The area inside the red line is the visceral fat area. The superficial fat area is calculated by subtracting the visceral fat area from the total fat area (yellow line) (reproduced with permission from Beddy et al, 2010[31]).

1.3.4 Epidemiology of obesity and cancer

Epidemiological studies have provided robust evidence for the association of obesity with cancer development at numerous sites: oesophagus (adenocarcinoma), pancreas, colorectum, breast (postmenopausal), endometrial and kidney[18,212]. The largest meta-analysis to date to date includes 282,000 patients from prospective observational studies with over 133 million person-years of follow up, and demonstrates that high body mass index is associated with an increased risk of cancer[17]. This association carries modest relative risk estimates of 1.1-1.6 per $5kg/m^2$ incremental increase in BMI, and is sex and site specific but consistent across geographic populations[17]. Emerging clinical evidence suggests that weight loss following bariatric surgery leads to a reduction in cancer incidence[213].

1.3.5 Epidemiology of obesity and oesophageal adenocarcinoma

As discussed in detail in section 1.1.2, obesity is an independent risk factor for OAC[14,19,26,214]. The relation between obesity and OAC persists even after accounting for GORD[14,215–217]. It is thus likely that the substantial effect of obesity is mediated via molecular pathways[10,32]. These pathways are discussed in more detail in section 1.1.2.

Table 1.2. Cancer risk and obesity

Table 1	Obesity related cancers			
Type of cancer	**Relative risk* with BMI of 25-30 kg/m²**	**Relative risk* with BMI of ≥30 kg/m²**	**PAF (%) US population‡**	**PAF (%) EU population§**
Colorectal (men)	1.5	2.0	35.4	27.5
Colorectal (women)	1.2	1.5	20.8	14.2
Female breast (Postmenopausal)	1.3	1.5	22.6	16.7
Endometrial	2.0	3.5	56.8	45.2
Kidney (renal cell)	1.5	2.5	42.5	31.1
Oesophageal (adenocarcinoma)	2.0	3.0	52.4	42.7
Pancreatic	1.3	1.7	26.9	19.3
Liver	ND	1.5-4.0	NDǁ	NDǁ
Gallbladder	1.5	2.0	35.5	27.1
Gastric cardia (adenocarcinoma)	1.5	2.0	35.5	27.1

Relative risks associated with overweight and obesity, and the percentage of cases attributable to overweight and obesity in the European Union (EU) and the United States (US). (Adapted from Calle et al, 2004[26]).

*Relative risk estimates are summarized from the literature cited in the main text.

‡Data on prevalence of overweight and obesity are from the National Health and Nutrition Examination Survey (1999-2000) for men and women from the United States aged from 59-69 years.

§Data on prevalence of overweight and obesity are from a range of sources for adult men and women residing in 15 European countries in the 1980s and 1990s.

ǁPAFs were not estimated because the magnitudes of the relative risks across studies are not sufficiently consistent.

PAF Population attributable fraction

ND Not determined

1.3.6 Obesity and outcomes

Obesity and outcomes in cancer

A prospective study of 900,000 adults in the USA reported that obesity could account for 14 per cent of all deaths from cancer in men and 20 per cent in women[18]. Survival rates may be influenced by differences in diagnosis, operative outcomes and treatment of cancer in the obese, as well as any specific biological effect of adiposity on cancer progression[218–220]. The treatment of cancer comprises surgery, radiotherapy, chemotherapy and hormonal treatment. These treatment modalities may be adversely affected by the presence of obesity. Surgery and anaesthesia are more hazardous in overweight patients, not least because of the increased incidence of cardiorespiratory comorbidity[221]. Resections in obese patients may be technically more challenging, with longer operative times, lower lymph node retrieval and increased complications[222–225].

Delivery of both chemotherapy and radiotherapy may also be hampered by obesity. The narrow therapeutic index of many chemotherapeutic drugs prompts concern that the high doses of chemotherapy required by the very obese will result in excess toxicity, thus obese patients are frequently treated at lower chemotherapy dose intensities compared to non-obese patients. Administering an adequate radiation dosage to obese patients receiving external beam radiotherapy may also be challenging. Organ motion and set-up error in obese patients exceeds that of normal weight patients, potentially resulting in a less-than-optimal radiation dose[226,227].

Obesity has been associated with increased risk for cancer recurrence and death following treatment.[228–239] However, a number of studies have reported no association between obesity and outcomes,[240–244] and of those with significant findings, there are inconsistencies about the measurement and level of obesity, treatment modality, and the role of gender[228,229,232,245].

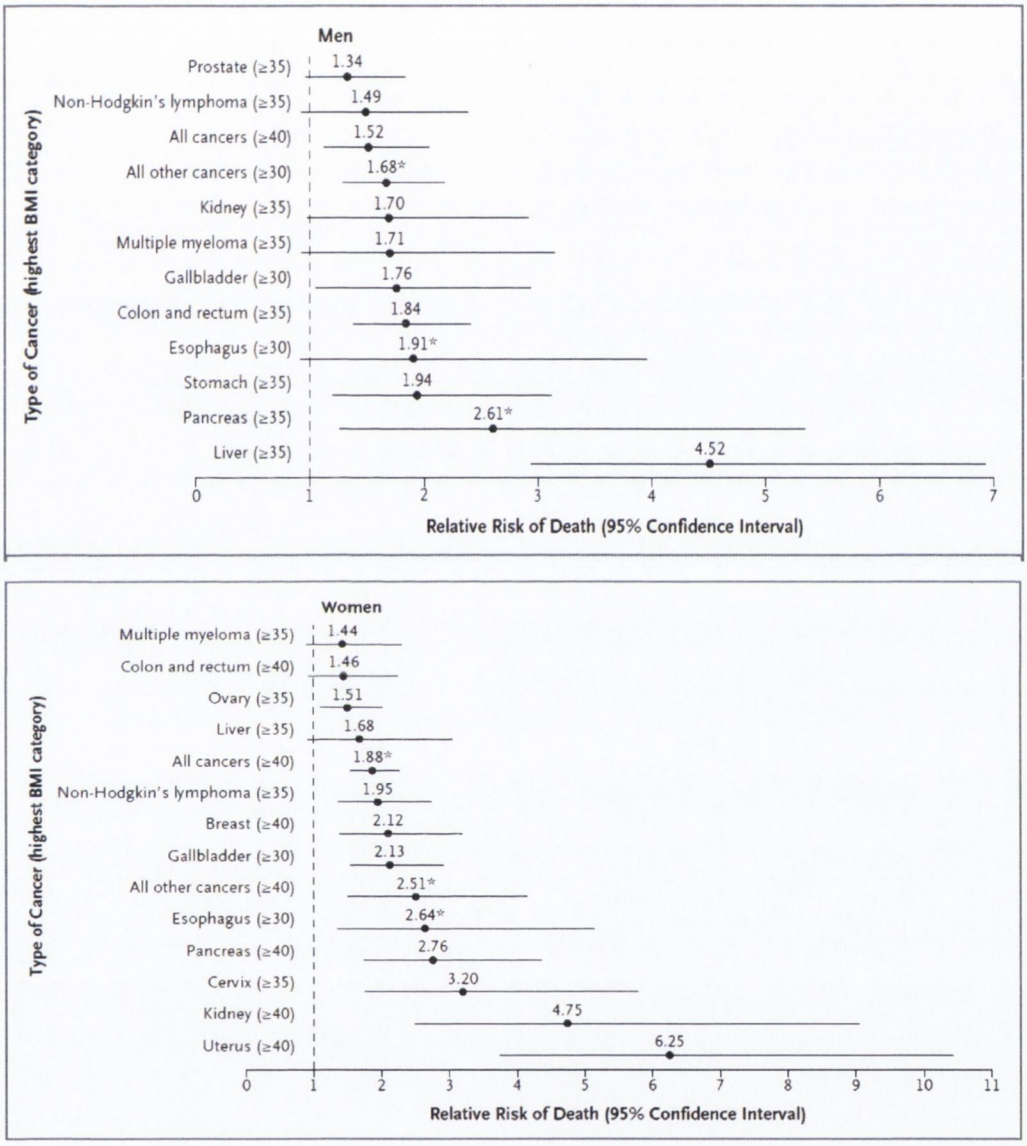


Figure 1.11. Summary of mortality from cancer according to BMI for (A) U.S. men and (B) U.S. women in the Cancer Prevention study II, 1982 through 1998

For each relative risk, the comparison was between men/women in the highest BMI category (indicated in parentheses), and men/women in the reference category (BMI 18.5-24.9). Results of the linear test for trend were significant ($p \leq 0.05$) for all cancer sites.

*Men/Women who never smoked (reproduced with permission from Calle et al, 2003[18]).

Obesity and treatment outcomes in OAC

Studies show that obese patients undergoing oesophagectomy for localized adenocarcinoma of the oesophagus or oesophagogastric junction have a longer hospital stay, an increased incidence of respiratory complications and radiologic anastomotic leaks, and greater requirements for blood products compared with non-obese patients, but no increase in in-hospital mortality[246]. As regards oncological outcomes following oesophagectomy, Healy et al. demonstrated a marked decrease in lymph node retrieval in obese patients[246], while other groups reported no statistically significant difference in number of lymph nodes between obese and non-obese patients[247,248]. Data on long term outcomes and obesity is inconsistent[246,247,249–251]. Four studies have investigated outcomes in OAC patients who have undergone neoadjuvant radiotherapy. No difference in survival was noted between obese and non-obese patients after oesophagectomy in 215 patients described by Morgan et al, of whom 49 received neoadjuvant CRT[247]. Obesity status did not affect survival in 150 patients who underwent resection for adenocarcinomas of the oesophagus or gastroesophageal junction, 81 of who also underwent neoadjuvant CRT[246]. Two recent studies focused on patients primarily treated with CRT with or without surgery, and found no correlation between BMI and oncologic outcome or survival[251,252]. As obesity rates rise, there will be more oesophagectomies performed for cancer in obese patients. The impact of obesity on survival of oesophageal cancer, in particular the response to neoadjuvant therapy, has not been adequately addressed to date.

1.3.7 Candidate molecular mechanisms linking obesity and cancer

The mechanisms by which visceral adiposity is thought to promote tumourigenesis are manifold. Until the 1990s, adipose tissue was generally regarded as metabolically inert, but it is now known that adipose tissue is a complex endocrine, metabolic and immune organ with a wide variety of functions[195,253]. Potentially relevant pathways include adipokine production, immunomodulation, alterations in insulin and the insulin-like growth factor (IGF) axis and sex steroids[253].

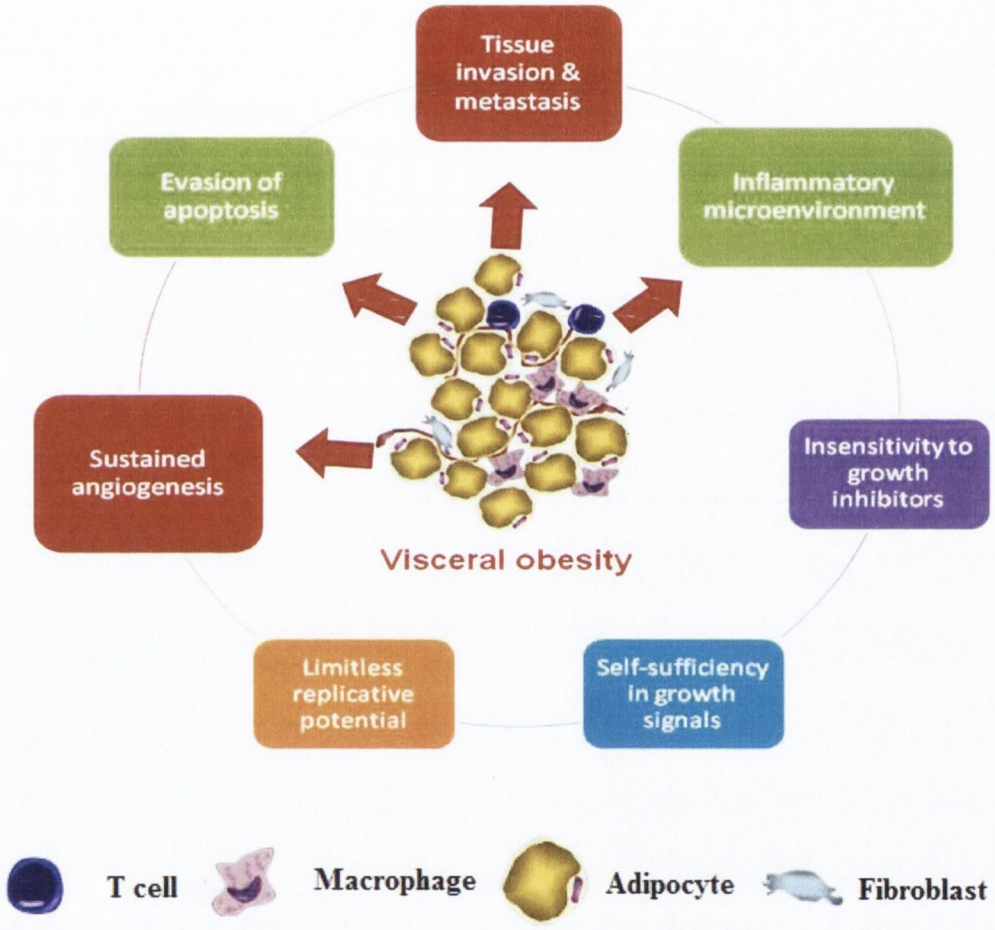


Figure 1.12. Hallmarks of cancer and potential role of visceral obesity in tumourigenesis

Increased visceral adiposity creates a pro-tumourigenic environment which can act to facilitate tumour development by promotion of the acquisition of some of the hallmarks properties that characterise cancerous lesions. As visceral adipose tissue expands it becomes infiltrated with macrophages, T-cells and fibroblasts. These immune cells and the adipocytes induce alterations in adipokine production, insulin and insulin-like growth factor (IGF) pathways, cancer cell signalling and inflammatory pathways and angiogenesis (reproduced with permission from Donohoe et al, 2011[253]).

1.3.7.1 Adipokine production

Adipocyte-conditioned media promotes tumourigenesis in cancer cells, by increasing cell proliferation, invasive potential, angiogenesis and induction of cross-talk between cancer cells and the surrounding extracellular matrix[254]. These actions are thought to be mediated by production of biologically active proteins such as adiponectin, leptin and inflammatory cytokines including TNF-α, IL-2, IL-8, IL-10 and IL-1 receptor agonist, collectively termed adipocytokines[255]. Adipose tissue products activate the key inflammatory pathways of NF-κB (nuclear factor-κB) and STAT3 (signal transducer and activation of transcription 3), leading to transcription of genes mediating proliferation, invasion, angiogenesis, survival and metastasis[256].

Adiponectin is the most abundant adipokine and is secreted mostly from visceral adipocytes: however its level is inversely associated with BMI[257]. It is highly anti-angiogenic, anti-proliferative, anti-inflammatory and insulin sensitising, may prevent the interaction of growth factors with their receptors[257–260]. Hypoadiponectinaemia is associated with induction of genomic instability, including telomere shortening[261]. Adiponectin effects are mediated via two receptors, adiponectin receptor 1 (AR1) and adiponectin receptor 2 (AR2), and expression of AR1 has been associated with prolonged survival in vitro in lung cancer[262,263].

Leptin, primarily produced by adipose tissue, is the most studied adipokine. Leptin is an adipocyte-specific hormone that acts centrally to regulate appetite and bodyweight[264]. Levels of leptin are positively associated with adiposity, cancer risk and poor prognosis[265–267]. We and others have shown that leptin and its receptor (LepR/ObR) are overexpressed in a number of cancers including OAC; in addition, expression of leptin and its receptor are associated with higher pathological stage[268–272]. *In vitro* studies from our unit and others have confirmed that leptin promotes cell proliferation, angiogenesis and metalloproteinase expression in oesophageal and colonic cancer cell lines[271,273–276].

Vascular endothelial growth factor (VEGF) is a pro-angiogenic and survival factor for a variety of solid malignancies, and has been shown to suppress radiation induced cell death in cancer cell lines[277–281]. A study from our unit demonstrated that levels of VEGF are significantly higher in conditioned media from visceral adipose tissue of centrally obese compared to non-obese patients[185]. The VEGF/VEGF-receptor axis is composed of multiple ligands and receptors[279]. There are three main subtypes of VEGFR 1, 2 and 3, as well as co-receptors including the neuropilins[282]. The VEGF family is comprised of six proteins, three of which bind neuropilins: VEGF-A (VEGF), VEGF-B, and VEGF-C. Contrary to endothelial cells, VEGFR-1/2 expression is not always detectable in certain tumour cells[283–285]. In contrast, NRP-1 is the most frequently expressed VEGF receptor in tumour cells. Neuropilin-1 is a co-receptor for VEGF on both

endothelial and tumour cells, which is involved in tumour initiation, growth, metastasis and immunity[286]. NRP-1 expression correlates with more aggressive clinical tumour behaviour and is associated with poor patient prognosis in a number of tumour types, including OAC[287–294].

Neutralisation of adipokines such as IL8 has been associated with inhibition of angiogenesis and metastasis, two well-defined hallmarks of cancer, in melanoma cells[295]. We have previously shown that VEGF neutralisation of ACM leads to significant decreases in cancer cell proliferation[185], demonstrating the pro-tumourigenic capacity of VEGF in ACM. We have also shown that neutralising both VEGF and IL8 in the ACM significantly decreased anaphase bridging in oesophageal cell lines, suggesting that these factors may be critical components of the visceral adipose tissue secretome in driving genomic and chromosomal instability[296]. Neutralisation and overexpression of VEGF and other adipokines such as adiponectin and leptin in radioresistant and radiosensitive OAC cell lines may reveal a role for these factors in the induction of chromosomal instability in radioresistant OAC.

1.3.7.2 Immunomodulation

Cancer related inflammation is a key component of the tumourigenic process and is increasingly referred to as the seventh hallmark of cancer[297]. Excess adiposity, in particular visceral obesity, results in elevated levels of pro-inflammatory adipokines, resulting in an imbalance between increased inflammatory stimuli and decreased anti-inflammatory mechanisms leading to a chronic state of systemic low-grade inflammation[195,298,299]. The level of adipokine production from adipose tissue is strongly influenced by immune cell populations present in adipose tissue[188,300–302]. Dense lymphoreticular structures within the human omentum, termed milky spots contain a range of innate and adaptive immune cells, including macrophages, mast cells, T- and B-cells, natural killer and invariant natural killer T-cell populations[303,304].

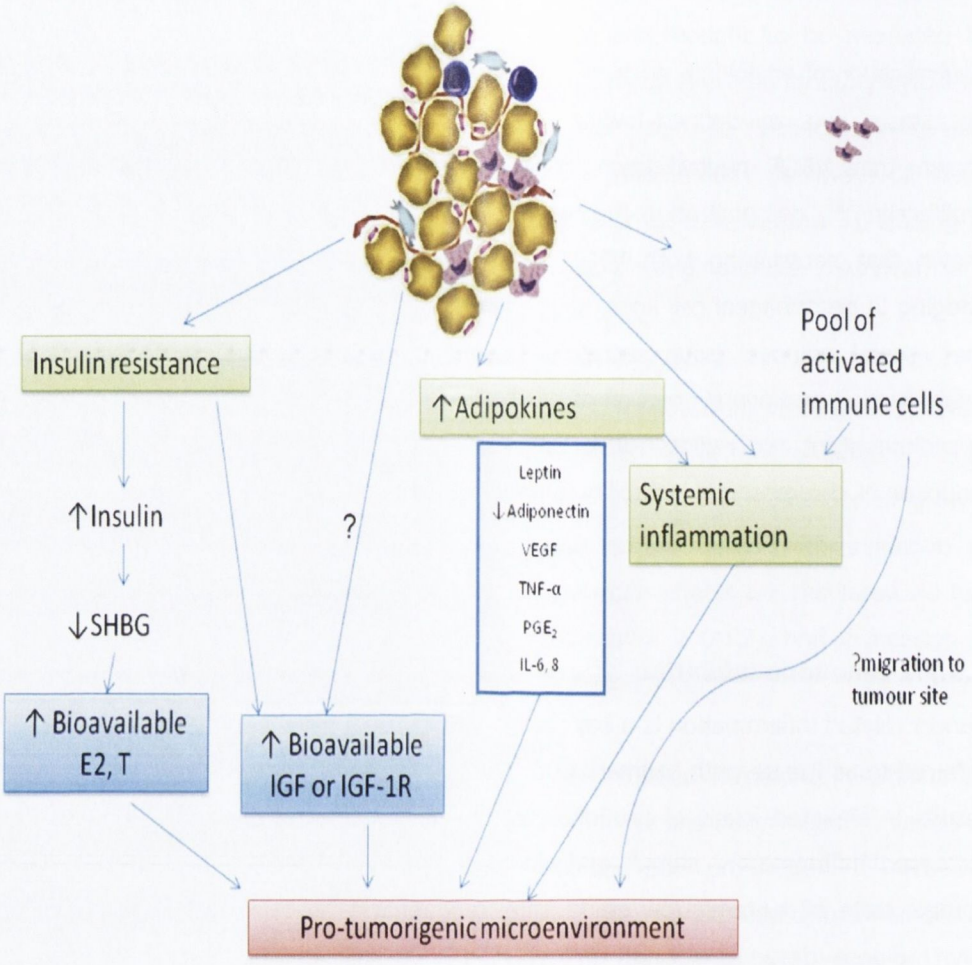


Figure 1.13. Systemic alterations in visceral adiposity which may contribute to a pro-tumourigenic microenvironment

Systemic alterations in obesity include chronic systemic inflammation, increased adipokine production, an altered immunological status and associated changes in the sex hormone profile. Insulin resistance develops as a consequence of visceral adiposity and there is a rise in insulin production, which may be associated with activation of the insulin-like growth factor (IGF) system. Adipose tissue becomes inflamed in obese patients. Adipocytes hypertrophy and the tissue becomes infiltrated with macrophages and T cells. These immune cells and the adipocytes produce adipokines including leptin, IL-6 and TNF-a. All of these changes which occur in tandem with the development of obesity have the ability to interact with each other. It is this altered systemic milieu which is thought to fuel cancer development and progression (reproduced with permission from Donohoe 2011[253]).

1.4 Genomic instability and cancer

1.4.1 Genomic instability as an enabling characteristic of cancer

A consensus is emerging that a crucial early event in carcinogenesis is the induction of the genomic instability phenotype, which enables an initiated cell to evolve into a cancer cell by achieving a greater proliferative capacity and the genetic plasticity to overcome host immunological resistance, localized toxic environments and suboptimal micronutrient supply[305,306]. Genomic instability is recognised as an emerging enabling characteristic of the hallmarks of cancer originally proposed by Hanahan and Weinberg in their landmark paper in 2000[33,297]. Most solid tumours undergo alterations in chromosomal structure and number, which is defined as chromosomal instability (CIN) and is found in 85% of non-hereditary carcinomas[307–309]. Numerous events may lead to CIN, including (a) abnormal centriole number leading to multipolar mitoses, (b) chromosome loss at anaphase as a result of kinetochore defects, (c) misalignment of chromosomes at anaphase as a result of defects in the separation of chromatids, (d) mitotic slippage caused by inhibition of mitosis leading to the formation of tetraploid cells, and (e) failure of cytokinesis following nuclear replication as a result of defects in microfilament assembly[310]. These defects can lead to CIN and drive the multistep tumourigenesis process[311–314].

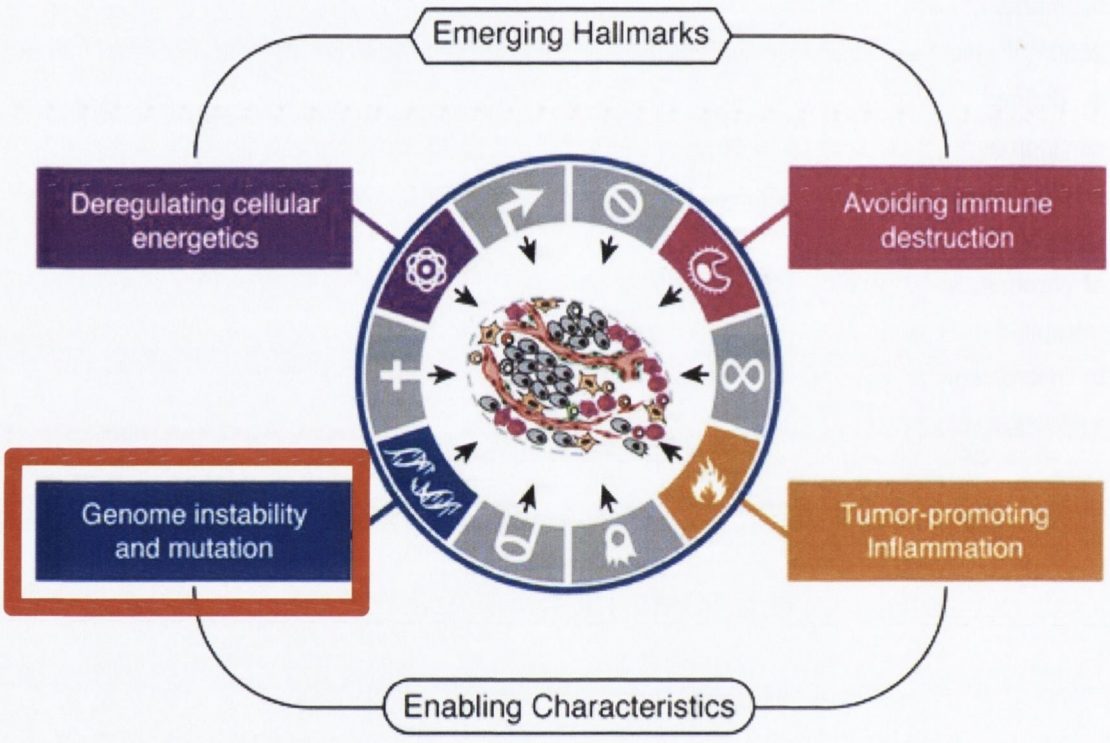


Figure 1.14. Genomic instability is an emerging enabling hallmark of cancer

In 2011 the authors of the original 'Hallmarks of Cancer' proposed an update to the six established hallmarks. Tumour promoting inflammation and genomic instability were proposed as enabling characteristics of cancer cells (Adapted from Hanahan and Weinberg, 2011[297]).

1.4.2 Telomeres and genomic instability

1.4.2.1 Telomere function

Telomeres, the natural ends of linear chromosomes, consist of a double stranded region comprised of tandem arrays of short repetitive G-rich sequences [TTAGGG], oriented 5'-to-3' towards the end of the chromosome, ending in a short overhang of single-stranded sequence at the 3' end[315–317]. Electron microscopy studies suggest that, in humans, this overhang can loop back and integrate into the duplex repeat tract, forming a 't-loop[318]. Telomeres have two principal functions: they must be recognized as functional domains, thus distinguishing them from random chromosomal breaks that will induce DNA damage checkpoint signalling, and they must prevent these DNA ends from fusing with other DNA ends[319].

1.4.2.2 Telomere shortening

In most normal somatic cells, telomeres shorten with every cell division, and telomere length is inversely correlated with age in humans[320–322]. Telomere shortening in human cells eventually results in either the initiation of apoptosis or an irreversible cell cycle arrest, termed replicative senescence, responses proposed to have evolved as tumour-suppressive mechanisms in large, long-lived organisms[320,323–327]. Once the shortening process starts, the t-loop can no longer form and the protective proteins detach from the telomeres. DNA in humans and all eukaryotes is linear,[328] and it was recognized in the early 1970s that the known DNA polymerases would be unable to replicate the very end of linear DNA molecules — a phenomenon known as the 'end replication problem'[328,329]. In this case, the chromosome ends can act as free DNA breaks and may be fused to other ends with short telomeres. Cells that are unable to senesce continue to divide and undergo severe telomere shortening, eventually resulting in "crisis," involving massive chromosome fusion and cell death[330]. Some cells can survive this crisis by regaining the ability to maintain telomere length, either through expression of telomerase or through an alternative pathway involving recombination and the activation of the ALT pathway[331,332]. Cancer cells typically demonstrate this ability to maintain telomeres, which is thought to be necessary for the extensive cell division required for the development of malignant cancer[323].

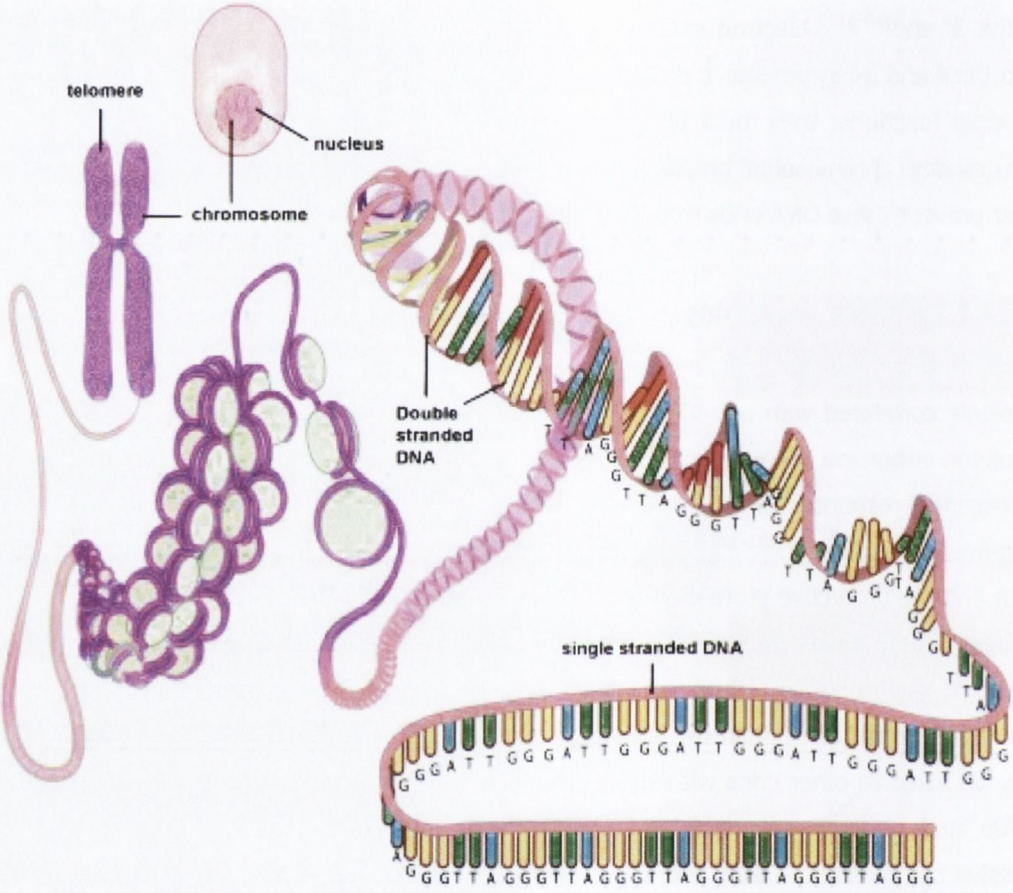


Figure 1.15. Telomere structure

Telomeres consist of a double stranded region comprised of telomeric repeats followed by a much shorter single stranded overhang on the 3' G-rich strand. In humans this G-rich strand folds back in a loop into the duplex region of the telomere tract to form the t-loop found at the end of the telomere (reproduced with permission from Zhu et al, 2011[333]).

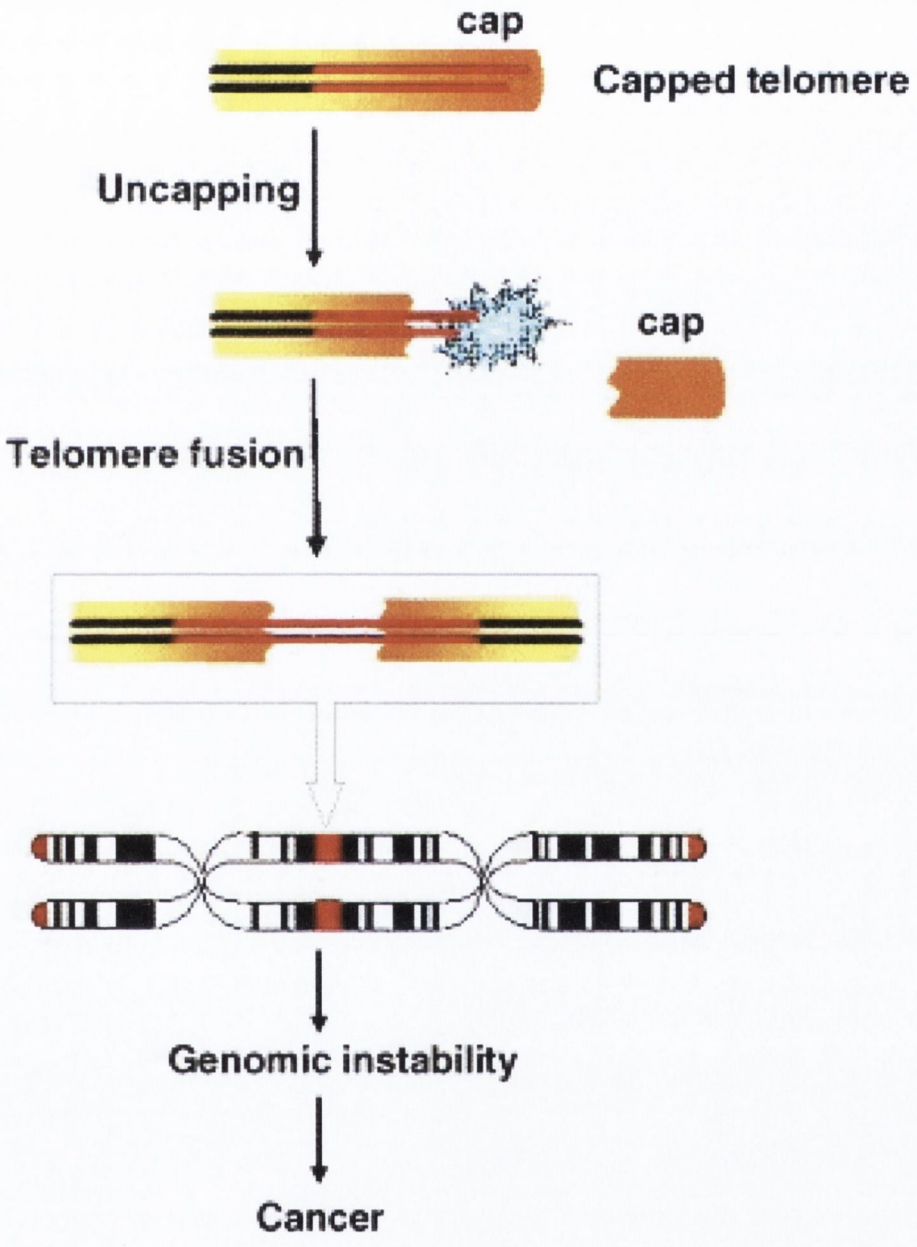


Figure 1.16. Telomere shortening leads to chromosomal fusion and genomic instability.
During cell replication, telomere DNA cannot be completely replicated, leading to telomere shortening with each cell division. Eventually telomere shortening leads to uncapping of the chromosomes, end to end fusions and genomic instability (reproduced with permission from Gilley et al, 2005[334]).

1.4.2.3 Telomerase

Telomerase is a ribonuclear protein complex consisting of protein reverse transcriptase (TERT) that uses an RNA component (TERC) as a template for telomere elongation, along with the subunits dyskerin (DKC1) and telomerase associated protein 1 (TEP1)[335,336]. The telomerase complex synthesises one strand of telomere DNA, the 5′ to 3′ strand, by copying the TERC template sequence[337]. Somatic adult cells display very little telomerase expression and activity, and telomere shortening elicits a DNA damage response, ultimately leading to permanent growth arrest and cellular senescence[320,338]. In contrast, cells that constitutively express telomerase can continue to divide almost indefinitely[339,340]. Telomerase activity has been reported in virtually all human tumours, but not in adjacent normal cells[341,342]. It is hypothesised that maintenance of telomere length is essential for the long term proliferation and immortality of tumour cells[343].

1.4.2.4 Shelterin complex

Telomeres are protected from degradation by associating with the shelterin complex. This complex consists of three proteins which bind telomeres directly; TRF1 (telomeric-repeat binding factor 1), TERF2 (telomeric-repeat binding factor 2) and POT1 (protection of telomeres 1), and these three are interconnected by additional proteins; TINF2 (TRF1 interacting nuclear factor 2) and TPP1 (tripeptidyl peptidase 1)[316]. Telomere end protection is compromised when components of the shelterin complex are perturbed, resulting in inappropriate processing of the telomere ends by the cell's DNA damage machinery, resulting in chromosomal fusions through the non-homologous end joining (NHEJ) or homologous recombination (HR) pathways[343]. In contrast to the telomerase complex, shelterin complex proteins are negative regulators of telomere elongation[82]. Three separate effects of shelterin on telomeres have been documented to date[344]. Shelterin controls the structure of the telomeric terminus, it is responsible for the generation of T-loops, and it mediates the recruitment and synthesis of telomeric repeats by telomerase[344].

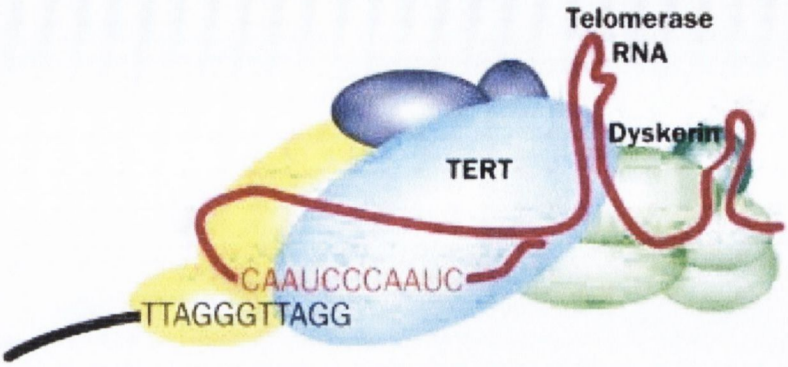


Figure 1.17. Telomerase structure
The telomerase complex consists of the telomerase reverse transcriptase (TERT) and the telomerase RNA template component (TERC), and a number of subunits including DKC1 and TEP1 (reproduced with permission from Wong et al, 2003[345]).

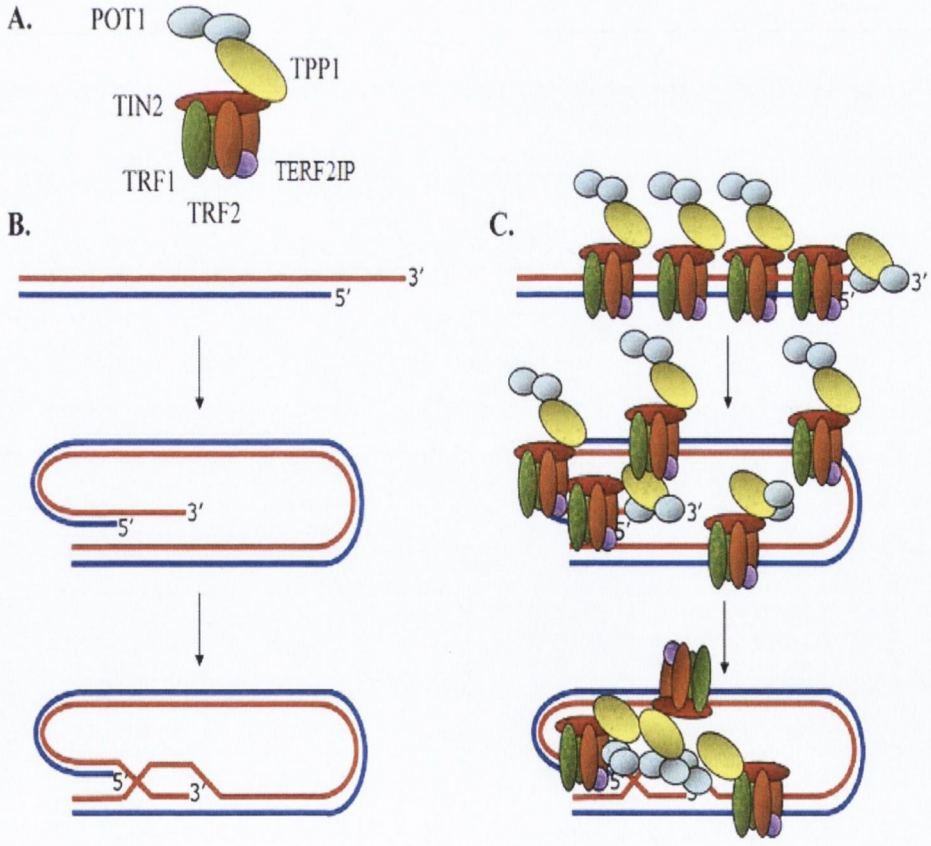


Figure 1.18. Shelterin complex structure
A protein complex termed the shelterin complex consisting of three proteins which bind telomeres directly (TERF1, TERF2 and POT1) interconnected by additional proteins (TINF2 and TPP1) (reproduced with permission from Moon and Jarstfer, 2007[346]).

1.4.3 Anaphase bridge formation and genomic instability

Anaphase bridges are a common cause and indicator of genomic instability, first described by Barbara McClintock in maize[347]. Anaphase bridges may be described as a chromatin fibre connecting the nuclei of daughter cells which fail to resolve following anaphase in cell division[348]. The majority of anaphase bridges formed will break, usually unevenly, giving rise to structural chromosomal rearrangement, with a net gain of chromosomal material in one daughter cell, and a corresponding net loss in the other daughter cell, contributing to CIN in both cell culture and tissues[348–352]. A bridge is thought to form from the fusion of two broken DNA ends, or as a result of telomere dysfunction; anaphase bridges have been shown to arise from telomere shortening, loss of telomeres or defects in telomerase[352–356]. Moreover, we and others have shown a significant correlation between telomere length and the frequency of endogenous bridges in cancer cells[349,357,358].

1.4.4 Breakage-fusion-bridge cycle

Breakage-fusion-bridge (BFB) cycles are now generally accepted as a mechanism explaining genetic plasticity in CIN tumours[359]. The BFB cycle begins when chromosome breakage results in two "reactive" chromosome arms. Dicentric chromosomes form when these two broken chromosomes fuse at their ends. During anaphase, the two centromeres of a dicentric chromosome are pulled to opposite poles of the mitotic spindle, forming an anaphase bridge. The two sister chromatids break apart from each other, but not necessarily at the site that they fused, resulting in one daughter cell acquiring a chromosome with a duplication on its end in the form of an inverted repeated, while the chromosome sequestered to the other daughter cell contains a terminal deletion[360]. Once started, the BFB cycle continues and chromosome fragments fuse with one another. The formation of a dicentric chromosome in some of these fusions can lead to mitotic segregation of the two centromeres to different poles and renewed breakage events[359].

BFB events resulting from telomere loss can produce chromosome rearrangements by terminal deletions, amplifications, inverted repeats and translocations[361]. Rearrangement events consistent with BFB cycles have been observed in human cancers[362–366]. Telomere instability is almost universal in epithelial tumours[367], and tumour samples show a correlation between anaphase bridges and abnormal karyotypes in sarcomas, pancreatic carcinomas, and colon carcinomas[350]. Many complex tumours exhibit dynamic BBF cycles, such as osteosarcoma, prostate, breast and colon cancer[327,349,361,368–372].

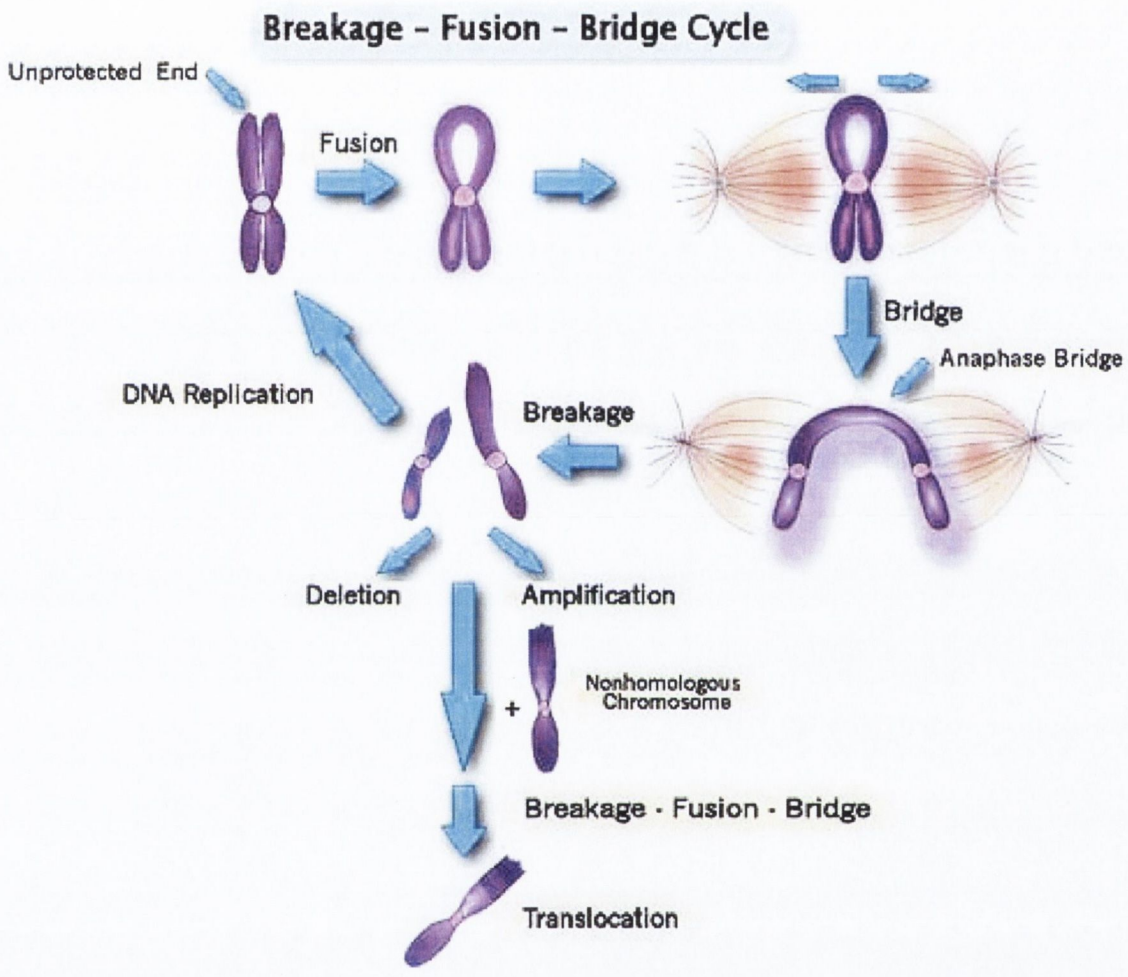


Figure 1.19. Repeated breakage-fusion-bridge cycles results in rampant genomic instability

In the setting of uncapped chromosome ends, telomeric fusions may occur between identical sister chromatids or between different chromosome. As sister chromatids are pulled to opposite poles, the fused chromosome ends are placed under tension and form anaphase bridges. These pulling forces result in chromosome breaks that contribute to deletions, amplifications, and translocations. Because of the further generation of unprotected chromosome ends, the cycle may be repeated (reproduced with permission from DeVita et al, 2010[373]).

1.4.5 Spindle assembly checkpoint

Spindle assembly checkpoint function in anaphase

The spindle assembly checkpoint (SAC) is a surveillance mechanism that ensures the fidelity of chromosome replication during mitosis[373]. This signalling pathway ensures the proper alignment of the chromosomes at the metaphase plate prior to chromosome segregation[373]. The SAC is activated in every cell cycle immediately upon entry into mitosis and functions to delay anaphase until all chromosomes are properly attached at the metaphase plate. When the kinetochores of chromosomes are not fully aligned at the metaphase plate, a signal comes from the unattached kinetochores, inactivating the cell division cycle 20 protein (CDC20)[374–377]. APC/C is regulated by the mitotic checkpoint complex (MCC), which includes SAC proteins, MAD2L2 (mitotic arrest deficient-like 2), BUB1b (budding uninhibited by benzimidazole 1, beta), and CDC20[378–382]. MAD2L2 and BUB1b prevent APC/C activation by binding the CDC20-APC/C complex[383–385]. At the same time that the MCC is being activated, CENPE (centromere associated protein E), activates BUB1b, which also blocks anaphase[386]. Once all kinetochores become stably attached to the spindle, the activity of the sensor proteins declines, CDC20 is released from MAD2L2 and can then activate the APC/CDC20 complex[386]. This leads to activation of a protease known as separase (encoded by the ESPL1 gene in humans), which is required to cleave the cohesin complex that holds chromatids together[385,387–391]. Cleavage of this cohesion complex is necessary to initiate anaphase[392–394].

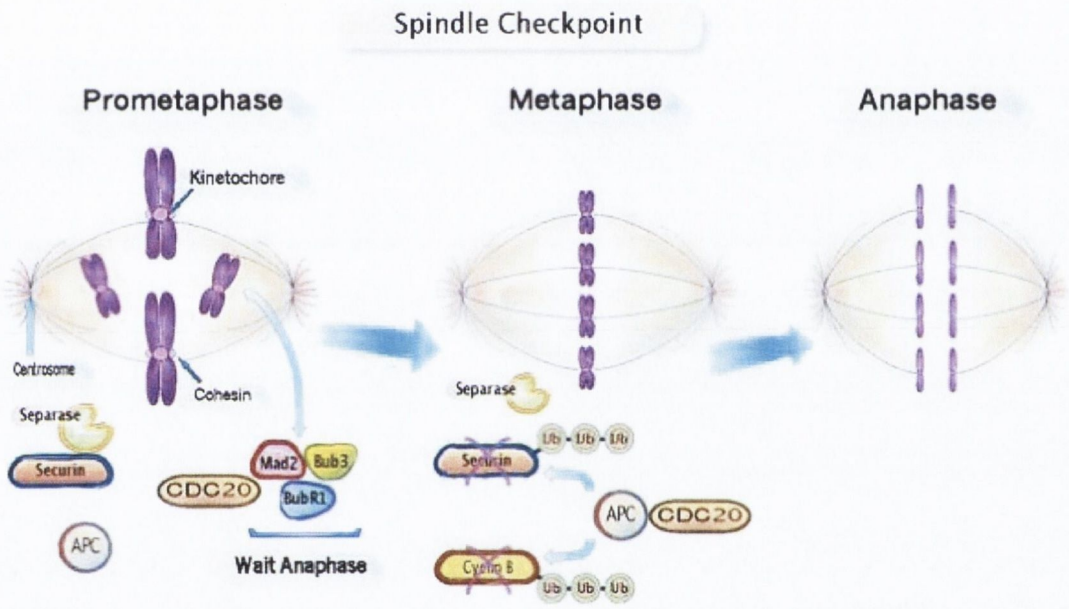


Figure 1.20. The spindle assembly checkpoint (SAC) ensures correct chromosomal alignment prior to anaphase

During metaphase, paired sister chromatids attach to the bipolar mitotic spindle apparatus at kinetochores. Kinetochores that are unattached to the spindle catalyse the formation of an active MCC complex (wait anaphase signal) that binds and inhibits CDC20. Once the final kinetochore is occupied by the spindle, the wait anaphase signal is lost, and CDC20 activates APC to ubiquitinate substrates such as cyclin B and securin. The resultant degradation of securin releases the enzyme separase to cleave cohesin and allow for sister chromatid separation under the tension of the mitotic spindle (reproduced with permission from Jr et al, 2010[373]).

Spindle assembly checkpoint and genomic instability

Failure of the spindle checkpoint may create conditions conducive to CIN[395–397]. Mouse models demonstrate that a compromised spindle checkpoint can promote tumourigenesis but also illustrate that there is no simple correlation between chromosome missegregation rates and the probability of developing cancer[397–401]. Dysregulations in the spindle assembly checkpoint have been documented in a number of human cancers[402–412]. Current evidence indicate that weakened mitotic spindle checkpoint signalling provides a favourable environment for tumourigenesis, but in itself may or may not drive the process[413,414].

1.4.6 Obesity and genomic instability

Significant negative relationships between adiposity measures (BMI, waist circumference, hip circumference, total body fat, and visceral adipose tissue) and leukocyte telomere length have been reported in some studies[415–419], while others have not confirmed this finding[420–424]. It is not apparent whether the reason for these inconsistencies is due to a difference in methods of measurements of telomere length, sample characteristics in the study, or simply there is no relationship between adiposity and telomere length. The studies reporting no association between obesity and telomere shortening relied almost exclusively on BMI measures, and many were not powered to show an association between anthropometric indices and telomere length. Adipocytes from obese adults have telomeres approximately 17% shorter than those in adipocytes from non-obese adults[425]. In addition to its relationship with telomere length, studies have found a significant inverse association between adiposity and telomerase activity[426–429]. It has been suggested that lifestyle changes, including a healthier diet, moderate aerobic exercise, and stress management can increase leukocyte telomerase enzyme activity[430]. There is very limited evidence linking shelterin complex dysfunction with adiposity. The gene that has the strongest association with human obesity is the fat mass and obesity associated (FTO) gene, which is thought to mediate its effect through epigenetic changes. A genome wide methylation profile of obese and non-obese carriers of the FTO risk allele revealed that TERF2IP, a component of the shelterin complex, was one of four sites with significantly increased methylation status[431]. Obesity has not been linked with deregulation of the SAC complex in humans. BUB1b and CDC20 expression is upregulated in tumour-bearing mice fed a high fat compared to normal diet[432]. Studies identifying causal mechanisms for SAC deregulation are limited, but oxidative stress has been linked to malfunction of the SAC in yeast, and oxidative stress is a known consequence of obesity[433,434].

1.4.7 Radiosensitivity and BFB events

The association between telomere length and radiosensitivity was initially based on the fact that accelerated telomere shortening is commonly observed in radiosensitive cells derived from patients with IR sensitive syndromes such as ataxia-telangiectasia, Nijmegen breakage and Fanconi anaemia syndrome[435–438]. Many studies demonstrated that fibroblasts with short telomeres are more radiosensitive than their counterparts with long telomeres, and radiosensitive human cells have shorter telomeres than normal cells[439–442]. The rate of anaphase bridging is higher in these radiosensitive cells than in wild type cells. Similarly in a range of cancer cell lines, short telomeres enhance radiosensitivity[443–445]. These results mirror those observed in *TERC* knock-out mice lacking the telomerase RNA component. This animal model suffers progressive telomere attrition both with age and with successive generations.[446] Progressive telomere shortening was associated with enhanced cellular and organismal sensitivity to ionizing radiation[439,447]. A significant inverse correlation between telomere length and chromosomal radiosensitivity was observed in lymphocytes from breast cancer patients as well as in healthy individuals[440,448]. Although some studies have suggested that telomerase expression *per se* influences radiosensitivity,[449,450] others suggest that telomere length is the primary determinant of radiosensitivity[439,447,451,452]. In these studies, ectopic telomerase expression or telomerase inhibition had no effect on sensitivity to IR until a measurable change in telomere length was observed. Although the end-result of telomerase suppression (enhanced radiosensitivity and delayed DNA repair kinetics) is similar to the effect observed with telomere shortening, telomerase suppression increased euchromatin content whereas telomere shortening increased heterochromatin content. This indicates that although telomerase repression and telomere shortening are closely intertwined, the two processes do not have identical consequences for the cell[442]. Most of the evidence linking telomere dysfunction to radiosensitivity relates to telomere length and telomerase inactivation, however studies have demonstrated that a set of genes related to the shelterin complex are altered in human laryngeal cancer cell lines with different radiosensitivities[453]. Furthermore, Tang et al observed that the expressions of POT1 and TPP1, components of the shelterin complex, were increased in radioresistant laryngeal cancer cell lines compared to more sensitive cell lines, at both gene and protein levels[454]. Dysregulation of the SAC has not been identified as a mediator of radiosensitivity, but inactivation of MAD2L2 and CDC20 has been observed to enhance the radiosensitivity of cells in vitro[455].

1.5 Overall Hypothesis

To date, no studies have investigated the interplay between obesity, radiation response and genomic instability, and there is a lack of clinicopathological parameters predicting the tumour response to CRT in oesophageal adenocarcinoma (OAC). The overall hypothesis of this thesis is that adiposity drives genomic instability events in OAC, resulting in a radioresistant phenotype. Consequently, we investigated the molecular mechanisms of radioresistance in oesophageal cancer using a novel, isogenic cell-line model of radioresistant oesophageal adenocarcinoma

Specific aims:

- Study the interaction between visceral adiposity and radioresponse in oesophageal cancer in vitro and in vivo
- Investigate the effect of visceral adipose tissue on telomere biology in OAC
- Elucidate the interaction between adipose tissue, anaphase bridge formation and SAC expression
- Identify potential gene markers of radioresistance by characterising novel genomic instability events in a radioresistant model

Chapter 2 The interaction between obesity and the radioresponse in oesophageal adenocarcinoma

In preparation for submission to Br J Cancer: AM Mongan, N Lynam-Lennon, S Maher, JV Reynolds, G Pidgeon, J O'Sullivan. Obesity influences the response to radiotherapy in oesophageal adenocarcinoma

2.1 Introduction

Incidence rates for OAC have been increasing in Western countries for several decades due in part to increases in the prevalence of known risk factors such as being overweight and obesity[23–25]. In fact, OAC may be considered the exemplar model of an obesity-related cancer. Obesity is associated with increased mortality in a number of cancers, including OAC[18,212], and is associated with increased risk of cancer recurrence and death following treatment[228–235,237,239,456,457]. However, a number of studies have reported no association between obesity and outcomes[240–244], and of those with significant findings, there are inconsistencies about the measurement and level of obesity, treatment modality, and the role of gender[228,229,232,245]. The impact of obesity on outcomes in oesophageal cancer, in particular the response to neoadjuvant chemoradiotherapy (NA CRT), is not clear. Although several studies have reported no difference in survival between obese and non-obese patients[246,247,252], others have reported better survival outcomes in patients with high BMIs[248,458]. One recent study focused on patients treated with NA CRT followed by surgery, and found no correlation between BMI and oncologic outcome or survival[251].

In addition to the lack of clarity regarding clinical studies on this topic, the relationship between adipose tissue and radioresponse has not been investigated at a molecular level. Mechanisms of radioresistance are still poorly understood. We and others have shown that a radioresistant phenotype is correlated with features such as altered DNA repair, cell cycle checkpoint operation, telomere biology, reactive oxygen species (ROS) biology, and induction of apoptosis[115,440,459–462]. Many of these processes are hypothesised to be affected by adiposity. We have shown that visceral adipose tissue is a major immune organ and a rich source of activated pro-inflammatory T cells[463]. Obesity is associated with a state of chronic inflammation and the production of active mediators, chemotactic molecules, cytokines, and adipokines, results in the excessive production of ROS causing systemic oxidative stress[434,464]. The induction of oxidative stress is one of the mechanisms by which ionizing radiation damages cells. The radioresistant phenotype has been associated with lower levels of ROS, which is likely to be due, at least in part, to enhanced ROS scavenging by antioxidant enzymes, particularly those involved in GSH processing such as GCLM (glutamate-cysteine ligase modifier subunit), GSS (glutathione synthetase) and GPX (glutathione peroxidase)[459,460]. Oxidative stress in adipose tissue over time is associated with inhibition of G_1-S phase transition, which is mediated via transcriptional repression of E2F target genes[465]. We have shown that ACM co-culture with oesophageal cancer cells alters expression of genes involved in cell cycle control[466]. However, the effect of adipose tissue on cell cycle kinetics has not been explored.

Obesity is associated with alterations in DNA repair mechanisms. Our group has demonstrated that the radioresistance of OE33R cells is due at least in part to alterations in DNA damage repair efficiency[174].

Murine models of obesity demonstrate increased levels of nuclear and mitochondrial DNA damage[467,468], and childhood obesity is associated with high levels of incompletely repaired DSBs[469]. Our unit has demonstrated that co-culture with adipose conditioned media (ACM) induces significant alterations in DNA repair pathway gene expression in healthy and malignant oesophageal cells[296,466].

Other putative pathophysiological mechanisms linking obesity and aggressive tumour behaviour include adipokine production, the insulin-like growth factor axis and sex steroids[253]. We have previously shown that co-culture with adipocytes has minimal transcriptomic effects on oesophageal cancer cells in comparison with whole adipose tissue and ACM co-culture, suggesting that the alterations in tumour biology are mediated not by adipocytes, but predominantly by secreted factors from the adipose tissue stromal vascular fraction[470]. We have shown that visceral ACM in OAC patients is a rich source of adiponectin, leptin and VEGF[185]. Adiponectin is the most abundant adipokine, inversely associated with BMI and visceral adipose tissue[257,471]. It is anti-angiogenic, anti-proliferative and anti-inflammatory, and circulating levels are lower in cancer patients[257–260]. Expression of the adiponectin receptor AR1 has been associated with prolonged survival *in vitro* and in vivo[263,472–474]. Leptin, which is positively associated with adiposity, promotes cell proliferation, angiogenesis and metalloproteinase expression in oesophageal cancer cell lines, and is a prognostic factor for poor outcome in gastric cancer[266,271,475]. VEGF is known to be pro-angiogenic and may have a role in modulating radioresponse[476]. Our unit has demonstrated that oesophageal cancer cells treated with recombinant VEGF demonstrate increased proliferation which is abrogated following treatment with VEGF-neutralizing antibody[185]. Its co-receptor NRP1 is upregulated in OAC and is associated with risk of invasive behaviour in Barrett's oesophagus[291]. Lysaght et al assessed expression of a panel of six proteins in ACM (IL-6, IL-8, TNF-α, VEGF, leptin and adiponectin) but a detailed metabolomic screen of the constituents of conditioned media from adipose tissue has yet to be performed[185].

This study uses the first isogenic model of radioresistance in oesophageal adenocarcinoma to assess the interaction between obesity and radioresponse in OAC[174]. Isogenic models of radioresistance, which use cells of the same origin that differ only in terms of radiosensitivity, are increasingly being used to study the biological mechanisms controlling radioresponse[477–479]. These model systems reduce the genetic variation that is present in patient samples and cell lines of different origin. Ionizing radiation induces multiple signalling pathways, so it is likely

that the mechanisms of radioresistance involve multigene interactions. The isogenic radioresistant oesophageal adenocarcinoma cell line model used in this study was generated by exposing OE33 oesophageal adenocarcinoma cells to clinically relevant fractionated doses of 2 Gy X-ray radiations (cumulative dose 50 Gy). Characterization of this model in terms of the standard parameters pertaining to radiosensitivity such as cell cycle, apoptosis and ROS biology, revealed no apparent alterations that could explain the enhanced radioresistance of OE33R cells[174]. Interestingly, radioresistant OE33R cells demonstrate greater efficiency in the repair of radiation-induced DNA damage compared to OE33P cells, which is likely contributing to radioresistance in this model[174]. However, given the complexity of the cellular response to IR, it is likely that multiple interacting processes can regulate sensitivity to radiation in OAC. The basis for the tumour response to radiotherapy lies in the interaction between the tumour microenvironment and the tumour cells themselves. The role of obesity in determining radiosensitivity is unknown, and warrants investigation.

2.2 Overall aim and specific objectives

The aim of this chapter was to study the interaction between visceral adiposity and the radioresponse in oesophageal adenocarcinoma, and to identify potential mechanisms by which adiposity may influence radioresistance.

Specific objectives:

- Determine if obesity status affects patient outcomes and radiation sensitivity in oesophageal adenocarcinoma (OAC) patients
- Investigate the effect of adipose conditioned media (ACM) on clonogenic survival following irradiation in the isogenic radioresistant OAC model
- Determine the effect of ACM on cell cycle kinetics in the isogenic radioresistant OAC model
- Investigate adipose receptor expression in the isogenic radioresistant OAC model
- Identify the most abundantly expressed metabolites in ACM from non-cancer patients, treatment naïve OAC patients, and OAC patients who had undergone neoadjuvant chemoradiotherapy (NA CRT)

2.3 Materials and methods

2.3.1 Retrospective analysis

A retrospective analysis of patients with resectable adenocarcinoma of the oesophagus or oesophagogastric junction treated with neoadjuvant chemoradiotherapy (NA CRT) at St. James's Hospital was performed. Clinical, pathological and survival data were retrieved from a prospectively maintained upper gastrointestinal cancer database in the Department of Surgery. A formal multidisciplinary team (MDT) discussed the management of each patient. Patients at St. James's Hospital were considered for a multimodal regimen if they fulfilled the following criteria: age under 77 years; satisfactory performance status and medical fitness for surgery; a biopsy proven invasive tumour of the oesophagus or oesophagogastric junction; and a staged tumour deemed resectable by the primary surgeon. All patients had a leukocyte count greater than 3500 per m^3, a platelet count above 100,000 per m^3, serum creatinine less than 1.4 mg/dL (124 mol/L), no previous chemotherapy or radiation therapy, and no previous cancer.

Multimodal regimen

Patients were given a standard protocol of CRT consisting of 40 Gy/15 fractions on days 1 to 5, 8 to 12, and 15 to 19, and concurrent chemotherapy of 5-fluorouracil (15 mg/kg) on days 1 to 5 and cisplatin (75 mg/m^2) on day seven. Chemotherapy was repeated on week six. Severity of chemotherapy adverse effects was defined according to the National Cancer Institute Common Toxicity Criteria version 2.0[480].

Surgical resection

Patients were restaged by CT and OGD at week eight and scheduled for surgery on week nine. Surgery occurred if the neutrophil count was >2x10^6/mL, if performance status had not significantly deteriorated, and if there was no evidence of local or systemic progression of disease on imaging. All patients had a thoracotomy as a component of their surgical management, either combined with an abdominal and neck exploration (three-stage) for mid- and upper-oesophageal cancers, or cancer arising in long- segment Barrett oesophagus, or with an abdominal exploration (two-stage) for most lower third and junctional tumours, or combined with a total gastrectomy for junctional tumours with significant gastric extension. A two-field lymphadenectomy (abdominal and thoracic) was performed in all cases. In the abdomen, nodal dissection routinely involved resection of N1 nodes as well as nodes along the left gastric artery, common hepatic artery, and splenic artery. In the thorax, clearance was obtained of nodes up to and including subcarinal nodes in all cases, and in selected cases paratracheal nodes were resected. Dissection of cervical lymph nodes was not performed. Pathologic assessment was performed as per standard guidelines[481]. The extent of residual carcinoma in the surgical specimen was assigned as per Mandard and colleagues as described in section

1.1.6. TRG 1-3 was considered to represent a good response to therapy, TRG 4-5 a poor response to therapy. Data were also analysed according to the three-point variation of the Mandard TRG described in section 1.1.6, which separates complete (TRG 1), partial (TRG2/3) and minimal (TRG 4/5), responses. Surgical complications were graded according to the Clavien-Dindo classification[482]. Patients were followed at three monthly intervals for the first year and at four to six monthly intervals for the subsequent four years. All patients had CT scans in the first and second post-treatment years or as clinically indicated.

2.3.2 Reagents

All laboratory chemicals and reagents were purchased from Sigma Chemical Company (MO, USA) unless otherwise stated, and prepared and stored according to manufacturer's specifications. Solid reagents were weighed using a Scout Pro electronic balance (Ohaus Corporation, NJ, USA) or an Explorer Pro fine electronic balance (Ohaus Corporation, NJ, USA), and made up using double distilled H_2O, unless otherwise stated. Solutions were autoclaved prior to use and stored at room temperature unless otherwise stated. Gilson pipettes (Gilson S.A., France), were used to transfer liquid volumes up to 1 mL, electronic pipette aids (Drummond, PA, USA) and disposable Pasteur pipettes (Sarstedt Ltd., Wexford, Ireland) were used for volumes greater than 1 mL and graduated cylinders were used for volumes in excess of 10 mL.

2.3.3 Cell culture

All cell culture media was purchased from Lonza (Basel, Switzerland) and all cell culture plastics were purchased from Sarstedt Ltd. (Wexford, Ireland) unless otherwise stated. Cell culture was carried out in a dedicated cell culture room which was cleaned and sterilised monthly. Cell culture was carried out in a Grade II laminar hood using aseptic technique while wearing a clean lab coat with elasticated cuffs and disposable latex gloves. The cabinet was cleaned with 70% (v/v) ethanol before and after each use and all reagents, media, and plastics were taken into the cabinet and cleaned in this manner.

Generation of the OE33R cell line

The human oesophageal adenocarcinoma OE33 cell line was purchased from the American Collection of Cell Cultures (ATCC, Virginia, USA). The radioresistant cell line OE33R was established as previously described[174]. Briefly, the OE33 cell line was exposed to clinically relevant fractionated doses of 2 Gray (Gy) X-ray radiation (cumulative dose 50 Gy) to create an isogenic radioresistant subline called OE33R. Both OE33R and its age and passage matched parental counterpart, OE33P, were cultured as monolayers in Roswell Park Memorial Institute (RPMI-1640) medium supplemented with 10% fetal calf serum and 1% penicillin-streptomycin

(hereafter known as complete medium), and maintained at 37^0C in 95% humidified air containing 5% CO_2. Cells were grown to approximately 50% confluence in vented 75 cm^2 culture flasks and exposed to 2 Gy X rays (250 keV, 15 mA, 38 s) using an X-ray generator (RS225) (Gulmay Medical, Surrey, UK). Cells were trypsinized (Lonza) and subcultured when they had reached 90% confluence. This procedure was repeated until cells had received a cumulative dose of 50 Gray. Parental cells (OE33P) were mock-irradiated. The OE33P and OE33R cell lines are age and passage-matched.

The enhanced survival of OE33R cells is specific to radiation, rather than a general phenotype to cytotoxic insult. This was demonstrated by treating OE33P and OE33R cells with the chemotherapy agents cisplatin and 5FU and measuring survival by clonogenic assay[174]. Treatment with IC_{50} doses of cisplatin or 5FU for 24 hours significantly decreased survival similarly in both cells lines[174]. While radiation, cisplatin and 5FU have DNA as a common primary target, the mode of action of each cytotoxic agent is different, with mechanisms of resistance that are generally distinct from one another.

Cell subculture

OE33P and OE33R were examined daily using an inverted phase contrast Nikon microscope (Nikon Corporation, Tokyo, Japan) and subcultured upon reaching 80-90% confluency. A 1 mL volume of trypsin Ethylene Diamine Tetra Acetic Acid (0.05% (w/v) trypsin, 0.02% (w/v) EDTA) was added to the flask and incubated at 37°C for three to five minutes or until the cells had detached from the surface of the flask. Complete media (2 mL) was added to inactivate the trypsin and cells were seeded at specific densities in vented T75 flasks.

2.3.4 Oesophageal tumour and adipose tissue biobank

All research was carried out in accordance with the Declaration of Helsinki, and ethical approval for this study was granted by the Joint St. James's Hospital/AMNCH Ethics Committee to carry out all aspects of this work. All patients provided fully informed consent. Patients were excluded from the study if they were pregnant, HIV or Hepatitis C positive or had diagnosed metastatic disease or a history of cancer in the previous 3 years.

Oesophageal tumour biobank

Histologically proven OAC patients undergoing elective surgical resections were invited to participate in the oesophageal tumour biobank, established in the Department of Surgery since 2004. Standard operating procedures for the collection, storage and analysis of specimens were optimised[483]. Tumour tissue was placed in in RNA*later*® (Qiagen, Sussex, UK) for the purpose of RNA extraction.

Adipose tissue biobank

An adipose biobank was established in the department of surgery in July 2007 and standard operating procedures were optimised from a previously published study[484]. Patients undergoing oesophagectomy for oesophageal cancer and elective non oncological gastrointestinal surgeries were recruited to the study with consent.

Patient anthropometry

Body weight, height, visceral fat area and central waist circumference were measured and body mass index (BMI) calculated for all patients. All anthropometric measurements were recorded on the morning of surgery. Height and weight were measured to the nearest 0.1 cm and 0.1 kg using SECA Alpha 770 digital scale (CMS Weighing Equipment Ltd, London, UK) and portable stadiometer (SECA, Vogel and Halke, Germany). Body mass index (BMI) was calculated as weight (kg) / height^2 (m^2). Waist circumference was measured to the nearest 0.1 cm using a tape measure midway between the uppermost border of the iliac crest and the lower border of the costal margin in the midaxillary line after respiratory exhalation while the patient was in a standing position[204].

All patients had a pre-operative diagnostic computed tomography (CT) scan and visceral fat area (VFA) was calculated by an experienced radiologist, using a previously described and validated technique[485,486]. The cross-sectional surface areas of the different abdominal fat compartments were calculated at the disc space between the L3 and L4 intervertebral space. All patients were scanned on a Siemens Emotion single slice or a multislice Somatom Sensation scanner (Siemens, Erlangen, Germany). Individual scans were analysed on a Siemens Leonardo workstation (Siemens) to calculate total (TFA), visceral (VFA) and subcutaneous fat area (SFA)[31,204]. All areas were measured in square centimetres. To quantify TFA, a line was drawn around the skin surface with a cursor. Then an automatic algorithm and a Hounsfield threshold value of − 50 to − 150 was used to determine the cross-sectional fat content within that area. VFA was calculated by repeating the technique with an area delineated by a line drawn around the inner layer of the abdominal wall musculature. SFA was calculated by subtracting VFA from TFA[31]. The accuracy of BMI to diagnose obesity is limited, particularly for individuals in the intermediate BMI ranges[197]. Waist circumference is a more accurate predictor of visceral fat but reflects total abdominal fat, failing to distinguish between subcutaneous and visceral compartments, and there are no clearly defined cut-off values which correlate with increased cancer risk. Computed tomography (CT) measurement of visceral fat area (VFA) is the gold standard marker of obesity and was used as the primary indicator of obesity status in this study[198,199]. A visceral fat area in excess of 163.8 m^2 (men) and 80.1 m^2 (women) is classified as obese for gastrointestinal cancer patients[204].

Adipose tissue processing

Omental adipose tissue specimens were excised at the beginning of the surgical resection and immediately transported in sterile transport buffer (glucose (0.15%), gentamycin (0.05 mg/mL) in PBS) for processing in a Grade II laminar air flow cabinet. The adipose tissue was minced with a pair of scissors and washed with sterile PBS. In a tissue culture dish, 5 g samples of minced and washed adipose tissue were incubated in 10 mL of serum free M199 media for 72 hours at 37°C and 5% CO_2. The adipose conditioned media (ACM) was filtered to remove adipose tissue fragments and the supernatant stored at -80°C.

Co-culture with adipose conditioned media

Cells were seeded in 12-well plates at a concentration of 1.2×10^5 cells/well (flow cytometry, karyotyping and array CGH), 2×10^4 cells/well (anaphase bridge enumeration), 6×10^4 cells/well (gene expression studies and telomere length analysis): in 6-well plates at a concentration of $1\text{-}6 \times 10^4$ cells/well (clonogenic assay): in 96-well plates at a concentration of 5×10^2 (crystal violet assay). Cells were allowed to adhere overnight. At 16 hours post seeding, cells were incubated with ACM or M199 (1 mL to 6-well plate, 0.5 mL to 12-well plate, 0.05 mL to 96-well plate) and plates were incubated at 37°C in 95% humidified air and 5% CO_2 for 24 or 72 hours.

Adipokine levels in adipose conditioned media

Previous investigations in this laboratory demonstrated that adipokine levels in adipose conditioned media from OAC patients is influenced by location of fat depot, obesity status and treatment modality. Comparing subcutaneous (sACM) and visceral adipose conditioned media (vACM), significantly higher levels of VEGF and IL6 were observed at mRNA and protein levels, along with higher proportions of CD+8 T cells and NKT cells (Table 2.1)[185,487]. Similar gene expression levels were observed for IL8, TNF-alpha and adiponectin between subcutaneous and visceral adipose tissue depots[185,487]. No significant differences in the proportions of myeloid DC, plasmacytoid B lymphocytes, CD4+ T cells, CD14+ monocytes or NK cells were observed in visceral compared with subcutaneous adipose tissue[185,487]. Following culture with oesophageal tumour cells, vACM induced a greater increase in proliferation compared to tumour cells co-cultured with sACM[185,487].

A selection of cytokines, chemokine and adipokines were measured in a cohort of obese and non-obese patients. Significantly higher levels of VEGF and lower levels of adiponectin were observed in the vACM of centrally obese compared to non-obese patients (Table 2.2)[466]. There was no significant difference in levels of leptin or IL6[466]. vACM from viscerally obese OAC

patients induces significantly more tumour cell proliferation than that of non-obese patients[185,466].

Levels of VEGF, adiponectin, leptin IL8, IL6, MCP1 and IFNγ were assessed at a gene and protein level in OAC patients treated with surgery and those treated with surgery and NA CRT. Patients who underwent surgery only had significantly higher levels of leptin and IL6 compared to patients who received NA CRT prior to surgery (Table 2.3)[487].

Table 2.1 Constituents of visceral compared to subcutaneous adipose conditioned media

Adipokines	Immune cells	Cell function
↑ IL6 expression	↑ NKT cells	↑ Proliferation in OE33
↑ VEGF expression	↑$CD8^+$ T cells	
↔ Adiponectin	↔ Myeloid DC	
↔ Leptin	↔ Plasmacytoid B cells	
↔ TNFα	↔ $CD4^+$ T cells	
	↔ $CD14^+$ monocytes	
	↔ NK cells	

Table 2.2 Constituents of obese compared to non-obese adipose conditioned media

Adipokines	Cell function
↑ VEGF expression	↑ Proliferation
↓ Adiponectin	
↔ Leptin	
↔ IL6	

Table 2.3 Constituents of adipose conditioned media from OAC patients treated with surgery only compared to OAC patients treated with NA CRT

Adipokines
↓ Leptin expression
↓ IL6
↔ Adiponectin
↔ IL8
↔ MCP1
↔ VEGF
↔ IFNγ

2.3.5 Investigation of gene expression

RNA isolation from cell lines using TriReagent method

RNA to be used for quantitative real time polymerase chain reaction (qPCR) was isolated from cell lines using the TriReagent method. Following co-culture with ACM, RNA was harvested from OE33P and OE33R cell lines using 1 mL of TriReagent (Molecular Research Centre, Montgomery Road, OH, USA), containing a mixture of guanidine thiocyanate and phenol in monophasic solution. Samples lysed in TriReagent were stored at -80°C until RNA extraction. Total RNA was isolated as follows: samples were thawed and stored at room temperature for 5 min following which 100 µL Bromo-3-chloro-propane (BCP) was added. Samples were vortexed for 15 s and allowed to stand at room temperature for 15 min. Following centrifugation at 12000 x g at 4°C for 15 min, the upper aqueous phase was carefully removed to a new tube and subsequent steps were carried out at room temperature. Isopropanol (500 µL) was added to the tube and incubated for 10 min followed by centrifugation at 12000 x g for 8 min. The supernatant was decanted and the pellet washed in 1 mL ethanol (75% v/v) by brief vortexing followed by centrifugation at 12000 x g for 5 minutes. The ethanol was decanted and the pellet allowed to air dry for 3-5 min. The pellet was resuspended in 40 µL RNase-free H_20.

Pre amplification of RNA

RNA from patient pre-treatment biopsy samples was amplified using a MessageAmp II aRNA amplification kit (Ambion). The procedure involves single-strand reverse transcription of RNA to cDNA. The cDNA undergoes a second-strand synthesis, and purification to provide a template for in vitro transcription, which generates antisense RNA (aRNA) copies of each mRNA in a sample. RNA (250ng) was made up to a final volume of 10 µL in nuclease-free H_20. A reverse transcription master mix was made up to contain (per reaction): 1 µL nuclease-free H_20, 1 µL T7 Oligo (dT) primer, 2 µL first strand buffer (10X), 4 µL dNTP mix, 1 µL RNase inhibitor and 1 µL array script reverse transcriptase enzyme. A 10 µL volume of master mix was added to each RNA sample and mixed by pipetting. Samples were incubated at 40^0C, with the lid at 50^0C in a G-Storm thermal cycle (Gene technologies Ltd) for 2 hours. Samples were centrifuged briefly to pool, and placed on ice until required.

A second strand cDNA synthesis master mix was made up to contain (per sample): 63 µL nuclease-free H_20, 10 µL second strand buffer (10X), 4 µL dNTP mix, 2 µL DNA polymerase enzyme and 1 µL RNase H. An 80 µL volume of master mix was added to each sample, and mixed by pipetting. Samples were pooled by brief centrifugation, and incubated at 16^0C in a pre-cooled G-Storm thermal cycler (Gene technologies Ltd) for 2 hours. It was ensured that the lid of the thermal cycler was inactivated, as temperatures above 16^0C may inhibit the second-strand cDNA synthesis reaction. A 250 µL volume of cDNA binding buffer was added to each

sample, and mixed by pipetting. The samples were centrifuged briefly to pool, and each sample was pipetted onto the centre of a cDNA filter cartridge placed in a plastic wash tube. Samples were centrifuged at 10,000 × g for 1 min or until the entire volume had passed through the filter and the flow-through were discarded. A 500 µL volume of wash buffer was added to the cDNA filter cartridge and centrifuged at 10,000 × g for 1 minute or until the entire volume had passed through the filter. The eluted cDNA was transferred to a 0.2 mL PCR tube.

A transcription master mix was made up to contain (per cDNA sample): 4 µL T7 ATP, 4 µL T7 CTP, 4 µL T7 GTP, 4 µL T7 UTP, 4 µL T7 (10X) reaction buffer and 4 µL T7 polymerase enzyme mix. A 24 µL volume of transcription master mix was added to each cDNA sample, mixed by pipetting and centrifuged briefly to pool. Samples were incubated at 37^0C with the lid at 100-105^0C in a G-Storm thermal cycler (Gene technologies Ltd) for 14 hours. The reaction was stopped by addition of 60 µL nuclease-free H_20 to each sample.

A clean-up of each sample was performed to ensure removal of enzymes and any unincorporated nucleotides from the amplified RNA. A 350 µL volume of aRNA binding buffer, followed by 250 µL ethanol was added to each sample, and mixed 3 times by pipetting. Each sample was then immediately transferred onto the centre of an aRNA filter cartridge placed in a plastic elution tube. Samples were centrifuged at 10,000 × g for 1 min or until the entire volume had passed through the filter and the flow-through were discarded. A 650 µL volume of wash buffer was pipetted onto the filter cartridge and centrifuged at 10,000 × g for 1 min or until the entire volume had passed through the filter. The flow-through was discarded, and the centrifugation was repeated to remove any trace amounts of wash buffer. The aRNA filter cartridge was transferred to a new collection tube, and 200 µL nuclease-free H_20 heated to 55^0C was pipetted onto the filter cartridge. Samples were incubated at 55^0C for 10 min, and centrifuged at 10,000 × g for 1.5 min or until the entire volume had passed through the filter.

RNA quantification and purity analysis

RNA quantification was determined spectrophotometrically, using a Nanodrop 1000 spectrophotometer (version 3.1.0, Nanodrop technologies, DE, USA). RNase-free H_2O (1 µL) was used to blank the instrument prior to RNA analysis. A 1 µL volume of each sample of isolated RNA was loaded onto the instrument and concentration was measured in ng/µL. 260:280 and 260:230 purity ratios were also recorded. A 260:280 ratio greater than 2.0 was indicative of a pure RNA yield, while a 260:230 ratio greater than 1.7 indicated the sample was free of phenol contamination.

cDNA synthesis cell lines and tumour samples

The reverse transcriptase enzyme and buffer were purchased from Bioline (Bioline, Kilkenny, Ireland); all other reagents were purchased from Invitrogen (Invitrogen Corp., CA, USA). cDNA was synthesised by adding random primers (1 µL) to 1 µg total RNA, adjusting the volume to 11 µL with RNase-free H_2O, and heating the sample to 70°C for 10 min, and immediately chilling on ice for at least 1 min. A master mix containing: RNaseOUT recombinant ribonuclease inhibitor (1 Unit/µl), dNTPs (10mM, prepared as a 1:1:1:1 ratio of dATP, dGTP, dTTP and dCTP), and Bioscript reverse transcriptase (200 units/µL) in 5X Bioscript reaction buffer was added to each sample. This mixture was incubated at 37°C for 3 hours and 70°C for 10 minutes. The resulting cDNA was stored at -20°C.

Table 2.4. Reagents and volumes used in cDNA synthesis

Reagent	**Volume per sample (µL)**
Random Primers	1.0
250ng of RNA + RNase free H_20	11.0
Heated for 10 min at 70°C and cooled on ice for 1 min then following mix added:	
5X Bioscript reaction buffer	4.0
H_20	2.0
DNTPs	1.0
RNase out	0.5
Bioscript Reverse Transcriptase	0.5
Total Volume	**20**

Quantitative real time PCR

TaqMan® assay kit (Applied Biosystems, CA, USA) were used for all gene expression experiments. The following PCR master mix was prepared for each sample to be amplified: 10 µL Taqman® Universal Master Mix (2X), 8.0 µL nuclease-free H_2O, 10 µL Taqman® gene expression assay. cDNA (1 µL) from each sample was added in triplicate to a 96-well MicroAmp™ Optical reaction plate (Applied Biosystems, CA, USA). A no-template control using 1 µL H_2O instead of DNA template was also included. The PCR master mix was added to each well, to give a final reaction volume of 20 µL. The reaction plate was sealed using an optical adhesive cover (Applied Biosystems), and the plate was centrifuged briefly to pool reagents and eliminate any bubbles. Real-time PCR detection was performed using an ABI Prism 7900HT real-time thermal cycler (Applied Biosystems). The plate was heated to 50°C for 2 min, 95°C for 10 min, followed by 40 cycles of 95°C for 15 s and 60°C for 1 min. Taqman fluorogenic gene expression probe sets (Applied Biosystems) were used for all gene expression experiments. All probe sets used were FAM (6-carboxyfluroscein) labelled.

Quantitative real time PCR data analysis

Data analysis was performed using SDS 2.3 and SDS RQ Manager 1.2 relative quantification software. A visual inspection of triplicate expression values was initially performed to exclude outliers. The threshold cycle (Ct) for each well was calculated and the expression levels of target genes were normalised to expression levels of an endogenous control gene (18S ribosomal RNA). For all pre-treatment biopsy tumour samples, target gene expression was normalised to proportion of tumour cells as determined by B actin expression. CT values for B actin were determined for each sample and stratified into low, moderate and high. CT values for each sample were divided by 1 (high), 2 (moderate) or 3 (low). Analysis of gene expression data was performed using the $2^{-\Delta\Delta Ct}$ relative quantification method, which describes the change in expression of a target gene relative to the expression of a reference group, such as an untreated control. One sample was set as the calibrator for the analysis. Gene changes were only reported if the transcript was amplified before 30 cycles.

2.3.6 X-Ray irradiation

Cells were seeded in 6-well plates and treated with control media or co-cultured with ACM as previously described (section 2.3.3). All irradiations were performed using a Gulmay Medical X-Ray generator, model (Rs225) (Gulmay Medical, Surrey, UK), at a dose rate of 3.25 Gy/min (2 Gy/38 s). The uniform delivery of ionising radiation to cells plated on culture dishes was ensured with the generation of a broad radiation beam (12.5 cm × 12.5 cm). Cells were irradiated at the centre of the beam, at a distance of 40 cm with a beam produced by 200 kV

and 15 mA. The dosimetry was performed by a qualified medical physicist, using ionisation chambers and thermoluminescent dosimeters.

Clonogenic assay

The sensitivity of cells to radiation was measured using the clonogenic assay, which is the gold standard method for measuring cytotoxicity[488]. This assay tests the ability of each cell in a population to retain its reproductive integrity following exposure to cytotoxic insults. Cells in the exponential growth phase were harvested by trypsinization as described previously (section 2.2.3) and a single cell suspension was obtained. The cell suspension was adjusted to the required density using complete medium, and the required numbers of cells (see Table 2.5) were seeded into 6-well plates (Sardstedt). Cells were allowed to adhere to plates overnight at 37^0C in 5% CO_2/95% air. Cells were irradiated at 0 or 2 Gy bolus dose, and incubated at 37^0C in 5% CO_2/95% air for 7–14 days to allow surviving colonies to reach maximum density without merging of colonies occurring.

Table 2.5. Optimum clonogenic cell seeding densities

Treatment	Cell seeding density (cells/well) (6-well plate)
M199 control media	4.0×10^3
M199 control media + 2 Gy IR	8.0×10^3
ACM	3.5×10^3
ACM + 2 Gy IR	6.0×10^3

Staining of colonies

Media were removed from wells and 0.5 mL staining/fixing solution (0.05% w/v crystal violet, 25% v/v Methanol) was added to each well. Plates were incubated for 30 minutes at room temperature, and the staining/fixing solution was removed from wells to a waste flask. Residual crystal violet was removed by gently submerging plates in a water bath. Plates were left to air dry. Crystal violet waste was inactivated using NaOH before disposal.

Colony counting

Colonies consisting of 50 cells or more were counted using a PC-software operated colony counter (ColCount™, Oxford Optronix Ltd, Oxford, UK). Colonies are imaged using wide-angled optics, and electro-luminescent trans-illumination is used to create maximal contrast with the crystal violet stain. The application of constant counting parameters eliminates bias and ensures objective results. Plating efficiencies (PE), which are the fraction of colonies from

untreated cells, were calculated using the formula: PE= No. colonies/No. cells seeded. The surviving fraction (SF), which is the number of colonies produced after treatment, expressed in terms of PE, was calculated using the formula: SF= No. colonies/(No. cells seeded × PE).

2.3.7 Propidium iodide cell cycle analysis

Cell cycle analysis was performed by Propidium iodide (PI) staining and flow cytometry[489]. Cells were seeded in 6-well plates, and allowed to adhere overnight at 37°C in 5% CO_2/95% humidified air. Cells were treated with 1 mL RPMI control media, M199 control media or ACM. Following treatment, cells were collected by trypsinization as described previously (section 2.3.3) and transferred to 5 mL falcon tubes (BD Biosciences). Cells were centrifuged at 180 × g for 3 min, and the supernatant decanted. Cell pellets were washed with 1 mL PBS and centrifuged as before. Cell pellets were fixed and permeabilised by drop-wise addition of 4.5 mL ice-cold ethanol (70% v/v in PBS) (Merck, Darmstadt, Germany), and incubated at 4°C for a minimum of 2 hours. The fixative was decanted following centrifugation at 180g for 3 min. Fixed cells were washed with 1 mL PBS and centrifuged as before. Each sample was resuspended in 0.5 mL PI staining solution [PI (0.02 mg/mL)/Triton X- 100 (0.1%)/RNase A (0.2 mg/mL)], except for appropriate controls. Samples were incubated at 37°C for 30 min and then at room temperature for 1.5 hours in PI staining solution. Unstained control samples used for instrumental setup were incubated in 1 mL PBS. Flow cytometry was performed using a FACSCalibur™ flow cytometer (Becton- Dickson, San Jose, CA), data acquired using Summit v4.3 software (Dako, Glostrup, Denmark) and data analysed by histogram plot using CELLQuest™ software. A minimum of 10,000 events were collected, and doublets were excluded from analysis using doublet discrimination. The X-axis of the histogram plot represents PI fluorescence or DNA content, whilst the Y-axis represents cell number.

2.3.8 Metabolomic screen of ACM

A volume of 250 µL deuterium and 10 µL sodium trimethyl [2,2,3,3-$^2H_4$] propionate (TSP) (0.005 g/mL) were added to each 330 µL sample of adipose conditioned media. Spectra were acquired on a 600-MHz Varian NMR spectrometer (Varian Limited, Oxford, United Kingdom) by using the first increment of a NOESY (Nuclear overhauser effect spectroscopy) pulse (sequence at 251C). ^1H NMR ACM spectra were processed manually with Chenomx software (version 6; Chenomx Edmonton, Canada) and were phase and baseline corrected. Spectra were integrated into bins consisting of spectral regions of 0.001 ppm. The water region was excluded, and data were normalized to the total area of the spectral integral. Discriminating metabolites were identified by using libraries of pure metabolites enveloped in house and the Chenomx database library. Acquisition of samples resulted in spectra containing a number of peaks, representing proton resonance in ^1H NMR.

2.3.9 Statistical analysis

Statistical analysis was performed using Graphpad Prism 5 software (GraphPad Software, Inc., CA, USA) and SPSS version 18 for Windows (IBM, Armonk, New York, USA) software. Unless otherwise stated, scientific data were expressed as mean ± standard error of the mean (SEM). SEM was calculated as the standard deviation of the original sample divided by the square root of the sample size. Clinical data was expressed as the median. Unpaired *t*-tests and the Mann-Whitney U test were used to examine statistical significance between unpaired groups of parametric and non-parametric data respectively. Categorical variables were analysed by Chi-square and Fisher's exact tests. Data analysis was performed by one way analysis of variance (ANOVA), where the number of groups in the experiment was three or more. A Tukey multiple comparisons post hoc test was necessary following ANOVA in order to determine which groups were significantly different to each other. RR refers to relative risk, 95% CI to 95% confidence interval. Survival analysis was performed using Kaplan-Meier curves and log-rank test. Survival was calculated from date of diagnosis to the first event (i.e. recurrence, progression, death or end of the follow-up period). For all analysis, $p \leq 0.05$ was considered to be statistically significant.

Statistical methods for the analysis of metabolomic data may be grouped into supervised and unsupervised approaches. Multivariate metabolite data analyses were performed with Simca-P+ software (version 11.0; Umetrics, Umea°, Sweden). The ^{1}H NMR spectra were analysed using two pattern recognition methods, principal component analysis (PCA) (unsupervised) and partial least square discriminant analysis (PLS-DA) (supervised). In PCA, the maximum variation in the dataset itself is described without providing information to the model about the class groupings. The output is a series of orthogonal principal components, describing the maximum to minimum variation in the data in turn through weighted peaks. In biological materials such as ACM, confounding or random data may mask the true differences in the samples, indicating that supervised analysis techniques may be more useful. PLS-DA uses multivariate metabolomic peak data to describe the assignment of samples to binary groups. Principal components analysis (PCA) was applied to data sets to explore any trends or outliers in the data. The difference between metabolite patterns was further explored by using partial least-squares discriminant analysis (PLS-DA). A scores plot was created to visualize the PLS-DA model, and the corresponding loadings provided information on the contribution of 1H NMR spectral regions to the separation of metabolite clusters. The variable importance in the projection (VIP) value of each variable in the model was calculated to indicate its contribution to the classification of samples. Variables with a VIP value >1.5 were considered important in discriminating between groups. The quality of all models was judged by the goodness-of-fit parameter (R^2) and the predictive ability parameter (Q^2), which is calculated by an internal

cross-validation of the data and the predictability calculated on a leave-out basis. For all analysis, $p \leq 0.05$ was considered to be statistically significant.

2.4 Results

2.4.1 Impact of obesity on radioresponse in OAC patients treated with neoadjuvant chemoradiotherapy.

Between 1990 and 2012, a total of 254 consecutive OAC patients were treated with neoadjuvant chemoradiotherapy (NA CRT) as part of their curative therapy, of whom 209 completed NA therapy and went on to have a surgical resection. According to BMI classification, eight patients were underweight (4%), 53 were normal weight (25%), 94 were overweight (45%) and 54 were obese (26%). Visceral fat area (VFA) is the gold standard marker of visceral obesity[490]. Visceral obesity status as measured by VFA was available on just 75 of the 209 patients (38 non-obese and 37 obese). The small sample size precluded analysis of outcomes in this subset, therefore BMI had to be used as the surrogate marker of obesity. Patients who were underweight were excluded from analysis. The remaining cohort of 201 patients comprised 33 women and 168 men, with a median age of 61 years (range 30-77 years). The normal (n=53) and overweight/obese (n=148) cohorts were not significantly different in terms of age, gender, ASA grade, smoking status, tumour site or clinical stage (Table 2.6). Overall, 188 patients were characterised as ASA 1 or 2 (94%), most patients were current or ex-smokers (n=190, 95%), most tumours were located in the oesophago-gastric junction (n=194, 97%) and deemed clinically to be stage T3 (n=166, 83%).

Table 2.6. Clinical details of normal and overweight/obese cohorts.

	NORMAL n=53		OVERWEIGHT & OBESE n=148		ALL n=201		P value
Age median (years)	61		62		61		0.19[a]
Age range (years)	30-75		37-77		30-77		
Male gender	42	79%	126	85%	16 8	86%	0.39[b]
ASA GRADE	**n**	**%**	**n**	**%**	**n**	**%**	
ASA Grade 1	26	49%	70	47%	96	48%	1.00[c]
ASA Grade 2	22	42%	70	47%	92	46%	
ASA Grade 3	5	9%	8	6%	13	6%	
SMOKING STATUS	**n**	**%**	**n**	**%**	**n**	**%**	
Current smoker	29	55%	101	68%	13 0	65%	0.37[d]
Ex smoker	13	24%	47	32%	60	30%	
Never smoked	11	21%	0		11	5%	
TUMOUR SITE	**n**	**%**	**n**	**%**	**n**	**%**	
Middle oesophagus	1	2%	2	1%	3	1%	0.44[e]
Lower oesophagus	1	2%	3	2%	4	2%	
Oesophago-gastric junction	51	96%	143	97%	19 4	97%	
OGJ I	*22*		*83*		*48*		
OGJ II	*23*		*53*		*20*		
OGJ III	*6*		*7*		*3*		
Clinical T stage	**n**	**%**	**n**	**%**	**n**	**%**	
Clinical stage Tis	1	2%	1	1%	2	1%	0.47[f]
Clinical stage T1	1	2%	3	2%	4	2%	
Clinical stage T2	6	11%	13	9%	19	10%	
Clinical stage T3	42	79%	124	84%	16 6	83%	
Clinical stage T4	1	2%	2	1%	3	1%	
Clinical stage Tx	2	4%	5	3%	7	3%	

ASA=American society of anaesthesiologists' classification of physical health; OGJ=Oesophago-gastric junction; Tis=In situ; Tx=Not assessed; a=Analysed by Mann Whitney U test; b=male vs. female analysed by χ^2 test; c=ASA 1 vs. ASA 2-3, analysed by χ^2 test; d=Current or ex-smoker vs. never smoked analysed by χ^2 test; e=AEG vs. other site analysed by χ^2 test; f=Clinical stage Tis-T0-T2 vs. T3-4 analysed by χ^2 test.

2.4.1.1 Pathological outcomes

Of the 201 resected tumours, 50% were ypT3 (n=101). A median of 15 nodes were analysed (range 1-37) and 100 patients (49%) had node positive disease (Table 2.7). An R0 resection was achieved in 163 (81%) of patients. A good TRG response (TRG 1-3) was seen in 148 patients (74%) and 32 (16%) had a TRG of 1. While clinical T stage prior to NA CRT did not differ between normal and overweight/obese patients, overweight and obese patients were more likely to have a lower pathological T stage at surgery (Relative Risk (RR) 1.495, 95% Confidence Interval (CI) 1.094-1.938, p=0.02) (Figure 2.1). The number of lymph nodes analysed and lymph node positivity did not differ between normal and overweight/obese cohorts. Overweight or obese patients were more likely to achieve a good TRG response compared to normal weight patients (RR=2.141, 95% CI=1.374-3.336, p=0.002) (Figure 2.2 A). When patients with TRG 3 were excluded from the analysis, overweight/obese patients were three times as likely to achieve a good (TRG 1-2) response following NA CRT (RR=3.259, 95% CI=1.269-8.368, p=0.004) (Figure 2.2 B). Direct logistic regression was performed to assess the impact of a number of factors on the likelihood of a good TRG response. The model contained six variables (age, gender, smoking history, ASA grade, clinical T stage, BMI classification). Only BMI classification independently predicted TRG response. Overweight and obese patients were three times more likely to achieve a good TRG response after controlling for all other factors in the model (OR=3.376, 95% CI=1.68-6.784, p=0.002). If data are analysed according to the three-point variation of the Mandard TRG which separates complete (TRG 1), partial i.e. fibrosis predominates (TRG2/3) and minimal i.e. cancer outweighs fibrosis (TRG 4/5), overweight and obese patients were still more likely to achieve a good TRG response compared to normal weight patients (p=0.003).

Table 2.7. Pathological details for normal and overweight/obese patient cohorts

TUMOUR PATHOLOGY	Normal n=53		Overweight & obese n=148		Overall n=201		P value
	n	%	n	%	n	%	
Pathological T Stage							
TiS	0	-	3	2%	3	1%	**0.02**[a]
T0	3	6%	26	18%	29	15%	
T1	6	11%	25	17%	31	16%	
T2	5	9%	26	18%	31	16%	
T3	38	72%	63	43%	101	50%	
T4	1	2%	2	-	3	1%	
Tx	0	-	3	2%	3	%	
Pathological N Stage							
N0	22	42%	77	52%	99	49%	0.20[b]
N1	25	47%	62	42%	87	43%	
N2	4	8%	5	3%	9	4%	
N3	2	4%	2	1%	4	2%	
Nx	0	-	2	1%	2	1%	
Analysed nodes							
Median	15		17		15		0.25[c]
Range	0-41		0-37		0-41		
Residual Tumour							
R0	43	81%	121	82%	164	81%	0.84[d]
R1	10	19%	26	17%	36	18%	
R2	0	-	1	1%	1	1%	
Tumour Regression Grade							
TRG 1	4	8%	28	19%	32	16%	**0.002**[e]
TRG 2	12	23%	38	26%	50	25%	
TRG 3	14	26%	52	35%	66	33%	
TRG 4	19	36%	28	19%	47	23%	
TRG 5	4	8%	2	1%	6	3%	

a=Tis/T0-T2 vs. T3-4, analysed by χ^2 test; b=N0 vs. N1-3, analysed by χ^2 test; c=analysed by unpaired two tailed t test; d=R0 vs. R1-2, analysed by χ^2 test; e=TRG1-3 vs. TRG 4-5 analysed by χ^2 test.

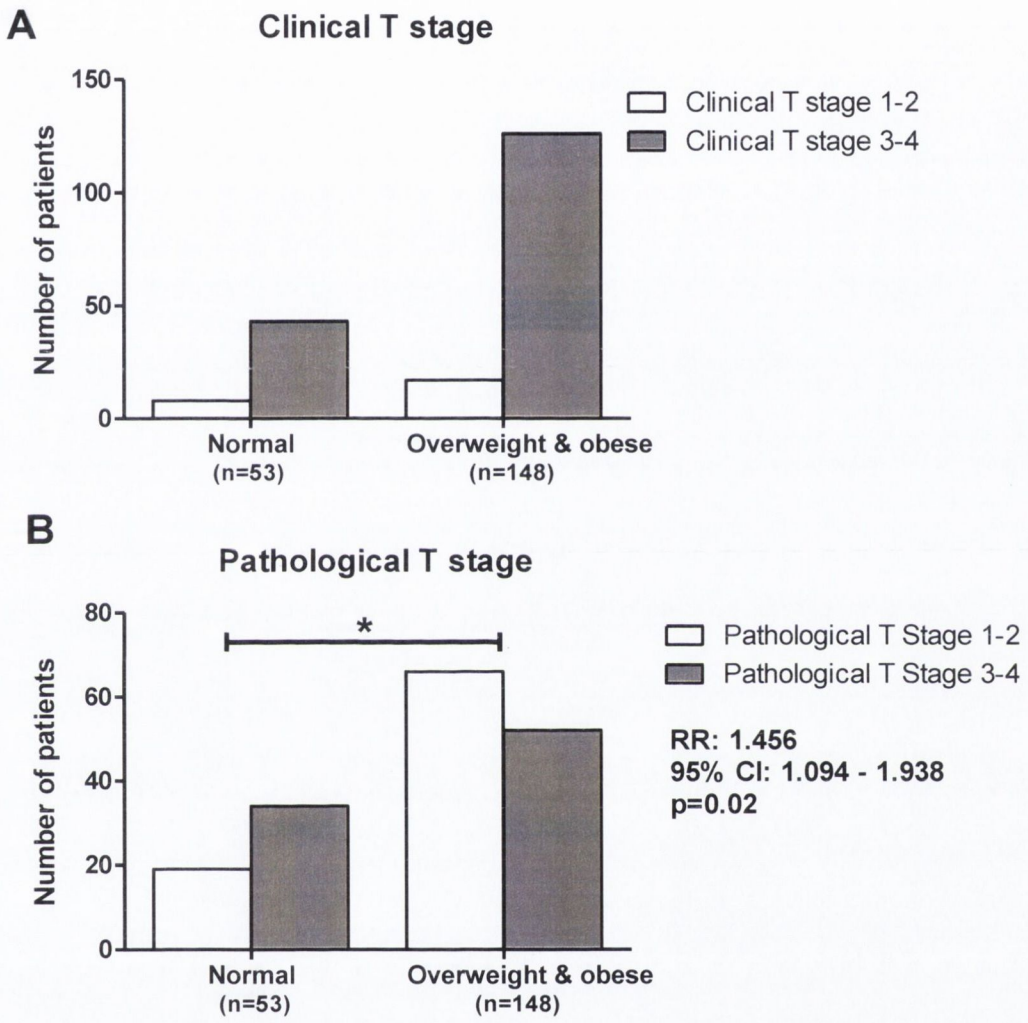


Figure 2.1. Comparison of clinical and pathological T stage in normal and overweight/obese patient cohorts

Comparison of patient cohorts was performed using χ^2 test. A p value of ≤ 0.05 was considered to be statistically significant. *p<0.05; RR=relative risk; 95% CI=95% confidence interval. **(A)** Normal and overweight/obese patients did not differ in terms of clinical T stage. **(B)** However, normal weight patients were more likely to have higher pathological T stage (T stage 3-4) at resection (RR=1.456, 95% CI=1.094-1.938, p=0.02).

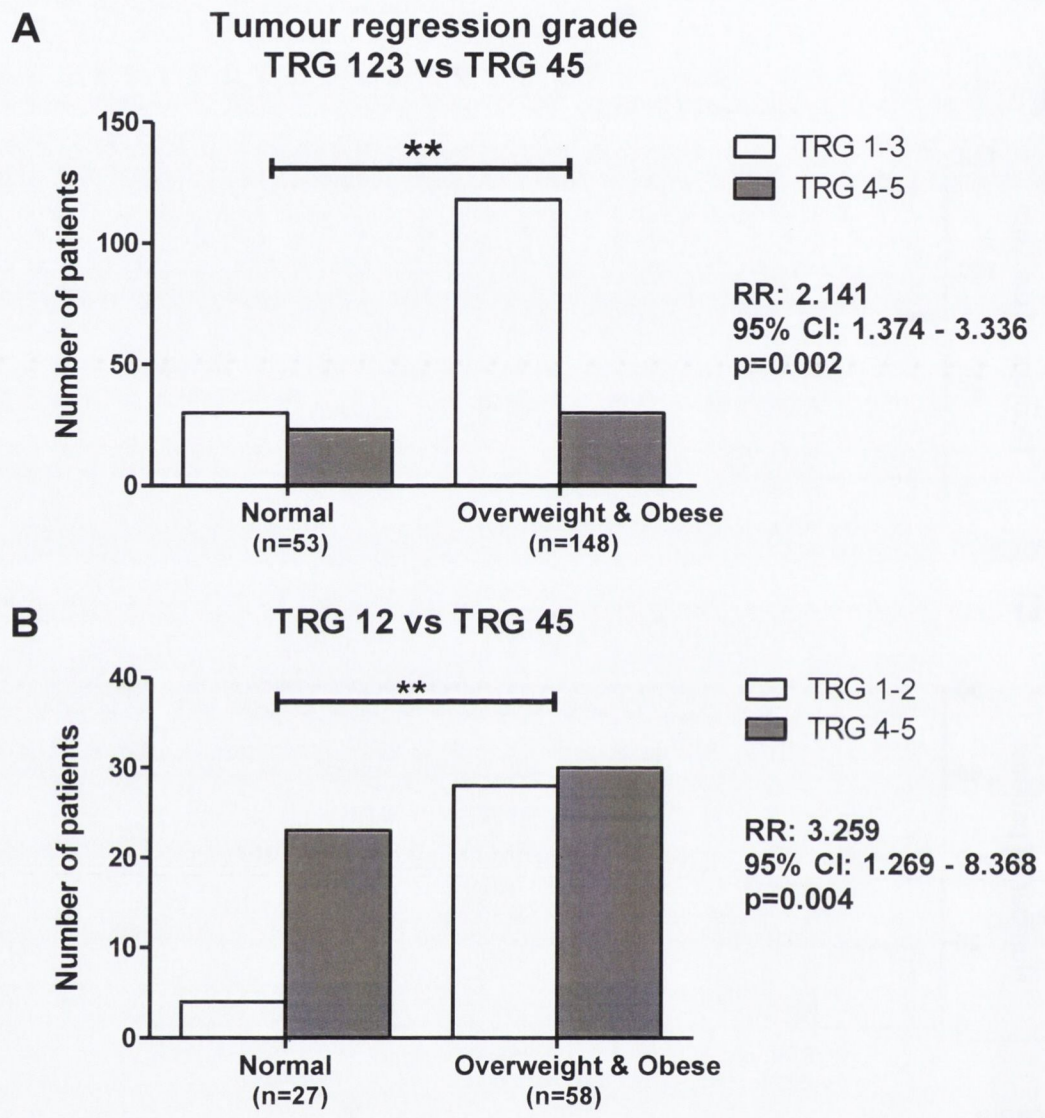


Figure 2.2. Comparison of tumour regression grade following NA CRT in normal and overweight/obese patient cohorts

Comparison of patient cohorts was performed using χ^2 test. A p value of ≤0.05 was considered to be statistically significant. **(A)** Overweight/obese patients were twice as likely to achieve a good (TRG 1-3) response following NA CRT (RR=2.141, 95% CI=1.374-3.336, p=0.002). **(B)** When patients with TRG 3 were excluded from the analysis, overweight/obese patients were three times as likely to achieve a good (TRG 1-2) response following NA CRT (RR=3.259, 95% CI=1.269-8.368, p=0.004). **p<0.001; RR=relative risk; 95% CI=95% confidence interval.

2.4.1.2 Surgical complications

Median time to surgery after diagnosis was 129 days (range 17-250 days) (Table 2.5). Overweight/obese patients had significantly longer time to surgery compared to normal weight patients (Figure 2.3 A). Most patients underwent a stage II oesophagectomy (n=167, 83%). Major postoperative complications (Clavien-Dindo grade III-IV) were detected in 57 patients (28%). Pneumonia represented the most common postoperative complication (n=12, 16%). Seventeen patients (8%) required an exploratory laparotomy postoperatively, and the in-hospital mortality was 7% (n=15). The frequency of postoperative complications did not differ between normal weight and overweight/obese patients, and both cohorts were equally likely to develop major complications (Grade III, IV, V) (Figure 2.3).

2.4.1.3 Recurrence and survival

At a median follow-up of 19 months, recurrence was noted in 118 patients (59%), with median time to recurrence of 9.2 months. Obesity status was not associated with risk of recurrence and did not affect survival (Figure 2.4). Five-year survival was 21% (Table 2.9), with overall median disease-specific survival of 27 months (median survival for normal weight patients was 23 months, overweight/obese median survival was 30 months).

Table 2.8. Surgical resection in normal and overweight/obese patient cohorts

SURGICAL RESECTION	Normal n=53		Overweight & Obese n=148		Overall n=201		P Value
Time to surgery from diagnosis							
Range (days)	17-209		63-250		17-250		**0.03**[a]
Median (days)	122		131		129		
OPERATION PERFORMED							
Stage II oesophagectomy	47	87%	120	81%	167	83%	0.26[b]
Stage III oesophagectomy	5	13%	25	17%	30	14%	
Transhiatal oesophagectomy	0		1	1%	1	1%	
Gastrectomy	0		2	1%	3	2%	
POST-OPERATIVE COMPLICATIONS[#]							
Any complication	35	66%	93	63%	128	64%	0.74[c]
Grade III-IV complications	20	38%	56	38%	57	28%	0.84[c]
Reoperation	5	9%	12	8%	17	8%	
MORTALITY							
In-hospital mortality	3	6%	12	8%	15	7%	0.76[c]
Median DSS (months)	23		30		27		0.88[d]

[#]As per the Clavien-Dindo (CD) classification of surgical complications
DSS=Disease specific survival

Overweight/obese patients had significantly longer time to surgery compared to normal weight patients. Normal weight patients compared to overweight/obese patient cohort did not differ in type of operation performed, postoperative complications or mortality rates.

[a]Analysed using unpaired two tailed t test

[b]Stage II vs. stage III oesophagectomy, analysed by χ^2 test

[c] Analysed by χ^2 test

[d] Analysed by log-rank test

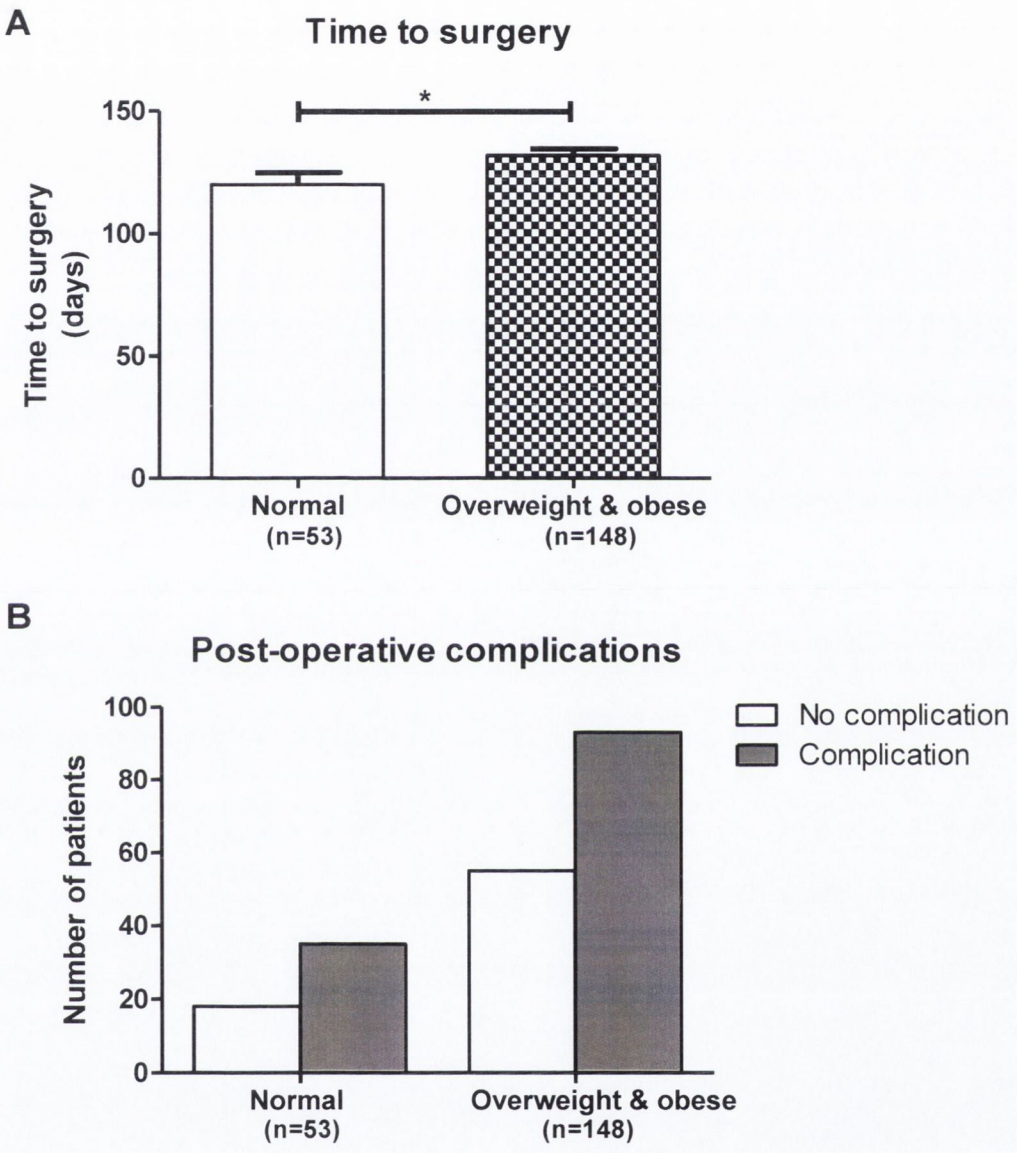


Figure 2.3. Operative outcomes in normal weight and overweight/obese patient cohorts

Comparison of patient cohorts was performed using Mann Whitney U for continuous data and χ^2 test for categorical variables. A p value of ≤ 0.05 was considered to be statistically significant; *$p<0.05$. **(A)** Normal weight patients had statistically shorter time to surgery following NA CRT (median time to surgery 120 days compared to 132 days delay for overweight/obese patients) ($p=0.03$). **(B)** Post-operative complication rates were similar in normal weight and overweight/obese patient cohorts.

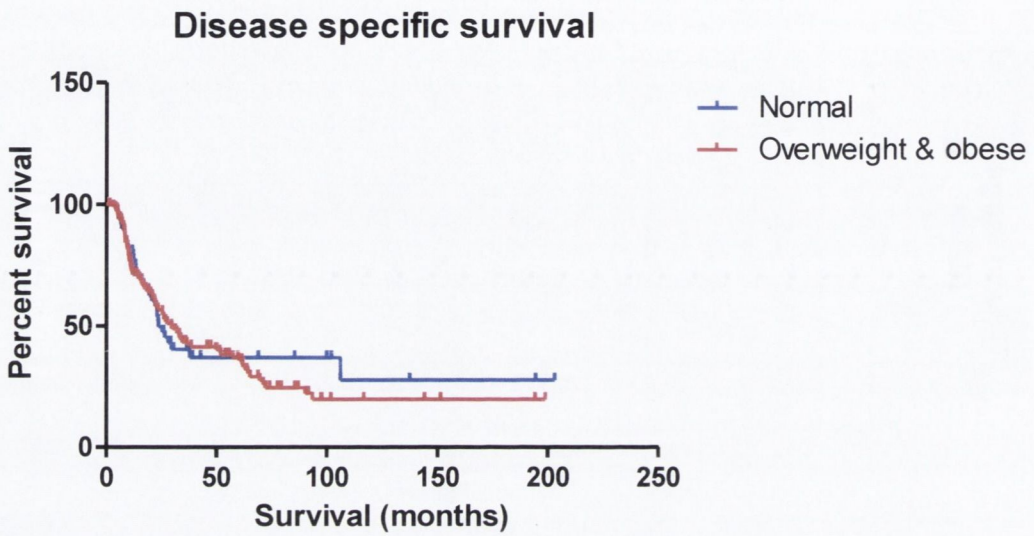


Figure 2.4. Disease specific survival of normal and overweight/obese patient cohorts

Survival was calculated from date of diagnosis to the first event (i.e. death or end of the follow-up period). Survival analysis was performed using Kaplan-Meier curves and log-rank test. There was no statistically significant difference in survival in normal weight compared to overweight/obese patients. Median survival was 23 and 30 months respectively.

Table 2.9. Actuarial life table analysis

OVERALL SURVIVAL (n=201)			
Survival Time	**No. At Risk**	**Deaths**	**Cumulative Survival**
1 year	201	52	72%
2 year	125	28	55%
3 year	83	19	42%
4 year	55	2	41%
5 year	48	16	21%
Median survival 26.8 months			

Overall survival in all patients treated with NA CRT from 1990 to 2013 (n=201). Overall five-year survival was 21%.

2.4.1.4 Recurrence and survival

Therefore, clinically we have shown that while there was no difference in preoperative clinical T stage between normal weight patients and overweight and obese patients, overweight and obese patients were more likely to have a lower pathological T stage at surgery and to achieve a good TRG response (TRG 1-3) at surgery. Obesity status did not influence rates of postoperative morbidity, recurrence or survival. To investigate if obesity did or did not increase radiosensitivity *in vitro,* survival of oesophageal cancer cells following co-culture with adipose conditioned media and irradiation was assessed using clonogenic assay.

2.4.2 Radiosensitivities of oesophageal cancer cell lines and optimisation of radiation seeding densities

Sensitivity to radiation was measured by clonogenic assay using methods described in section 2.3.6. M199 media was used as the control treatment for all clonogenic assays. A critical parameter of the clonogenic assay that can affect colony formation is the density at which cells are initially seeded. At least 100 viable colonies at the end of the clonogenic incubation period are required to ensure statistical accuracy. These colonies should be discrete and not overlapping or they do not provide a reliable result. The optimal cell seeding densities were previously determined for OE33P and OE33R cell lines irradiated with a 2 Gy dose[491]. Clonogenic survival cell seeding densities were optimised for OE33P and OE33R cell lines following treatment with ACM (ensuring that at least 100 viable colonies were present at the end of the clonogenic incubation period). Figure 2.5 shows representative images of clonogenic assays performed on OE33P cells treated with control media and 2 Gy irradiation (IR) (Figure 2.5 A), OE33P cells co-cultured with ACM and irradiated at 2 Gy, (Figure 2.5 B), OE33R cells treated with control media and 2 Gy IR (Figure 2.5 C), and OE33R cells co-cultured with ACM and irradiated at 2 Gy (Figure 2.5 D). OE33P demonstrated decreased survival compared to OE33R cells at baseline (p=0.008) (Figure 2.6).

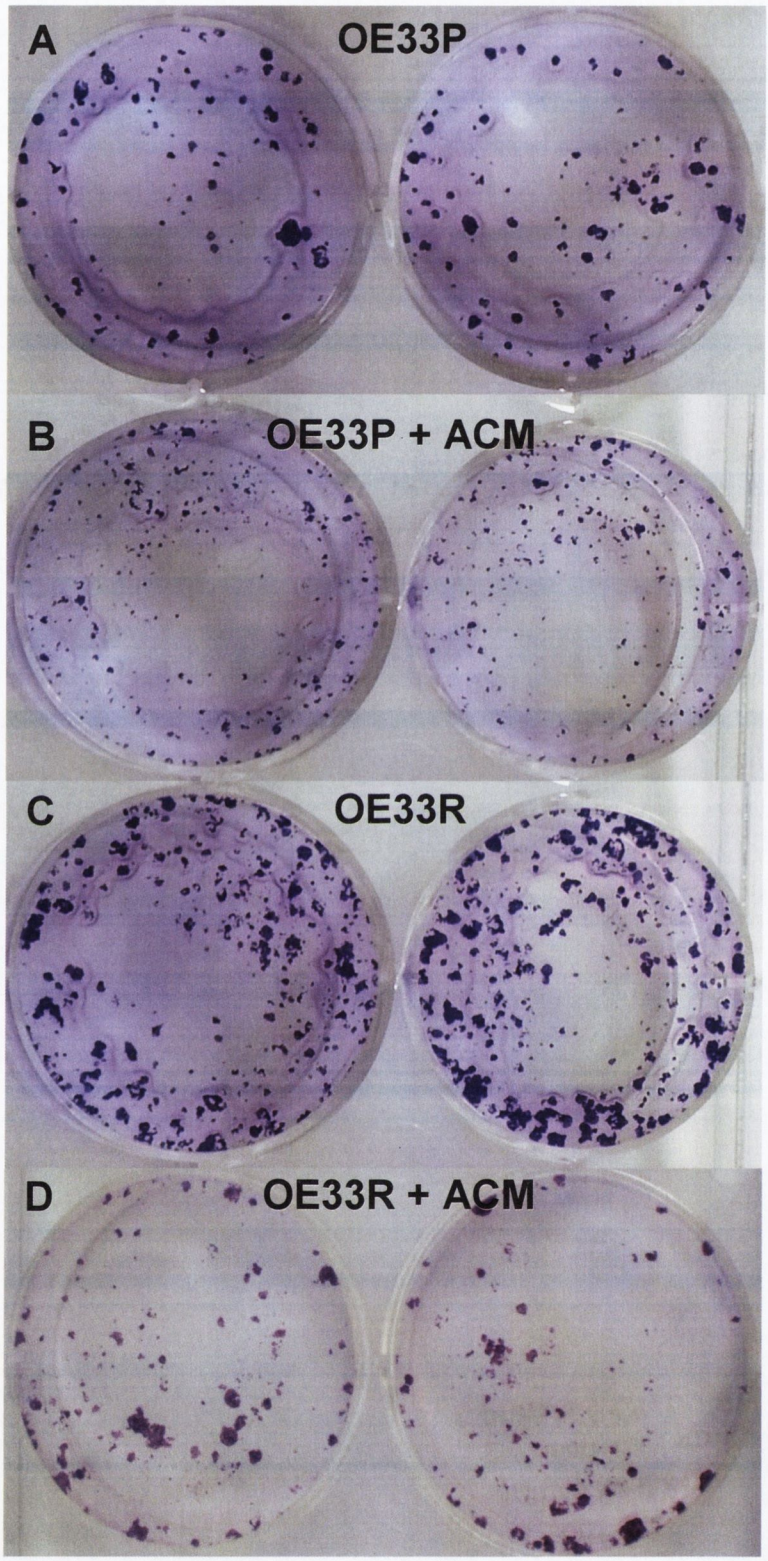


Figure 2.5. Clonogenic assay of OE33P and O33R cells
Representative images of **(A)** OE33P cells treated with 2 Gy irradiation (IR); **(B)** OE33P cells treated with ACM and 2 Gy IR; **(C)** OE33R cells treated with 2 Gy IR and **(D)** OE33R cells treated with ACM and 2 Gy IR.

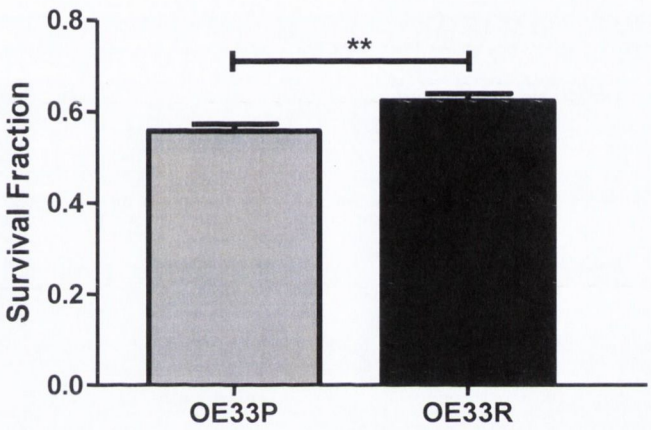


Figure 2.6. OE33P cells are more radioresponsive than OE33R cells

OE33P demonstrated decreased survival compared to OE33R cells at baseline ($p=0.008$). Data are expressed as mean ± SEM. Statistical analysis was performed using unpaired t test comparing ACM treated cells versus control; $^{**}p<0.001$.

2.4.3 Treatment with ACM decreases radioresistance in OE33P and OE33R

OE33P and OE33R cell lines were exposed to 2 Gy IR following treatment with control media or ACM from non-cancer patients (non-cancer cohort, n=5) (Figure 2.7 A, B), ACM from OAC patients who had not undergone NA CRT prior to surgery (surgery only OAC cohort, n=14) (Figure 2.7 C, D), and ACM from OAC patients who received NA CRT therapy prior to surgery (NA CRT OAC cohort, n=10) (Figure 2.7 E, F). Patient characteristics are shown in Table 2.10. Decreased radioresistance was seen in OE33P cells treated with ACM from the non-cancer and surgery only OAC cohort; however this did not reach statistical significance (Figure 2.7 A and C). OE33P cells treated with ACM from the NA CRT OAC cohort demonstrated a statistically significant decrease in radioresistance compared to cells treated with control media ($p=0.009$, Figure 2.7 E).

Decreased radioresistance was detected in OE33R cells following co-culture with ACM from the non-cancer cohort ($p=0.03$, Figure 2.7 B), ACM from the surgery only OAC cohort ($p=0.002$, Figure 2.7 D) and ACM from the NA CRT OAC cohort ($p<0.0001$, Figure 2.6 F). The ACM used in this study was generated from obese and non-obese OAC patients. No difference in survival fraction in OE33P and OE33R cells was seen when ACM from non-obese compared to obese patients was used.

Radiosensitivity was compared in OE33P and OE33R cells treated with ACM from three patient cohorts. There was no difference in survival fraction in OE33P cells treated with ACM from three patient cohorts (Figure 2.8 A). Radioresistance was significantly lower in OE33R cells treated with ACM from NA CRT OAC patients compared to cells treated with ACM from the radiation naïve OAC patient cohort ($p=0.003$) (Figure 2.8 B).

Table 2.10. A-C Anthropometric data for patient ACM used in clonogenic assays

A Non-cancer cohort (n=5)

Patient	Age	Gender	BMI (kg/m^2)	WC (cm)	VFA (cm^2)
1	60	Female	23.0	79	94.5
2	61	Female	29.4	89	212.4
3	44	Female	29.1	105	264.4
4	47	Female	37.3	121	236.9
5	64	Female	37.9	112	

B Surgery only OAC cohort (n=14)

Patient	Age	Gender	BMI (kg/m^2)	WC (cm)	VFA (cm^2)
1	60	Female	25.4	86	73.7
2	44	Male	22.4	79	34.1
3	52	Male	23.5	90	109
4	69	Female	21.5	76	25.2
5	61	Female	29.8	91	124.2
6	47	Male	33.4	118	345.2
7	64	Male	26.8	95	235.1
8	67	Male	27.2	102	216.8
9	62	Male	33.8	126	383.8
10	71	Male	22.9	88	227.0
11	68	Female	42.6	129	299.3
12	59	Male	26.3	94	217.1
13	60	Male	32.9	NS	221.7
14	69	Male	27.6	97	165.5

C NA CRT OAC cohort (n=10)

Patient	Age	Gender	BMI (kg/m^2)	WC (cm)	VFA (cm^2)
1	58	Male	20.6	80	30.8
2	63	Male		83	34.7
3	58	Male	28.0	74	91.0
4	55	Male	24.4	81	120.2
5	76	Male	30.7	114	354.6
6	51	Male	30.6	112	210.6
7	72	Male	27.9	97	228.8
8	62	Male	30.9	94	237.4
9	69	Male	30.2	101	280.8
10	63	Male	32.7	106	247.45

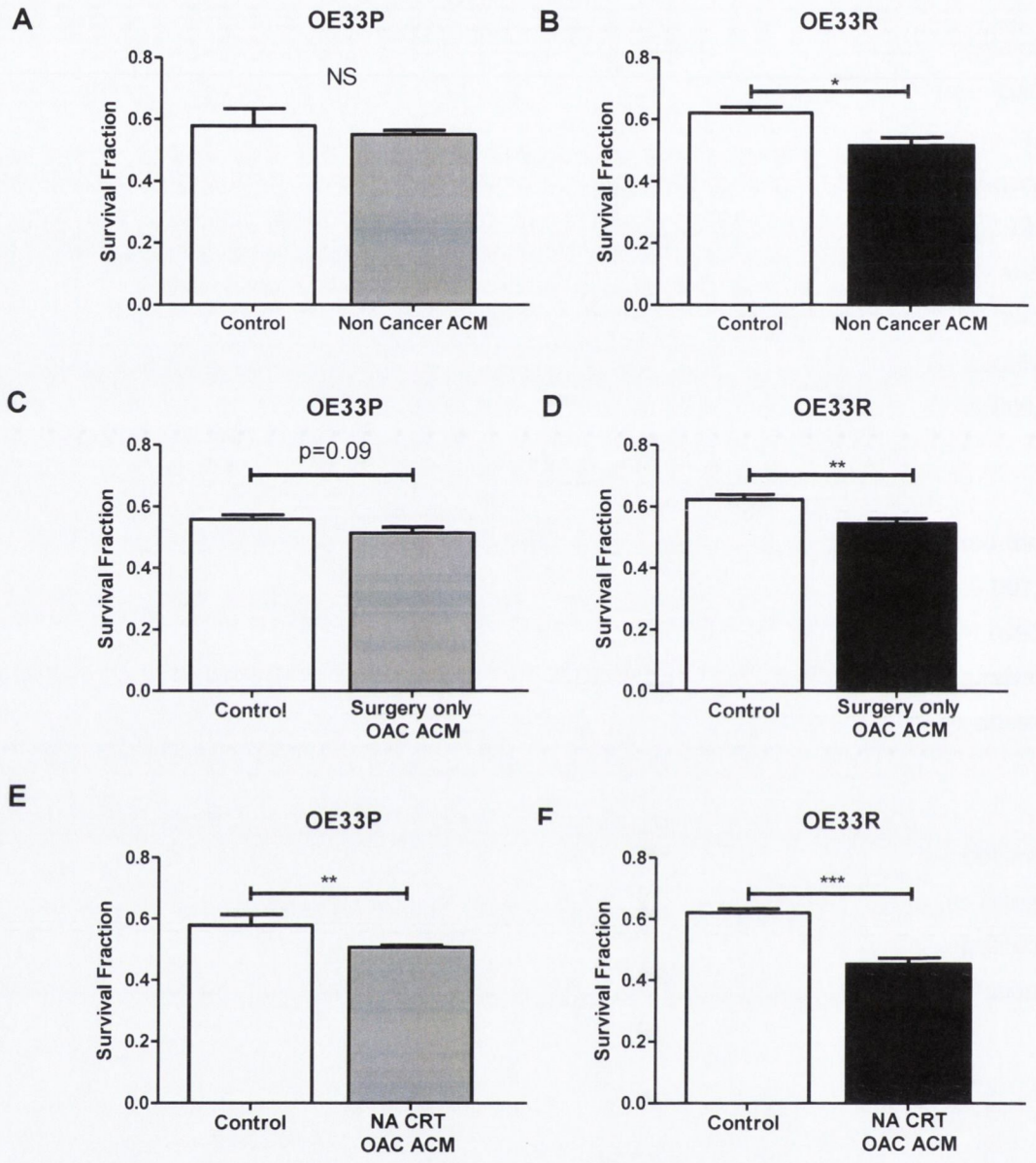


Figure 2.7. ACM treatment decreases radioresistance in OE33P and OE33R
OE33P and OE33R cells were treated ACM from three patient cohorts (non-cancer cohort n=5, surgery only OAC cohort n=18, and NA CRT OAC cohort n=14). Data are expressed as mean ± SEM. Statistical analysis was performed using unpaired two tailed t test; *p<0.05, **p<0.001, ***p<0.0001, *NS*=not significant. **(A)** Co-culture of OE33P cells with ACM from non-cancer patients did not significantly alter radioresistance. **(B)** Co-culture of OE33R cells with ACM from non-cancer patients resulted in decreased radioresistance (p=0.03) **(C)** OE33P cells co-cultured with ACM from surgery only OAC patients did not demonstrate significantly altered radioresistance. **(D)** OE33R cells co-cultured with ACM from surgery only OAC patients demonstrated decreased radioresistance (p=0.002). **(E)** Treatment with ACM from irradiated OAC patients resulted in decreased radioresistance (p=0.009). **(F)** OE33R cells treated with ACM from non-cancer patients demonstrated decreased radioresistance (p<0.0001).

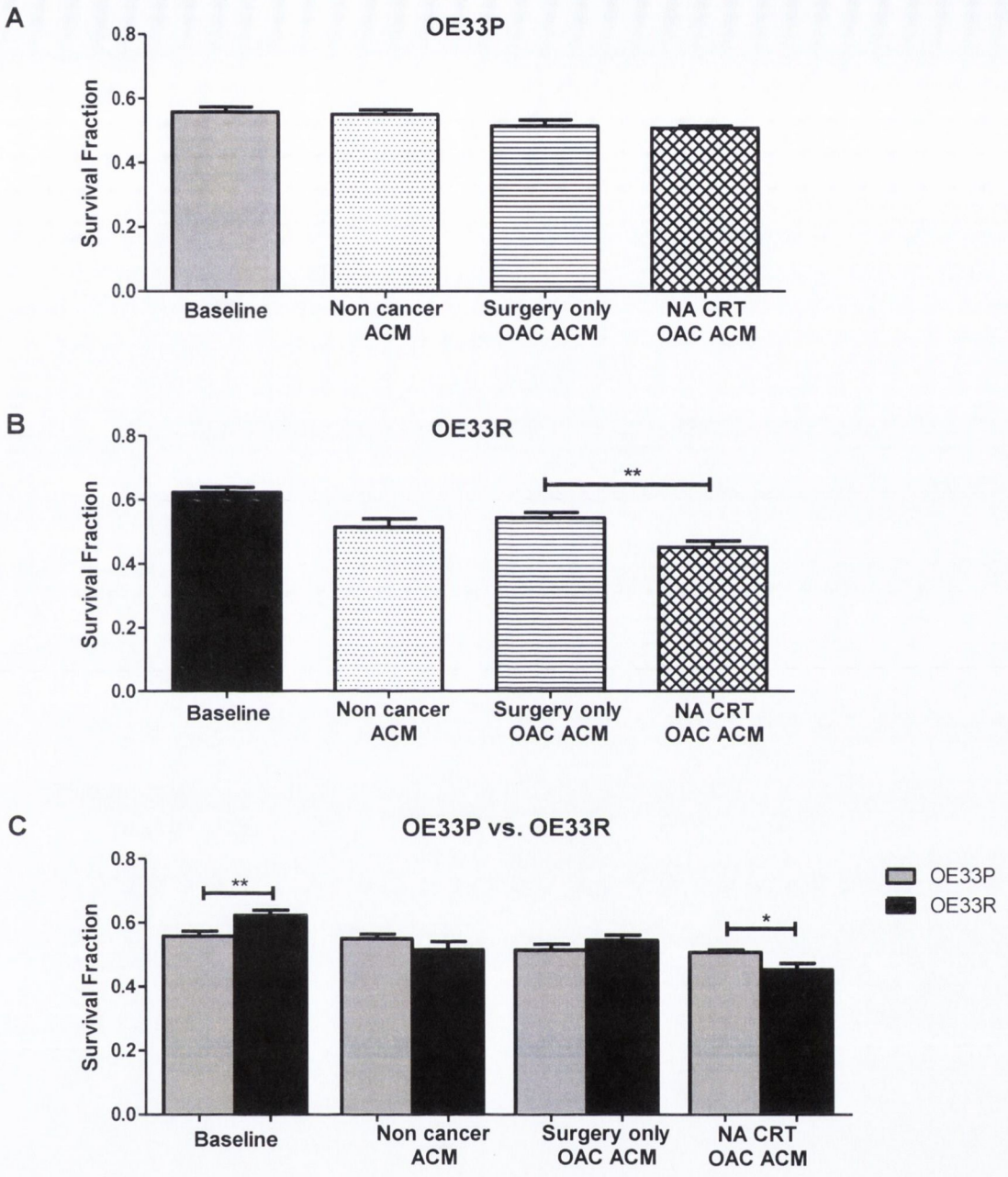


Figure 2.8. Comparison of the effect of ACM from three patient cohorts on radiosensitivity of OE33P and OE33R

Data are expressed as mean ± SEM. Statistical analysis was performed using one-way ANOVA with Tukey *post-hoc* correction; *p<0.05, **p<0.001. **(A)** There was no difference in survival fraction in OE33P cells treated with ACM from three patient cohorts. **(B)** OE33R cells treated with ACM from NA CRT OAC patients showed decreased radioresistance compared to cells treated with ACM from surgery only OAC patients (p=0.003). **(C)** Following treatment with ACM from non-cancer and surgery only OAC patients, there was no difference in survival fraction in OE33P compared to OE33R cells. Following co-culture with ACM from NA CRT OAC patients, OE33P cells demonstrated higher radioresistance compared to OE33R cells.

2.4.4 ACM treatment alters cell cycle kinetics in OE33P and OE33R cells

Cell cycle position affects radiosensitivity, however the effect of ACM on cell cycle progression is unknown. Cells in the G_2/M phase are most sensitive to radiation, while cells in S phase are most resistant[148]. Cell cycle distribution was analysed in OE33P and OE33R cells following co-culture with control media or ACM from three obese OAC patients (patient data shown in Table 2.11). OE33P cells treated with ACM had a lower proportion of cells in the more radioresistant S phase compared to cells treated with control media ($p=0.05$) (Figure 2.9). OE33R cells treated with ACM had a lower proportion of cells in the more radioresistant S phase ($p=0.05$), but a higher proportion of cells in G_0/G_1 phase ($p=0.05$) (Figure 2.10). While statistically significant, the magnitude of the difference in cell cycle distribution between control and ACM-treated cells is small, and unlikely to account for the difference in radiosensitivity between treated and untreated cells.

OE33P cells treated with ACM had a higher proportion of cells in S phase compared to ACM-treated OE33R cells ($p=0.004$), and a lower proportion of cells in G_0/G_1 phase ($p=0.002$). There was no difference in the proportion of cells in G_2/M phase in OE33P compared to OE33R cells following ACM treatment.

Table 2.11. Anthropometric data for patient ACM used in cell cycle analysis

Patient	Age	Gender	BMI (kg/m^2)	WC (cm)	VFA (cm^2)	Neoadjuvant CRT
1	42	Male	31.2	106.0	172.0	No
2	69	Male	27.6	97.0	165.5	No
3	67	Male	30.5	98.0	185.4	No

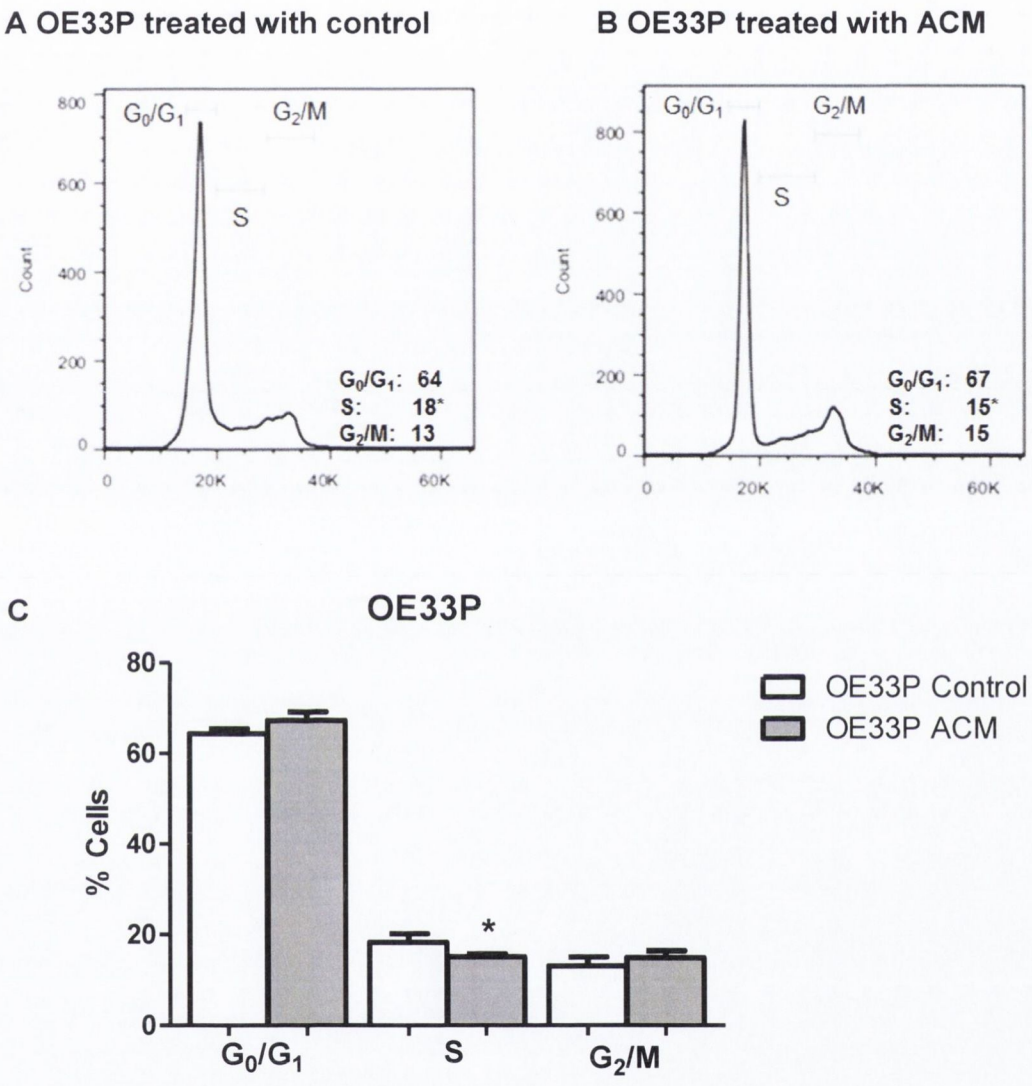


Figure 2.9. Cell cycle kinetics in OE33P following ACM treatment

Cell cycle analysis was performed by PI staining and flow cytometry. **(A)** Cell cycle analysis of OE33P cells treated with control media. **(B)** Cell cycle analysis of OE33P cells treated with ACM. **(C)** A greater percentage of OE33P cells was observed in S phase following treatment with M199 control media when compared to OE33P cells treated with ACM ($p=0.05$). Data are expressed as mean ± SEM. Statistical analysis was performed using unpaired student t test; *$p<0.05$.

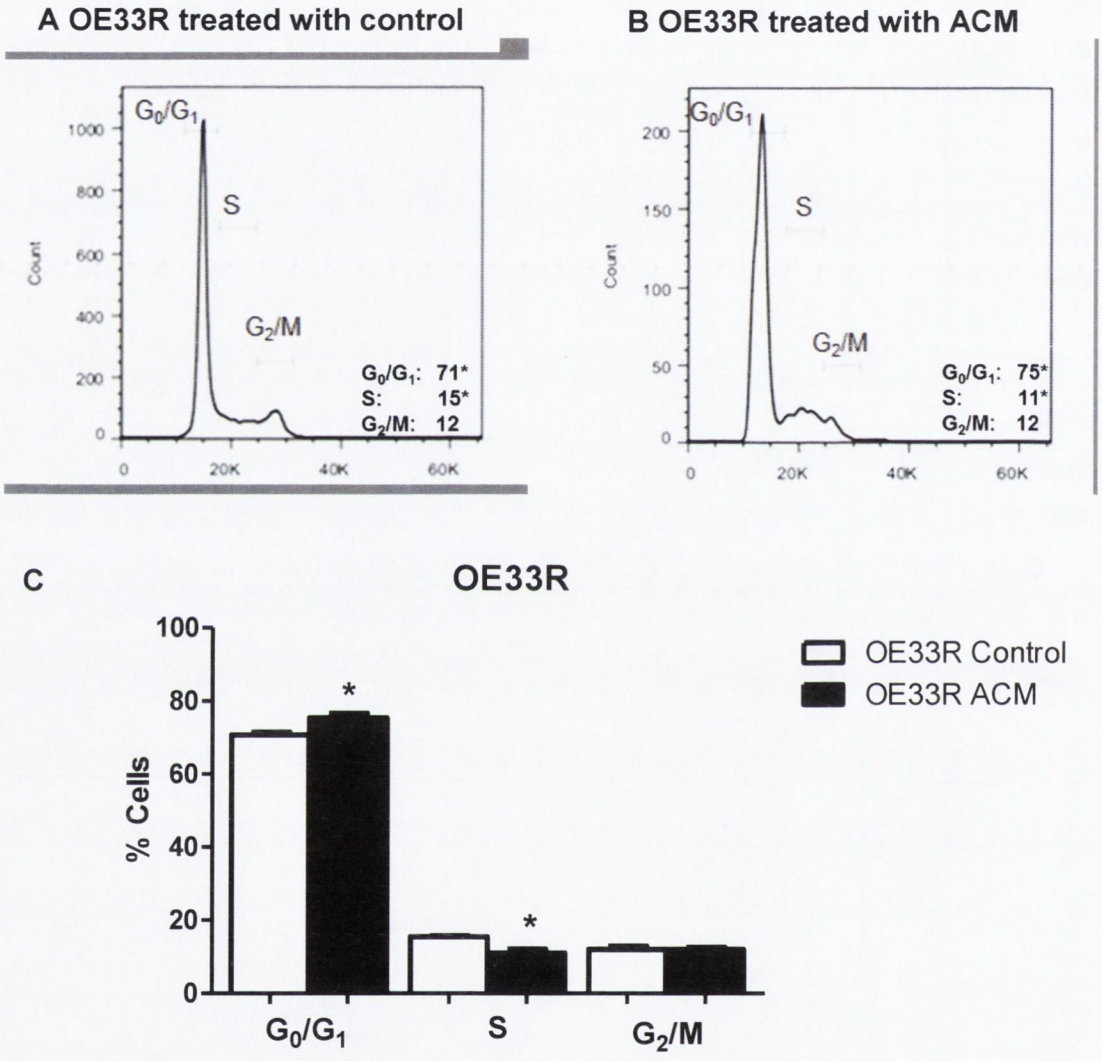


Figure 2.10. Cell cycle kinetics in OE33R following ACM treatment
Flow cytometry cell cycle analysis demonstrating cell cycle distribution of OE33R cells treated with **(A)** M199 control media and **(B)** ACM. **(C)** OE33R cells treated with ACM demonstrated a lower proportion of cells in the more radioresistant S phase ($p=0.04$), but a higher proportion of cells in the G_0/G_1 phase ($p=0.05$). Data are expressed as mean ± SEM. Statistical analysis was performed using unpaired student t test; *$p<0.05$.

2.4.5 ACM treatment alters AR1 and NRP1 expression

Cell cycle distribution did not explain the alteration in radiosensitivity induced by ACM. Therefore, we examined the role of adipokines in the ACM. ACM treatment of OE33P and OE33R reduced radioresistance to a greater degree in OE33R compared to OE33P cells. OE33P and OE33R cells were treated with ACM generated from the same patients, therefore heterogeneity in ACM composition did not explain the difference detected. We speculated that the different response seen in OE33P compared to OE33R cells might be attributable to alterations in adipokine receptor expression between OE33P and OE33R. Expression of a panel of four adipokine receptors representing abundant adipokines in non-obese and obese visceral ACM was assessed in OE33P and OE33R cell lines at baseline and following co-culture with ACM for 24 hours. We investigated the expression of adiponectin receptor 1 (AR1); adiponectin receptor 2 (AR2); leptin receptor (LepR); and the VEGF receptor neuropilin-1 (NRP1). ACM was generated from obese and non-obese OAC patients, and anthropometric characteristics of patients are summarised in Table 2.12.

There was a significant 2-fold downregulation in AR1 expression in OE33P cells following 24 hours of ACM treatment compared to cells treated with control media ($p=0.02$). ACM treatment did not alter AR1 expression in OE33R (Figure 2.11 A). AR2 expression following ACM treatment was not altered in OE33P or OE33R (Figure 2.11 B). Expression of AR1 and AR2 in OE33P and OE33R did not differ following treatment with ACM generated from non-obese compared to obese patients or following treatment with ACM from patients treated with surgery only compared to patients who underwent NA CRT. LepR expression following ACM treatment was not altered in OE33P or OE33R (Figure 2.11 C). However, LepR expression in OE33P cells following treatment with ACM from patients who underwent NA CRT was increased two-fold compared to controls ($p=0.05$), and was significantly higher compared with OE33P cells treated with ACM from surgery only patients ($p=0.02$). LepR expression in ACM-treated OE33R cells was not influenced by obesity status or treatment status of the patient ACM. ACM induced a 13-fold upregulation in NRP1 expression in OE33P cells ($p=0.05$), but did not alter NRP1 expression in OE33R cells (Figure 2.11 D). Expression of NRP1 in OE33P and OE33R did not differ following treatment with ACM generated from non-obese compared to obese patients or following treatment with ACM from patients treated with surgery only compared to patients who underwent NA CRT.

Table 2.12. Patient cohort details (ACM used in adipokine receptor gene expression and genomic instability *in vitro* experiments).

Patient	Age	Gender	Body Mass Index (kg/m^2)	Waist Circumference (cm)	Visceral Fat Area (cm^2)
1	68	Male	25	95	127.5
2	58	Male	-	-	83.0
3	50	Male	23.2	94	87.6
4	46	Male	-	100.3	17.0
5	58	Male	20.6	80	30.8
6	68	Male	28.8	104	284.8
7	72	Male	30.1	106.7	240.6
8	67	Male	27.2	102	216.8
9	62	Male	33.8	126	383.8
10	71	Male	22.9	88	227.0

Anthropometric data for patient ACM used in adipokine receptor gene expression studies, telomere length measurement, telomerase and shelterin gene expression studies, anaphase bridge enumeration and SAC gene expression studies.

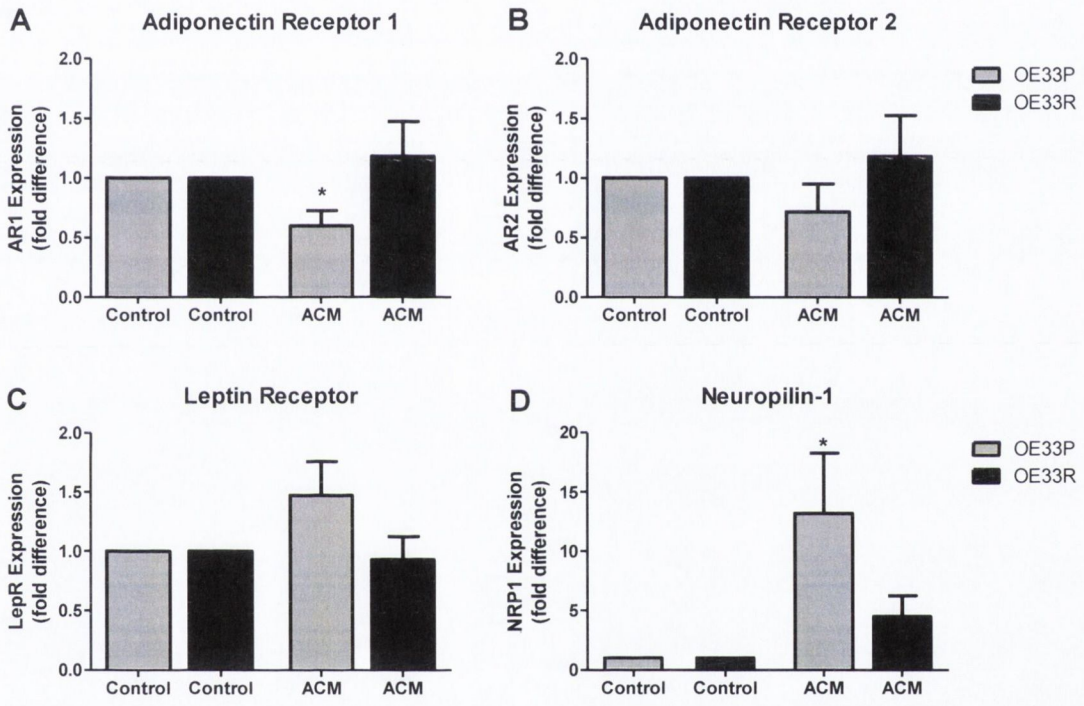


Figure 2.11. The effect of ACM on adipokine receptor expression
OE33P and OE33R cells were co-cultured with ACM from ten OAC patients. Data are expressed as mean ± SEM. Statistical analysis was performed using paired two-tailed student's *t*-test to compare ACM treated cells versus control; *p<0.05. **(A)** ACM induced a two-fold downregulation in AR1 expression in OE33P cells (p=0.008), but did not alter AR1 expression in OE33R. **(B)** No significant difference in AR2 expression was seen in OE33P or OE33R cells treated with ACM for 24 hours. **(C)** ACM treatment did not alter LepR expression in OE33P or OE33R. **(D)** ACM upregulated NRP1 expression in OE33P cells 13-fold (p=0.05), however NRP1 expression in OE33R cells was not altered following ACM treatment.

2.4.6 Adipokine receptor expression is influenced by radiosensitivity status

Adipokine receptor expression in OE33P cells at baseline and following ACM treatment was compared to adipokine receptor expression in OE33R cells (Table 2.10). Expression of AR1 and AR2 was significantly higher in OE33P cells compared to OE33R cells at baseline ($p=0.0008$ and $p=0.02$ respectively) (Figure 2.12 A, B). Expression of AR1 and AR2 following ACM treatment was not different between OE33P and OE33R. In contrast, levels of LepR and NRP1 were significantly lower in OE33P cells compared to OE33R cells ($p=0.002$, and $p=0.04$ respectively) (Figure 2.12 C, D). Expression of NRP1 following ACM treatment was not different between OE33P and OE33R, however, expression of LepR was higher in OE33R cells compared to OE33P cells following ACM treatment ($p=0.0004$) (Figure 2.13).

2.4.7 Adipokine receptor expression changed during the generation of the radioresistant OE33R line

Expression of four adipokine receptors (AR1, AR2, LepR, NRP1) was assessed across a sequence of increasing passage OE33R sublines (OE33R-4, OE33R-8, OE33R-19) representing sequential stages in the generation of the resistant cell line (Figure 2.14). OE33P and OE33R are plotted for reference. Increasing expression of AR1, AR2 and LepR is seen across the sequence, while decreasing expression of NRP1 is seen across the sequence.

Table 2.13. Adipokine receptor expression in OE33P compared to OE33R cells

	AR1	AR2	LepR	NRP1
OE33P vs. OE33R Baseline (Relative RQ)	**0.9 vs. 0.5**	**0.9 vs. 0.5**	**1.3 vs. 7**	**1.3 vs. 2.8**
p value	***0.008***	***0.02***	***0.002***	***0.04***
OE33P vs. OE33R 24hr ACM (Fold change)	-1.8 vs. 1.2	-1.6 vs. 1.2	1.5. vs. -1.1	13 vs. 4.5
p value	*0.10*	*0.30*	*0.24*	*0.18*

AR1 and AR2 gene expression was significantly higher in OE33P compared to OE33R cells, while LepR and NRP1 gene expression was significantly lower in OE33P compared to OE33R cells at baseline. Expression of the four adipose receptor genes AR1, AR2, LepR and NRP1 did not differ in ACM treated OE33P cells compared to ACM treated OE33R cells. Data are expressed as mean fold change in expression. Values highlighted in bold represent statistically significant alterations in gene expression. Statistical analysis was performed using unpaired two-tailed student's t test.

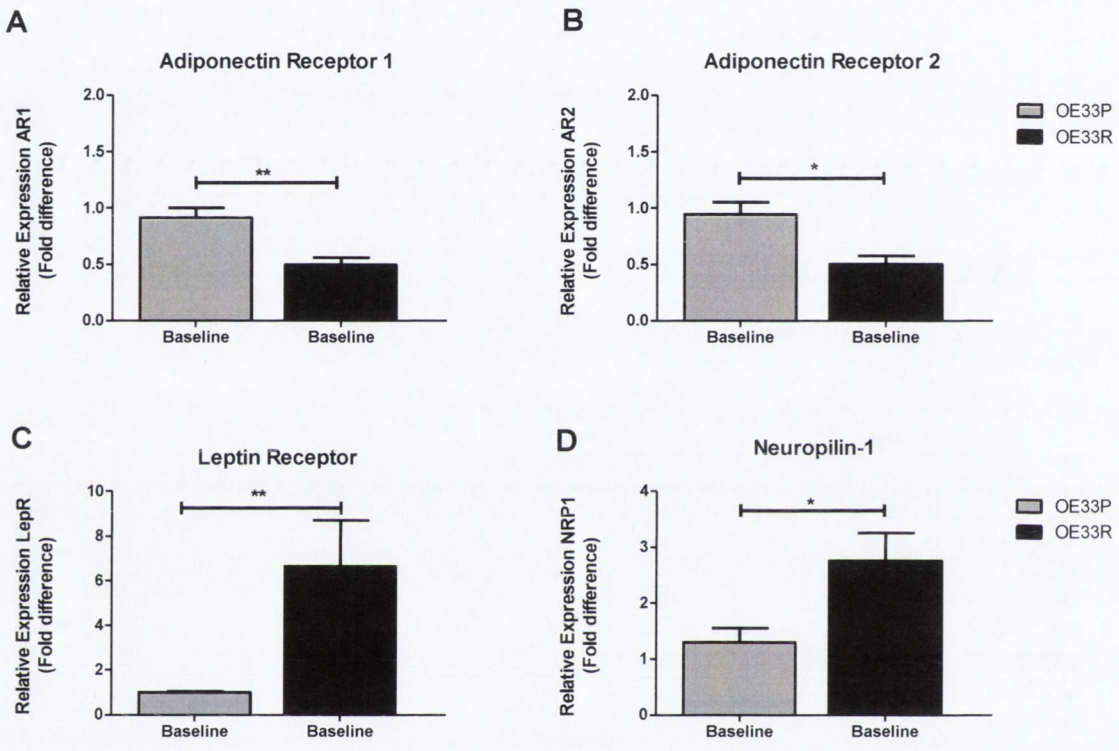


Figure 2.12. Adipokine receptor expression in OE33P compared to OE33R
Expression of a panel of adipokine receptors was assessed in OE33P and OE33R cell lines using qPCR. Data are expressed as mean ± SEM. Statistical analysis was performed using unpaired two tailed student's t test; *$p<0.05$, **$p<0.001$. **(A)** Expression of AR1 was significantly higher in OE33P compared to OE33R ($p=0.008$). **(B)** Similarly, AR2 expression was higher in OE33P compared to OE33R ($p=0.02$). **(C)** LepR expression was lower in OE33P compared to OE33R ($p=0.002$). **(D)** NRP1 expression was significantly lower in OE33P compared to OE33R ($p=0.04$).

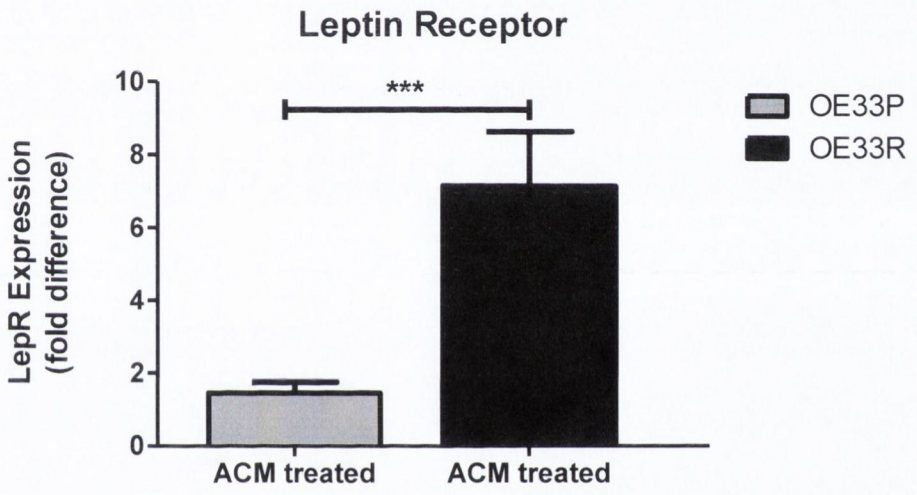


Figure 2.13. LepR expression is greater in ACM treated OE33R compared to ACM treated OE33P cells

Data are expressed as mean fold change in expression ± SEM. Statistical analysis was performed using unpaired two-tailed student's *t*-test; ***p<0.0001. Expression of LepR was higher in OE33R cells compared to OE33P cells following ACM treatment (p=0.0004).

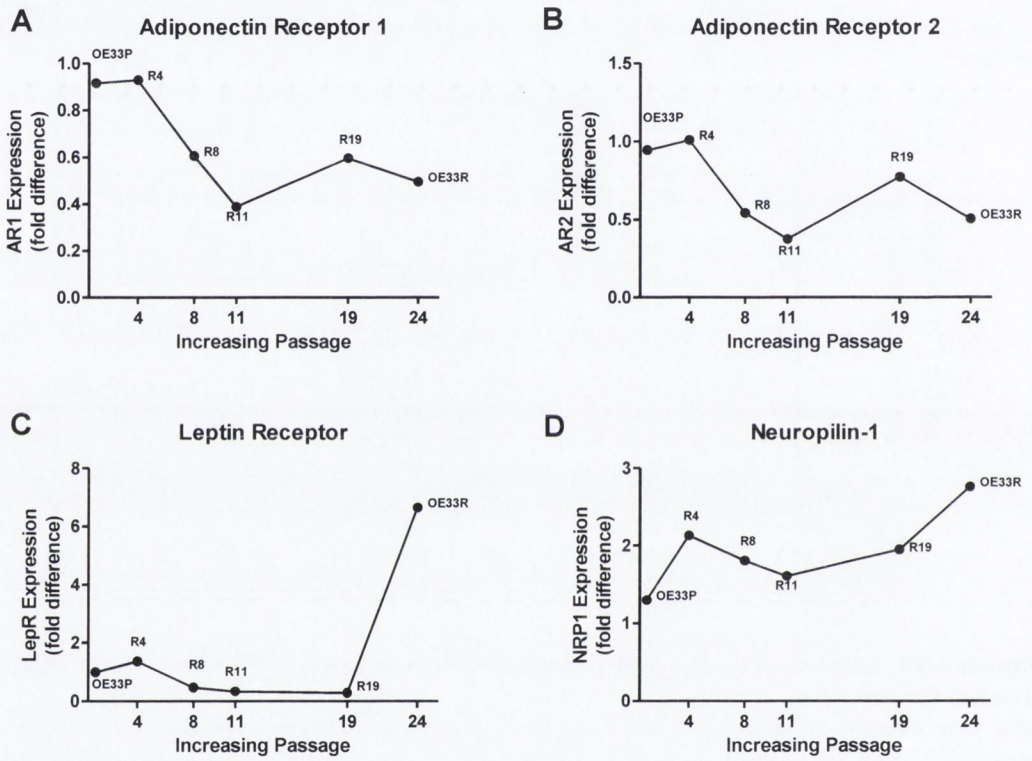


Figure 2.14. Expression of adipokine receptors across a sequence of increasing passage OE33 cell lines during generation of the radioresistant OE33R cell line

Expression of a panel of four adipokine receptors was assessed across a sequence of increasing passage OE33 cells (OE33P, OE33R-4, OE33R-8, OE33R-19, OE33R) representing sequential stages in the generation of the resistant cell line. OE33P and OE33R are plotted for reference.

2.4.8 Adipokine receptor expression in responder and non-responder patient cohort

Expression of AR1, AR2, LepR and NRP was determined in oesophageal adenocarcinoma pre-treatment biopsy samples from patients who had a good TRG response (TRG 1-3, responder) and poor TRG response (TRG 4-5, non-responder) at resection (patient details are outlined in table 2.14). There was increased expression of AR1 and AR2 in responder compared to non-responder patients but this did not reach statistical significance ($p=0.40$ and $p=0.70$ respectively) (Figure 2.15 A, B). There was lower expression of LepR and NRP1 in responder compared to non-responder patients, but this did not reach statistical significance ($p=0.43$ and $p=0.12$ respectively) (Figure 2.15 C, D).

Table 2.14. Characteristics of responder and non-responder OAC patients.

	Responder TRG 1-3 n=11	Non-responder TRG 4-5 n=19	p Value
Age at surgery (years)*	64 (53-67)	61 (44-70)	NS[a]
Gender			NS[b]
Male	9	15	
Female	2	5	
Obesity Status			
Body mass index (kg/m^2)*	29.1 (19.8-31.1)	27.3 (19.5-40.5)	NS[a]
Waist circumference (cm)*	97.5 (90-121)	92 (77-114)	NS[a]
Visceral fat area (cm)*	183.5 (84-338.5)	141 (42.8-283.7)	NS[a]
Pathological T Stage			0.001[c]
Tis	0	0	
T0	5	0	
T1	2	0	
T2	1	3	
T3	2	15	
T4	0	1	
Tx	1	0	
Nodal status			0.007[d]
Node negative	9	5	
Node positive	2	14	

*Values given are median (range); NS=Not significant; a=Analysis performed using Mann Whitney U test; b=Analysis performed using Fisher's exact test; c=Pathological T stage 0-2 compared to pathological T stage 3-4, RR=4.2, 95% CI=1.2-14.8; d=Analysis performed using Fisher's exact test, RR=4.1, 95% CI=1.1-14.6.

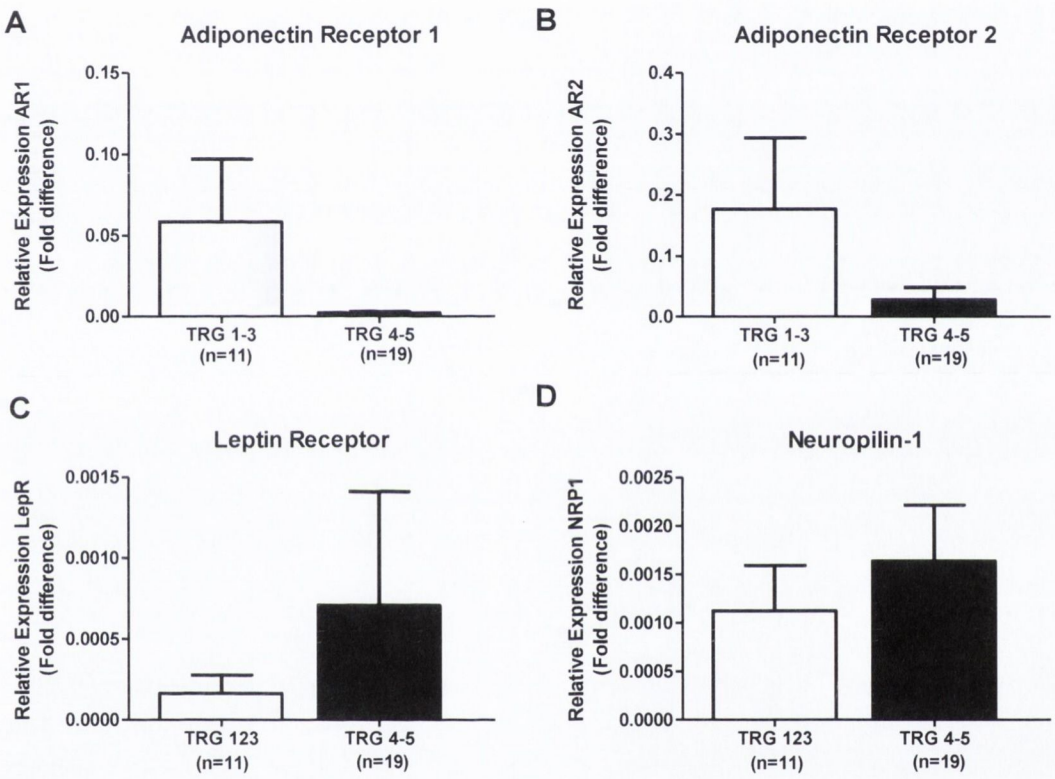


Figure 2.15. Adipokine receptor expression in responder and non-responder OAC patients

Adipokine receptor expression was determined in pre-treatment OAC tumour biopsy samples from responder (n=11) and non-responder (n=19) patients using quantitative real-time PCR. Data are expressed as mean ± SEM. Statistical analysis was performed using Mann-Whitney U test. There was no statistically significant difference in expression of **(A)** Adiponectin receptor 1 **(B)** Adiponectin receptor 2, **(C)** Leptin receptor and **(D)** Neuropilin-1 in pre-treatment biopsy tumour samples from responder patients compared to biopsy samples from non-responder patients.

2.4.9 Metabolomic profile of ACM from non-cancer compared to OAC patients

We hypothesised that adipokines in ACM may influence the radioresponse, and showed that adipokine receptor expression differed in OE33P compared to OE33R cells. In this section, we investigate the metabolomic profile of ACM from non-cancer patients and OAC patients using nuclear magnetic resonance spectroscopy (NMR). Anthropometric details are outlined in Tables 2.15, 2.16 and 2.17.

The initial principal components analysis (PCA) of ^{1}H NMR ACM data showed one outlying sample: the NMR spectra were inspected, and it was noted that the spectrum was of poor quality and as a result, this sample was removed from further analysis. A representative PCA plot that showed separation on the basis of the three patient cohorts (non-cancer, surgery only OAC, NA CRT OAC) is depicted in Figure 2.18A. To investigate this further, a partial least-squares discriminant analysis (PLS-DA) model was constructed (Figure 2.18 B). Separation of the three patient cohorts was seen, but the Q^2 value indicated that the model was weak. Therefore pairwise PCA plots were constructed comparing non cancer ACM with surgery only OAC ACM (Figure 2.19), and non-cancer ACM with NA CRT OAC ACM (Figure 2.20).

Two robust models were built when comparing ACM profiles of different patient cohorts. Representative PCA plots showing separation on the basis of two patient cohorts (non-cancer versus surgery only OAC patients, and non-cancer versus NA CRT OAC patients) are depicted in Figure 2.19A and 2.20A. To investigate this further, pairwise PLS-DA models were constructed (Figure 2.19B, 2.20B). Analysis of the VIP values revealed the metabolites responsible for the separation of non-cancer and surgery only OAC cohorts (Table 2.18). The most discriminating metabolites included lactate, threonine, glucose, lysine and valine. Concentrations of lactate, threonine, lysine and valine were significantly higher in the ACM of surgery only OAC patients, whereas glucose was significantly higher in the ACM of non-cancer patients (Table 2.18). The metabolites responsible for the separation of non-cancer and NA CRT OAC cohorts are listed in Table 2.19 and included threonine, glucose, lysine, valine and isoleucine. Concentrations of threonine, lysine, valine and isoleucine were significantly higher in the ACM of NA CRT OAC patients, whereas glucose was significantly higher in the ACM of non-cancer patients.

A representative PCA plot showing separation of the surgery only OAC and NA CRT OAC cohorts is depicted in Figure 2.19 A. To investigate this further, a PLS-DA model was constructed (Figure 2.19 B). Separation of the two patient cohorts was seen, but the Q^2 value indicated that the model was weak.

Table 2.15. Anthropometric details of non-cancer patients

Patient	Age	Gender	BMI (kg/m^2)	WC (cm)	VFA (cm^2)
1	58	Male	20.6	80	30.8
2	51	Male	30.6	112	210.6
3	72	Male	27.9	97	228.8
4	62	Male	30.9	94	237.4
5	69	Male	30.2	101	280.8
6	63	Male	32.7	106	247.45

Table 2.16. Anthropometric details of surgery only OAC patients

Patient	Age	Gender	BMI (kg/m^2)	WC (cm)	VFA (cm^2)
1	58	Male	20.6	80	30.8
2	51	Male	30.6	112	210.6
3	72	Male	27.9	97	228.8
4	62	Male	30.9	94	237.4
5	69	Male	30.2	101	280.8
6	63	Male	32.7	106	247.45

Table 2.17. Anthropometric details of NA CRT OAC patients

Patient	Age	Gender	BMI (kg/m^2)	WC (cm)	VFA (cm^2)
1	58	Male	20.6	80	30.8
2	51	Male	30.6	112	210.6
3	72	Male	27.9	97	228.8
4	62	Male	30.9	94	237.4
5	69	Male	30.2	101	280.8
6	63	Male	32.7	106	247.45

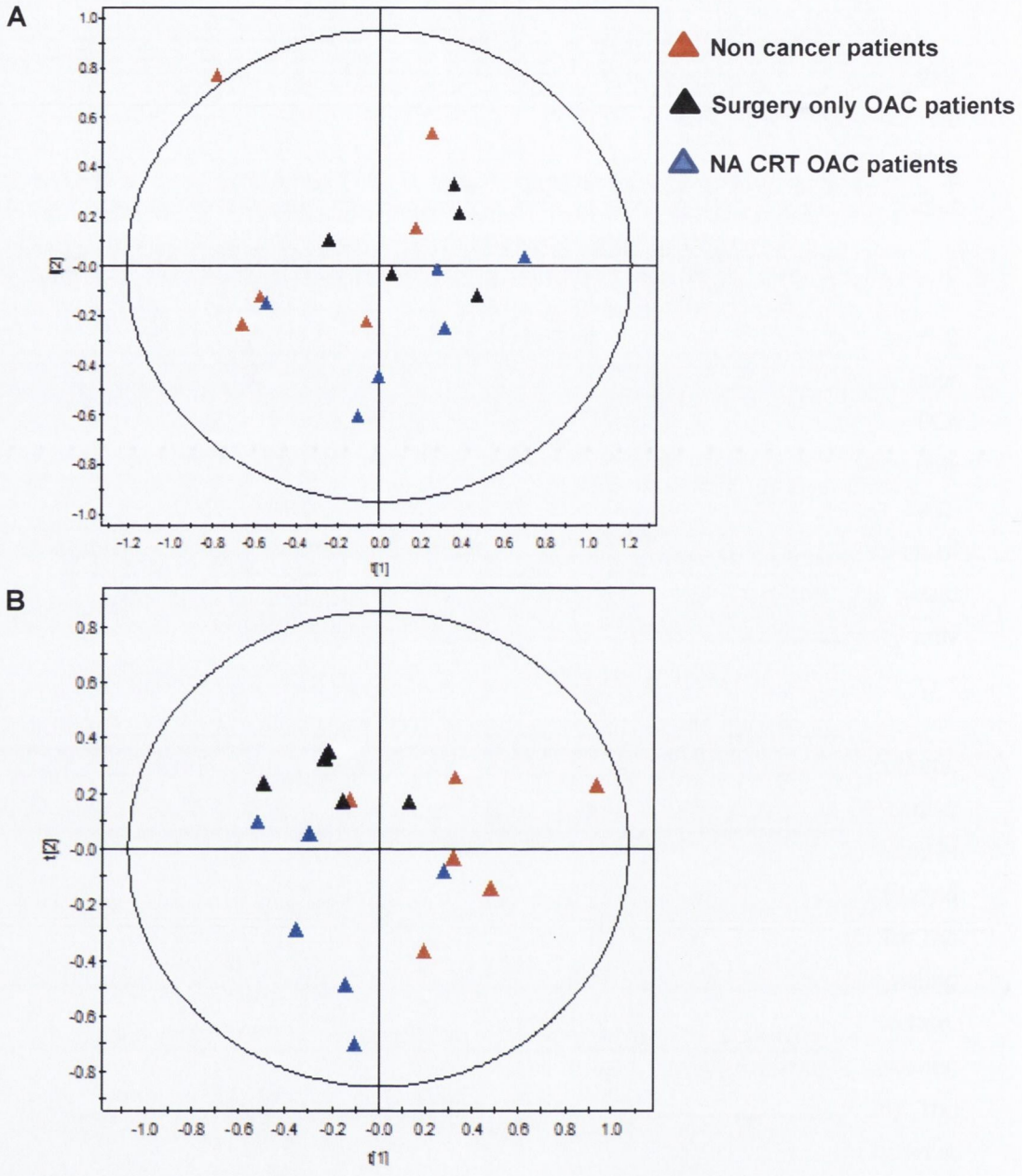


Figure 2.16. Separation of patient cohorts on the basis of metabolomic profile
(A) Principal component analysis (PCA) of ^{1}H nuclear magnetic resonance ACM data for three patient cohorts (non-cancer cohort, surgery only OAC cohort, NA CRT OAC cohort, n=6 for all, R^2=0.736). t[1]= PCA component 1, t[2]= PCA component 2. **(B)** Partial least-squares discriminant analysis (PLS-DA) of ^{1}H NMR plasma data for three patients cohorts (non-cancer cohort, surgery only OAC cohort, NA CRT OAC cohort), (R^2=0.453, Q^2=0.0012). Red triangles represent non cancer patients, blue triangles surgery only OAC patients, and black triangles represent NA CRT OAC patients.

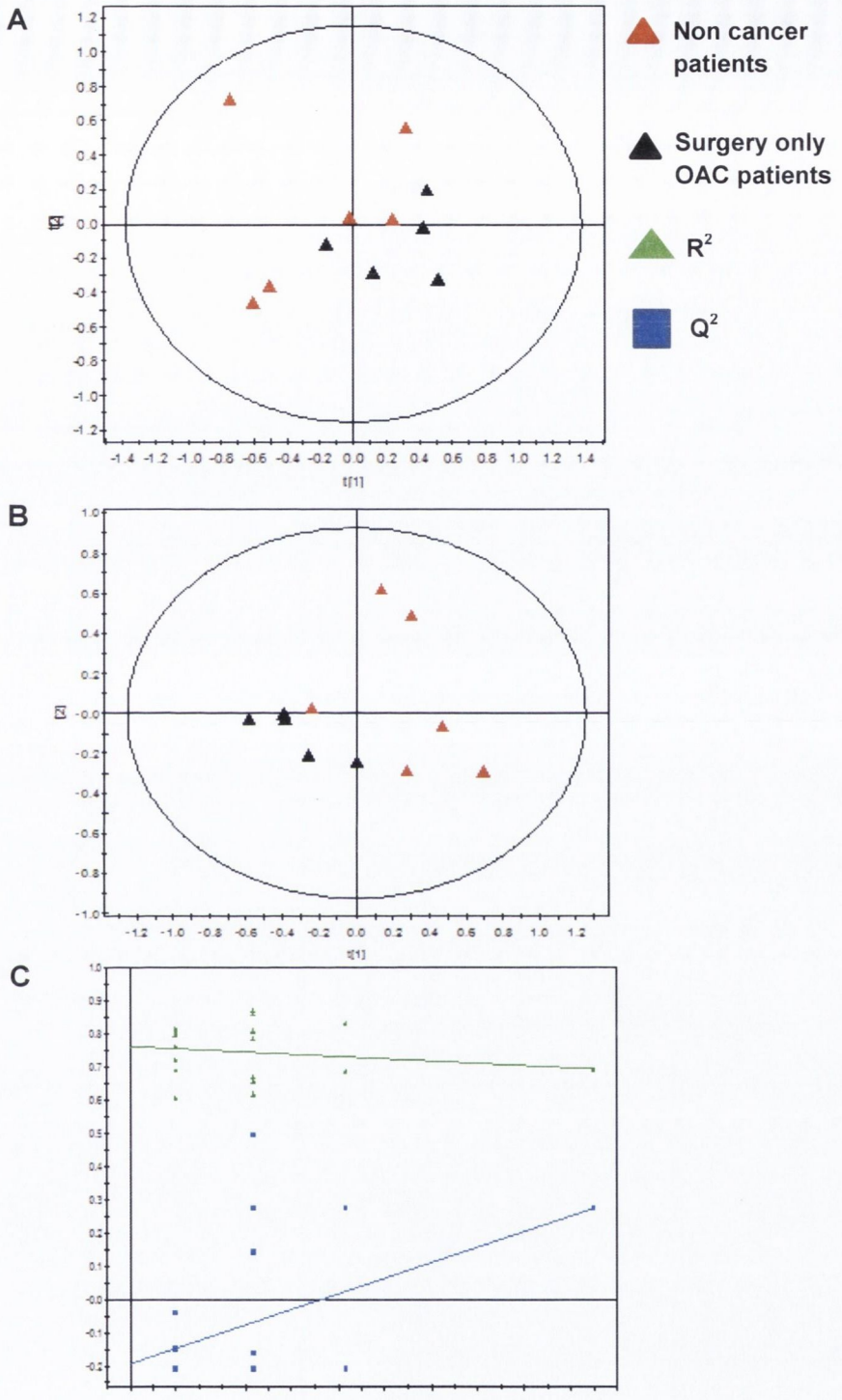


Figure 2.17. Non-cancer and surgery only OAC patients are associated with different metabolomes

(A) Principal component analysis (PCA) of ^{1}H nuclear magnetic resonance ACM data for two patient cohorts (non-cancer versus surgery only OAC patients, R^2=0.699). t[1]=PCA component 1, t[2]=PCA component 2. **(B)** Partial least-squares discriminant analysis (PLS-DA) of ^{1}H NMR plasma data for two patient cohorts (non-cancer cohort versus surgery only OAC cohort), (R^2=0.479, Q^2=0.273). **(C)** Validation model. Red triangles represent non cancer patients, black triangles represent NA CRT OAC patients, n=6 for each cohort

Table 2.18. Relative intensities and VIP values of the most discriminating metabolites generated from the PLS-DA for comparison of ACM from non-cancer *versus* surgery only OAC patients

VIPS (ppm)	M5.VIP					Metabolite	p-value
		Non cancer cohort		Surgery only OAC cohort			
		Mean	SD	Mean	SD		
1.315	7.33073	0.0492	0.0402	0.0827	0.0277	Lactate	NS
1.325	5.31929	0.0582	0.0484	0.0834	0.0284	Lactate	NS
1.305	6.58509	0.0128	0.0106	0.0304	0.0080	Threonine	0.014
1.295	4.15207	0.0005	0.0061	0.0082	0.0029	Threonine	0.031
3.825	2.35536	0.0032	0.0022	0.0007	0.0002	Glucose	0.039
3.835	2.09140	0.0023	0.0014	0.0004	0.0001	Glucose	0.022
3.845	2.02298	0.0022	0.0012	0.0005	0.0002	Glucose	0.019
1.865	2.22582	0.0019	0.0014	0.0039	0.0008	Lysine	0.017
1.875	2.13270	0.0016	0.0010	0.0035	0.0015	Lysine	0.025
1.035	1.95987	0.0011	0.0010	0.0027	0.0011	Valine	0.029
3.515	3.03494	0.0008	0.0003	0.0019	0.0013	Glycerol	NS

VIP values indicate the contribution of metabolites to the classification of samples. VIP values were calculated for the partial least-squares discriminant analysis model that compared non-cancer and surgery only OAC cohorts. P values are based on two-tailed, unpaired t-test. VIP=Variable importance in the projection, ppm=parts per million

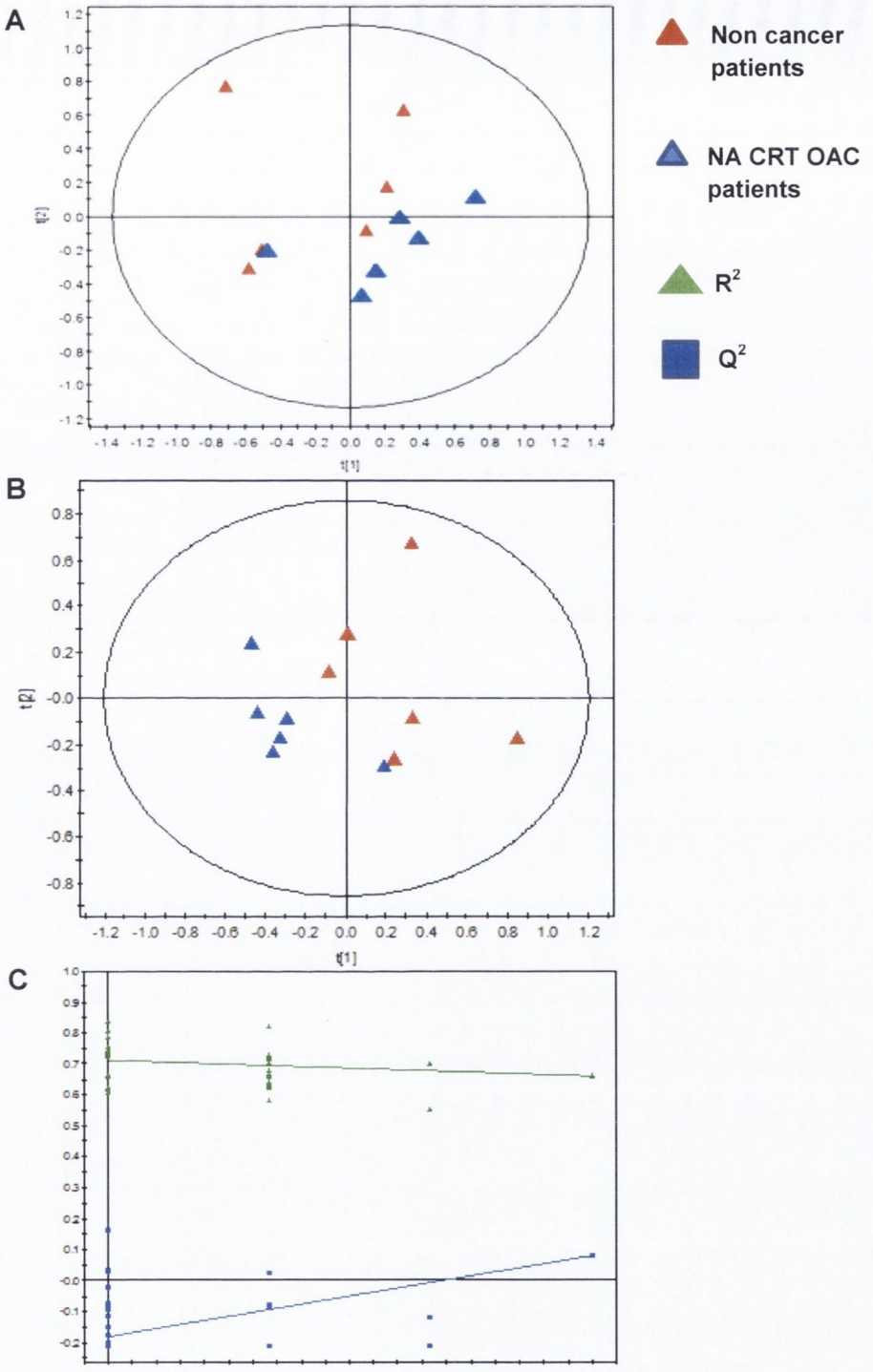


Figure 2.18. Non cancer and NA CRT OAC patients express different metabolomic profiles

(A) Principal component analysis (PCA) of ^{1}H nuclear magnetic resonance ACM data for two patient cohorts (non-cancer versus NA CRT OAC patients, R^2=0.819). t[1]= PCA component 1. t[2]= PCA component 2. **(B)** Partial least-squares discriminant analysis (PLS-DA) of ^{1}H NMR plasma data for two patient cohorts (non-cancer cohort versus NA CRT OAC cohort), (R^2=0.489, Q^2=0.079). **(C)** Validation model. Red triangles represent non cancer patients, black triangle represents NA CRT OAC patients, n=6 for each cohort

Table 2.19. Relative intensities and VIP values of the most discriminating metabolites generated from the PLS-DA for comparison of ACM from non-cancer versus NA CRT OAC patients

VIPS (ppm)	M7.VIP					Metabolite	p-value
		Non cancer cohort		NA CRT OAC cohort			
		Mean	SD	Mean	SD		
1.295	5.67466	0.0005	0.0061	0.0114	0.0042	Threonine	0.005
3.825	2.35468	0.0032	0.0022	0.0009	0.0005	Glucose	0.034
3.735	2.22689	0.0028	0.0014	0.0010	0.0004	Glucose	0.024
3.745	2.09995	0.0025	0.0010	0.0011	0.0002	Glucose	0.012
1.865	2.74278	0.0019	0.0014	0.0045	0.0013	Lysine	0.007
1.875	2.56597	0.0016	0.0010	0.0038	0.0013	Lysine	0.006
1.855	2.09317	0.0023	0.0014	0.0042	0.0014	Lysine	0.042
1.885	2.18606	0.0013	0.0005	0.0029	0.0010	Lysine	0.004
1.035	2.26945	0.0011	0.0010	0.0029	0.0008	Valine	0.007
3.535	5.24455	0.0083	0.0076	0.0205	0.0111	Glycine	0.05
1.245	2.19622	0.0022	0.0024	0.0045	0.0014	Isoleucine	NS
1.225	2.15509	0.0011	0.0017	0.0030	0.0011	Isoleucine	0.039
1.225	2.10611	0.0025	0.0025	0.0047	0.0015	Isoleucine	NS
1.275	2.10165	0.0034	0.0022	0.0056	0.0022	Isoleucine	NS
1.445	3.68593	0.0085	0.0072	0.0023	0.0006	Alanine	NS
1.285	3.45395	0.0030	0.0038	0.0082	0.0042		0.049

VIP values indicate the contribution of metabolites to the classification of samples. VIP values were calculated for the partial least-squares discriminant analysis model that compared non-cancer and surgery only OAC cohorts. P values are based on two-tailed, unpaired t test. VIP=Variable importance in the projection, ppm=parts per million

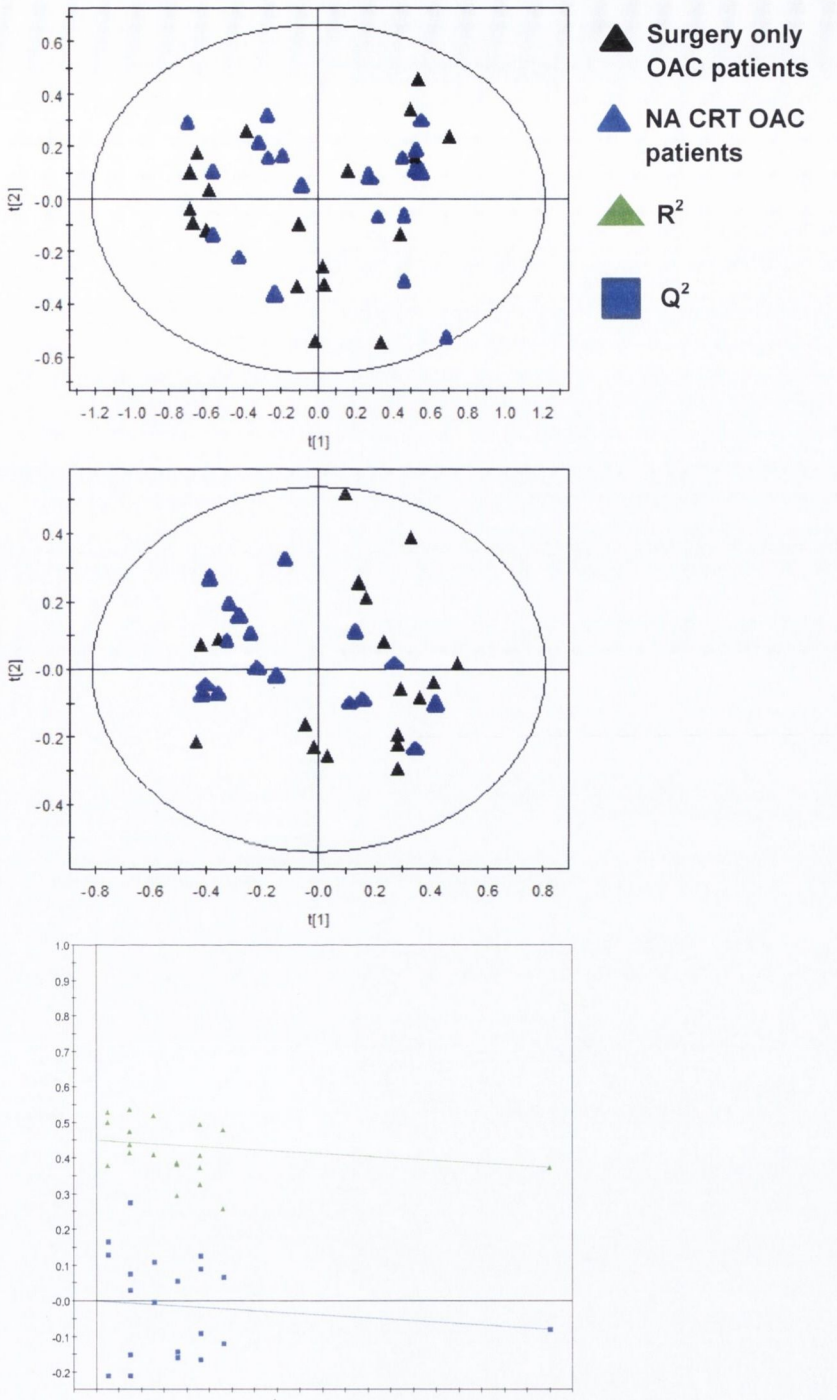


Figure 2.19. Metabolomic profile of surgery only OAC and NA CRT OAC patient cohorts

(A) Principal component analysis (PCA) of ^{1}H nuclear magnetic resonance ACM data for two patient cohorts (surgery versus NA CRT OAC patients, R^2=0.672). t[1]= PCA component 1. t[2]= PCA component 2. **(B)** Partial least-squares discriminant analysis (PLS-DA) of ^{1}H NMR plasma data for two patient cohorts (non-cancer cohort versus NA CRT OAC cohort), (R^2=0.423, Q^2=-ve 0.08). **(C)** Validation model. Black triangles represent surgery only OAC patients, blue triangle represents NA CRT OAC patients, n=6 for each cohort

2.4.10 Metabolomic profile of ACM from obese compared to non-obese OAC patients

The ^{1}H NMR ACM profiles from OAC patients showed separation on the basis of obesity status (anthropometric details are summarised in table 2.20) (Figure 2.20 A). To investigate this further, a pairwise PLS-DA plot was constructed comparing non-obese OAC ACM with obese OAC ACM (Figure 2.20 B). Analysis of the VIP values revealed the metabolites responsible for the separation of non-obese and obese OAC cohorts (Table 2.21). The most discriminating metabolites included lactate, glycerol, alanine and pyruvate. The concentration of lactate was significantly higher in the ACM of non-obese OAC patients, whereas glycerol, alanine and pyruvate were significantly higher in the ACM of obese OAC patients (Table 2.21).

Table 2.20 Anthropometric details of non-obese and obese OAC patients

	Non-obese n=20	Obese n=20	p Value
Age at surgery (years)*	62 (43-86)	64 (45-76)	NS[a]
Gender			
Male/Female	17/3	20/0	NS[b]
Obesity Status			
Body mass index (kg/m^2)*	23.4 (10.1-33.6)	29.3 (18.3-39)	<0.0001[a]
Waist circumference (cm)*	88 (61-109)	101 (85-130)	<0.0001[a]
Visceral fat area (cm)*	73.9 (4.3-158)	211.4 (110.6-381.1)	<0.0001[a]
Neoadjuvant therapy			
Yes/No	10/10	10/10	NS[b]

*Values given are median (range); NS=Not significant; a=Analysis performed using Mann Whitney U test; b=Analysis performed using Fisher's exact test.

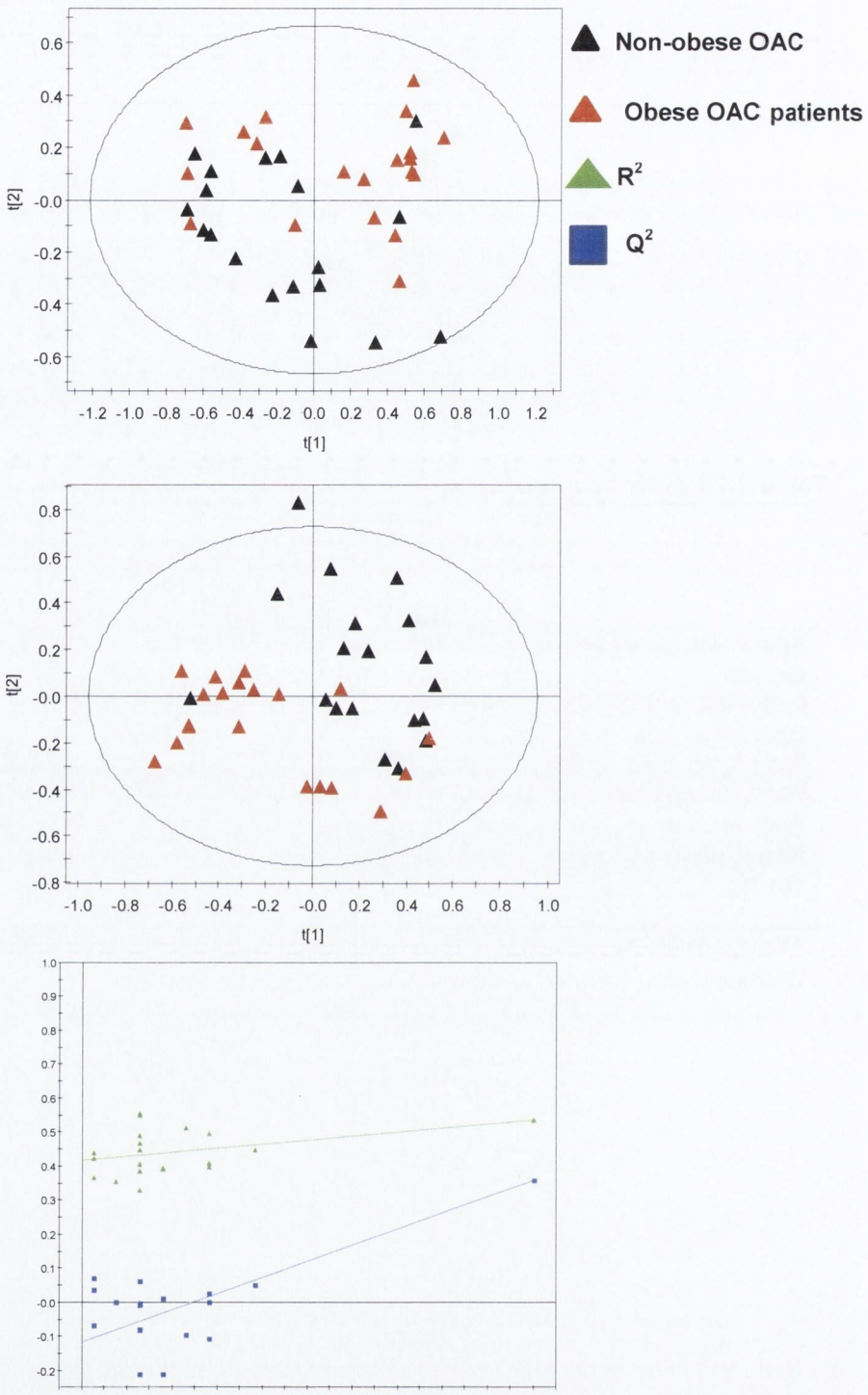


Figure 2.20. Metabolomic profile of non-obese OAC and obese OAC patient cohorts
(A) Principal component analysis (PCA) of ^{1}H nuclear magnetic resonance ACM data for two patient cohorts (non-obese OAC versus obese OAC patients, R^2=0.672). t[1]=PCA component 1, t[2]=PCA component 2. **(B)** Partial least-squares discriminant analysis (PLS-DA) of ^{1}H NMR ACM data for two patient cohorts (non-obese OAC cohort versus obese OAC cohort), (R^2=0.461, Q^2=0.361). **(C)** Validation model. Black triangles represent non-obese OAC patients, red triangles represent obese OAC patients, n=20 for each cohort

Table 2.21 Relative intensities and VIP values of the most discriminating metabolites generated from the PLS-DA for comparison of ACM from non-obese *versus* obese OAC patients

VIPS (ppm)	M7.VIP					Metabolite	p-value
		Non-obese OAC cohort		Obese OAC cohort			
		Mean	SD	Mean	SD		
1.317	11.65333	0.0022	0.0009	0.0068	0.0039	Lactate	0.004
3.547	3.19	0.0005	0.0003	0.0009	0.0005	Glycerol	0.041
1.446	2.92	0.0005	0.0003	0.0010	0.0004	Alanine	0.029
2.360	2.74	0.0001	0.0001	0.0011	0.0002	Pyruvate	0.042
0.948	2.85	0.0004	0.0002	0.0008	0.0006	Leucine	NS

VIP values indicate the contribution of metabolites to the classification of samples. VIP values were calculated for the partial least-squares discriminant analysis model that compared non-obese and obese OAC cohorts. P values are based on two-tailed, unpaired t test. VIP=Variable importance in the projection, ppm=parts per million

2.5 Discussion

The relationship between obesity and the radioresponse in OAC has not previously been addressed and mechanisms of radioresistance are poorly understood. OAC is an aggressive disease with low treatment response rates and extremely poor five-year survival indicating that mechanisms of treatment resistance are of great significance[25,60]. Analysis of standard clinicopathologic parameters does not predict the response of oesophageal cancer to neoadjuvant CRT[159]. There is a distinct lack of studies evaluating obesity status and radioresponse in OAC. This is the first study to suggest that BMI status influences TRG response in OAC. We have shown that patients who were overweight or obese were more likely to have a lower pathological T stage than normal weight patients, despite having similar clinical T stages prior to treatment and were more likely to achieve a good TRG response (TRG 1-3) than normal weight patients. One study, performed by Shridhar et al., specifically examined oncological and survival outcomes in a cohort of OAC patients who received NA CRT; BMI was not associated with tumour response[251]. That study stratified tumour responses into complete, partial and no response; whether this was based on the TRG classification used in our study is not clear, and may potentially explain the disparity in our findings[251]. In our study, obesity status was not associated with recurrence or survival. Four studies investigating outcomes in OAC patients in relation to BMI have included a cohort of patients who received NA RT, none of which demonstrated a difference in survival between obese and non-obese patients[246,247,251,252].

A significant limitation of this retrospective study is the use of BMI as a marker of obesity status. VFA is the gold standard marker of visceral obesity, and visceral obesity contributes to obesity related disease risk more than overall adiposity[198,199,490]. In addition, conditioned media derived from visceral adipose tissue is used to examine the effect of adiposity *in vitro*, thus specific measurement of visceral adiposity would be a more appropriate measure. Prospective studies assessing the link between obesity and radioresponse in OAC using VFA as a marker of obesity should be performed to confirm the findings from this retrospective analysis.

Clinical data indicating a potential association between increased adiposity and improved radioresponse was supported by our results from the clonogenic assay showing that ACM influences radiosensitivity in both OE33P and OE33R. The effect of adipose tissue or adipose conditioned media on the clonogenic survival of cancer cells has not previously been studied. OE33P and OE33R cells treated with ACM demonstrated decreased radioresistance. This effect was seen with ACM from three patient cohorts, including radiation naïve OAC patients as well as previously irradiated patients, suggesting that this outcome is not merely a bystander effect caused by previous exposure to radiation, nor is it a secondary effect of malignancy. Radioresistance was significantly lower in cells treated with ACM from NA CRT patients, compared to the radiation naïve OAC cohort, suggesting that previous exposure to irradiation

may have induced a bystander effect on the visceral fat, thus releasing an altered panel of adipokines which stimulated a more radioresponsive phenotype. Previous work from this unit demonstrated that ACM generated from NA CRT OAC patients contains higher levels of Leptin and IL-6 (Interleukin 6) compared to surgery only OAC patients, and higher levels of IL6, IL8 (Interleukin 8), MCP1 (Monocyte chemoattractant protein 1), and IFNγ (Interferon-gamma), compared to ACM from non-cancer patients. IL6 levels are increased in the adipocytes of obese subjects and may be important either as a circulating hormone or as a local regulator of insulin action[492]. Secretion of IL6 is increased in healthy and malignant cell lines following exposure to ionizing radiation (IR)[493–495]. IL6 expression positively correlates with radioresistance in cancer cell lines[496–498], while IL6 inhibition attenuates radioresistance[496–499]. Similarly, IL8 levels are elevated in obese subjects[500], induction of IL8 is stimulated by irradiation[501,502], and it is associated with radioresistance and poor outcomes in cancer patients[498,499,503]. Neither IL6 nor IL8 have been linked with radiosensitivity *in vitro* or *in vivo,* making them unlikely mediators of radiosensitivity in this model. Circulating levels of MCP1 are raised in obese patients[500], and MCP1 expression in cancer cells is induced by irradiation[504,505]. However, MCP1 expression has not been investigated in relation to radioresponse. Elevated IFNγ is observed in obese subjects[506], and is associated with radiosensitivity in murine immune cells[507]. The radiosensitising effect of IFNγ is thought to be mediated via downregulation of the cell cycle regulatory gene Chk1 (Checkpoint kinase 1). However, the mechanisms of action of IFNγ are complex and not well understood. IFNγ induces attenuation of telomerase activity, and lower hTERT expression[508]; low levels of telomerase activity are associated with radiosensitivity in cancer cell lines[441,444]. In addition, IFNγ inhibits proliferation and promotes accumulation of cancer cells in the radiosensitive G_2/M phase[509]; G_2/M accumulation was not seen in the isogenic model following ACM treatment in this study.

Cells in the M and G_2 phase are, in general, the most sensitive to radiation, cells with a long cycle time demonstrate another peak of resistance in early G_1 phase, whilst cells in S phase are most resistant[144,148]. Chronic irradiation of OE33R during its generation altered its basal cell cycle distribution, with OE33R cells demonstrating a lower proportion of cells in G_0/G_1 phase and a concomitant higher proportion of cells in the G_2/M phase, compared to OE33P cells, which is surprising given that the G_2/M phase is most sensitive to radiation[174,510]. However, these differences were extremely small (4% difference in G_2/M phase distribution) and highly unlikely to be a major factor contributing to the enhanced radioresistance of OE33R[174]. The synchronization of cells into radiosensitive phases has been recognized as a method by which to improve the efficacy of radiation therapy[511,512]. IR-induced DNA damage stimulates temporary cell cycle arrest in G1, S and G2 phases allowing time for repair of DNA damage, and can also permanently prevent proliferation of severely damaged cells[150]. ACM induced a small but statistically significant decrease in the proportion of cells in the radioresistant S phase in

both OE33P and OE33R. An increase of cells in the relatively radiosensitive G_0/G_1 phase was seen in OE33R cells following ACM treatment. The G_1 checkpoint pathway involves the phosphorylation of the IFNγ-induced Chk1[513]. Abrogation of this checkpoint has been shown to alter cellular sensitivity to radiation[514,515]. The changes in cell cycle distribution induced by ACM parallel the changes in radioresponse. These differences were small however, (3% change in S phase distribution in OE33P, 4% change in S phase and G_0/G_1 phase distribution in OE33R) suggesting that other mechanisms must play a greater role in affecting radioresponse in OE33P and OE33R.

ACM induced a greater change in radioresponse in OE33R compared to OE33P cells. Both cell lines were treated with identical patient ACM, suggesting that differences in cell line receptor expression may account for the difference in response. With this in mind, we assessed the expression of a panel of four adipokine receptors in the two cell lines and demonstrated that adipokine receptor expression differs between OE33P and OE33R; AR1 and AR2 expression was higher in OE33P compared to OE33R, while LepR and NRP1 expression was lower in OE33P compared to OE33R. These adipokines are known to be highly expressed in visceral fat and are associated with prognosis in cancer[185,262,263,267,277–281]. Adiponectin is the most abundant adipokine[258], and over 90% of oesophageal and junctional adenocarcinomas express the adiponectin receptors AR1 and AR2[271]. Overexpression of AR1 and AR2 has been implicated in poor prognostic indicators such as high grade, advanced stage and lymph node involvement[271,516,517]. Conversely, high expression of AR1 and AR2 is associated with prolonged survival in lung, thyroid and gastric cancer[263,472–474]. These findings are consistent with our *in vitro* data demonstrating that AR1 and AR2 levels are higher in radioresponsive compared to radioresistant cancer. Adiponectin exerts protective effects against oxidative damage *in vivo* and *in vitro*[518]. Oxidative stress is one of the main mechanisms through which irradiation causes damage to DNA and other cellular components[519,520], and a relationship between increased oxidative stress and decreased circulating levels of adiponectin in normal weight and metabolically obese humans has been observed[521,522], suggesting a radioprotective role for adiponectin. However, adiponectin has been shown to inhibit tumour growth in animals[258], and recombinant adiponectin has antiproliferative and proapoptotic effects on oesophageal adenocarcinoma cell lines that express both AR1 and AR2[523,524]. Adiponectin-induced inhibition of cellular proliferation may potentially contribute to delaying recovery from DNA damage following irradiation, enhancing radiosensitivity.

In contrast, expression of LepR and NRP1 correlates with aggressive tumour behaviour in OAC, and poor prognosis in a range of cancers[271,287–294]. The association of these receptors with radiosensitivity status has not previously been investigated. Our study has shown that LepR and NRP1 are upregulated in radioresistant OAC. Studies from this unit and others confirm that

leptin promotes cell proliferation, angiogenesis and metalloproteinase expression in oesophageal and colonic cancer cell lines[271,273–276]. A close relationship has been observed between leptin expression and decreased efficacy of anti-oestrogen therapies in breast cancer[525–527]. In addition, leptin interferes with non-hormonal therapies, and can reduce the antiproliferative effect of 5FU, taxol and vinblastine in breast cancer cells[525]. This effect may be cancer-type specific; leptin enhances the cytotoxic effect of chemotherapy in colon cancer cells[528]. The interaction of leptin and the radioresponse has not been studied in cancer; however the obese db/db mouse which lacks the LepR, demonstrates increased susceptibility to IR[529], and leptin upregulation is known to suppress therapy-induced apoptosis by inhibiting caspase activation[530]. VEGF is critical for development, angiogenesis, growth and metastasis of tumours, and its expression levels have been demonstrated to be predictive of resistance to treatment[531,532] Low VEGF levels are a predictor of good oncological outcomes following NA CRT in colorectal cancer[533]. Antitumour effects were noted in a variety of tumour model systems following treatment with anti-VEGF therapies prior to radiotherapy[278,534–536]. IR activates the MAPK pathway via ROS stimulation, resulting in upregulation of VEGF expression and reduced response to radiotherapy in head and neck squamous cancer[537,538]. VEGF is currently under investigation as a therapeutic target for radiosensitization in rectal cancer[539]. The radiosensitising effect of VEGF blockade was thought to be mediated via an anti-angiogenic effect[476]; emerging data now suggest that multiple mechanisms account for the efficacy of VEGF-targeted therapies in patients with cancer[540]. These include modulating vascular function, directly mediating migration and invasion of cancer cells, and establishing immune privilege of tumour cells[540]. The clinical benefit and enhancement of radiation therapy response have been confirmed in a neoadjuvant phase I/II trial with bevacizumab in combination with 5-FU and radiation therapy in patients with rectal cancer[476]. NRP1 is also undergoing investigation as a target for cancer therapy, and it is interesting to note that combined anti-VEGF and anti-NRP1 therapy with monoclonal antibodies is synergistic in mouse models of cancer[541].

Higher levels of AR1 and AR2 were noted in the OE33P cell line while OE33R cells expressed higher levels of the leptin receptor and the VEGF co-receptor NRP1. While the same trend was seen in the responder and non-responder patient samples, the differences in expression did not reach statistical significance. This may be due to the small sample size (n=11 responders, n=19 non-responders) or to a genuine lack of effect in vivo. The patient cohort used for this study was the maximum number available in the departmental bioresource that met the inclusion criteria. Given the small sample size, the results warrant further investigation of adipokine receptor expression as a potential in vivo biomarker to predict response in OAC through multicentre studies. These mRNA expression study results indicate a potentially useful association between adipokine receptor gene expression and radiosensitivity. A drawback of

this approach is that alterations in mRNA expression were not validated at the protein and functional level, and this may be an important area for future investigation.

High levels of lactate correlate with malignancy, metastasis, and reduced overall survival in several types of cancers[542–546]. Mass spectrometry-based metabolomics has demonstrated utility for identifying biomarkers of ionizing radiation exposure in cellular, mouse and rat in vivo radiation models[547]. Metabolomic profiling of ACM did not reveal markers of radioresponse in OAC patients in this study. The most widely used clinical diagnostic fluids in metabolomic studies are plasma and urine[548]. Metabolomic mapping of ovarian, endometrial, lung, renal and colorectal cancer have demonstrated alterations in serum or urine profiles[548]. This is the first study however, to identify an altered metabolome in the ACM of OAC compared to non-cancer patients. Higher levels of threonine, lysine and valine, and lower levels of glucose were seen in the metabolome of OAC patients compared to non-cancer patients. In addition, obesity status influenced the metabolomic profile of OAC patients. The metabolome of obese OAC patients demonstrated an increase in lactate and a reduction in alanine levels, perhaps indicating a diversion of pyruvate to alanine. An emerging area for metabolic profiling is the characterization of the role of the metabolites produced by gut microbiota in cancer and obesity, however, metabolomic profiling of the ACM of non-obese and obese cancer patients has not previously been performed. The role of adipose tissue metabolites in modulating cancer risk in obese individuals requires further investigation. Small-molecule ligands of nuclear receptors govern the transcriptional regulation of metabolism, however these ligands remain poorly characterized, primarily due to lack of robust analytical techniques. While the role of the adipokine receptors in OAC biology is under investigation, the signalling pathways through which these receptors and their ligands influence tumour behaviour are very poorly understood. Future analysis may allow the metabolic pathways associated with adipokine receptors to be identified based on the results of metabolomics analysis.

In conclusion, this large single-institution study of OAC patients treated with NA CRT demonstrates that higher BMI is associated with improved response to therapy. Currently, 47% of the population is overweight or obese and it is estimated that obesity rates will continue to rise by at least 1% per annum[549–551]. Ireland has the fourth highest prevalence of overweight and obesity in men in the EU and the seventh highest prevalence among women[552]. Parallel to this increase in obesity, there has been a dramatic rise in the incidence of several cancers, particularly OAC[17]. The diagnosis of oesophageal cancer confers a poor prognosis with an overall cure rate of 15%-25%[25,60]. A subset of patients achieving a complete pathologic response to NA therapy, have improved outcomes[55,61–65]. This occurs in only 35% to 50% of cases receiving NA CRT and it is not understood why tumours of identical pre-treatment stage, undergoing identical neo-adjuvant regimens, respond differently to NA CRT[55,61–65]. CRT is

expensive and time-consuming, carries the risk of treatment associated toxicity and increased peri-operative morbidity as well as the risk of developing secondary tumours. The ability to identify and select only patients sensitive to or resistant to CRT, ideally before or in the early stages of treatment, would confer a major clinical advance, both in terms of the optimization of current treatment regimens, and the development of clinical trials. BMI, and potentially VFA, measured before starting therapy is likely to be a useful predictive biomarker in operable OAC, and may have relevance to other cancer types. Clinicians should be aware of higher BMI status as a host factor influencing tumour response to NA CRT. This is particularly important given that patients with severe obesity-associated medical co-morbidities (including diabetes, hypertension, and coronary artery disease) are more likely to be excluded from radical curative therapies. Patients with low BMI might either not benefit from NA CRT or require a higher dosage. If further validation studies corroborate our results, the measurement of BMI/VFA will have to be included in clinical trials for NA CRT in OAC, thereby taking into account tumour parameters and also host parameters. This isogenic model of radioresistance largely avoids the influence of confounding factors, facilitating the identification of specific markers or radioresponse/radioresistance. The association of adipose tissue with radiosensitivity identifies a novel area of research for biomarkers of radioresponse, and therapeutic targets in radioresistant cancer. In this study adipose tissue influenced radioresponse in OAC cell lines and adipose receptor expression differed in the radioresponsive and radioresistant cell lines, suggesting that obesity has a key role in regulating radioresponse in OAC. These data call for further studies to determine whether the predictive effect of high BMI is related to adipokine production or other novel mechanisms. Taken together, this data demonstrates for the first time a role for adipose tissue in modulating the cellular response to radiation in oesophageal cancer, potentially by adipokine production.

Chapter 3 Obesity drives telomere dysfunction in oesophageal adenocarcinoma

In preparation for submission to Cancer Lett: AM Mongan, N Lynam-Lennon, R Casey, S Maher, JV Reynolds, G Pidgeon, J O'Sullivan. Adiposity drives telomere dysfunction in oesophageal adenocarcinoma

3.1 Introduction

Oesophageal cancer represents a significant and increasing health problem. Worldwide, it is the sixth most common cause of cancer death[2]. The vast majority of oesophageal cancers may be classified into two histological subtypes, squamous cell carcinoma or adenocarcinoma (OAC)[3]. There has been a dramatic epidemiological shift toward adenocarcinoma in recent decades and OAC is now the most prevalent form of oesophageal cancer in the Western world[4,553]. The incidence of OAC is increasing more than any other cancer in the western world, paralleling the current epidemic of obesity[4,554]. Robust epidemiological studies have identified obesity as a risk factor for a number of different cancers including gastrointestinal malignancies such as OAC and colorectal cancer[26,555,556]. In fact, OAC is the strongest model of a cancer associated with obesity, making it the ideal model for studying the molecular effects of obesity[18,26,556]. As the prevalence of obesity continues to rise globally, an increasing number of obese patients will undergo treatment.

Emerging concepts position centrally located, visceral adipose tissue as key to the pathogenesis of the co-morbidities associated with obesity. Adipose tissue, particularly visceral fat, is an important metabolic organ which secretes factors in a paracrine and systemic manner, altering the immunological, metabolic and endocrine milieu, creating a pro-neoplastic environment which facilitates tumour development by promotion of the acquisition of some of the hallmarks of cancer[253]. One of these emerging hallmarks of cancer is genomic instability, which is an established feature of most forms of cancer as well as pre-malignant conditions such as Barrett's Oesophagus[297,307–309,423]. Genomic instability refers to the increased tendency of the genome to acquire mutations when the various processes involved in maintaining and replicating the genome are dysfunctional. Telomeres are composed of tandem repeats of TTAGGG and are associated with a wide variety of telomere binding proteins which mediate their function[315,317,359]. DNA polymerase are unable to replicate the ends of linear DNA, a phenomenon termed the 'end replication problem'[328,329]. Therefore, during cell replication, telomere DNA cannot be completely replicated, leading to progressive telomere shortening over time[329]. Eventually, telomere shortening will reach a threshold, and cells can enter replicative senescence[315]. Cancer cells escape this cell senescence by increasing telomerase expression and activity[331,332]. Telomerase is an enzyme complex which maintains and elongates telomere length and gives immortality to cancer cells[331]. This ribonucleo protein consists of two main components which elongate telomeres through the *de novo* addition of TTAGGG repeats by TERT onto chromosome ends using an associated RNA component (TERC) as a template[359]. Along with members of the telomerase complex, TEP1 and DKC1 are known to bind telomeres and are direct regulation of telomere length[335,336]. While telomeres protect the end of chromosomes from degradation, the telomeres themselves are protected from degradation by a six protein complex termed the shelterin complex[557,558]. This complex consists of three proteins

which bind telomeres directly; TERF1, TERF2, and POT1, and these are interconnected by additional proteins; TINF2 and TPP1. In contrast to the telomerase complex, shelterin complex proteins are negative regulators of telomere elongation[559]. Telomere dysfunction has been linked to radiosensitivity status *in vitro* and in animal models: telomere shortening and telomerase inactivation are associated with a radiosensitive phenotype[439,440,442,449,450,560].

Obesity has been shown to drive carcinogenesis and is implicated in genomic instability events such as telomere shortening[253,561]. Significant negative relationships exist between adiposity measures (BMI, waist circumference, hip circumference, total body fat, and visceral adipose tissue) and leukocyte telomere length[415–419]. Short telomere length is associated with increased risk of cancer; the strongest evidence exists for bladder, oesophageal, gastric, and renal cancers[562]. Telomere length is inversely associated with increasing OAC risk,[423,563] and telomere shortening occurs early in the aetiology of oesophageal carcinogenesis[372]. A potential interaction has been demonstrated between telomere length and lifestyle measures including WHR (waist hip ratio) with risk of OAC in patients with Barrett's oesophagus[423].

OAC risk is strongly affected by obesity,[6,14,17–22] which, interestingly, is also known to be related to telomere length,[415–419] a marker of radiosensitivity[439,440,442,449,450,560]. The interaction between obesity, telomere dynamics and the radioresponse in OAC has not been investigated. Currently a multi-modal approach to treatment, by which patients receive neoadjuvant chemoradiotherapy (CRT) followed by surgery, has replaced single modality treatment[564,565]. Radiation therapy plays a central role in treatment, however resistance to radiation therapy remains a significant clinical problem with only 15-30% of patient's achieving a complete pathological response following CRT[565,71,79,566]. The identification of obesity-induced telomere dysfunction as a marker and mechanism of radiosensitivity would be a novel finding, which would be of substantial clinical benefit.

3.2 Overall aims and specific objectives

The overall aim of this chapter is to investigate the effect of visceral adipose tissue on telomere biology in OAC. Telomere length and telomere associated gene expression alterations were investigated in our isogenic radioresistant model following co-culture with adipose conditioned media and selected gene targets validated in OAC patient cohorts.

Specific aims:

- Determine if ACM drives telomere shortening in the isogenic radioresponsive and radioresistant oesophageal cancer cell lines
- Determine the effect of adipose conditioned media on telomerase and shelterin gene expression
- Determine if obesity status influences expression of selected telomerase complex and shelterin genes in OAC patient tumour samples
- Investigate if radiosensitivity status influences expression of selected telomerase complex and shelterin genes in OAC patient pre-treatment biopsy samples

3.3 Materials and methods

3.3.1 Cell Culture

Cell culture was performed as described in section 2.3.3

3.3.2 Telomere length measurement

DNA extraction

Cells were seeded in 12 well plates at a concentration of 3 x 104 cells/ml and allowed to adhere for 6 hr. Cells were co-cultured with ACM for 24 and 72 hours. Genomic DNA was extracted by adding 1ml DNA lysis buffer directly to each well. The constituents of the lysis buffer were: 5ml 10mM Tris HCL (pH 8.0), 0.5ml 0.5M EDTA, 1ml 10% SDS, 2ml 5M NaCl, 0.25ml 20mg/ml proteinase K and 41.25ml deionised H_20. Cells were transferred to 2ml eppendorfs and were incubated at 37°C for 3 hours. 1ml of isopropanol was added to the lysate and samples were left to stand at room temperature for 30 min before centrifugation at 12000 x g at 4°C. The supernatant was decanted and 0.5 ml of 70% (v/v) ethanol was added to the DNA pellet. Samples were subsequently centrifuged at 3500 x g for 5 min and the pellet was resuspended in 30µl of DNase free water.

DNA quantification and purity analysis

DNA quantification was determined spectrophotometrically, using a Nanodrop 1000 spectrophotometer (version 3.1.0, Nanodrop technologies, DE, USA). 1µl of DNAse free water was used to blank the instrument prior to DNA analysis. 1µl of each sample of isolated DNA was loaded onto the instrument and concentration was measured in ng/µl. 260:280 and 260:230 purity ratios were recorded. A 260:280 ratio greater than 1.65 was indicative of a relatively pure DNA yield, while a 260:230 ratio greater than 1.7 indicated the sample was free of contamination.

Telomere length PCR

Telomere length was measured by Quantitative-PCR (qPCR) using a method adapted from that originally described by Cawthon.[567] For each sample, two PCRs were performed: the first one to amplify the telomeric DNA and the second one to amplify a single-copy control gene (36B4, acidic ribosomal phosphoprotein PO). This provided an internal control to normalize the starting amount of DNA. A five-point standard curve (two-fold serial dilutions from 10 to 0.625ng of DNA) was included in all PCRs to allow the transformation of Ct (cycle threshold) into nanograms of DNA. All samples were run in triplicate and the median was used for subsequent calculations. The amount of telomeric DNA was divided by the amount of control-gene DNA, producing a relative measurement of the telomere length of the sample. Two control samples

were run in each experiment to allow for normalization between experiments and periodical reproducibility experiments were performed to guarantee correct measurements.

All telomere length PCR reactions were run in the ABI Prism 7500 (ABI Biosystems, CA, USA) real time thermal cycler. 2ng of genomic DNA was run per sample per well and all samples were run in duplicate in a final volume of 20µl. Each reaction included 2X Quantifast ™ SYBR green PCR master mix (Qiagen Inc., CA, USA), 1µl of forward and reverse primer (Metabion, Germany) and 7µl of DNase free water. The telomere PCR used 300nM of each primer (tel1b: GGTTTGTTTGGGTTTGGGTTTGGGTTTGGGTTTGGGTT;tel2b:GGCTTGCCTTACCCTTACCCTTACCC TTACCCTTACCCT), and 30 cycles of amplification at 95°C for 15 seconds and at 56°C for 60 seconds. The control PCR gene used 300nM of forward primer (36B4u: CAGCAAGTGGGAAGGTGTAATCC) and 500nM (36B4d:CCCATTCTATCATCAACGGGTACAA) of reverse primer and 35 cycles of amplification at 95°C for 15 seconds and at 56°C for 20 seconds and 72°C for 20 seconds. Both PCR reactions had an initial denaturation step at 95°C for 15 min. Ct values for each sample were converted into nanograms of DNA using standard curves. Ct values from the telomere assay were normalized to the single gene reference. The telomere length (x) from each sample was based on the telomere to single copy gene ratio (T/S ratio) and was based on the calculation of the ΔCT [CT(telomere)/CT(single gene)]. Telomere length was expressed as a relative T/S ratio, which was normalized to the average T/S ratio of the reference sample [$2^{-(\Delta CTx \cdot \Delta CTr)} = 2^{-\Delta\Delta CT}$]

3.3.3 Oesophageal tumour and adipose tissue biobank

Patient samples were processed as outlined in section 2.3.4.

3.3.4 Investigation of gene expression

RNA isolation from tumour samples

OAC tumour specimens were taken from patients following recruitment to the upper gastrointestinal biobank. Samples were briefly stored on saline gauze at room temperature before transfer to the lab. RNA was extracted using Qiagen Rneasy Mini kit (Qiagen Inc., CA, USA). Samples were homogenised in 600 µL Buffer RLT using a Qiagen TissueLyser (Retsch GmbH & Co., Haan, Germany) at 250 x g for 6 min with one 5 mm stainless steel bead (Qiagen Inc., CA, USA) added to each sample to aid homogenisation. The bead was removed and samples were centrifuged at 12000 x g for 3 minutes at 4°C, and supernatant was transferred to a new tube by pipetting. A 600 µL volume of ethanol (70% v/v) was added to the supernatant and mixed immediately by pipetting and transferred in volumes of 700 µL to an Rneasy spin column placed in a 2 mL collection tube. The spin column was centrifuged at 12000 x g for 15 s and the flow through was discarded. The spin column was washed by first

applying 700 µL buffer RW1, then 500 µL buffer RPE with centrifugation at 12000 x g for 15 s at room temperature between each step. A final wash step in 500 µL buffer RPW was centrifuged for 2 min in order to dry the membrane and ensure no ethanol was carried over. RNA was eluted in 30 µL of RNase-free H_2O by centrifugation for 1 min at 12000 x g at room temperature.

RNA quantification and purity analysis, cDNA synthesis and quantitative real time PCR

Gene expression was investigated as described in section 2.3.5

3.3.5 Statistical analysis

Statistical analysis was performed using Graphpad Prism 5 software (GraphPad Software, Inc., CA, USA) and SPSS version 18 for Windows (IBM, Armonk, New York, USA) software. Unless otherwise stated, data are expressed as mean ± standard error of the mean (SEM). SEM was calculated as the standard deviation of the original sample divided by the square root of the sample size. In cases where data were paired (ie untreated versus ACM-treated cells) a two-tailed paired t-test was used for statistical analysis. A two-tailed unpaired t-test was used to analyze unpaired parametric data. The Mann-Whitney U test was used to examine statistical significance between unpaired groups of non-parametric data. For all statistical analysis, a probability of (p) of ≤ 0.05 was considered to represent significant difference between groups.

3.4 Results

3.4.1 ACM drives telomere shortening in OE33P and OE33R

Telomere length was assessed in OE33P and OE33R cell lines using qPCR following 24 and 72 hour treatment with either control M199 media or ACM generated from obese and non-obese OAC patients (anthropometric characteristics of patients are summarised in Table 2.9). The T/S ratio is an indicator of telomere length; a lower T/S ratio reflects shorter telomere length. There was no difference in telomere length in untreated OE33P and OE33R cells (Figure 3.1). ACM stimulated telomere shortening in OE33P and OE33R cell lines following 24 and 72 hours of treatment ($p<0.0001$ for each) (Figure 3.1 A, B). Telomere length did not differ between 24 and 72 hour time points. There was no difference in the effect induced by ACM from non-obese compared to obese patients. The relationship between telomere length in ACM treated OE33P and OE33R cells and visceral obesity status (as measured by visceral fat area) was investigated using Pearson correlation coefficient. Telomere length did not correlate with visceral obesity.

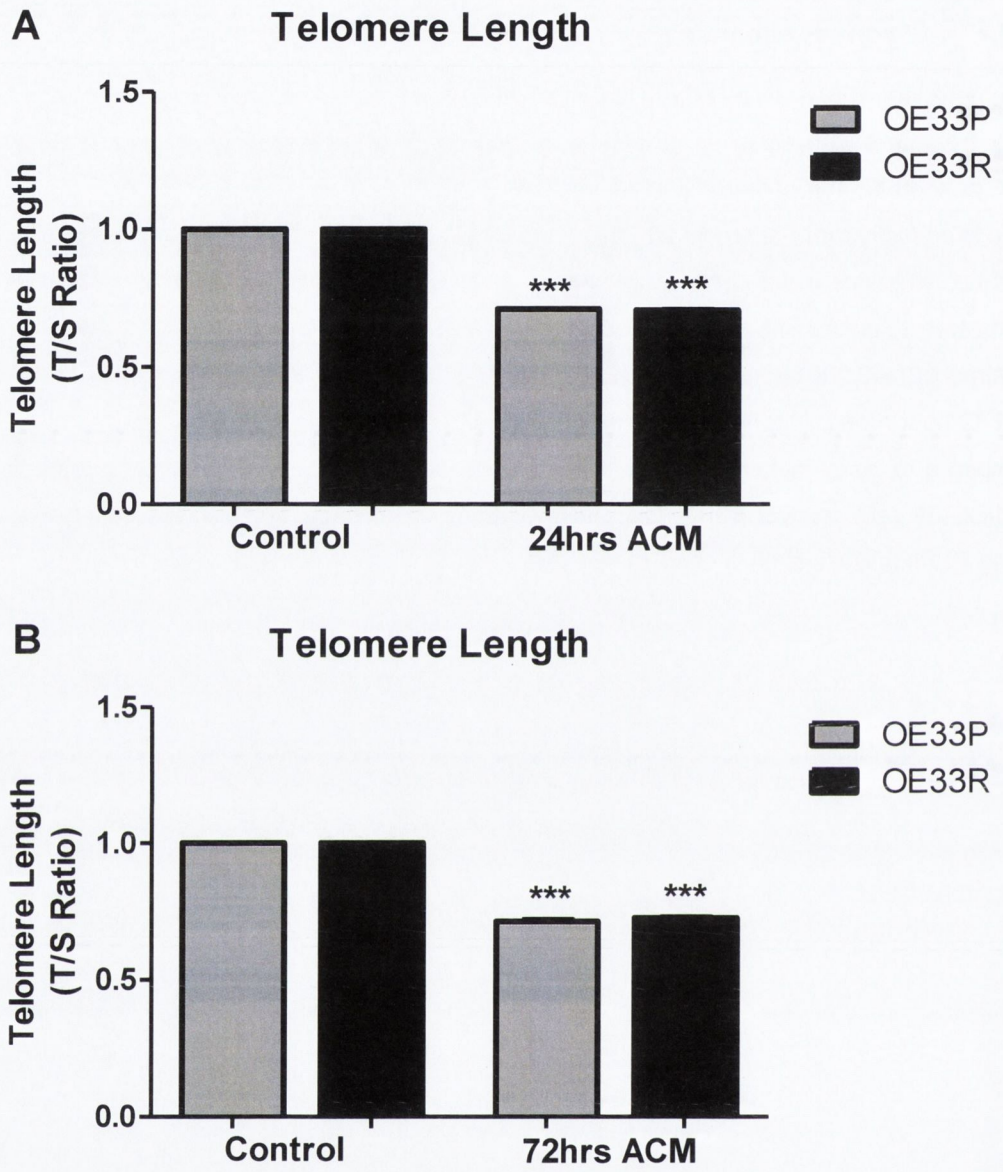


Figure 3.1. ACM drives telomere shortening in OE33P and OE33R

The average T/S ratio is an indicator of telomere length; a lower T/S ratio reflects shorter telomere length. **(A)** ACM induced telomere shortening in both OE33P and OE33R cells at 24 hours ($p<0.0001$). Telomere length did not differ in OE33P compared to OE33R cells. **(B)** ACM induced telomere shortening in OE33P and OE334 cell lines at 72 hours ($p<0.0001$). There was no difference in telomere length in OE33P versus OE33R following 72 hours of ACM treatment. Data are expressed as mean telomere length ± SEM. Statistical analysis was performed using paired, two-tailed student's t-test for ACM treated OE33P and OE33R cells versus control, ***$p<0.0001$; an unpaired, two-tailed student's t test was used to compare ACM treated OE33P cells to ACM treated OE33R cells.

3.4.2 ACM drives dysregulation of telomerase gene expression in OE33P and OE33R

OE33P and OE33R cells were treated with control media or ACM for 24 and 72 hours and the expression of four telomerase genes (TERC, TERT, TEP1 and DKC1) was investigated using quantitative real-time PCR. TERC expression was upregulated two-fold in both OE33P and OE33R cells following ACM treatment for 24 hours ($p=0.05$ and $p=0.03$ respectively) (Figure 3.2 A). A 20-fold upregulation was seen in OE33P cells following 72 hours of ACM treatment, and a 12-fold upregulation was seen in OE33R cells at 72 hours ($p=0.01$ and $p=0.03$ respectively) (Figure 3.2 B). Levels of TERC expression did not differ in OE33P compared to OE33R cells following 24 or 72 hours ACM treatment. TERC expression in both OE33P and OE33R cells was lower at 24 compared to 72 hours ($p=0.01$, $p=0.03$ respectively). ACM induced a five-fold downregulation in TERT expression in OE33P cells at 24 hours ($p<0.0001$), but did not alter expression in OE33R cells (Figure 3.2 C). TERT expression was significantly higher in OE33R compared to OE33P cells at 24 hours ($p=0.005$). At 72 hours, ACM did not alter TERT expression in OE33P cells, but induced a ten-fold upregulation in OE33R cells ($p=0.03$) (Figure 3.2 D). TERT expression was significantly higher in OE33R compared to OE33P cells at the 72 hour time point ($p=0.02$). TERT expression in both OE33P and OE33R cells was lower at 24 compared to 72 hours ($p=0.05$, $p=0.02$ respectively).

ACM did not alter TEP1 expression in OE33P cells at 24 hours, but induced a three-fold increase in expression in OE33R cells at 24 hours ($p=0.02$) (Figure 3.3 A). TEP1 expression was significantly higher in OE33R compared to OE33P cells ($p=0.04$). TEP1 expression in OE33P cells was unaffected by 72 hours of ACM treatment. However, ACM stimulated an eight-fold upregulation in TEP1 expression in OE33R cells at 72 hours ($p=0.01$) (Figure 3.3 B). TEP1 expression was significantly higher in OE33R compared to OE33P cells ($p=0.01$). TEP1 expression in OE33P cells did not differ following 24 compared to 72 hours of ACM treatment, however expression in OE33R cells was lower at 24 compared to 72 hours ($p=0.05$). DKC1 expression in OE33P cells was downregulated two-fold following 24 hours of ACM treatment ($p=0.0004$), but expression was not altered in OE33R cells at 24 hours (Figure 3.3 C). ACM did not alter DKC1 expression in OE33P cells at 72 hours, but caused a seven-fold upregulation in OE33R cells ($p=0.02$) (Figure 3.3 D). DKC1 expression in both OE33P and OE33R cells was lower at 24 compared to 72 hours ($p=0.01$ and $p=0.009$ respectively).

The ACM used in this study was generated from the visceral fat of obese or non-obese OAC patients. No difference in TERC, TERT, DKC1 or TEP1 gene expression in OE33P and OE33R cells was seen when ACM from non-obese compared to obese patients was used at 24 and 72 hour time points.

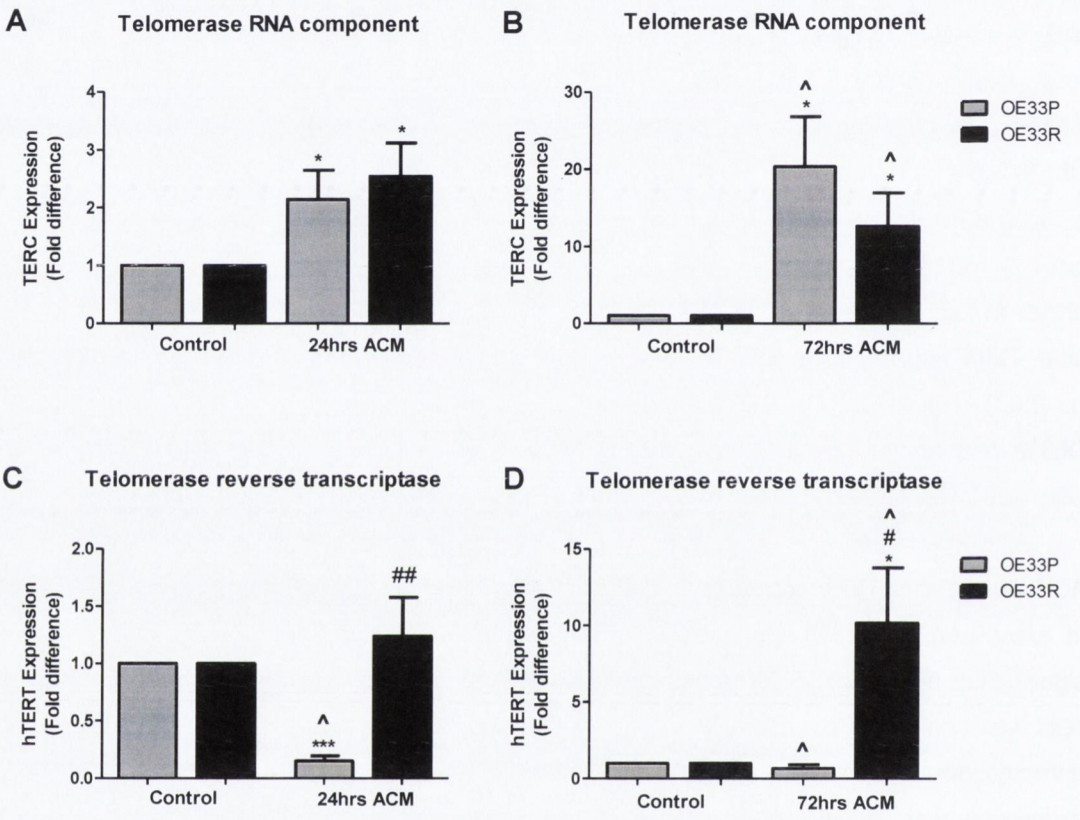


Figure 3.2. ACM alters TERC and TERT expression in OE33P and OE33R
(A) ACM induced a two-fold upregulation in TERC expression in OE33P and OE33R cells following 24 hours of ACM treatment ($p=0.05$ and $p=0.03$ respectively) **(B)** ACM upregulated TERC expression 20-fold in OE33P and 13-fold in OE33R at the 72 hour time point ($p=0.01$ and $p=0.03$ respectively). **(C)** TERT expression was downregulated five-fold in OE33P cells following 24 hours of ACM treatment ($p<0.0001$). **(D)** ACM treatment stimulated an eight-fold upregulation in TERT expression in OE33R cells ($p=0.01$). Data are expressed as mean fold change in expression following ACM treatment compared to controls ± SEM. Statistical analysis was performed using paired, two-tailed student's t test for ACM treated cells compared to control *$p<0.05$, ***$p<0.0001$; an unpaired, two tailed student's t test was used to compare ACM treated OE33P cells to ACM treated OE33R cells, #$p<0.05$, ##$p<0.001$; and to compare cells treated with ACM for 24 hours vs. 72 hours, ^$p<0.05$.

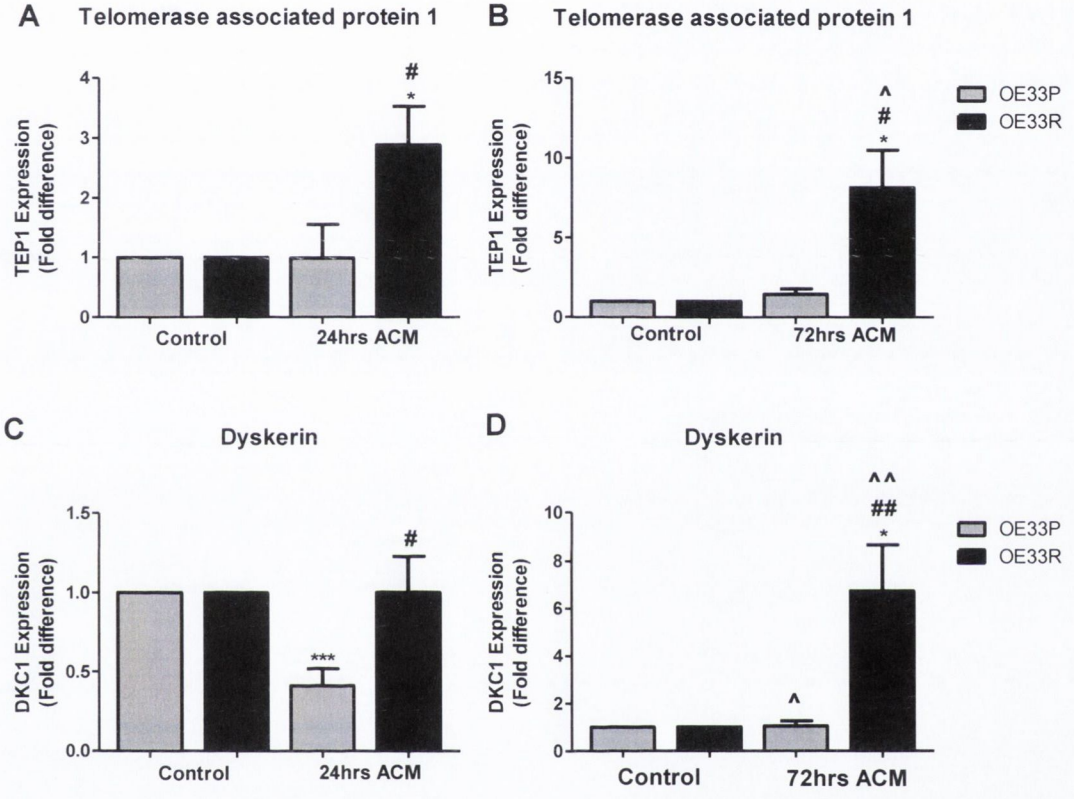


Figure 3.3. ACM alters DKC1 and TEP1 expression

(A) There was a three-fold upregulation in TEP1 expression in OE33R following 24 hours ACM treatment ($p=0.02$). **(B)** At 72 hours there was a ten-fold upregulation in TEP1 expression in OE33R cells ($p<0.05$). **(C)** ACM induced a two-fold downregulation in DKC1 expression in OE33P cells at 24 hours ($p<0.0001$). **(D)** Following 72 hours of ACM treatment there was a seven-fold upregulation of DKC1DKC1 expression in OE33R ($p<0.05$), and expression was significantly higher in OE33R compared to OE33P cells ($p<0.001$) Data are expressed as mean fold change in expression in ACM treated compared to control cells ± SEM. Statistical analysis was performed using paired, two-tailed student's t test for ACM treated cells compared to control *$p<0.05$, ***$p<0.0001$; an unpaired two-tailed student's t test was used to compare ACM treated OE33P cells to ACM treated OE33R cells, #$p<0.05$, ##$p<0.001$; and to compare cells treated with ACM for 24 hours vs. 72 hours, ^$p<0.05$.

3.4.3 TERC gene expression in OE33R cells correlates with visceral obesity

The relationship between telomerase gene expression in OE33P and OE33R cells at 24 and 72 hours following ACM treatment, and visceral obesity status (as measured by visceral fat area) was investigated using Pearson correlation coefficient. Results are summarised in Table 3.2. There was a strong, positive correlation between TERC expression in OE33R cells at 24 hours and VFA ($r= 0.794$ $p=0.006$), with higher levels of TERC expression associated with higher VFA (Figure 3.4). TERT, DKC1 and TEP1 expression in OE33R and OE33P cells following 24 or 72 hours of ACM treatment did not correlate with visceral obesity (Table 3.1).

Table 3.1. Telomerase gene expression correlates with visceral obesity.

	TERC r	TERT r	TEP1 r	DKC1 r
OE33P 24hr ACM VFA	0.226	0.103	0.076	0.196
p value	*0.53*	*0.77*	*0.44*	*0.59*
OE33R 24hr ACM VFA	**0.684**	0.441	0.392	0.610
p value	***0.03***	*0.20*	*0.10*	*0.06*
OE33P 72hr ACM VFA	0.205	0.027	0.584	0.442
p value	*0.55*	*0.94*	*0.08*	*0.20*
OE33R 72hr ACM VFA	0.338	0.507	0.070	0.245
p value	*0.34*	*0.16*	*0.68*	*0.49*

The relationship between telomerase gene expression in OE33P and OE33R cells at 24 and 72 hours following ACM treatment, and obesity status (as measured by visceral fat area) was investigated using Pearson correlation coefficient. Pearson's correlation coefficient r values highlighted in bold represent statistically significant correlations, blue represents negative correlations, and red represents positive correlations. *r*=Pearson's correlation coefficient, VFA=visceral fat area

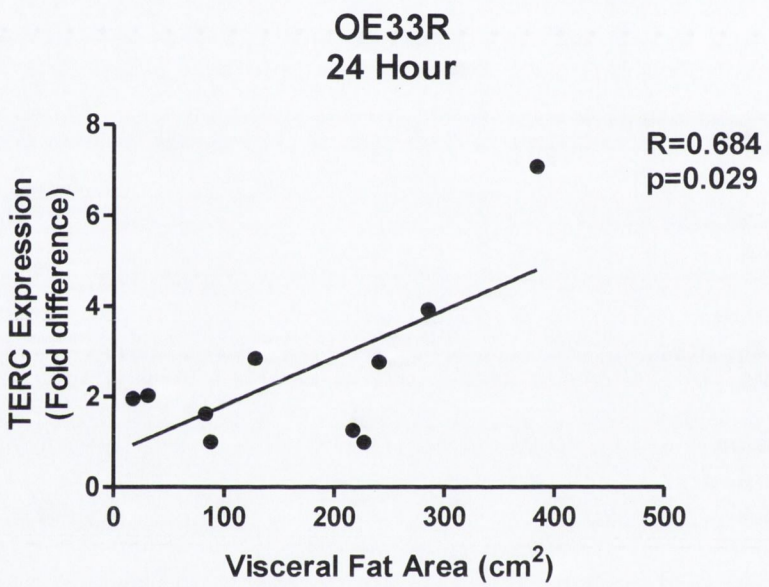


Figure 3.4. TERC expression correlates with visceral obesity
The relationship between TERC expression in OE33R cells post 24 hours ACM treatment and visceral fat area was investigated using Pearson correlation coefficient. There was a positive correlation between TERC expression in OE33R cells post 24 hours of ACM treatment and visceral fat area, with higher TERC expression associated with higher visceral fat area (R=0.684, p=0.029).

3.4.4 ACM drives dysregulation of shelterin complex gene expression

OE33P and OE33R cells were treated with control media or ACM for 24 and 72 hours and the expression of five shelterin complex genes (TERF1, TERF2, POT1, TPP and TINF2) was investigated using quantitative real-time PCR (results are summarised in Table 3.3). TERF1 expression in OE33P and OE33R cells was not altered following ACM treatment for 24 hours, but ACM treatment for 72 hours caused a significant five-fold upregulation of TERF1 in OE33P cells, and a nine-fold upregulation in OE33R cells ($p=0.03$ for both) (Figure 3.5 A). TERF1 expression in OE33P did not differ from OE33R at th72 hour time point. TERF1 expression in both OE33P and OE33R cells was lower at 24 compared to 72 hours ($p=0.02$, $p=0.01$ respectively). ACM treatment did not alter TERF2 or POT1 expression in OE33P or OE33R cells at either 24 or 72 hours following treatment. TPP1 expression was unchanged in both OE33P and OE33R cells following 24 hours of ACM treatment, but was upregulated seven-fold in OE33P cells following 72 hours of ACM treatment ($p=0.03$) (Figure 3.5 B). TPP1 expression did not differ in OE33P compared to OE33R cells at 72 hours ACM treatment. TPP1 expression in OE33P cells was lower following 24 compared to 72 hours ACM treatment ($p=0.03$), however expression in OE33R cells was not different at 24 compared to 72 hours. ACM did not alter TINF2 expression in OE33P cells at 24 hours, but stimulated a four-fold upregulation in expression in OE33R cells ($p=0.05$) (Figure 3.6 A). TINF2 expression was significantly higher in OE33R compared to OE33P cells at 24 hours ACM treatment ($p=0.04$). TINF2 expression was upregulated six-fold in OE33P ($p=0.009$) and nine-fold in OE33R cells ($p=0.04$) following 72 hours ACM treatment (Figure 3.6 B). TINF2 expression did not differ in OE33P compared to OE33R cells following 72 hours ACM treatment. TINF2 expression in OE33P cells was lower following 24 compared to 72 hours ACM treatment ($p=0.007$), however expression in OE33R cells was not different at 24 compared to 72 hours. No difference in shelterin gene expression in OE33P and OE33R cells was seen when ACM from non-obese compared to ACM from obese patients was used at 24 or 72 hour time points.

Table 3.2. ACM upregulates shelterin gene expression in OE33P and OE33R.

	TERF1 Fold change	TERF2 Fold change	POT1 Fold change	TPP1 Fold change	TINF2 Fold change
OE33P 24hr ACM	1.0	-1.3	1.4	1.0	1.1
p value	*0.83*	*0.25*	*0.29*	*0.85*	*0.48*
OE33R 24hr ACM	-1.2	1.6	1.6	2.0	**3.6**
p value	*0.43*	*0.49*	*0.36*	*0.25*	***0.05***
OE33P 72hr ACM	**4.8**	1.9	1.8	**7.2**	**5.9**
p value	***0.03***	*0.20*	*0.21*	***0.03***	***0.009***
OE33R 72hr ACM	**9.3**	7.4	3.4	7.1	**8.6**
p value	***0.03***	*0.07*	*0.09*	*0.06*	***0.04***

OE33P and OE33R cells were co-cultured with control media or ACM from ten OAC patients. Expression of five shelterin complex genes TERF1, TERF2, POT1, TPP1 and TINF2 was assessed. Data are expressed as mean fold change in gene expression in ACM treated OE33P and OE33R cells compared to cells treated with control media. Fold changes highlighted in bold represent statistically significant alterations in gene expression, blue represents downregulation, and red represents upregulation. Statistical analysis was performed using paired, two-tailed student's t test.

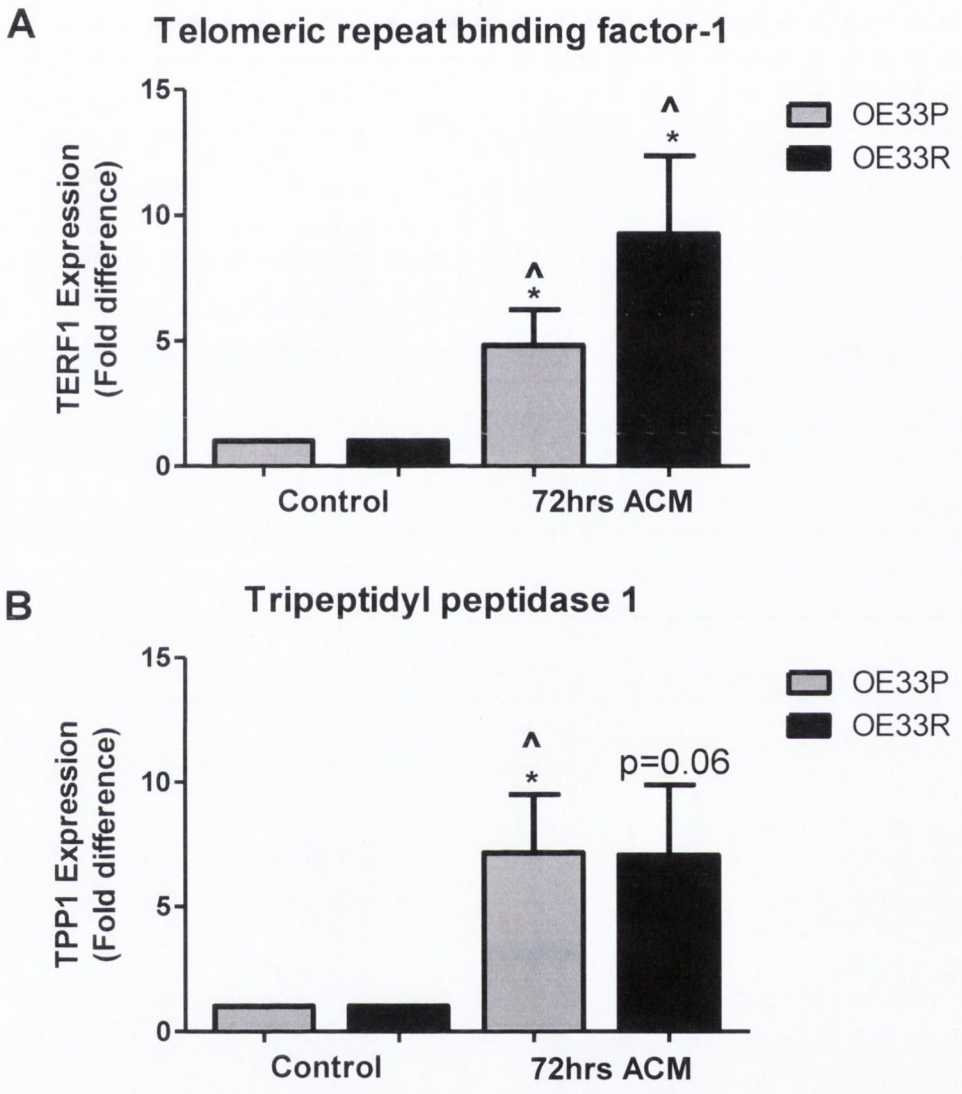


Figure 3.5. ACM upregulates shelterin complex gene expression in OE33P and OE33R

(A) ACM induced a five-fold upregulation in TERF1 expression in OE33P and a nine-fold upregulation in OE33R at 72 hours ($p=0.03$ for all). **(B)** There was a seven-fold upregulation in TPP1 expression in both OE33P and OE33R following 72 hours of ACM treatment, but this did not reach statistical significance in OE33R cells ($p=0.03$ for OE33P). Data are expressed as mean fold change in expression ± SEM. Statistical analysis was performed using paired two-tailed student's t test for ACM treated cells compared to control $*p<0.05$; an unpaired two-tailed student's t test was used to compare ACM treated OE33P cells to ACM treated OE33R cells; and to compare cells treated with ACM for 24 hours vs. 72 hours, $^p<0.05$.

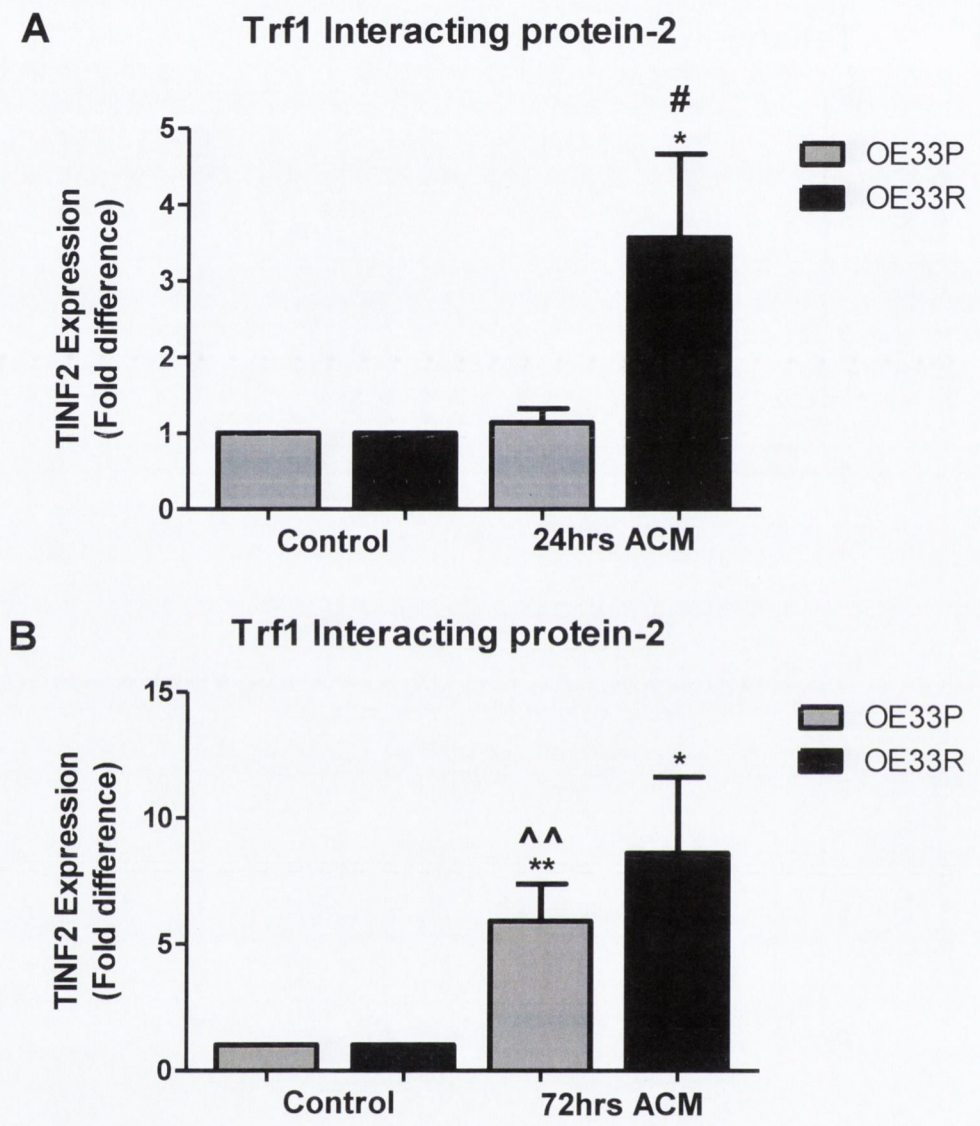


Figure 3.6. ACM upregulates TINF2 gene expression in OE33P and OE33R
(A) ACM induced a four-fold upregulation in TINF2 expression in OE33R cells ($p=0.05$). TINF2 expression was significantly higher in OE33R compared to OE33P cells ($p=0.04$). **(B)** There was a six-fold upregulation in TINF2 expression in OE33P and a nine-fold upregulation in OE33R cells following 72 hours of ACM treatment ($p=0.009$ and $p=0.04$, respectively). Data are expressed as mean fold change in expression ± SEM. Statistical analysis was performed using paired two-tailed student's t test for ACM treated cells compared to control *$p<0.05$, **$p<0.001$; an unpaired two-tailed student's t test was used to compare ACM treated OE33P cells to ACM treated OE33R cells, ##$p<0.001$; and to compare cells treated with ACM for 24 hours vs. 72 hours, ^$p<0.05$.

3.4.5 TERF1, TPP1 and TINF2 gene expression in OE33R correlates with visceral obesity

The relationship between shelterin complex gene expression in ACM treated OE33P and OE33R cells and visceral obesity status (as measured by visceral fat area) was investigated using Pearson correlation coefficient. Results are summarised in Table 3.3. Levels of shelterin gene expression (TERF1, TERF2, POT1, TPP1 and TINF2) in OE33P cells following 24 hours of ACM treatment did not correlate with visceral obesity. However, there was a strong positive correlation between TERF1 expression in OE33R cells treated with ACM for 24 hours and visceral obesity, with higher levels of TERF1 expression associated with higher VFA ($r=0.685$, $p=0.04$) Figure 3.7 A). TERF2 and POT1 expression in ACM treated OE33R cells at 24 hours did not correlate with visceral obesity. Levels of TPP1 expression in OE33R cells following 24 hours of ACM treatment correlated with visceral obesity, with higher gene expression associated with higher VFA ($r=0.873$, $p=0.05$) (Figure 3.7 B). Similarly, TINF2 gene expression in OE33R cells following 24 hours of ACM treatment correlated with visceral obesity, with higher gene expression associated with higher VFA ($r=0.654$, $p=0.05$) (Figure 3.7 C). There was no correlation between levels of TERF1, TERF2, POT1, TPP1 and TINF2 gene expression in OE33P or OE33R cells treated with ACM for 72 hours and visceral obesity.

Table 3.3. Shelterin gene expression correlates with visceral obesity

	TERF1 R	TERF2 R	POT1 R	TPP1 R	TINF2 R
OE33P 24hr ACM VFA	-0.519	0.088	-0.204	-0.051	-0.543
p value	*0.15*	*0.81*	*0.57*	*0.90*	*0.13*
OE33R 24hr ACM VFA	**0.685**	0.143	0.195	**0.873**	**0.654**
p value	***0.04***	*0.69*	*0.59*	***0.05***	***0.05***
OE33P 72hr ACM VFA	0.170	0.501	0.486	0.256	0.369
p value	*0.64*	*0.17*	*0.18*	*0.48*	*0.29*
OE33R 72hr ACM VFA	-0.187	0.580	0.485	0.099	0.252
p value	*0.63*	*0.10*	*0.19*	*0.80*	*0.51*

The relationship between shelterin gene expression in OE33P and OE33R cells at 24 and 72 hours post ACM treatment, and obesity status (as measured by visceral fat area) was investigated using Pearson product-moment correlation coefficient. Pearson's correlation coefficient R values highlighted in bold represent statistically significant correlations, blue represents negative correlations, and red represents positive correlations. R=Pearson's correlation coefficient, VFA=visceral fat area.

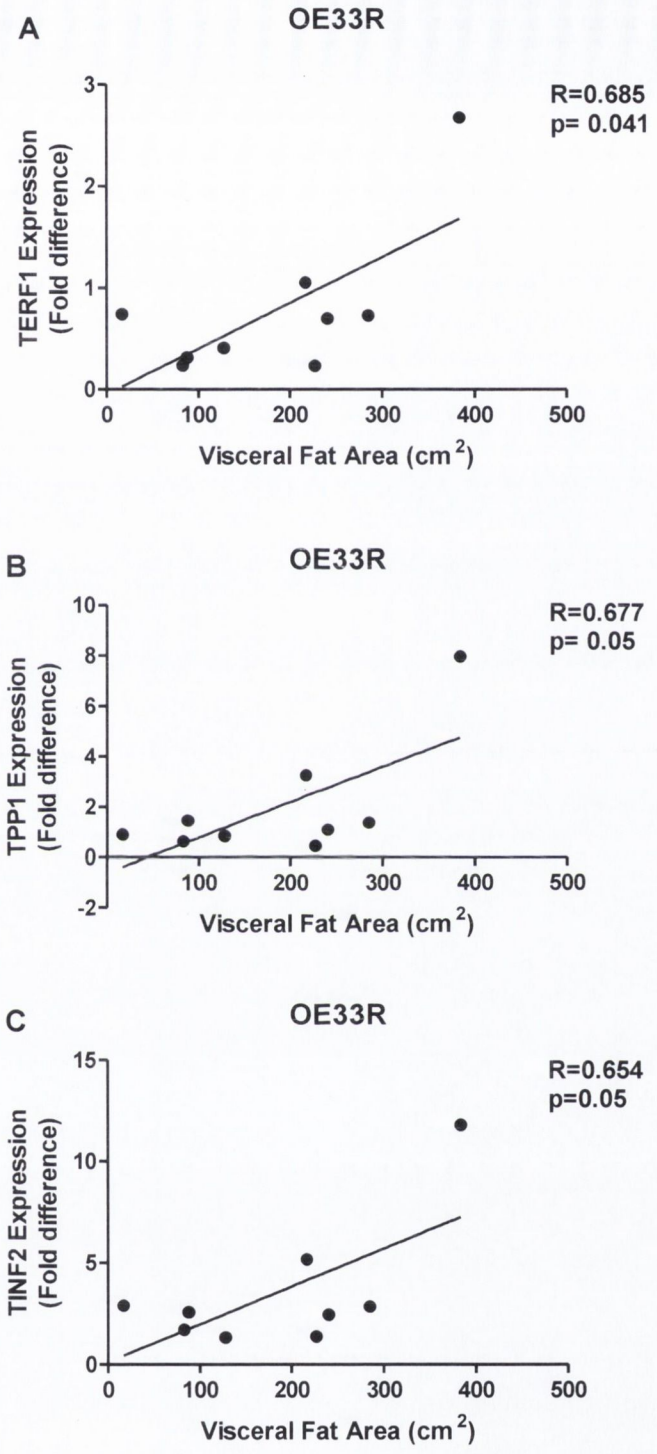


Figure 3.7. Shelterin gene expression in ACM treated OE33R cells correlates with visceral obesity

The relationship between shelterin gene expression in OE33R cells post 24 hours ACM treatment and visceral fat area was investigated using Pearson correlation coefficient. There was a positive correlation between visceral fat area and expression of **(A)** TERF1 (r=0.685, p=0.4), **(B)** TPP1 (r=0.677, p=0.05) and **(C)** TINF2 (r=0.654, p=0.05), in OE33R cells post 24 hours of ACM treatment.

3.4.6 Telomere gene expression in obese and non-obese oesophageal cancer patients

From the panel of four telomerase and five shelterin genes, four telomerase genes (TERC, TERT, DKC1 and TEP1) and three shelterin genes (TERF1, TINF2 and TPP1) were upregulated in OAC cells following ACM treatment. Because these genes were upregulated by ACM and due to their functional importance, TERC, TERT and TINF2 were selected for validation in obese and non-obese OAC tumour samples. Gene expression levels were determined in oesophageal adenocarcinoma tumour tissue samples from viscerally non-obese and obese patients using quantitative real-time PCR (patient details are outlined in table 3.4). Tumour samples from obese patients demonstrated similar levels of TERC expression compared to tumour samples from non-obese patients (Figure 3.8 A). TERT expression however, was significantly higher in obese compared to non-obese patients ($p=0.02$) (Figure 3.8 B). TINF2 expression did not differ in obese compared to non-obese patient tumour samples (Figure 3.8 C).

The relationship between TERC, TERT and TINF2 gene expression in tumour samples and visceral obesity status (as measured by visceral fat area) was investigated using Spearman rho test. Levels of TERC and TINF2 gene expression did not correlate with visceral obesity. However, there was a positive correlation between TERT and visceral obesity, with higher levels of TERT expression associated with higher VFA, but this did not reach statistical significance ($r=0.260$, $p=0.08$).

Table 3.4. OAC tumour patient characteristics (in which TERC, TERT and TINF2 gene expression was measured)

	Non-obese n=46	Obese n=41	p Value
Age at surgery (years)*	65 (42-86)	64 (45-83)	NS[a]
Gender			
Male/Female	35/11	33/8	NS[b]
Obesity Status			
Body mass index (kg/m^2)*	23.4 (10.1-33.6)	29.3 (18.3-39)	<0.0001[a]
Waist circumference (cm)*	88 (61-109)	101 (85-130)	<0.0001[a]
Visceral fat area (cm)*	73.9 (4.3-158)	211.4 (110.6-381.1)	<0.0001[a]
Neoadjuvant therapy			
Yes/No	23/23	21/18	NS[b]
Pathological T Stage			NS[c]
Tis	0	1	
T0	5	19	
T1	6	0	
T2	6	7	
T3	29	12	
T4	0	1	
Tx	0	1	
Nodal status			NS[b]
Node negative	20	18	
Node positive	17	17	

*Values given are median (range); NS=Not significant; a=Analysis performed using Mann Whitney U test; b=Analysis performed using Fisher's exact test; c=Pathological T stage 0-2 compared to pathological T stage 3-4, analysis performed using Fisher's exact test.

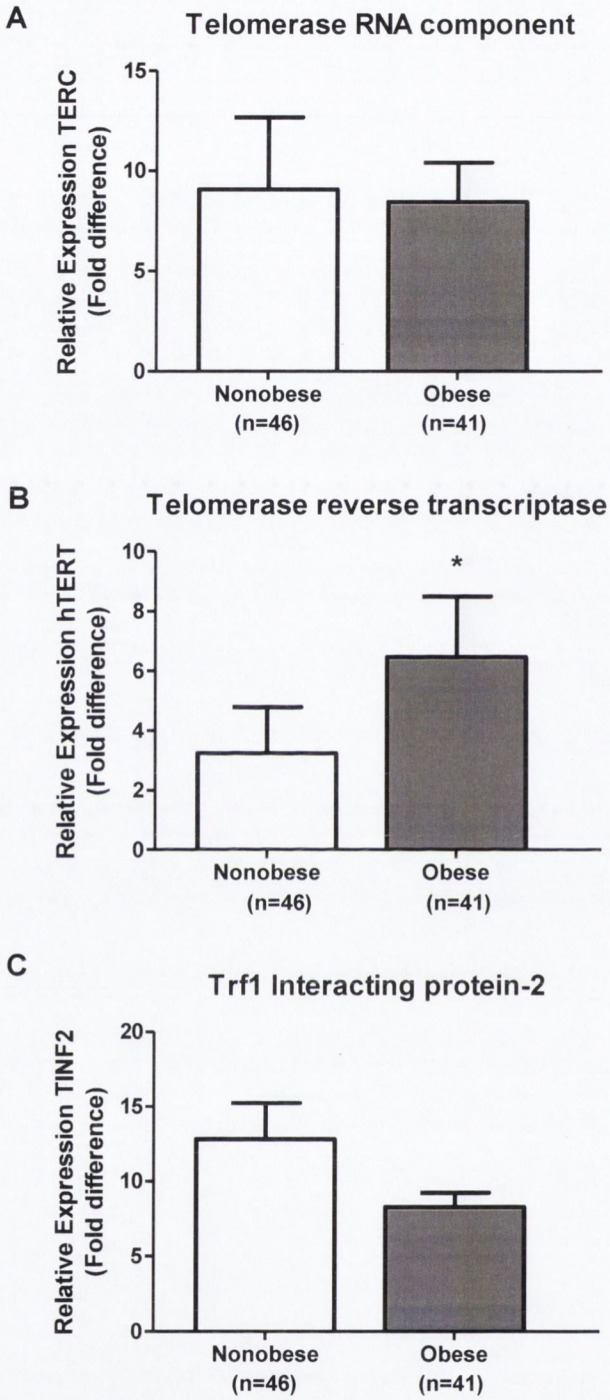


Figure 3.8. Telomerase and shelterin gene expression in obese and non-obese patient cohorts

TERC, TERT and TINF2 expression levels were determined in oesophageal adenocarcinoma tumour samples from non-obese (n=46) and obese (n=41) patients using quantitative real-time PCR. **(A)** Similar levels of TERC expression was seen in tumour samples from obese and non-obese patients. **(B)** TERT expression was significantly higher in tumour samples from obese compared to non-obese patients ($p=0.02$) **(C)** TINF2 expression did not differ in tumour samples from obese compared to non-obese patients. Data are expressed as mean RQ values ± SEM. Statistical analysis was performed using Mann-Whitney U test, *$p<0.05$, **$p<0.001$, ***$p<0.0001$.

3.4.7 Radiosensitivity status influences telomerase and TINF2 expression, but not telomere shortening

Telomere length was similar in untreated OE33P cells compared to untreated OE33R cells (Figure 3.9). ACM induced the same degree of telomere shortening in both OE33P and OE33R cells. Telomerase and shelterin gene expression in OE33P and OE33R was compared at baseline and following ACM treatment (Table 3.5 and 3.6). Basal expression of all four telomerase genes (TERC, TERT, DKC1 and TEP1) was equivalent in untreated OE33P and OE33R cell lines. Following ACM treatment, expression of TERC was similar in OE33P compared to OE33R cells at both 24 and 72 hours. TERT, TEP1 and DKC1 expression was significantly greater in the OE33R cell line compared to OE33P at both 24 and 72 hour time points. There was no difference in basal or ACM-induced expression of TERF1, TERF2, POT1 and TPP1 in OE33P compared to OE33R cells. TINF2 expression was five-fold greater in OE33P cells compared to OE33R cells at baseline ($p=0.05$). This was reversed following ACM treatment for 24 hours when TINF2 expression was three-fold greater in OE33R compared to OE33P cells. ($p=0.05$) Higher TINF2 expression was seen in the OE33R cell line at 72 hours, but this was not statistically significant.

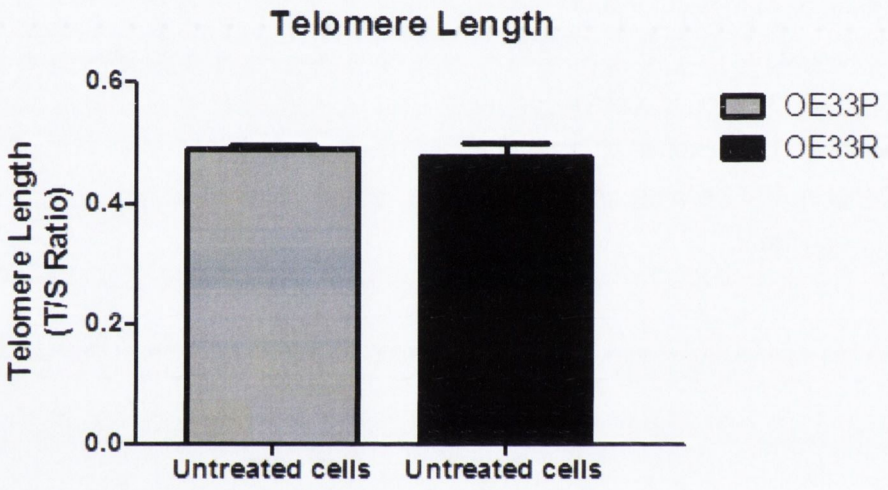


Figure 3.9. Telomere length did not differ in untreated OE33P compared to OE33R cells

The average T/S ratio is an indicator of telomere length; a lower T/S ratio reflects shorter telomere length. No significant difference in telomere length was seen in OE33P cells compared to OE33R cells treated with control media only. Data are expressed as mean telomere length ± SEM. Statistical analysis was performed using unpaired, two tailed student's *t*-test.

Table 3.5. Comparison of telomerase gene expression in OE33P and OE33R cell lines at baseline and following ACM treatment.

	TERC Fold change	hTERT Fold change	TEP1 Fold change	DKC1 Fold change
OE33P vs. OE33R Baseline (Relative RQ)	3.6 vs. 1.8	0.8 vs. 0.4	0.9 vs. 0.4	0.8 vs. 0.6
p value	*0.24*	*0.48*	*0.50*	*0.62*
OE33P vs. OE33R 24hr ACM (Fold change)	2.1 vs. 2.5	**-5.0 vs. 1.2**	**-2.0 vs. 1.0**	**1.0 vs. 2.9**
p value	*0.61*	***0.005***	***0.04***	***0.03***
OE33P vs. OE33R 72hr ACM (Fold change)	20.4 vs. 12.6	**-1.3 vs. 10.2**	**1.4 vs. 8.1**	**1.1 vs. 6.7**
p value	*0.34*	***0.02***	***0.01***	***0.009***

Expression of the four telomerase genes TERC, TERT, TEP1 and DKC1 did not differ in untreated OE33P cells compared to untreated OE33R cells. TERC expression did not differ in OE33P compared to OE33R cells following 24 and 72 hours of ACM treatment. In contrast, TERT, TEP1 and DKC1 expression was significantly different in ACM treated OE33P cells compared to ACM treated OE33R cells at both 24 and 72 hours. Data are expressed as mean fold change in expression. Fold changes highlighted in bold represent statistically significant alterations in gene expression, blue represents downregulation, and red represents upregulation. Statistical analysis was performed using student's t test; NS=Non-significant.

Table 3.6. Comparison of shelterin expression in OE33P and OE33R cell lines at baseline and following ACM treatment.

	TERF1	TERF2	POT1	TPP1	TINF2
OE33P vs. OE33R Baseline (Relative RQ)	0.9 vs. 1.3	0.6 vs. 0.9	2.4 vs. 1.7	0.9 vs. 1.2	**1.6 vs. -3.0**
p value	*0.56*	*0.36*	*0.56*	*0.21*	***0.05***
OE33P vs. OE33R 24hr ACM (Fold change)	1.0 vs. -1.2	-1.3 vs. 1.7	1.4 vs. 1.6	1.0 vs. 2.0	**1.1 vs. 3.6**
p value	*0.43*	*0.33*	*0.77*	*0.26*	***0.05***
OE33P vs. OE33R 72hr ACM (Fold change)	4.8 vs. 9.3	1.9 vs. 7.4	1.8 vs. 3.4	7.2 vs. 7.1	5.9 vs. 8.6
p value	*0.20*	*0.09*	*0.26*	*0.98*	*0.42*

Levels of TERF1, TERF2, POT1 and TPP1 gene expression did not differ in untreated OE33P compared to OE33R cells, or following 24 and 72 hours of ACM treatment. TINF2 gene expression was significantly higher in untreated OE33P compared to untreated OE33R cells ($p=0.05$). TINF2 expression was significantly higher in OE33R cells treated with ACM for 24 hours compared to OE33P cells treated with ACM for 24 hours ($p=0.05$). However, TINF2 expression did not differ in OE33P and OE33R cells following 72 hours of ACM treatment. Data are expressed as mean fold change in expression. Fold changes highlighted in bold represent statistically significant alterations in gene expression, blue represents downregulation, and red represents upregulation. Statistical analysis was performed using two-tailed, unpaired student's t test, *$p<0.05$, **$p<0.001$, ***$p<0.0001$, NS=Non-significant.

3.4.8 Shelterin and telomerase gene expression in responder and non-responder patient cohort

Four telomerase (TERC, TERT, DKC1 and TEP1) and one shelterin gene (TINF2) demonstrated altered expression in OE33P compared to OE33R cells. Due to their functional importance and association with radiosensitivity, TERT and TINF2 were selected for validation in OAC pre-treatment biopsy samples. Gene expression was determined in OAC pre-treatment biopsy samples from patients who went on to have a good pathological response (TRG 1-3; responder), and poor TRG response (TRG 4-5; non-responder) at resection (patient details are outlined in table 2.7). Pre-treatment biopsy tumour samples from responder patients demonstrated lower TERT expression compared to non-responder patients, but this did not reach statistical significance ($p=0.46$) (Figure 3.10 A). Pre-treatment biopsy tumour samples from responder patients demonstrated higher TINF2 expression compared to non-responder patients, but this did not reach statistical significance($p=0.71$) (Figure 3.10 B).

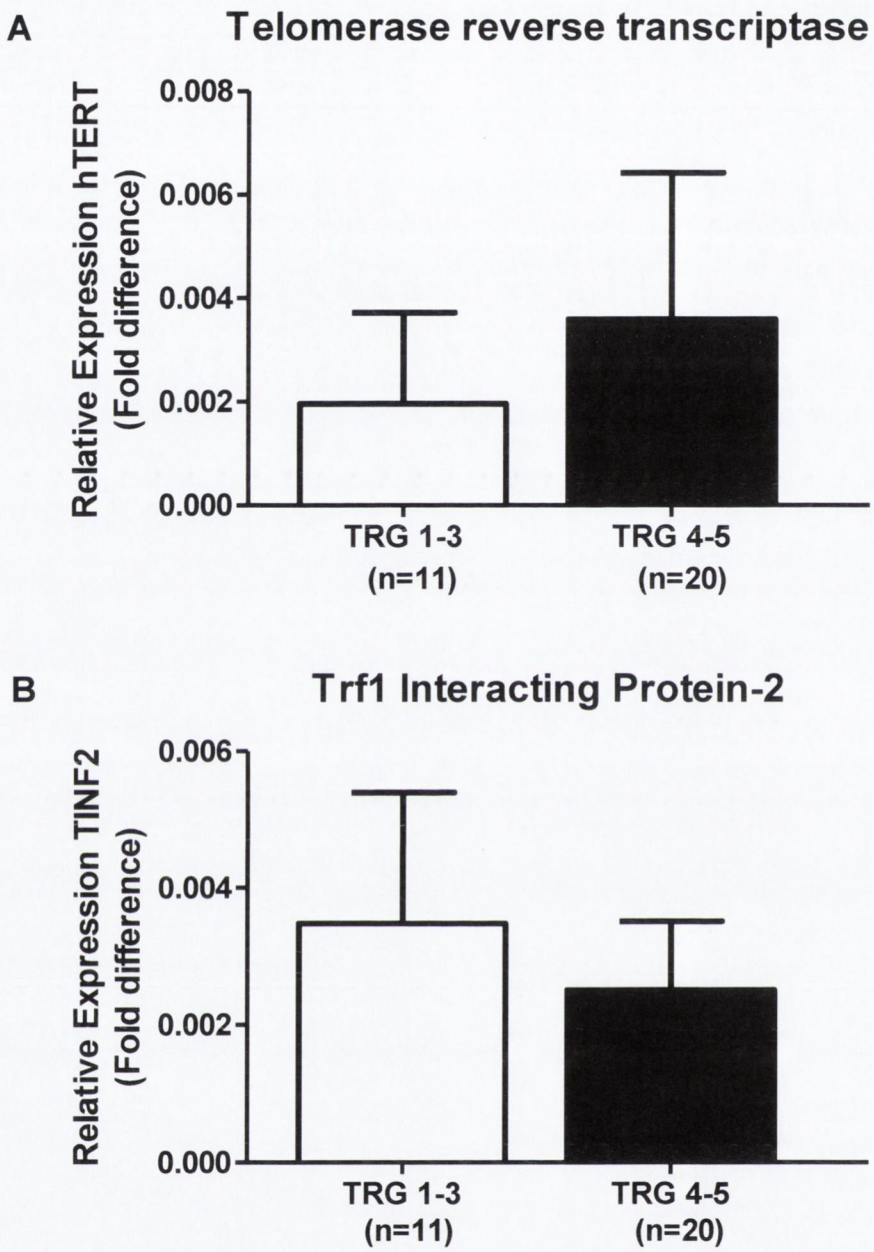


Figure 3.10. TERT and TINF2 gene expression in responder and non-responder patient cohorts

TERT and TINF2 gene expression was determined in OAC pre-treatment tumour biopsy samples from responder and non-responder patients using quantitative real-time PCR. Data are expressed as mean RQ values ± SEM. Statistical analysis was performed using Mann Whitney U test. **(A)** Pre-treatment biopsy tumour samples from responder patients demonstrated lower TERT expression compared to non-responder patients, but this did not reach statistical significance. **(B)** Pre-treatment biopsy tumour samples from responder patients demonstrated higher TINF2 expression compared to non-responder patients, but this did not reach statistical significance

3.5 Discussion

In chapter two we showed that adipose tissue influences radiosensitivity in OAC; the aim of this chapter was to investigate if telomere dysfunction was implicated in the interaction between obesity and radioresponse. In summary, this chapter demonstrated that ACM promoted telomere shortening and dysregulation of telomerase and the shelterin complex, and that obesity status influences TERT gene expression in OAC patients. TERT, TEP1, DKC1 and TINF2 expression, but not telomere length, were associated with radioresistance in the isogenic model.

ACM induced telomere shortening in OE33P and OE33R cells. The number of epidemiologic studies of associations between telomere length and obesity status has grown rapidly in recent years[561]. Short telomeres in leucocytes and adipocytes are associated with measurements of obesity such as BMI and waist circumference, in addition to obesity related conditions such as insulin resistance, diabetes mellitus, and cardiovascular disease[561]. Telomere length is inversely correlated with cancer risk, including oesophageal adenocarcinoma[423,562,563]; telomere shortening is an early event in OAC carcinogenesis[568]. Our findings highlight telomere shortening as a potential mechanism for the pro-tumourigenic environment associated with obesity. The molecular basis for the established link between obesity and telomere dysfunction is not fully understood[416,422,425–427,569–574]. In this study, adipose conditioned media derived from the visceral fat of OAC patients induced telomere shortening in OAC cells. The adipokine profile of visceral ACM has been characterised by our group; VEGF, Adiponectin, IL-6, IL-8, TNF-α and Leptin are all expressed in ACM and may have a role in driving telomere abnormalities[185]. Few studies have focused on the interaction between these adipokines and telomere length. Telomere length is not associated with leptin or TNF-α expression in a healthy paediatric population[575]. Serum levels of adiponectin correlate with telomere shortening in obese diabetic patients[261]. The effect of IL-6 and IL-8 levels on telomere length has not been investigated. These inflammatory cytokines can upregulate NF-κB which leads to an increase in nitric oxide (NO), a substrate for reactive oxygen species (ROS). It has been suggested that oxidative stress may be the underlying mechanism for the association between obesity and shorter telomeres[417]. Oxidative stress induces SSBs in DNA[576]. Telomeric sequences are G-rich and thus more susceptible to acute oxidative damage compared with genomic DNA. In addition, telomeric DNA has a reduced capacity for DNA repair. This causes accelerated telomere loss and replicative senescence during each cell cycle[576]. The effect is enhanced in obesity, since increasing adiposity aggravates oxidative stress processes and the release of inflammatory cytokines[434]. Adipocytes under oxidative stress exhibit increased reactive oxygen species (ROS) generation, DNA damage, shortened telomeres and switch to a pro-inflammatory phenotype with impaired glucose uptake. Adipose tissue has not previously been shown to stimulate telomere shortening in healthy or cancer cells; this is the first study to suggest a causative

rather than correlative relationship between adiposity and telomere dysfunction. Further studies are required to delineate the precise mechanism(s) by which adipose tissue regulates telomere length in OAC.

The relationship between TERC expression and obesity in cancer is not clear. Telomerase activity negatively correlates with obesity status in healthy cells[426]; however, TERC expression does not always parallel telomerase activity, and has been detected in cells that do not normally show telomerase activity[577]. The association of TERC expression per se with markers of obesity has not previously been investigated. In addition to stimulating telomere shortening, ACM altered expression of telomerase and shelterin genes. ACM stimulated upregulation of TERC, the RNA component of telomerase, in OAC cells, and TERC expression correlated with visceral obesity. These novel *in vitro* findings did not translate to patient samples; similar levels of TERC mRNA were demonstrated in obese and non-obese OAC patients. This indicates that the factors in ACM driving TERC expression are visceral fat factors which are expressed at similar levels in non-obese compared to obese patients. A study from this unit compared levels of VEGF, Adiponectin, Leptin and IL6 in ACM derived from the visceral fat of non-obese and obese OAC patients and revealed significantly higher VEGF and significantly lower adiponectin in the ACM from centrally obese patients[185]. No significant difference was observed in IL-6 or leptin levels in the ACM from non-obese compared to obese patient[185], although circulating leptin levels correlate with body mass index. Our results suggest a potential role for leptin and IL6 in regulating TERC expression which has not previously been noted and warrants investigation.

The interaction between TERT expression and obesity status in OAC has not been adequately addressed in the literature. In this study, TERT was upregulated in OAC cells in response to ACM treatment, and TERT expression was significantly higher in obese compared to non-obese OAC patients, confirming findings from our *in vitro* experiments. Our findings contradict a study reporting a significant inverse association between adiposity and telomerase activity in normal healthy cells[401]. Studies have suggested that enhanced expression of TERT, the catalytic subunit of telomerase, is a direct determinant of telomerase activity in cancers as expression of TERT is restricted to cells with telomerase activity only[339,578–583]. Nonetheless, TERT mRNA expression doesn't directly correlate with telomerase enzyme activity, as it depends on posttranscriptional and posttranslational modifications of TERT[583], and our results are consistent with the findings of Rahmati-Yamchi et al. who demonstrated that increased TERT mRNA expression in breast cancer tissue is associated with high BMI[429]. The mechanism linking TERT expression with obesity is uncertain. TERT expression was higher in ACM-treated OE33R cells compared to ACM-treated OE33P cells. In chapter one, we demonstrated that expression of the VEGF co-receptor NRP1 and the leptin receptor was higher in OE33R compared to OE33P cells.

These findings suggest a role for VEGF or Leptin in mediating the upregulation of TERT in OE33R cells in response to ACM. Expression of VEGF, an angiogenic factor known to be an abundant constituent in our ACM, correlates with TERT expression in prostrate, breast and head and neck cancer[584–586]. VEGF has been shown to induce telomerase activity in ovarian cancer through upregulation of TERT expression[185,587]. Leptin is known to induce telomerase activation and upregulate TERT expression in breast cancer cells directly and via the transcription factor STAT3[427]. The relationship between adiponectin levels and telomerase gene expression in cancer patients has not been investigated to date[261]. Hong et al demonstrated that expression of IL-6 and IL-8 does not correlate with telomerase activity in head and neck cancer[585]. In endothelial cells however, IL-8 protects against oxidative stress-induced senescence via upregulation of hTERT expression[588]. While other studies demonstrated a correlation between TERT expression and adiposity measures[429], this is the first study to show that adipose tissue upregulates TERT expression; this effect is likely mediated via adipokine production, but the exact mechanism has yet to be elucidated.

ACM stimulated upregulation of the shelterin complex components TERF1, TINF2 and TPP1, and expression of these three genes correlated with visceral obesity. TINF2 is a central component of shelterin; it connects TPP1 to TERF1. Downregulation of TERF1, TINF2 and TPP1 is seen in colorectal cancer tissue[589], while upregulation of these three genes is related to telomere shortening during hepatocarcinogenesis[590]. Dysregulation of these three genes has not previously been linked with obesity. TINF2 expression was assessed in non-obese and obese OAC patient samples; however obesity status did not influence gene expression levels. A potential limitation of this study is that oesophageal adenocarcinoma tumour samples without laser microcapture dissection were used for gene expression analysis. Thus there is potential for contamination of samples with non-tumour tissue, which may impact the genetic signature of the tissue. Conversely, the inclusion of such cells may provide a more representative picture of the tumour microenvironment.

In this study, telomere length in untreated OE33P cells was similar to telomere length in untreated OE33R cells, and ACM induced the same degree of telomere shortening in both cell lines. An inverse relationship between telomere length and radiosensitivity has previously been reported in healthy fibroblast cell lines[441,448], in addition to cancer cell lines including breast, laryngeal and hepatocellular carcinoma[443,591]. Studies have shown that cells with short telomeres are more radiosensitive than cells with long telomeres; however, long telomeres do not render a cell radioresistant[441]. The connection between telomere length and radiosensitivity is supported by murine studies on the $TERC^{-/-}$ mouse[439,447]. Telomerase deficient mice null for the essential telomerase RNA component gene TERC undergo progressive telomere shortening and are highly sensitive to IR[439]. Other studies dispute this association: Zongaro et al report

that in the presence of telomerase, short telomeres are stabilised and not associated with a radiosensitive phenotype in immortalized fibroblasts[592], while telomere length in peripheral lymphocytes of breast cancer patients does not correlate with radiosensitivity[593]. Studies have shown that in certain cell lines and murine models it is not average telomere length, but rather individual critically short telomeres that trigger cellular responses and render cells radiosensitive[594,595]. Our findings suggest that average telomere length is not indicative of radiosensitivity in our isogenic model.

TERT expression was significantly higher in ACM-treated OE33R cells compared to OE33P cells. Haploinsufficiency of TERT results in a reduction of telomerase activity, telomere shortening and radiosensitivity in colorectal cancer cell lines[596], while TERT expression in rectal carcinoma biopsy samples predicts tumour radiosensitivity, local recurrence and disease free survival[597]. Telomerase is thought to impact radiosensitivity through an indirect effect on telomere length[598]. In this study telomere length did not correlate with expression of the telomerase genes. Low levels of telomerase activity and short telomeres are associated with radiosensitivity in primary human and cancer cell lines[441,444]. Telomerase expression has little effect on the radiosensitivity of human cells with similar telomere lengths[441]. This is supported by studies on $TERC^{-/-}$ mice: the emergence of telomere loss in late generation $TERC^{-/-}$ mice coincided with the emergence of a radiosensitive phenotype associated with accelerated mortality, suggesting that telomere shortening rather than telomerase loss per se impact radioresponse[447]. These studies highlight that although telomerase repression and telomere shortening are closely linked, the two processes may not have identical consequences for the cell[442]. In addition, studies show that TERT mRNA expression doesn't directly correlate with telomerase enzyme activity[583], and TERT has additional functions in tumourigenesis unrelated to telomerase activity, including cellular proliferation, gene expression regulation and mitochondrial function[599]. This suggests that TERT expression may mediate radioresistance without altering telomere length. TERT increases resistance to chemotherapeutic agents and pro-apoptotic stimuli, possibly by inhibition of Bcl-2 mediated mitochondrial apoptosis[600–602]. While our results demonstrate a role for TERT expression as a biomarker of radioresistance in our isogenic model, TERT expression is a target for anti-cancer therapies in vivo[603]. It has been shown that modulation of telomerase activity by telomerase inhibitors can shorten telomere length and increase radiosensitivity in human neuroblastoma and glioma cells[445,604], suggesting telomerase activity may be exploited to sensitize cells to radiotherapy. Radiosensitization by telomerase inhibition is attractive because human malignant cells have shorter telomeres than matched somatic and peripheral blood cells, and telomerase inhibitors are already in phase II trials as a therapeutic modality for human cancer[603]. Available pre-treatment biopsy tissue from our bioresource demonstrated a trend for increased TERT expression in tumour tissue from non-responder patients compared to responder patients. This trend did not reach statistical

significance however, and a larger sample size is required to confirm this effect in future studies.

Telomere function not only depends on telomeric DNA length and telomerase activity, but also on the shelterin complex. We have shown that TINF2 expression differs in untreated and ACM-treated OE33P and OE33R cells. Few studies have focused on the interaction between shelterin complex genes and radioresponse. Cells with telomere shortening secondary to overexpression of TINF2 demonstrate enhanced radiosensitivity compared to cells with longer telomeres due to dominant mutant TINF2-13, but this effect cannot be distinguished from the effect of telomere shortening on radioresponse[560]. TINF2 negatively regulates telomere length in a TERT dependent fashion but does not directly alter TERT expression[605], and depletion of TINF2 is associated with decreased recruitment of telomerase to telomeres. Our in vivo findings demonstrated lower expression of TINF2 in patients with a poor response to CRT, but this did not reach statistical significance. TINF2 forms complexes with other shelterin subunits, in addition to several factors involved in the DNA damage response[606], however no other shelterin genes were associated with radioresistance in our isogenic model.

The precise mechanisms linking radiosensitivity and telomere dysfunction are unknown, but alterations in DNA damage response (DDR) processes may play a role. Telomere maintenance mechanisms are directly or indirectly related to DDR[591,607]. Proteins involved in DDR localize to telomeres and are required for normal telomere maintenance, yet are also involved in the cellular response to telomere shortening and dysfunction. Our group has demonstrated that the radioresistance of the OE33R cells is due at least in part to alterations in DNA damage repair efficiency[174]. Expression of PARP1, a miR-31-regulated gene target, is significantly decreased in OE33P cells compared to OE33R cells, and in oesophageal tumours sensitive to neoadjuvant CRT. PARP1 depletion is also associated with telomere dysfunction: PARP1 is known to be recruited to eroded telomeres, and PARP1 knockout in cell culture systems results in telomere shortening, while the $PARP1^{-/-}$ mouse undergoes 30% telomere loss. The interaction between PARP1 and telomere length is thought be mediated via the interaction between PARP1 and TERF2. Individuals with short telomeres present higher frequencies of radio-induced damage than individuals with long telomeres[448]. Cells with short or dysfunctional telomeres activate a damage response similar to the response observed with DNA DSBs, including activation of ATM, phosphorylation of ATM targets, and formation of nuclear foci containing protein complexes involved in DNA repair[608,609]. The emerging hypothesis is that critically short telomeres act as if they were true DSBs and activate the DNA-damage response is reinforced by studies demonstrating that DNA damage-response factors such as cH2AX, 53BP1, MDC1 and NBS1 form foci on shortened telomeres in senescent human fibroblasts[609].

In this study, telomere shortening, and telomerase and shelterin function were associated with adiposity, while TINF2 and TERT expression was associated with radioresistance in our isogenic model. The molecular basis for these associations remains unclear. With the advent of telomerase inhibition therapies[603], elucidating the mechanisms underpinning the relationship between telomerase and radioresponse in OAC would be of substantial clinical benefit; allowing us to utilize TERT expression in tumour cells as a biomarker to predict radioresponse and to exploit TERT dysfunction in tumour cells to sensitize these cells to radiation[439,461]. Further studies are needed to confirm this relationship in OAC patients.

Chapter 4 Obesity stimulates anaphase bridge formation and spindle assembly checkpoint dysregulation in oesophageal adenocarcinoma

Under review with J Mol Med: AM Mongan, N Lynam-Lennon, R Casey, S Maher, JV Reynolds, G Pidgeon, J O'Sullivan. Obesity drives anaphase bridge formation and spindle assembly checkpoint dysregulation in radioresistant oesophageal adenocarcinoma.

4.1 Introduction

Oesophageal adenocarcinoma (OAC) is now the most prevalent form of oesophageal cancer in the Western world[4]. The incidence of OAC is increasing more than any other cancer in the western world, paralleling the current epidemic of obesity[4]. Obesity is associated with poor survival in a range of cancers including oesophageal[18], and studies have demonstrated that increased visceral obesity is an independent predictor of outcome following anti-angiogenic treatment in colorectal and renal cell carcinoma[505,506]. Standard of care in OAC comprises a multimodal approach with neoadjuvant CRT followed by surgical resection[75,612,613]. Given that 55% of OAC patients in this unit are viscerally obese, investigating the cellular and molecular interaction between obesity and the radioresponse is clinically relevant[185].

Anaphase bridges were first described by McClintock in maize[347], where it is hypothesised that nondisjunction of chromosomes would lead to gains and losses of genetic material via the formation of anaphase bridges and recurrent bridge-breakage-fusion cycles[347]. Anaphase bridging has been reported in cell cultures[348] and in tissues,[614] leading to structural and numerical chromosome changes which are strongly linked to tumourigenesis[349,352]. Anaphase bridges are a common cause and indicator of genomic instability[347]. Increasing levels of telomere dysfunction correlate with higher probabilities of anaphase bridges, while restoration of telomerase results in diminished levels of bridging[615,616]. While telomere shortening in leucocytes has been linked to obesity markers such as BMI and waist circumference[561], the exposures or lifestyle factors driving anaphase bridge formation have not yet been elucidated.

Activation of the spindle assembly checkpoint (SAC) is also essential in the prevention of genomic instability[400]. The SAC is a mitotic metaphase-to-anaphase checkpoint which, when activated, arrests cell cycle progression until all kinetochores (the protein complexes assembled at each centromere) are attached to both poles of the mitotic spindle, ensuring equal allocation of the chromosomes between daughter cells[409]. This represents the major cell cycle control mechanism protecting against aneuploidy[617]. Defects in the spindle assembly checkpoint may drive aneuploidy during carcinogenesis. The genes associated with this process include MAD2L2, BUB1b, CDC20, CENPE and ESPL1[400,618]. Cells with an impaired spindle assembly checkpoint enter anaphase prematurely before all kinetochores are attached and can suffer chromosomal rearrangement which may ultimately drive tumourigenesis[619]. Checkpoint proteins are recruited onto unattached kinetochores where they generate a diffusible signal to prevent anaphase onset during mitosis[620]. Even though mutations in mitotic checkpoint genes are not tolerated well, and are found in only a small number of tumours, SAC function is compromised in virtually all genomically unstable tumours[621]. These data have led to the suggestion that changes in the expression levels of checkpoint proteins, and not their mutation, may account for aneuploidy.

MAD2L2 is an essential component of the SAC. Inactivation or hyperactivation of this protein drives tumourigenesis in mice[622]. Mutations in BUB1b, and related family members BUBR1 and BUB3, have been identified in numerous cancers, though at a low frequency,[623] BUB1b is thought to be essential for precise regulation of the SAC and expression of a mutant BUB1b protein leads to a compromised checkpoint, facilitating genomic instability[624]. BUB1B is a candidate tumour suppressor gene in the oesophagus whose downregulation in normal oesophageal tissue is associated with cancer development. CDC20 is a co-factor of the APC/C and dysregulation of CDC20 is reported in many cancers[619,625]. CENPE is required for the maintenance of chromosomal stability through stabilization of microtubule capture at kinetochores[626]. Studies have shown an interaction between CENPE with SAC genes BUB1b and MAD2L2, which are important in kinetochore attachment to the chromosomes during the end of metaphase[626]. Dysregulation of CENPE function drives aneuploidy both *in vitro* and in an age dependant manner in mice[627]. ESPL1, regulated by securin, is involved in the separation of sister chromatids, which takes place at the metaphase-to-anaphase transition. Depletion of securin impairs DNA repair after radiation, increasing DNA damage and promoting senescence in surviving cells,[628] while ESPL1 overexpression has been shown to drive aneuploidy and tumourigenesis in mice[399].

Cycles of anaphase bridge formation and BFB lead to an increased generation of genetic changes. Malfunction of checkpoint systems that normally cause cell-cycle arrest and apoptosis when recognizing DNA damage or mitotic dysfunction will result in a decreased elimination of cells that have sustained genetic alterations[413,414]. This provides a flexible genetic system for clonal evolution and progression, leading to variability of phenotypic and genetic traits within a cell population[348]. Accumulation of chromosomal instability is associated with resistance to therapy across a range of cancer cell lines[455,629,630], and with poor prognosis in cancer patients[630–632]. An incompetent mitotic checkpoint plays a role in regulating response to therapy in cancer cells[455,633,634].

Obesity fuels tumour progression and may be implicated in the initiation of genomic instability events[415–419,425,431,432]. The aim of this study was to assess if adipose conditioned media drives genomic instability events (anaphase bridges and dysregulated SAC expression) and identify if these instability events are associated with a radioresistant phenotype in oesophageal cancer.

4.2 Overall aim and specific objectives

In chapter 3, we demonstrated that adipose conditioned media induced telomere dysfunction in OE33P and OE33R. Currently there is no published data on the role of adipose tissue in stimulating the downstream bridge-breakage-fusion events anaphase bridge formation and spindle assembly checkpoint dysregulation in oesophageal cancer. Therefore, the aim of this chapter was to elucidate the interaction between adipose tissue, anaphase bridge formation and SAC expression in a radioresistant OAC model, and to investigate the expression of SAC genes in obese and non-obese OAC patients and responder and non-responder OAC patient cohorts.

Specific objectives:

- Investigate the effect of adipose conditioned media on anaphase bridge formation in OE33P and OE33R
- Investigate the effect of adipose conditioned media on SAC (MAD2L2, BUB1b, CDC20, CENPE and ESPL1) gene expression in OE33P and OE33R
- Determine if the expression of SAC genes in tumour samples from oesophageal cancer patients correlates with obesity status
- Investigate if the expression of MAD2L2, BUB1b, CDC20, CENPE and ESPL1 genes in diagnostic pre-treatment biopsies from OAC patients is associated with response to neoadjuvant CRT as determined by tumour regression grade

4.3 Materials and methods

4.3.1 Cell Culture

Cell culture was performed as described in section 2.3.3

4.3.2 Anaphase bridge enumeration

Crystal violet staining

Crystal violet assays were performed to determine fold change in cell number in OE33P and OE33R cells following ACM treatment. Cell number was assessed at the same time as anaphase bridge level enumeration to allow for normalisation to change in cell number. Cells were seeded in triplicate in 96 well plates at a concentration of 5000 cells/well and allowed to adhere overnight prior to co-culture with 50µl ACM or M199 control media for 24 and 72 hours at 37^{0}C. Following 24 and 72 hours, the media was decanted. Cells were washed with PBS and fixed with 1% glutaraldehyde at room temperature for 15 minutes. Cells were washed with PBS and stained with 500µl 0.1% crystal violet at room temperature for 30 minutes. Crystal violet was discarded and the plate washed gently with tap water, then left to air dry upside down for ten minutes. Cells were resuspended in 400µl Triton X solution and incubated on a shaker for 15 minutes at room temperature. 100µl of sample was transferred into a 96 well plate. The absorbance was read at 590nm in a VERSAMax microplate reader (Molecular devices, CA, USA).

Staining of anaphase bridges

Cells were seeded in triplicate in 12 well plates at a concentration of $2x10^4$ cells/well, and allowed to adhere for at least 6 hours prior to co-culture with ACM or M199 control media for 24 and 72 hours at 37^{0}C. Cells were washed with PBS and fixed with 3.7% paraformaldehyde at room temperature for 15 minutes. Cells were stained with haematoxylin for 30 minutes at room temperature. Fixed cells were washed with tap water to remove excess stain, and washed in 50%, 70% and 100% ethanol before drying on the bench for 1 hour. Anaphase bridges were counted using an Olympus CKX41 (Tokyo, Japan) microscope at 20x magnification. Anaphase bridges were defined as one or more interconnected strands between daughter nuclei. Numbers of anaphase bridges counted were normalised to increase in cell number assessed by crystal violet assay, and expressed as a fold change compared to the M199 control.

4.3.3 Oesophageal tumour and adipose tissue biobank

Patient samples were processed as outlined in section 3.3.5.

4.3.4 Investigation of gene expression

Gene expression was investigated as described in section 2.3.5.

4.3.5 Statistical analysis

Statistical analysis was performed using Graphpad Prism 5 software (GraphPad Software, Inc., CA, USA) and SPSS version 18 for Windows (IBM, Armonk, New York, USA) software. Unless otherwise stated, data are expressed as mean ± standard error of the mean (SEM). SEM was calculated as the standard deviation of the original sample divided by the square root of the sample size. In cases where data were paired (i.e. untreated versus ACM-treated cells) a two-tailed paired t-test was used for statistical analysis. A two-tailed unpaired t-test was used to analyse unpaired parametric data. The Mann-Whitney U test was used to examine statistical significance between unpaired groups of non-parametric data. Data analysis was performed by one way analysis of variance (ANOVA), where the number of groups in the experiment was three or more. A Tukey multiple comparisons post hoc test was necessary following ANOVA in order to determine which groups were significantly different to each other. For all statistical analysis, a probability of (p) of ≤ 0.05 was considered to represent significant difference between groups.

4.4 Results

4.4.1 ACM stimulates cell growth in OE33P and OE33R

In order to normalise levels of anaphase bridges to changes in cell growth induced by ACM, cell number was assessed in OE33P and OE33R cell lines following 24 and 72 hour treatment with either control media or ACM using a crystal violet assay. Anthropometric characteristics of patients are summarised in chapter three (Table 3.1). ACM stimulated a 1.5-fold increase in cell growth in OE33P and OE33R cell lines following 24 hours of treatment ($p<0.0001$ and $p=0.003$ respectively) (Figure 4.1 A). There was no difference in cell number in OE33P cells compared to OE33R cells following 24 hours of ACM treatment. ACM increased cell number two-fold in OE33P cells at the 72 hour time point ($p=0.02$) (Figure 4.1 B). There was no change in cell number in OE33R cells following 72 hours of ACM treatment (Figure 4.1 B). Cell number in OE33P cells following ACM treatment was greater than cell number in ACM treated OE33R cells at the 72 hour time point ($p=0.009$). There was no difference in cell number in OE33P and OE33R cells following 24 compared to 72 hours ACM treatment. There was no difference in cell number in OE33P and OE33R cells following treatment with ACM generated from non-obese compared to obese patients.

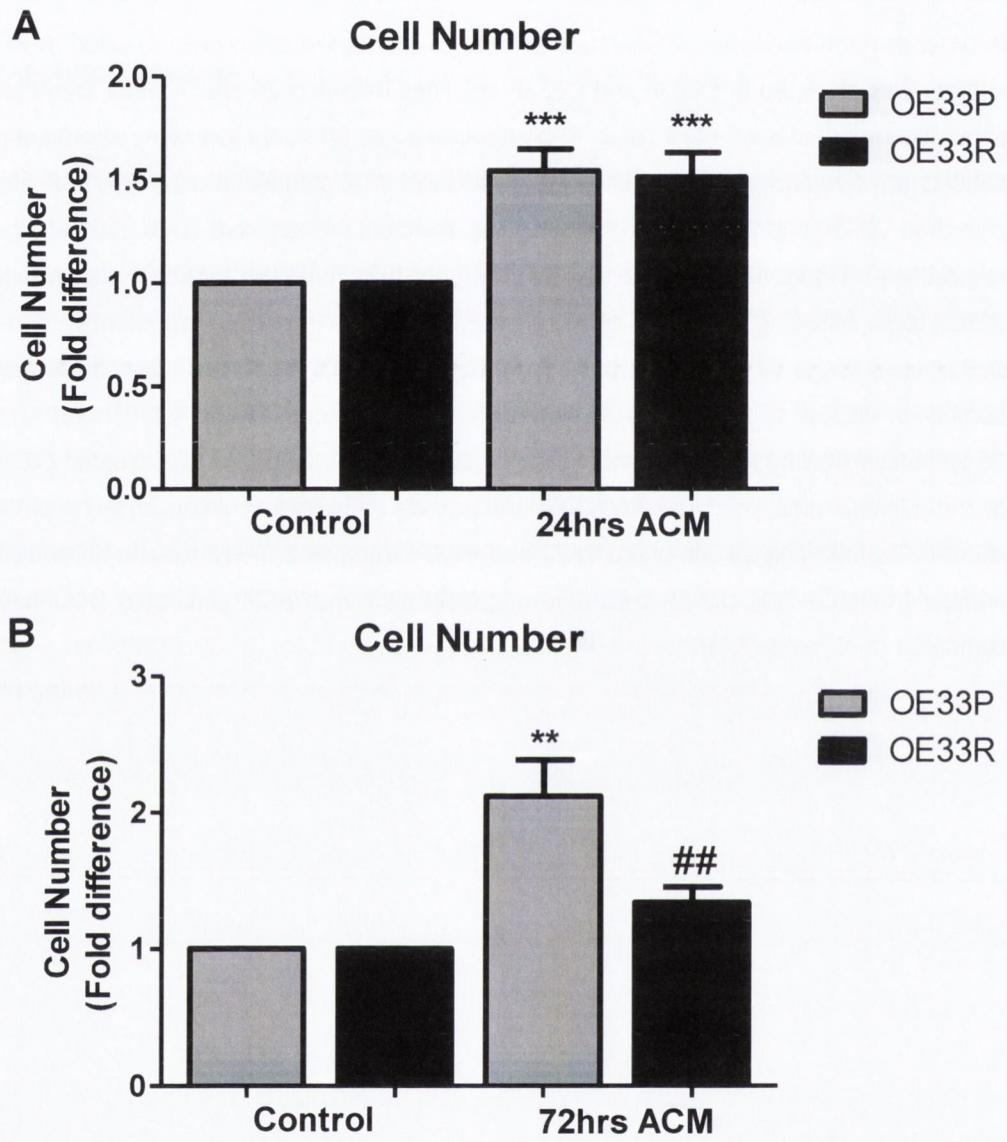


Figure 4.1. ACM stimulated cell growth in OE33P and OE33R cells at 24 hours
(A) ACM stimulated a 1.5-fold increase in cell number in both OE33P and OE33R cells following 24 hours of ACM treatment ($p<0.0001$ and $p=0.003$ respectively). Cell number did not differ in OE33P compared to OE33R cells following 24 hours ACM treatment. **(B)** ACM increased cell number two-fold in OE33P cells at 72 hours ($p=0.02$), but did not alter cell number in OE33R. There was no difference in cell number in OE33P cells compared to OE33R cells following 72 hours of ACM treatment. Data are expressed as fold change in cell number in ACM treated cells compared to cells treated with control media ± SEM. Statistical analysis was performed using paired, two-tailed student's t-test when comparing ACM treated OE33P and OE33R cells versus control, **$p<0.001$, ***$p<0.0001$; an unpaired, two-tailed student's t test was used to compare ACM treated OE33P cells to ACM treated OE33R cells, ##$p<0.001$.

4.4.2 ACM stimulates anaphase bridge formation in OE33P and OE33R

Figure 4.2 illustrates anaphase bridges representing lagging chromosomes that do not fully resolve during anaphase (Figure 4.2 A-C). OE33P and OE33R cell lines were cultured with control M199 media and ACM for 24 and 72 hours. The anthropometric characteristics of patients are summarised in chapter three (Table 3.1). Cell growth rates and anaphase bridge levels were assessed at both time points. Results were expressed as fold increase in anaphase bridge formation per fold increase in cell number. There was no difference in levels of anaphase bridges between OE33P and OE33R cell lines following treatment with control media. OE33P cells exposed to ACM for 24 hours showed a two-fold increase in anaphase bridge levels compared to OE33P cells exposed to control media ($p=0.001$) (Figure 4.3 A). OE33R cells exposed to ACM for 24 hours showed a six-fold increase in anaphase bridge levels compared to OE33R cells exposed to control media ($p=0.001$) (Figure 4.3 A). Levels of anaphase bridging following ACM treatment were higher in OE33R cells compared to the OE33P cells at 24 hours ($p<0.01$) (Figure 4.3 A).

OE33P cells exposed to ACM for 72 hours demonstrated significantly lower levels of bridges compared to cells exposed to control media (two-fold decrease, $p<0.0001$) (Figure 4.3 B). OE33R cells exposed to ACM for 72 hours demonstrated a 1.5-fold increase in levels of anaphase bridge formation compared to cells exposed to control media ($p=0.006$) (Figure 4.3 B). Levels of anaphase bridging following ACM treatment were higher in OE33R cells compared to the OE33P cells at 72 hours ($p<0.0001$) (Figure 4.3 B). Significantly higher levels of anaphase bridge formation were seen in OE33P at 24 compared to 72 hours ($p<0.0001$). Significantly higher levels of anaphase bridges were seen in OE33R at 24 compared to 72 hours ($p=0.002$). Levels of anaphase bridges in OE33P and OE33R cells did not differ in response to ACM generated from non-obese compared to obese patients.

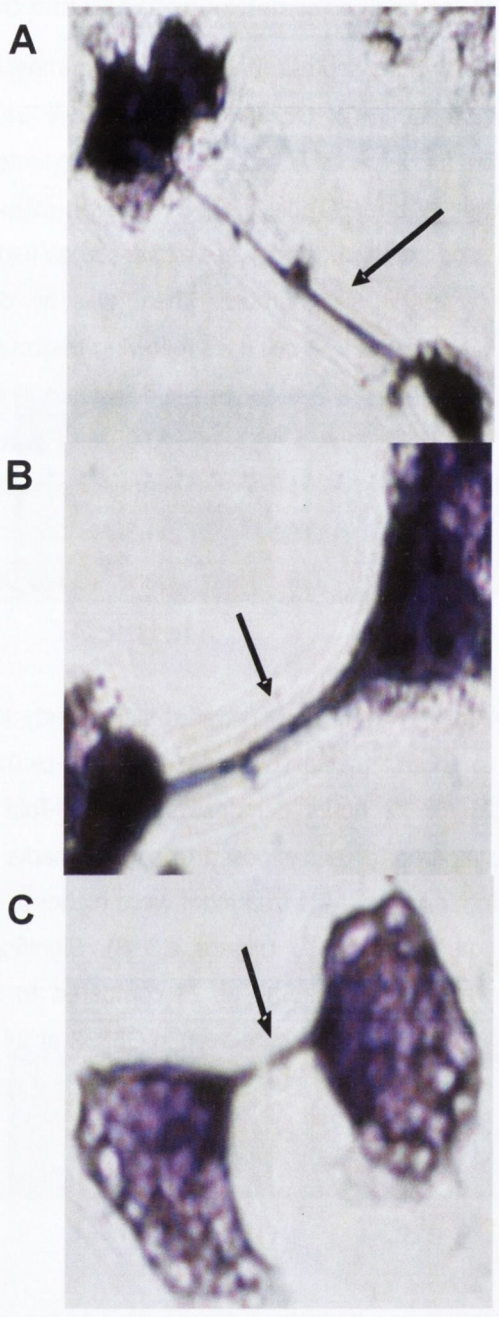


Figure 4.2 Anaphase bridge formation in OE33P and OE33R cells
OE33P and OE33R cells were co-cultured with ACM generated from non-obese and obese OAC patients. Anaphase bridges were enumerated post ACM treatment. **(A, B, C)** This panel illustrates representative images of anaphase bridges enumerated in this study.

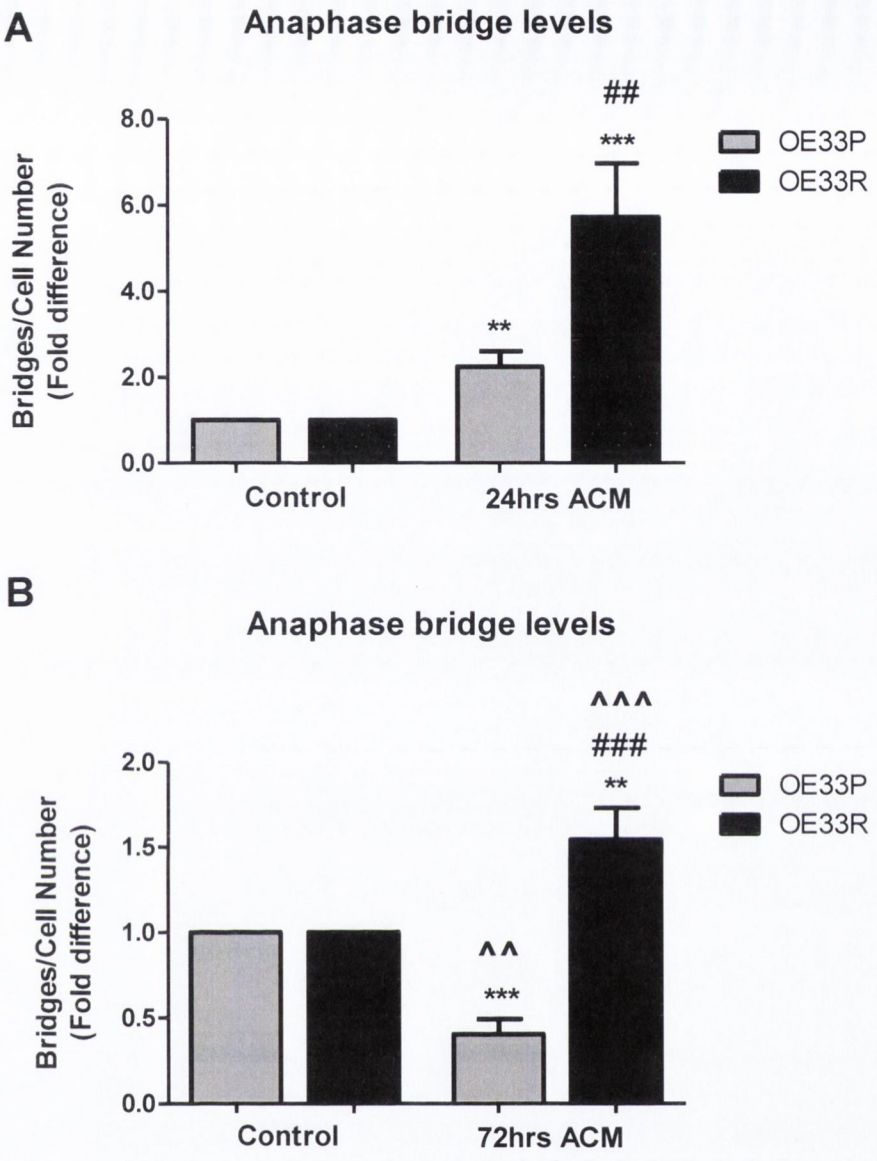


Figure 4.3. Anaphase bridge levels in OE33P and OE33R cells following ACM treatment

(A) Increased anaphase bridge levels at 24 hours post ACM treatment were detected in both OE33P (two-fold increase, p=0.001) and OE33R cells (six-fold increase, p=0.001) compared to controls. Levels of bridging induced by ACM were higher in OE33R compared to OE33P cells at 24 hours (p=0.004). **(B)** A two-fold decrease in anaphase bridge levels was detected in OE33P cells following 72 hours of ACM treatment (p<0.0001). ACM increased anaphase bridge levels 1.5-fold in OE33R cells at 72 hours (p=0.006). Levels of bridging induced by ACM were higher in OE33R compared to OE33P cells at 72 hours (p<0.0001). Significantly higher levels of anaphase bridges were seen in OE33P (p<0.0001), and OE33R (P=0.002) at 24 hours compared to 72 hours. Data are expressed as fold increase in anaphase bridges per fold increase in cell number. Analysis was performed using paired two-tailed student's *t*-test for ACM treated OE33P and OE33R cells versus control, **p<0.001, ***p<0.0001; an unpaired, two-tailed student's t test was used to compare ACM treated OE33P cells to ACM treated OE33R cells, ##p<0.001, ###p<0.0001, and when comparing cells treated with ACM for 24 versus 72 hours, ^^p<0.001, ^^^p<0.0001.

4.4.3 Anaphase bridge levels in ACM treated OE33R cells correlate with visceral obesity.

The correlation of anaphase bridge levels in OE33P and OE33R cells at 24 and 72 hours post ACM treatment with visceral obesity status (as measured by visceral fat area) was investigated using Pearson correlation coefficient. Anaphase bridge levels following 24 hours of ACM exposure did not correlate with visceral obesity (Table 4.1). However, there was a positive correlation between anaphase bridge levels in OE33R cells treated with ACM for 72 hours and VFA ($R=0.794$ $p=0.006$), with higher levels of anaphase bridge formation associated with higher VFA (Figure 4.4).

Table 4.1. Levels of anaphase bridges in ACM treated OE33R cells correlate with visceral obesity

	OE33P 24hr R	OE33R 24hr R	OE33P 72hr R	OE33R 72hr R
VFA	0.198	-0.040	0.205	**0.795**
p value	*0.58*	*0.91*	*0.57*	***0.006***

R=Pearson's correlation coefficient. Figures in bold represent statistically significant correlations, figures in red represent positive correlations

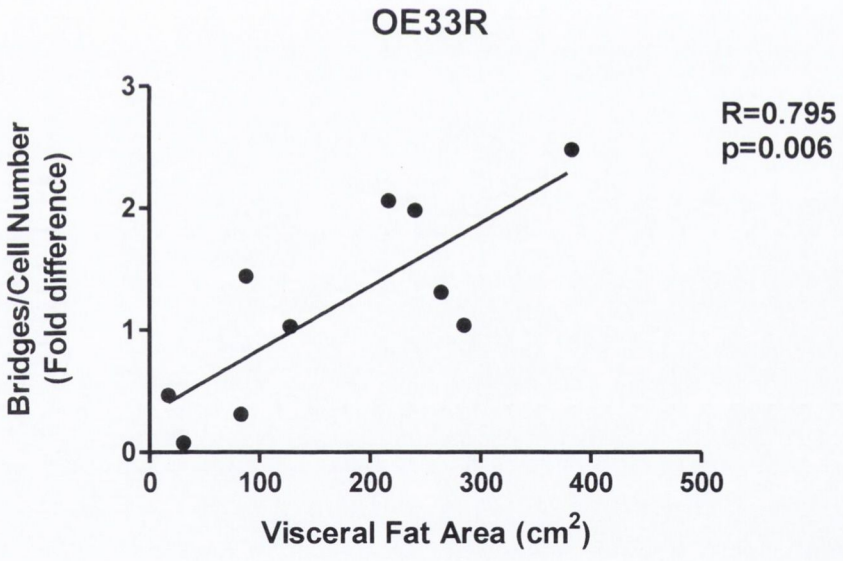


Figure 4.4. Anaphase bridge levels correlate with obesity status in OE33R cells following ACM treatment

The relationship between anaphase bridge levels in OE33R cells at 72 hours post ACM treatment and visceral obesity was investigated using Pearson correlation coefficient. There was a positive correlation between anaphase bridge formation in OE33R and VFA (R=0.795, p=0.006), with high levels of anaphase bridges associated with visceral obesity status.

4.4.4 Anaphase bridge levels correlate with TERC, TERT and DKC1 gene expression in ACM treated cells

The relationship between TERC, TERT, TEP1 and DKC1 gene expression in OE33P and OE33R cells at 24 and 72 hours post ACM treatment, and anaphase bridge levels was investigated using Pearson correlation coefficient. Results are summarised in Table 4.2. Anaphase bridge levels were negatively correlated with TERC expression in OE33P cells following 24 hour of ACM treatment (R= -0.712, p=0.03) (Figure 4.5 A). A negative correlation was detected between levels of anaphase bridging in OE33R cells at 24 hours and gene expression of TERT (R= -0.687, p=0.04) and DKC1 (R= -0.661, p=0.05) with higher anaphase bridge levels associated with lower TERT and DKC1 expression (Figure 4.5 B and C). There was no correlation between anaphase bridge levels and TEP1 gene expression in ACM treated OE33P and OE33R. The relationship between shelterin gene expression in OE33P and OE33R cells at 24 and 72 hours post ACM treatment, and anaphase bridge levels was investigated using Pearson correlation coefficient. There was no correlation between anaphase bridge levels and TERF1, TERF2, POT1, TINF2 or TPP1 expression in ACM treated OE33P and OE33R cells (Table 4.3).

Table 4.2. TERC, TERT and DKC1 gene expression correlates with anaphase bridge levels in ACM treated OAC cells

	TERC R	TERT R	TEP1 R	DKC1 R
OE33P 24hr ACM Anaphase Bridging	**-0.712**	-0.199	-0.136	-0.139
p value	***0.03***	*0.61*	*0.73*	*0.72*
OE33R 24hr ACM Anaphase Bridging	-0.453	**-0.687**	-0.562	**-0.661**
p value	*0.22*	***0.04***	*0.11*	***0.05***
OE33P 24hr ACM Anaphase Bridging	0.042	-0.215	0.615	-0.133
p value	*0.92*	*0.61*	*0.08*	*0.75*
OE33R 72hr ACM Anaphase Bridging	-0.061	-0.507	0.070	0.356
p value	*0.87*	*0.16*	*0.86*	*0.36*

The relationship between telomerase gene expression in OE33P and OE33R cells following 24 and 72 hours of ACM treatment and anaphase bridge levels was investigated using Pearson correlation coefficient. Anaphase bridge levels were negatively correlated with TERC expression in OE33P cells following 24 hour of ACM treatment (R= -0.712, p=0.03). A negative correlation was detected between TERT expression and anaphase bridge levels in OE33R cells following 24 hours ACM treatment (R= -0.687, p=0.04). There was a negative correlation between DKC1 expression and anaphase bridge formation in OE33R cells following 24 hours ACM treatment (R= -0.661, p=0.05). There was no correlation between anaphase bridge levels and TEP1 gene expression in OE33P or OE33R. R values highlighted in bold represent statistically significant correlations; blue represents negative correlations; red represents positive correlations.

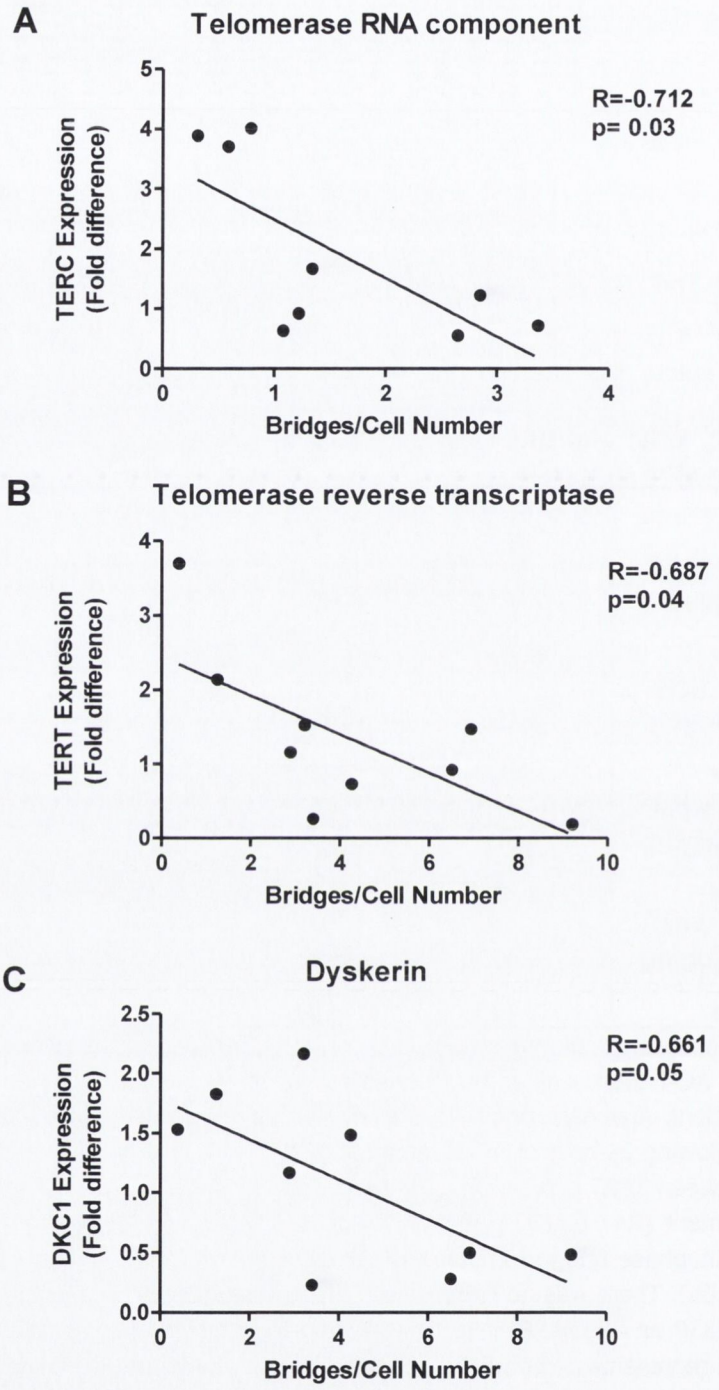


Figure 4.5. Telomerase gene expression correlates with anaphase bridge levels in ACM treated OE33P and OE33R cells

The relationship between telomerase gene expression in OE33P and OE33R cells following 24 and 72 hours of ACM treatment and visceral fat area was investigated using Pearson correlation coefficient. **(A)** A negative correlation between TERC expression and anaphase bridge levels was detected in OE33P cells following 24 hours ACM treatment (R= -0.712, p=0.03). **(B)** There was a negative correlation between TERT expression and anaphase bridge levels in OE33R cells following 24 hours ACM treatment (R= -0.687, p=0.04). **(C)** A negative correlation was detected between DKC1 expression and anaphase bridge levels in OE33R cells following 24 hours ACM treatment (R= -0.661, p=0.05).

Table 4.3. Shelterin gene expression does not correlate with anaphase bridge formation.

	TERF1 R	TERF2 R	POT1 R	TINF2 R	TPP1 R
OE33P 24hr ACM Anaphase Bridging	-0.524	-0.462	-0.491	-0.332	-0.180
p value	*0.18*	*0.21*	*0.18*	*0.42*	*0.67*
OE33R 24hr ACM Anaphase Bridging	-0.388	-0.273	-0.432	-0.248	-0.218
p value	*0.34*	*0.48*	*0.25*	*0.55*	*0.60*
OE33P 72hr ACM Anaphase Bridging	0.039	0.140	0.091	0.154	0.022
p value	*0.92*	*0.74*	*0.13*	*0.69*	*0.95*
OE33R 72hr ACM Anaphase Bridging	-0.485	0.138	0.078	0.036	-0.209
p value	*0.23*	*0.74*	*0.85*	*0.93*	*0.62*

The relationship between shelterin gene expression in OE33P and OE33R cells post ACM treatment and visceral fat area was investigated using Pearson correlation coefficient. There was no correlation between visceral fat area and shelterin gene expression in OE33P or OE33R.

4.4.5 ACM drives dysregulated spindle assembly checkpoint gene expression in OE33P and OE33R

Expression of five spindle assembly checkpoint genes (MAD2L2, BUB1b, CDC20, CENPE and ESPL1) in OE33P and OE33R cells treated with ACM, was investigated using quantitative real-time PCR. The anthropometric characteristics of patients are summarised in chapter three (Table 3.1).

There was a significant six-fold upregulation in MAD2L2 expression in OE33P cells following 24 hours ACM treatment compared to cells treated with control media ($p=0.0007$). MAD2L2 expression increased ten-fold in OE33R cells following ACM treatment for 24 hours ($p=0.004$) (Figure 4.6 A). MAD2L2 expression did not differ in ACM treated OE33P cells compared to ACM treated OE33R cells. A two-fold increase in expression was detected in OE33P following exposure to ACM for 72 hours ($p=0.01$) but MAD2L2 expression was unchanged in OE33R cells following 72 hours treatment with ACM (Figure 4.6 B). MAD2L2 expression was significantly higher in OE33P compared to OE33R cells at this time point ($p=0.004$). Significantly higher MAD2L2 expression was detected in OE33P ($p=0.002$), and OE33R ($p=0.002$) cells treated with ACM for 24 compared to 72 hours. MAD2L2 expression in OE33P and OE33R did not differ following treatment with ACM generated from non-obese compared to obese patients.

BUB1b expression did not differ in ACM treated OE33P cells compared to ACM treated OE33R cells at 24 hours. There was a five-fold increase in BUB1b expression ($p=0.008$) in OE33P cells following 24 hours of treatment with ACM. BUB1b expression was upregulated six-fold in OE33R cells treated with ACM for 24 hours ($p<0.01$) (Figure 4.6 C). In contrast there was a two-fold decrease in BUB1b expression in OE33P cells following 72 hours of ACM treatment ($p=0.0004$), and a five-fold downregulation of expression in OE33R cells treated for 72 hours ($p<0.001$) (Figure 4.6 D). BUB1b expression was higher in OE33R cells compared to OE33P cells at this time point ($p=0.004$). Significantly higher BUB1b expression was detected in OE33P ($p=0.003$) cells following ACM treatment for 24 compared to 72 hours. Similarly, BUB1b expression was higher in OE33R cells following ACM treatment for 24 compared to 72 hours ($p=0.001$). Expression of BUB1b in OE33P and OE33R did not differ following treatment with ACM generated from non-obese compared to obese patients.

Figure 4.6 demonstrates a five-fold upregulation in CDC20 expression in OE33P in response to ACM treatment for 24 hours ($p=0.007$). CDC20 expression was upregulated six-fold in resistant cells following ACM treatment for 24 hours ($p<0.0001$) (Figure 4.7 A). There was no difference in CDC20 expression in OE33P compared to OE33R cells following 24 hours ACM treatment. CDC20 expression was downregulated two-fold in OE33P cells in response to ACM treatment for 72 hours ($p=0.001$). There was a three-fold downregulation in CDC20 expression in OE33R in response to ACM ($p=0.001$) (Figure 4.7 B). There was no difference in CDC20 expression in

OE33P compared to OE33R cells following 72 hours ACM treatment. CDC20 expression in OE33P and OE33R cells was significantly higher at 24 compared to 72 hours ACM treatment ($p=0.004$ and $p<0.0001$, respectively). Expression of CDC20 in OE33P and OE33R did not differ following treatment with ACM generated from non-obese compared to obese patients.

Twenty-four hours ACM treatment increased expression of CENPE four-fold in parental cells ($p=0.05$), however no change was detected in resistant cells (Figure 4.7 C). CENPE expression was higher in OE33P compared to OE33R cells treated with ACM for 24 hours ($p=05$). There was a ten–fold downregulation of CENPE in OE33P in response to ACM treatment for 72 hours ($p<0.0001$) (Figure 4.7 D). ACM treatment did not affect CENPE expression in OE33R following 72 hours of ACM treatment (Figure 4.6 D). CENPE expression was lower in OE33P compared to OE33R cells treated with ACM for 72 hours ($p=05$). Expression was higher in OE33P cells following 24 compared 72 hours ACM treatment ($p=0.01$). There was no difference in CENPE expression in OE33R at 24 hours compared to the 72 hour time point. CENPE expression in OE33P and OE33R did not differ following treatment with ACM generated from non-obese compared to obese patients.

ACM did not stimulate an alteration in ESPL1 expression in OE33P or OE33R cells treated with ACM for 24 hours, and no significant difference in ESPL1 expression was detected in ACM treated OE33P cells compared ACM treated OE33R cells (Figure 4.8 A). In contrast, treatment with ACM for 72 hours resulted in a ten-fold downregulation in ESPL1 expression in OE33P ($p=0.009$). ESPL1 expression in OE33R was not altered post ACM treatment for 72 hours, and ESPL1 expression was significantly higher in OE33R cells compared to OE33P cells post ACM treatment ($p=0.05$) (Figure 4.8 B). ESPL1 expression in OE33P was higher following 24 compared to 72 hours ACM treatment ($p=0.005$). ESPL1 expression in OE33P and OE33R did not differ following treatment with ACM generated from non-obese compared to obese patients.

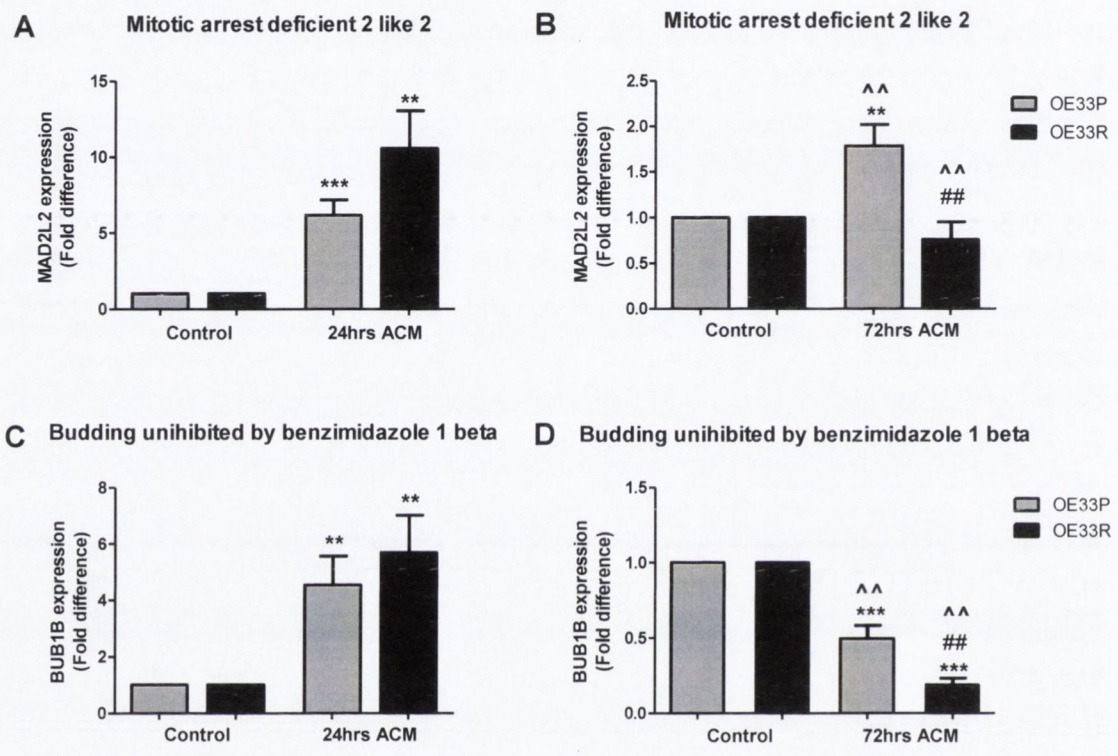


Figure 4.6. ACM upregulates MAD2L2 and BUB1b expression in OE33P and OE33R
(A) A six-fold upregulation of MAD2L2 expression was detected in OE33P following 24 hours of ACM treatment (p=0.0007). ACM stimulated a ten-fold upregulation of MAD2L2 expression in OE33R at 24 hours (p=0.004). **(B)** ACM increased expression two-fold in OE33P at 72 hours (p=0.01), but did not alter expression in OE33R. **(C)** ACM upregulated BUB1b expression five-fold in OE33P (p=0.008), and six-fold in OE33R (p=0.007), at 24 hours post ACM treatment. **(D)** ACM downregulated BUB1b expression two-fold in OE33P (p=0.0004) and five-fold OE33R (p<0.0001) following 72 hour of ACM treatment. Data are expressed as mean fold change in expression ± SEM. Analysis was performed using paired two-tailed student's *t*-test for ACM treated OE33P and OE33R cells versus control, **p<0.001, ***p<0.0001; an unpaired, two-tailed student's t test was used to compare ACM treated OE33P cells to ACM treated OE33R cells, ##p<0.001; and when comparing cells treated with ACM for 24 versus 72 hours, ^^p<0.001.

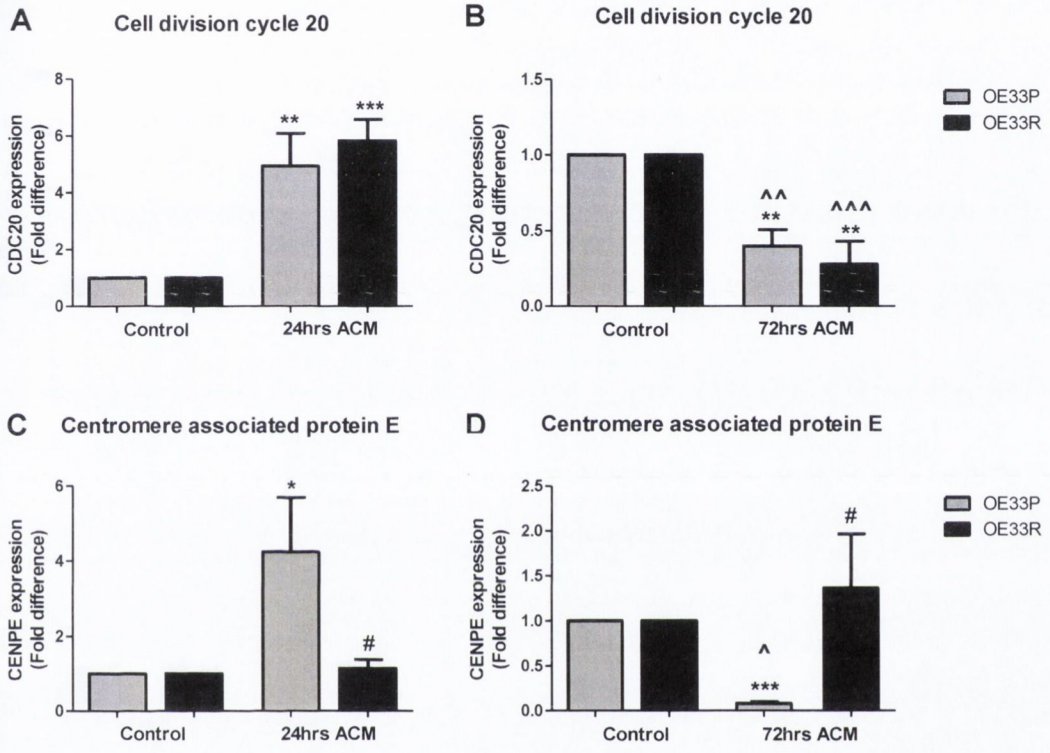


Figure 4.7. ACM alters CDC20 and CENPE expression in OE33P and OE33R
(A) A five-fold upregulation of CDC20 expression was detected in OE33P cells following 24 hours of ACM treatment ($p=0.007$) and a six-fold upregulation was detected in OE33R cells ($p<0.0001$). **(B)** ACM downregulated CDC20 expression two-fold in OE33P cells and three-fold in OE33R cells at 72 hours post ACM treatment ($p=0.001$ for all). **(C)** ACM upregulated CENPE expression four-fold in OE33P at 24 hours post ACM treatment ($p=0.05$), but did not alter expression in OE33R. **(D)** ACM treatment for 72 hours downregulated CENPE expression ten-fold in OE33P cells ($p<0.0001$). ACM did not affect CENPE expression in OE33R following 72 hours of ACM treatment. Data are expressed as mean fold change in expression ± SEM. Analysis was performed using paired two-tailed student's *t*-test for ACM treated OE33P and OE33R cells versus control, *$p<0.05$, **$p<0.001$, ***$p<0.0001$; an unpaired, two-tailed student's t test was used to compare ACM treated OE33P cells to ACM treated OE33R cells, #$p<0.05$; and when comparing cells treated with ACM for 24 versus 72 hours, ^$p<0.05$, ^^$p<0.001$, ^^^$p<0.0001$.

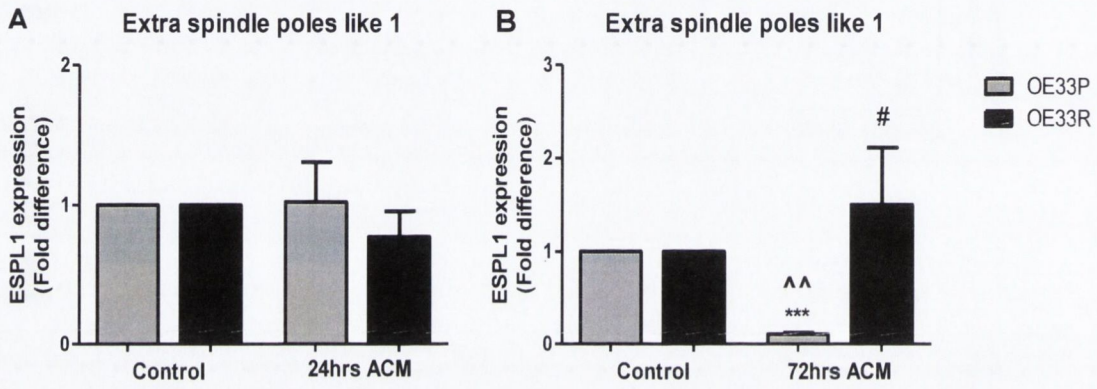


Figure 4.8. ESPL1 expression in OE33P cells was downregulated following 72 hours of ACM treatment

(A) No significant difference in ESPL1 expression was detected in OE33P or OE33R cells treated with ACM for 24 hours. **(B)** ACM downregulated ESPL1 expression ten-fold in OE33P at 72 hours post ACM treatment ($p=0.009$). ESPL1 expression in OE33R was not altered at 72 hours post ACM treatment. Data are expressed as mean fold change in expression ± SEM. Analysis was performed using paired two-tailed student's *t*-test for ACM treated OE33P and OE33R cells versus control, ***$p<0.0001$; an unpaired, two-tailed student's t test was used to compare ACM treated OE33P cells to ACM treated OE33R cells, #$p<0.05$; and when comparing cells treated with ACM for 24 versus 72 hours, ^^$p<0.001$.

4.4.6 SAC gene expression does not correlate with visceral obesity

The relationship between MAD2L2, BUB1b, CDC20, CENPE and ESPL1 gene expression in OE33P and OE33R cells at 24 and 72 hours post ACM treatment, and obesity status was investigated using Pearson correlation coefficient (Table 4.4). There was no correlation between MAD2L2, CDC20, CENPE and ESPL1 expression in OE33P or OE33R cells treated with ACM, and visceral obesity.

Table 4.4. SAC gene expression in OE33P and OE33R cells treated with ACM does not correlate with visceral obesity.

	MAD2L2 R	**BUB1b R**	**CDC20 R**	**CENPE R**	**ESPL1 R**
OE33P 24hr ACM VFA	-0.704	-0.206	-0.524	0.074	0.209
p value	*0.18*	*0.74*	*0.36*	*0.83*	*0.56*
OE33R 24hr ACM VFA	0.483	0.433	0.267	0.347	0.497
p value	*0.16*	*0.21*	*0.45*	*0.33*	*0.14*
OE33P 72hr ACM VFA	0.651	0.299	-0.496	-0.502	-0.005
p value	*0.06*	*0.43*	*0.17*	*0.14*	*0.99*
OE33R 72hr ACM VFA	0.135	-0.429	-0.543	-0.616	-0.317
p value	*0.73*	*0.25*	*0.13*	*0.06*	*0.37*

The relationship between SAC expression in OE33P and OE33R cells at 24 and 72 hours post ACM treatment, and obesity status (as measured by visceral fat area) was investigated using Pearson correlation coefficient. Pearson's correlation coefficient R values highlighted in bold represent statistically significant correlations. *R*=Pearson's correlation coefficient, VFA=visceral fat area

4.4.7 MAD2L2 and BUB1b expression in obese and non-obese oesophageal cancer patients

Because these genes were upregulated by ACM and due to their functional importance in the SAC, MAD2L2 and BUB1b were selected for measurement in OAC tumour samples from our panel of five SAC genes. Expression of MAD2L2 and BUB1b in oesophageal adenocarcinoma tumour tissue samples from viscerally non-obese and obese patients was assessed using quantitative real-time PCR. Data are expressed as mean RQ values ± SEM. Statistical analysis was performed using Mann-Whitney U test. Oesophageal tumour samples from obese patients (n=46) demonstrated significantly higher levels of MAD2L2 expression compared to tumour samples from non-obese patients (n=41, p=0.05, Figure 4.9 A). There was no difference in BUB1b expression between tumour tissue from obese (n=46) compared with non-obese patients (n=41, p=0.5). Anthropometric characteristics of patients are summarised in Table 3.5, chapter 3.

The relationship between MAD2L2 and BUB1b gene expression in obese and non-obese oesophageal cancer patients and visceral obesity status (as measured by visceral fat area) was investigated using Pearson correlation coefficient. There was a positive correlation between MAD2L2 expression in patient tumour samples and VFA (r=0.214 p=0.05), with higher levels of MAD2L2 expression associated with higher VFA. There was no correlation between BUB1b expression and visceral fat area.

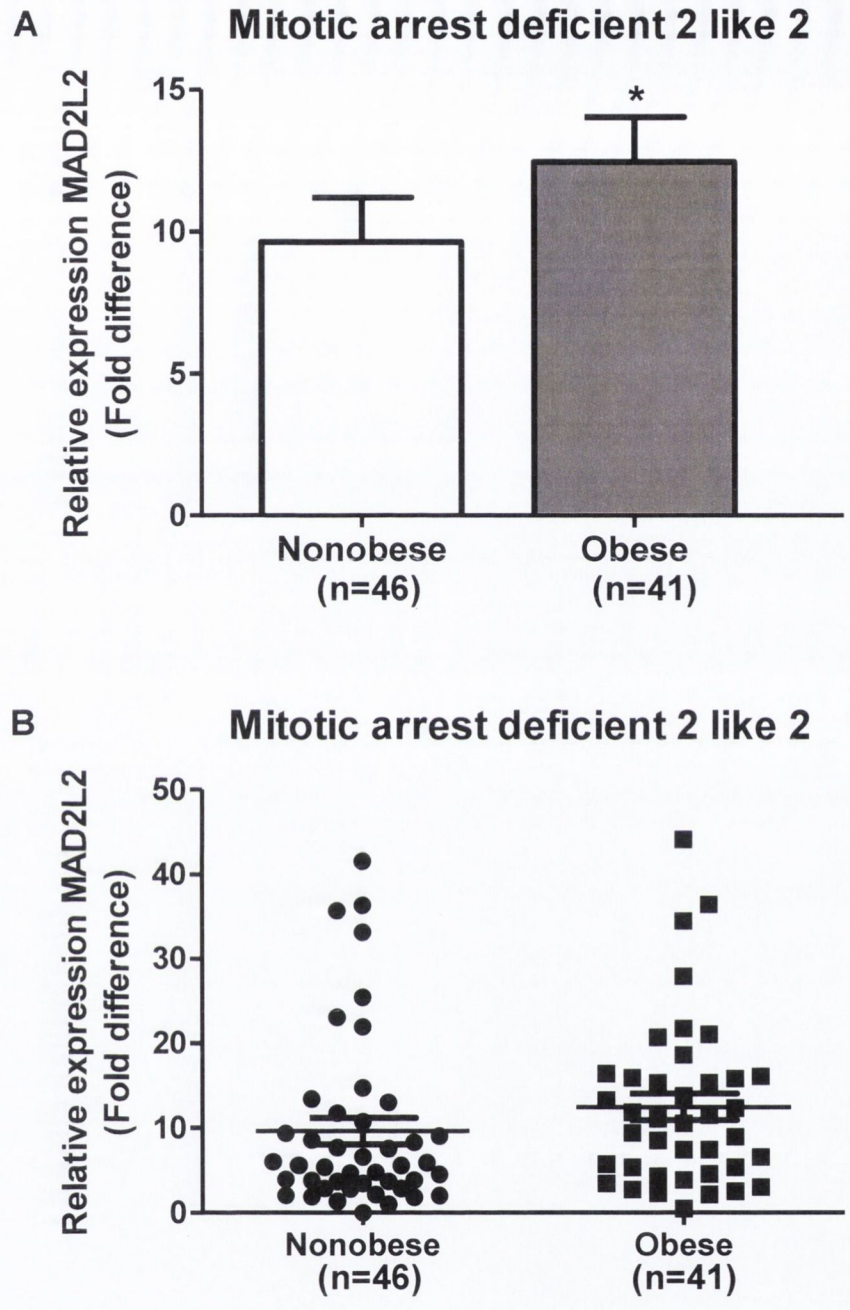


Figure 4.9. MAD2L2 and BUB1b expression in obese and non-obese oesophageal cancer patients

MAD2L2 and BUB1b expression levels were determined in oesophageal adenocarcinoma tumour samples from non-obese and obese patients using quantitative real-time PCR. Tumour samples from obese patients demonstrated higher levels of MAD2L2 expression compared to tumour samples from non-obese patients ($p=0.05$). Data are expressed as mean RQ values ± SEM and represented on **(A)** a column bar chart and **(B)** a dot plot. Statistical analysis was performed using Mann-Whitney U test, *$p \leq 0.05$.

4.4.8 Anaphase bridge levels correlate with CENPE and ESPL1 gene expression in OE33R

The relationship between SAC gene expression in OE33P and OE33R cells at 24 and 72 hours post ACM treatment, and anaphase bridge levels was investigated using Pearson correlation coefficient. Results are summarised in Table 4.5. There was no correlation between MAD2L2, BUB1b or CDC20 expression in ACM treated OE33P and OE33R cells and anaphase bridging. CENPE expression in OE33R cells following 72 hours of ACM treatment negatively correlated with anaphase bridge formation ($R=0.679$, $p=0.04$), with higher CENPE expression associated with lower anaphase bridge levels (Figure 4.10 A). A negative correlation was detected between ESPL1 expression in OE33R cells post 72 hours of ACM treatment and anaphase bridge levels at this time point, with higher ESPL1 expression associated with lower anaphase bridge formation ($R=0.705$, $p=0.03$) (Figure 4.10 B).

Table 4.5. CENPE and ESPL1 gene expression correlates with anaphase bridge levels in ACM treated OE33R cells

	MAD2L2 R	BUB1b R	CDC20 R	CENPE R	ESPL1 R
OE33P 24hr ACM ABL	-0.402	0.284	-0.514	-0.631	-0.480
p value	*0.50*	*0.64*	*0.38*	*0.06*	*0.19*
OE33R 24hr ACM ABL	0.178	-0.260	-0.191	-0.547	**-0.705**
p value	*0.65*	*0.50*	*0.62*	*0.13*	***0.03***
OE33P 72hr ACM ABL	0.173	0.450	0.334	-0.140	-0.189
p value	*0.68*	*0.26*	*0.42*	*0.72*	*0.63*
OE33R 72hr ACM ABL	0.092	0.166	0.614	**-0.679**	-0.556
p value	*0.83*	*0.70*	*0.11*	***0.04***	*0.12*

The relationship between SAC expression in ACM treated OE33P and OE33R cells and anaphase bridge formation was investigated using Pearson product-moment correlation coefficient. Pearson's correlation coefficient r values highlighted in bold represent statistically significant correlations; blue represents negative correlations; *ABL*=Anaphase bridge levels; *r*=Pearson's correlation coefficient.

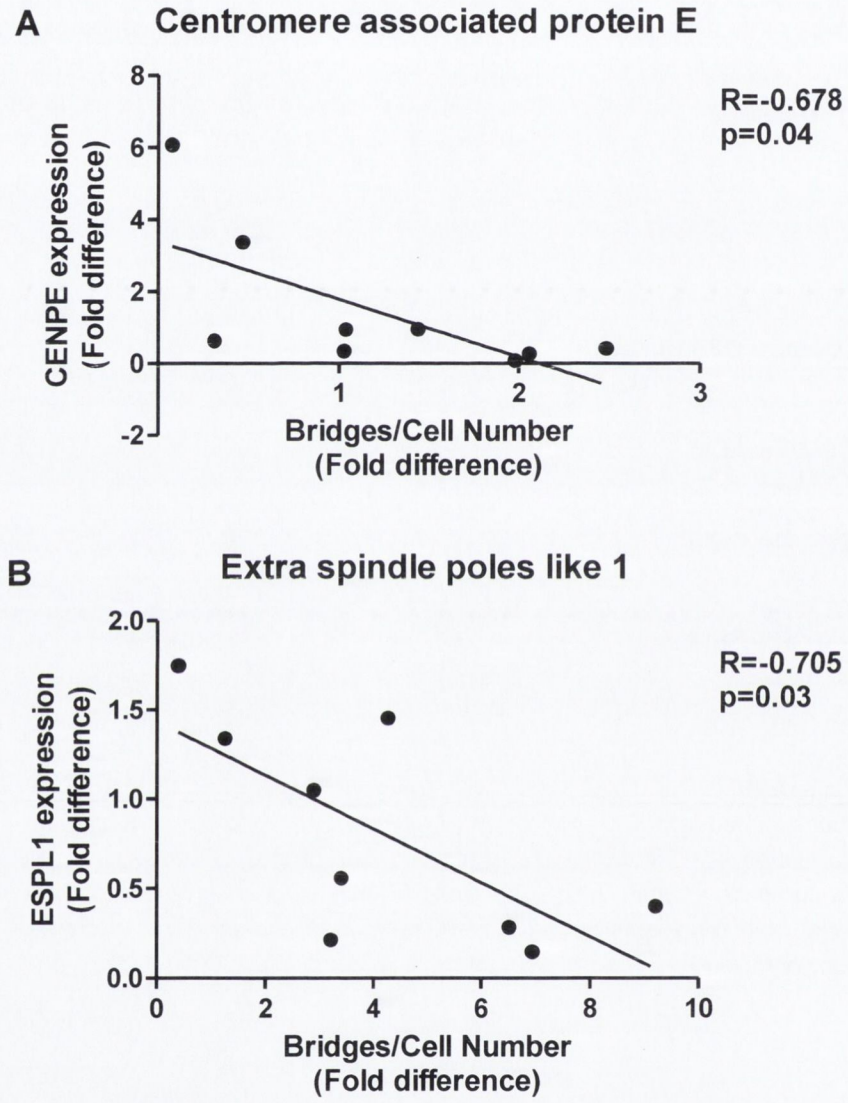


Figure 4.10. CENPE and ESPL1 expression in OE33R cells treated with ACM negatively correlates with anaphase bridge levels

The relationship between CENPE and ESPL1 expression in OE33P and OE33R cells post ACM treatment and anaphase bridge formation was investigated using Pearson correlation coefficient. **(A)** There was a negative correlation between CENPE expression in OE33R cells following 72 hours of ACM treatment and anaphase bridge formation (R=-0.679, p=0.04), with higher CENPE expression associated with lower anaphase bridge formation. **(B)** A negative correlation was detected between ESPL1 expression in OE33R cells post 72 hours of ACM treatment and anaphase bridge formation at this time point (R=-0.705, p=0.03), with higher ESPL1 expression associated with lower anaphase bridge formation.

4.4.9 Radiosensitivity status influences MAD2L2, CENPE and ESPL1 expression in oesophageal cancer cells following ACM treatment

SAC expression in OE33P cells at baseline and post ACM treatment was compared to SAC expression in OE33R cells (Table 4.4). Data are expressed as mean fold change in gene expression. Statistical analysis was performed using unpaired two tailed student's *t*-test. There was no difference in basal SAC gene expression in OE33P cells compared to OE33R cells. MAD2L2 expression was upregulated in both cell lines in following 24 hours ACM treatment, but this increase was greater in the OE33R cells compared to the OE33P cells; this difference reached statistical significance at the 72 hour time point ($p=0.003$). BUB1b expression following 72 hours ACM treatment was higher in OE33P compared to OE33R cells ($p=0.007$). Lower levels of CENPE expression were noted in OE33R cells compared to OE33P cells following 24 hours of ACM treatment ($p=0.05$). In contrast, higher levels of CENPE expression were seen in the OE33R cell line at 72 hours ($p=0.05$). ESPL1 expression was significantly higher in OE33R compared to OE33P cells following 72 hours treatment with ACM ($p=0.03$). There was no significant difference in CDC20 expression in ACM treated OE33P compared to OE33R cells.

Table 4.6. SAC gene expression in OE33P compared to OE33R cells.

	MAD2L2	BUB1b	CDC20	CENPE	ESPL1
OE33P vs. OE33R Baseline (RQ Value)	1.0 vs. 0.9	1.0 vs. 0.8	1.0 vs. 0.5	1.0 vs. 2.0	1.0 vs. 0.9
p value	*0.89*	*0.60*	*0.45*	*0.45*	*0.89*
OE33P vs. OE33R 24hr ACM (Fold change)	5.7 vs. 10.6	4.6 vs. 5.7	-4.5 vs. 5.8	**4.2 vs. 1.1**	1.0 vs. -1.2
p value	*0.09*	*0.56*	*0.33*	***0.05***	*0.47*
OE33P vs. OE33R 72hr ACM (Fold change)	**1.8 vs. -1.2**	**-2 vs. -5**	-2 vs. -3	**-10 vs. 1.4**	**-10 vs. 1.5**
p value	***0.003***	*0.007*	*0.53*	***0.05***	***0.03***

SAC expression levels in OE33P and OE33R were compared at baseline and following ACM treatment for 24 and 72 hours. Data are expressed as mean fold change in expression for n=10 samples. Statistical analysis was performed using unpaired two tailed student's *t*-test. Fold changes highlighted in bold represent statistically significant alterations in gene expression; blue represents downregulation; and red represents upregulation.

4.4.10 SAC expression in responder and non-responder OAC patients

From the panel of five SAC genes, MAD2L2, CENPE and ESPL1 were selected for measurement in OAC pre-treatment biopsy samples. Gene expression was determined in oesophageal adenocarcinoma pre-treatment biopsy samples from patients who went on to have a good pathological response (TRG 1-3, responder), or poor TRG response (TRG 4-5, non-responder) at resection (patient details are outlined in chapter two, table 2.7). There was no difference in MAD2L2, CENPE or ESPL1 expression between pre-treatment biopsy tissues from good compared to poor responders (Figure 4.11 A, B, C).

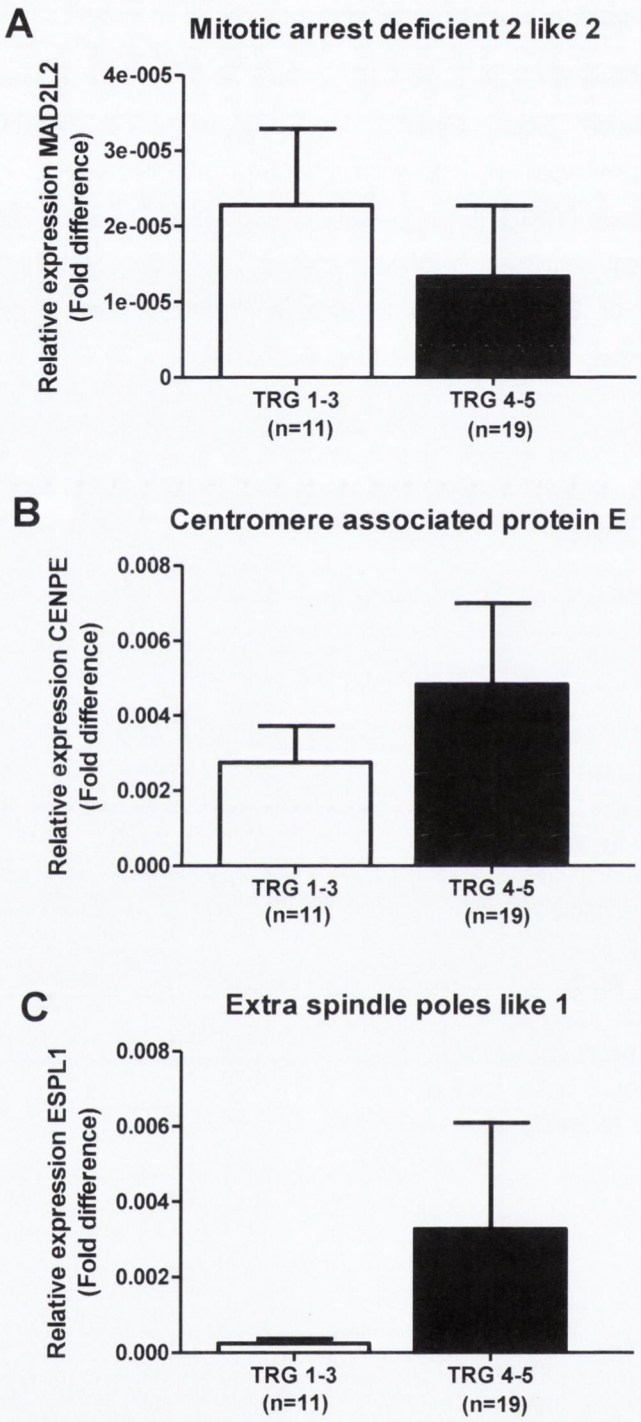


Figure 4.11. SAC expression in responder and non-responder OAC patient cohorts
MAD2L2, CENPE and ESPL1 expression was determined in oesophageal adenocarcinoma pre-treatment tumour biopsy samples from responder and non-responder patients using quantitative real-time PCR. Data are expressed as mean RQ values ± SEM. Statistical analysis was performed using Mann Whitney U. There was no difference in **(A)** MAD2L2 expression, **(B)** CENPE expression or **(C)** ESPL1 expression in pre-treatment biopsy tumour samples from responder patients compared to biopsy samples from non-responder patients.

4.1 Discussion

This study reveals that adipose tissue drives the genomic instability events anaphase bridge formation and spindle assembly complex dysregulation; obese OAC patients demonstrate increased MAD2L2 expression compared to non-obese patients. Furthermore, anaphase bridge levels are higher in radioresistant compared to radioresponsive oesophageal cancer cells.

Viscerally located adipose tissue is metabolically active, associated with systemic metabolic changes and the concomitant modification of the paracrine and endocrine panel of adipokines[185,635]. This is the first study to demonstrate that adipose tissue stimulates anaphase bridge formation in OAC. The breakage-fusion-bridge (BFB) cycle links telomere shortening, anaphase bridge formation and induction of chromosomal instability (CIN). The question if lifestyle factors drive anaphase bridge formation has not previously been addressed in the literature. Telomere shortening in leucocytes correlates with indicators of obesity including BMI and waist circumference, and is associated with obesity related conditions such as insulin resistance, diabetes mellitus, and cardiovascular risk[422,570,572], and in chapter three we showed that adipose tissue induces telomere shortening in OAC cells. This is the first study to demonstrate that adipose tissue induces BFB events downstream of telomere shortening. This study strengthens the association between obesity and stimulation of chromosomal instability events, and suggests that factors in adipose conditioned media are driving this association. Adipose tissue produces a range of other adipokines with biological effects in cancer, including TNF-α, IL-6, Resistin, Adiponectin and Leptin[636]. This unit has previously demonstrated that ACM generated from obese and non-obese OAC patients contains VEGF and IL-8[185], and that ACM-induced anaphase bridge formation in healthy oesophageal squamous cells is abrogated by neutralising VEGF and IL-8[296]. In this study, anaphase bridge levels correlated with visceral obesity in radioresistant oesophageal cancer cells, implying that adipokines associated with visceral obesity are implicated in anaphase bridge formation. This unit has previously demonstrated that concentrations of adipokines in ACM directly relate to the degree of obesity in humans. Levels of VEGF, IL6, leptin and adiponectin in ACM from viscerally obese patients were compared to levels in non-obese patients[185]. ACM from obese patients has significantly higher levels of VEGF and lower levels of adiponectin, but no significant difference in IL6 or leptin was observed[185]. OE33R demonstrated higher levels of anaphase bridges compared to OE33P. Both cell lines were treated with identical patient ACM, suggesting that differences in cell line receptor expression may account for the difference in response. In chapter two we demonstrated that LepR and NRP1 expression was higher in OE33R compared to OE33P, suggesting a role for leptin or VEGF in mediating anaphase bridge induction. It appears likely that adipokines such as VEGF are key to adipose-induced anaphase bridge formation, however further studies are warranted to confirm which adipose derived factors drive anaphase bridge formation in OAC.

This study showed that ACM upregulates expression of MAD2L2 and BUB1b in radioresponsive and radioresistant OAC. Obese OAC patients demonstrate increased expression of MAD2L2 but not BUB1b in their tumour specimens. Alterations in MAD2L2 expression drive tumourigenesis in mice and aberrant MAD2L2 expression is seen in number of human epithelial cancers[357,622]. BUB1b has a number of roles in the SAC and overexpression of this gene has been reported in colorectal cancer[623]. Doak et al reported both under and over expression of both MAD2L2 and BUB1b genes in Barrett's Oesophagus specimens, but SAC disruption has not previously been documented in OAC[637]. Obesity has never previously been linked with deregulation of the SAC complex in OAC. Studies identifying causal mechanisms for SAC deregulation are lacking, although oxidative stress has been linked to malfunction of the SAC in cancer cells[433]. Oxidative stress overrides the spindle checkpoint mechanism, possibly by interfering with the binding of MAD2 to CDC20[433], and increasing adiposity aggravates oxidative stress processes[434]. Adipose tissue is a rich source of pro-inflammatory cytokines including TNFα, IL1 (interleukin 1) and IL6, which are potent stimulators of ROS production, however the interaction of these factors with SAC expression has yet to be investigated[638]. We have shown that ACM alters SAC expression in OAC, but a more detailed understanding of the role of adipose tissue and adipokines in the dysregulation of the SAC in OAC is required.

In this study anaphase bridge levels following ACM treatment were higher at 24 compared to 72 hours. One possible explanation is that this reflects the higher SAC gene expression at 24 compared to 72 hours. However there was no positive correlation between anaphase bridge levels and SAC gene expression. SAC function may be affected by both under- and overexpression of the component genes[357,623]. Anaphase bridge levels negatively correlated with CENPE and ESPL1 expression following ACM treatment, but not with BUB1b, MAD2L2, or CDC20 expression. Prencipe et al demonstrated that downregulation of MAD2L2 was associated with increased anaphase bridge formation and polyploidy in breast cancer cell lines[357]. SAC deregulation is linked to genomic instability in a number of cancer types, but genomic instability may still occur in the presence of an intact SAC, suggesting that while both anaphase bridge formation and a compromised SAC are conducive to aneuploidy and carcinogenesis, these processes may occur independently of each other[357,623]. A weakened SAC may function as a facilitator rather than a driving force of tumourigenesis.

This is the first study demonstrating that increased levels of anaphase bridges are associated with radioresistance. A study by McCaul et al, found no relationship between anaphase bridge levels and radiosensitivity to clinically relevant doses of 2 Gy in 16 oral squamous cell carcinoma cell lines[444]. The same study found that in some cell lines, anaphase bridge levels were inversely correlated with radiosensitivity to higher 4 Gy doses of radiation[444]. The cell lines which demonstrated this relationship between high levels of bridging and radiosensitivity were

cell lines with high anaphase bridge levels, indicating that a certain threshold of bridging is necessary for this association to hold true[444]. Furthermore, the cell lines used in this study also demonstrated varying degrees of telomere dysfunction[444]. Telomere dysfunction has been associated with altered radiosensitivity of cells and organisms[444,447], and telomerase deficient $TERC^{-/-}$ mice who demonstrated telomere shortening and increased anaphase bridge formation exhibited a radiosensitive phenotype associated with accelerated mortality[439,447]. Given the number of possible factors that can influence intrinsic radioresistance, it is not surprising that the relationship between anaphase bridging and radiosensitivity may differ in individual cancer types. Anaphase bridge levels may be readily measured *in vitro*, however, due to the heterogeneous cell population typical of tumour samples and the low proportion of cells in this transient configuration, anaphase bridge quantification in patient samples is very difficult to evaluate[614]. Therefore anaphase bridge measurement has limited usefulness as a biomarker of radioresistance in vivo. Characterisation of the mechanisms underlying the link between anaphase bridges and radioresistance may yield important clinical benefits. The induced radioresistance of OE33R cells is likely a combination of both acquired mutation from adaptation of cells to the cytotoxicity of radiation, and the selection of a subpopulation of radioresistant cells. Our group has demonstrated that the radioresistance of OE33R cells is due at least in part to alterations in DNA damage repair efficiency[174]. OE33R cells demonstrate a greater efficiency in the repair of radiation-induced DNA damage compared to OE33P cells[174], and downregulation of miR-31, which has been shown to alter the expression of 13 genes involved in DNA repair[175]. These data suggest the possibility of inherent DNA repair alterations as a key factor in the radioresistance of OE33R. Anaphase bridges are associated with DNA double strand breaks (DSBs)[639]. While the majority of DSBs are repaired correctly, restoring the original chromosome structure, misalignment of two nonmatching ends may also occur resulting in anaphase bridges and chromosomal instability[640,641]. Non homologous end joining (NHEJ) acts to prevent anaphase bridges and in its absence the activity of homologous recombination (HR) leads to anaphase bridge formation; indeed, intrinsic NHEJ activity correlates with the induction of anaphase bridges[639], suggesting a mechanistic link between genomic instability and radioresistance[639].

MAD2L2, CENPE and ESPL1 expression differed in radioresponsive compared to radioresistant cells. Interestingly, expression of CENPE and ESPL1 also correlated with anaphase bridge levels, suggesting the possibility that expression of these SAC genes may be involved in the link between the anaphase bridge formation and radiosensitivity. The cohort of oesophageal cancer patients who had a poor response to RT demonstrated higher levels of MAD2L2 expression compared to patients who had a good response to treatment; however this was not statistically significant. MAD2L2 expression has been implicated in the radioresponse; suppression of MAD2L2 is associated with enhanced radiosensitivity in glioma cells through activation of

apoptosis via increased cleavage of PARP[455]. We have previously identified that PARP1 is overexpressed in oesophageal tumour tissue of poor responders[175]. In this study, CENPE expression was highest in oesophageal tumour tissue from patients showing the least response to radiation. Overexpression of CENPE is associated with recurrence in patients with pituitary tumours, and with chemoresistance in ovarian cancer patients[642]. ESPL1 expression was higher in tumour tissue from non-responders compared to responders. Overexpression of the ESPL1-encoded protein separase strongly correlates with high incidence of relapse and lower 5 year survival rate in breast and prostate cancer patients[643]. Separase is regulated by securin, the depletion of which is associated with radiosensitivity *in vitro*[628]. Pharmacologic inhibition of the SAC has been putatively proposed as a promising strategy for anticancer treatment[644]. The indolocarbazole compound Gö6976 overrides spindle checkpoint-mediated mitotic arrest by abrogating the phosphorylation and kinetochore localization of several spindle checkpoint proteins, resulting in apoptosis in various human cancer cell lines, including spindle checkpoint-compromised cancer cells[644]. MAD2L2, CENPE and ESPL1 expression was higher in radioresponder compared to non-responder oesophageal cancer patients, but this did not reach statistical significance. Our cohort had small numbers; therefore a larger study is required to investigate this association.

This study demonstrates a novel role for visceral obesity in the induction of genomic instability events and highlights the complex interaction between obesity, genomic instability and radioresponse in OAC. Further studies are required to elucidate the association between the SAC and radioresponse in vivo. Identification of the factors driving anaphase bridge formation could identify shared pathways as potential preventative and therapeutic targets, enabling the stratification of patients based on predicted response to therapy and ultimately to the manipulation of these factors to sensitize resistant cells to radiation.

Chapter 5 Identification of novel genomic instability events in radioresistant oesophageal adenocarcinoma using array comparative genomic hybridization

In preparation for submission to Radiation Research: AM Mongan, K Geiersbach, C Paxton, N Lynam-Lennon, R Casey, S Maher, Bronner M, JV Reynolds, G Pidgeon, J O'Sullivan. Novel genomic instability events in radioresistant oesophageal adenocarcinoma identified using array comparative genomic hybridization

5.1 Introduction

Incidence rates and incidence-based mortality for adenocarcinoma of the oesophagus have been increasing in Western countries for several decades, due in part to increases in the prevalence of factors such as overweight and obesity[5]. Locally advanced disease is generally treated with curative intent with a multimodal approach that includes surgery[59,61]. NA-CRT results in improved overall survival compared to surgery alone, and pCR rates which are higher than those from NA CT or RT when given alone[66,68,74–76]. Improved and standardised surgical techniques as well as advances in supportive care have contributed to an increase in the rate of curative resection, but five-year survival rates of patients with local-regional oesophageal cancer who have undergone curative resection remains low (approximately 35-50%)[55,61–65]. Therefore, oesophageal adenocarcinoma is a treatable but rarely curable disease. An improved understanding of the molecular, cellular and immunological mechanisms, which lie behind the progression of OAC, is required for the development of more efficacious treatments. This could in part be achieved by the study *in vitro* of cells derived from OAC tumours. Isogenic models of radioresistance, which use cells of the same origin that differ only in terms of radiosensitivity, are increasingly being used to study the radioresponse[477–479]. These model systems allow the comparison of cell lines with the same origin, but distinctly different radiosensitivities, thus avoiding the influence of confounding factors such as genetic variation, allowing for the detection of molecular mechanisms specifically involved in radiosensitivity. The radioresistant model used in this study, OE33R, was generated by the chronic exposure of OE33 cells to X-ray radiation. The JROECL33/OE33 cell line was derived from a poorly differentiated stage IIA adenocarcinoma in Barrett's oesophagus, from a 73 year old lady. The cell line was 14 months old at time of development in September 1994, following 19 subcultures[645]. The cell line was characterised as aneuploid, near tetraploid, and karyotyped in detail in 2002[646], however, it has not been characterised since then, and OE33R has never been karyotyped.

Advances in microarray technology have facilitated the investigation of the complex network of genes associated with the cellular response to IR, allowing high throughput profiling of large numbers of genes simultaneously[647]. This technology allows genome-wide scanning for genomic losses and gains over large numbers of targets and detects alteration-prone chromosomal regions. The use of a genome wide measure of genetic instability is appealing since all cancers progress through some type of genetic instability[648,649]. While some cancers may display little overall copy number instability, e.g., MIN cancers, these generally represent a minority of solid tumours, and certainly a minority of OACs[650]. A large body of evidence now suggests that most OACs arise in association with a process of gain or loss of whole chromosomes or large portions of chromosomes, using a variety of detection methods with various resolutions including conventional comparative genomic hybridization (CGH), microsatellite mapping, array CGH and SNP arrays[651–656]. A recent 317K SNP array study of 23

OACs reported an average of 97 copy number changes (range 23-208) per cancer that ranged in size from small homozygous deletions to large chromosome regions[651]. Copy gain, loss and copy neutral LOH averaged 13, 18 and 23MB, respectively. Findings from copy number profiling studies in OAC have resulted in the compilation of a well-established genomic landscape of OAC; recurrent genomic events include gains of 7p, 8q, and 17q and losses of 3p, 4p, 5q, and 17p[651,652,657–660]. These results indicate the complexity of genomic changes in OAC and suggest there will be both opportunities and challenges for risk stratification, cancer prevention and early detection. DNA copy number alterations (CNAs) can play significant roles in tumour behaviour and provide insight into gene deregulation and cancer biology, as exemplified by DNA amplifications of the oncogenes *HER-2* and *EGFR*[661,662]. Novel targeted biologic agents have resulted in improved outcomes in a number of cancers, including gastroesophageal cancers. HER2 (*ERBB2*) is amplified in approximately 10–20% of OAC. Traztuzumab antibody treatment was evaluated in a large randomized phase III trial (ToGA) in combination with chemotherapy, and was reported to have a modest improvement in overall median survival versus chemotherapy alone in a select *ERBB2* amplified subgroup of gastric and gastro-oesophageal junction adenocarcinoma patients[663].

Genome-wide studies on various cancers support the notion that biological difference reflected in gene expression profiles of tumours may dictate the prognosis of cancer patients[664–668]. For example, Van't Veer and van de Vijver et al have developed a highly successful predictive gene signature, the so called "Mammaprint," effective in identifying patients with primary breast cancer at a high risk of recurrence after local treatment alone[667,669]. Array-comparative genomic hybridisation and gene expression microarray profiling have been used separately to identify molecular aberrations in small cohorts of oesophageal adenocarcinoma patients[651,652,657,658,670–674]. Integrative genomics have been used to identify novel prognostic markers and therapeutic targets such as RON (Recepteur d'origine nantais) and RFC3 (Replication Factor C 3) in OAC[675,676]. Goh et al integrated data from an array CGH platform with corresponding gene expression microarray profiles from 56 fresh frozen OAC resection samples to generate a potential prognostic signature for OAC[660]. This study identified 16 probes which conferred poor prognosis in OAC patients, including six novel molecular targets not previously associated with OAC. The utility of CNAs as biomarkers of risk assessment response to therapy, however, has not been well studied. Chen et al used array CGH to identify a 58-probe pathological response prediction model associated with response to NA CRT in locally advanced rectal cancer[677], but genome-wide studies identifying genomic alteration "signatures" in OAC CRT responders and non-responders are lacking. To continue to explore and improve the discriminatory ability of genomic markers for radioresponse in OAC, we used array-based comparative genomic hybridization to examine CNAs in OE33R compared to OE33P.

5.2 Overall aim and specific objectives

The overall aim of this chapter was to investigate novel genomic alterations between radioresponsive OE33P and radioresistant OE33R cells. A comprehensive genome-wide microarray analysis was performed on OE33P and OE33R cell lines at the Department of Pathology at the University of Utah in Salt Lake City. Altered gene loci were validated *in vitro* and in vivo.

Specific objectives:

- Investigate genomic alterations in OE33P and OE33R using array CGH
- Use ChAs software to identify regions of chromosomal aberrations and copy number variations between OE33P and OE33R
- Investigate target gene expression in OE33P and OE33R cell lines
- Investigate if radiosensitivity status affects expression of selected target genes in OAC patient samples

5.3 Materials and methods

5.3.1 Cell Culture

Cell culture was performed as described in section 2.3.3

5.3.2 Karyotyping of OE33P and OE33R

Harvesting cell pellets for FISH

Cells were seeded in 12-well plates at a concentration of 1.2 x 10^5 cells/well and allowed to adhere for 24 hours. The plate was incubated at 37°C and 5% CO_2 for 24 hours. Cells were collected by trypsinization as described previously (section 3.2.3) and transferred to a 15 mL tube before centrifuging at 1100 RPM for 8 minutes. The supernatant was removed using a Pasteur pipette leaving 0.5-1 mL of supernatant above the cell pellet. The cell pellet was gently resuspended using a vortex. 10 mL of warmed 0.075% KCL hypotonic solution was added to the samples while vortexing. Samples were incubated at 37^0C for 25 minutes, and 1 mL of modified Carnoy's fixative (3:1 methanol HPLC grade: glacial acetic acid) was added. Samples were mixed by inverting the tubes and centrifuged at 1100 RPM, and supernatant removed. A volume of 10 mL of modified Carnoy's fixative was added to the samples while gently mixing using a vortex. Samples were incubated at room temperature for 30 minutes before being centrifuged and decanted as described previously. Samples were incubated at room temperature for a further 20 minutes. Samples were centrifuged, decanted, resuspended and 10ml modified Carnoy's fixative added before incubating at room temperature a further two times.

Precipitating the probe

Fluorescence *in situ* hybridization (FISH) analysis was performed at the department of pathology in the University of Utah in association with ARUP laboratories in Salt Lake City, Utah. A volume of 5 µL (~100 ng) of the D15S11 probe from Abbott Molecular (Des Plaines, IL) of the nick translation reaction mixture was pipetted into each sample microcentrifuge tube. COT-1 DNA (1 µg), human placental DNA (2 µg) and purified water (4 µL) were added to the tubes. A volume of 1.2 µL (0.1 volume) 3 M sodium acetate and 30 µL (2.5 volumes) of 100% EtOH was added. Samples were vortexed, placed on dry ice for 15 min and centrifuged at 12,000 rpm for 30 minutes at 4 °C to pellet the DNA. Supernatants were removed and pellets dried for 10 - 15 minutes under a vacuum at room temperature. Pellets were resuspended in 3 µL purified water and 7 µL Hybridization Buffer. Probes were denatured by heating the probe mix for 5 minutes in a 73 °C water bath.

Hybridizing the probe to the target metaphase

Hybridization areas were marked on the slide using a tipped scribe. Slides containing normal metaphase spreads were immersed into denaturation solution (70% formamide in2X SSC, pH 7.0 - 8.0) at 75 °C for 5 min. Slides were dehydrated for 1 min in 70% EtOH, followed by 1 minute in 85% EtOH, and 1 minute in 100% EtOH. Slides were blotted dry and placed on a slide warmer at 45°C to allow remaining EtOH to evaporate. A volume of 10 µL of denatured probe mix was added to the slides and coverslips immediately applied and sealed with rubber cement. Slides were placed in a sealed, humidified box in a 37 °C incubator for 16 hours for hybridization. The 0.4X SSC/0.3% NP-40 wash solution was heated to 73°C in a water bath for at least 30 mins. The rubber cement seal and the coverslip were removed and the slide placed into the wash solution and agitated for 1 - 3 seconds. Slides were let stand for 2 mins, and then placed in 2X SSC/0.1% NP-40 wash solution at room temperature. Slides were agitated for 1-3 sec, let stand for 5 sec and air dried in darkness for 10 mins. To visualise the hybridisation, a 10 µL volume of DAPI II counterstain and a coverslip was applied to each hybridization location. FISH probes were evaluated by fluorescence microscopy (Olympus, Centre Valley, PA).

5.3.3 Array CGH analysis of OE33P and OE33R

OE33P and OE33R cell lines were tested using Affymetrix CytoScan HD Array® (1,953,246 oligonucleotides and 743,304 SNP probes). I travelled to Salt Lake City to perform this array analysis at the department of pathology in the University of Utah in association with ARUP laboratories in Salt Lake City, Utah.

DNA Extraction for array CGH

Cells were seeded in 12-well plates at a concentration of 1.2×10^5 cells/well, and allowed to adhere for 24 hours. Following treatment with 0.5 mL control M199 media or ACM, cells were incubated at 37°C and 5% CO_2 for 24 hours. Cells were collected by trypsinization as described previously (section 3.2.3) and transferred to a 15 mL tube before centrifuging at 1500 RPM for 3 minutes. The supernatant was aspirated leaving a pellet and approximately 20µl of residual fluid. These samples were analysed in the Department of Pathology at the University of Utah in association with ARUP laboratories in Salt Lake City, Utah. The pellet was vortexed to resuspend the cells in the residual fluid. Cell lysis solution (600 µL) was added to the samples which were vortexed to lyse the cells. Proteinase K solution (3.0 µL) was added and samples incubated at 55°C for 1 hour. A 3.0 µL volume of RNase A solution was added. Samples were mixed by inverting the tube 25 times, pulse centrifuged to collect the contents, and incubated in a water bath at 37°C for 35 minutes before cooling on ice for 1 minute. 200 µL of protein precipitation solution was added and the samples were vortexed vigorously for 20 seconds and placed on ice for 5 minutes. Samples were centrifuged at 17,000 x g for 3 minutes.

Supernatants were transferred to 1.5 mL screw top centrifuge tubes containing 600 µL of isopropanol and mixed by inverting 50 times before centrifuging at 17,000 x g for 3 minutes. Supernatants were aspirated and discarded. A 600 µL volume of 70% ethanol was added and samples inverted to wash the pellet. Supernatants were aspirated and 600 µL of 70% ethanol added before inverting the tube several times. Samples were allowed to air dry for 10 minutes before 30 µL of DNA hydration solution was added. Samples were incubated overnight at room temperature.

Digestion

Genomic DNA (5.00 µl/250 ng) was added to the plate. 5 µl of the positive control was added to the well marked "+" and 5 µL of low EDTA TE as negative control added to the well marked "-". The digestion master mix was prepared as per table 5.1, vortexed, centrifuged, then 14.75 µl added to the samples. The plate was sealed with an adhesive film, vortexed, centrifuged, then loaded onto a preheated thermal cycler at 37°C for two hours, 65°C for 20 minutes and held at 4°C.

Table 5.1. Digestion master mix

Reagent	Per sample
Chilled Affymetrix nuclease-free water	11.55 µl
10X Nsp I buffer	2.00 µl
100X BSA	0.20 µl
Nsp I	1.00 µl
Total volume	**14.75 µl**

Ligation

The 10X T4 DNA ligase buffer and 50 µM adaptor Nsp I were thawed at RT, vortexed and placed on ice. The ligation master mix was prepared as per table 5.2, vortexed, centrifuged and 5.25 µL added to the samples. The plate was sealed with an adhesive film, vortexed, centrifuged and loaded onto the thermal cycler at 16°C for three hours, 70°C for 20 minutes and then at 4°C.

Table 5.2. Ligation master mix

Reagent	Per sample
10 X T4 DNA Ligase Buffer	2.50 µl
50 µM Adaptor Nsp I	0.75 µl
T4 DNA Ligase	2.00 µl
Total volume	**5.25 µl**

PCR

The sealed ligation plate was centrifuged and the ligated samples diluted as per table 5.3. The plate was sealed with an adhesive film, vortexed twice and four 10 µL aliquots of each sample transferred to the PCR plate. The 10X TITANIUM Taq PCR Buffer, dNTP mixture, PCR Primer 002 and diluted ligated samples were thawed at RT, and once thawed, immediately placed on ice, vortexed and centrifuged. The PCR master mix was prepared on ice as per table 5.4, vortexed and 90 µL added to the samples. The PCR plate was sealed, vortexed, centrifuged and loaded onto preheated thermal cycler as per the Cytoscan PCR program outlined in table 5.5. The four PCR products for each sample were pooled by transferring the samples to appropriately marked 1.5 mL eppendorf safe-lock tubes. 720 µL of purification beads were added to each sample. The samples were inverted ten times, incubated at RT for ten minutes, and centrifuged for three minutes. The supernatant was pipetted off and discarded. 1.0mL purification wash buffer was added to each tube. The tubes were vortexed, centrifuged, and the supernatant pipetted off. Tubes were again centrifuged, any remaining purification wash buffer pipetted off, and then left uncapped at RT for ten minutes. 52 µL of elution buffer was added to each tube. The samples were vortexed, centrifuged, and left to stand for ten minutes. 47 µL of eluted sample was transferred to a fresh 96-well plate. The plate was sealed, vortexed and centrifuged.

Table 5.3. PCR Dilution

Reagent	**Volume/sample**
Ligated sample	25 µl
Chilled Affymetrix ® Nuclease-free water	75 µl
Total volume	**100 µl**

Table 5.4. PCR master mix

Reagent	**Per sample**
Chilled Affymetrix® Nuclease-free water	39.5 µl
10X TITANIUM™ Taq PCR Buffer	10.0 µl
GC-Melt Reagent	20.0 µl
dNTP Mixture (2.5 mM each)	14.0 µl
PCR Primer 002	4.5 µl
50X TITANIUM™ Taq DNA Polymerase	2.0 µl
Total volume	**90.0 µl**

Table 5.5. Cytoscan PCR program

Temp	Time	Cycle
94°C	3 min	-
94°C	30 sec	30
60°C	45 sec	30
68°C	15 sec	30
68°C	7 min	-
4°C	Hold	-

Quantification

198 µL of Affymetrix nuclease-free water was aliquoted into a UV plate. 2 µL of each purified sample was added. The plate was sealed, vortexed and centrifuged. The OD of each PCR product was measured at 260, 280 and 320nm, and one OD reading was calculated for every sample: OD= (Sample OD) – (Average water blank OD). The undiluted concentration for each sample in µG/µL was calculated: OD x 0.05 µG/µL x 100. (OD260/OD280 ratio should be between 1.8 and 2.0, OD320 measurement should be very close to zero)

Fragmentation

The fragmentation master mix was prepared as per table 5.6 (all reagents, including water, kept on ice, and all additions performed on ice), vortexed, and 10 µL aliquoted to each sample. The sample plate was sealed with an adhesive film, vortexed, centrifuged and loaded onto a preheated thermal cycler at 37°C for 35 minutes, 95°C for 15 minutes and held at 4°C.

Table 5.6. Fragmentation master mix

Reagent	Fragmentation Reagent Concentration 2.0 U/µl
Chilled Affymetrix nuclease-free water	122.4 µl
10X Fragmentation Buffer	158.4 µl
Fragmentation Reagent	7.2 µl
Total volume	**288.0 µl**

Labelling

The labelling master mix was prepared as per table 5.7, vortex, centrifuge and aliquot 19.5 µL to each sample. The plate was sealed, vortexed, centrifuged and loaded onto the thermal cycler at 37°C for four hours, 95°C for 15 minutes and then at 4°C.

Table 5.7. Labelling master mix

Reagent	Per sample
5X Tdt Buffer	14.0 µl
30 mM DNA Labelling Reagent	2.0 µl
TdT	3.5 µl
Total volume	**19.5 µl**

Hybridisation

The hybridization master mix was prepared as per table 5.8 in a 15mL conical tube on ice, then vortexed, and 190µl added to each sample. The plate was sealed, vortexed, centrifuged and loaded onto the thermal cycler at 95°C for ten minutes and then at 49°C.

Table 5.8. Hybridisation master mix

Reagent	Per sample
Hyb Buffer Part 1	165.0 µl
Hyb Buffer Part 2	15.0 µl
Hyb Buffer Part 3	7.0 µl
Hyb Buffer Part 4	1.0 µl
Oligo Control Reagent 0100	2.0 µl
Total volume	**190.0 µl**

Wash, stain and scan

The following three reagents were aliquoted into separate 1.5 mL microfuge tubes: 500 µL Stain Buffer 1: 500µL Stain Buffer 2: 800 µL Array Holding Buffer. The fluidics station was primed with the wash buffers, the stain solutions were loaded and the CytoScan750K_Array450' protocol selected. The arrays were loaded onto the fluidics station and scanned.

Chromosomal microarray data analysis

Chromosomal microarray analysis (CMA) was performed using Affymetrix CytoScan HD microarray. This microarray consists of 2,696,550 oligonucleotide probes across the genome, including 1,953,246 unique non-polymorphic probes, and 743,304 SNP (single nucleotide polymorphism) probes. Patient hybridization parameters were compared to data derived from phenotypically-normal individuals. Deletions smaller than 50 kb, and duplications smaller than 400 kb, were not reviewed. Detected copy number variations (CNVs) and copy neutral loss of heterozygosity (CN-LOH) were reported when found to have clear or suspected clinical

relevance. CNVs devoid of relevant gene content or reported as common findings in the general population may not be reported. Genomic linear positions are given relative to NCBI build 37 (hg19).

This microarray and associated software (Chromosome Analysis Suite or ChAs) is manufactured by Affymetrix and used by ARUP Laboratories for the purpose of identifying DNA copy number gains and losses associated with large chromosomal imbalances. This analysis will not detect all forms of polyploidy, balanced rearrangements (e.g. inversions and balanced chromosomal translocations), small deletions, point mutations, and some mosaic conditions. This assay has been extensively validated by ARUP Laboratories and other clinical laboratories per ACMG guidelines; however, it is not feasible to validate every potential genomic imbalance in the human genome. Furthermore, this technique only identifies the regions of imbalance; it does not provide information regarding the arrangement or mechanisms responsible. For these reasons, some chromosomal microarray results were characterized by FISH.

5.3.4 Investigation of gene expression

Gene expression was investigated as described in section 2.3.5.

5.3.5 Statistical analysis

Statistical analysis was performed using Graphpad Prism 5 software (GraphPad Software, Inc., CA, USA) and SPSS version 18 for Windows (IBM, Armonk, New York, USA) software. Unless otherwise stated, data are expressed as mean ± standard error of the mean (SEM). SEM was calculated as the standard deviation of the original sample divided by the square root of the sample size. A two-tailed unpaired t-test was used to analyse unpaired parametric data. The Mann-Whitney U test was used to examine statistical significance between unpaired groups of non-parametric data. For all statistical analysis, a probability of (p) of ≤ 0.05 was considered to represent significant difference between groups.

5.4 Results

5.4.1 OE33P and OE33R have a complex, near tetraploid karyotype

OE33P and OE33R are age and passage-matched. OE33P and OE33R cell lines were karyotyped using FISH and array CGH analysis. FISH on interphase cells from prepared culture suspensions showed four copies of the D15S11 probe loci in >90% of cells in the OE33P and OE33R cell lines, confirming the karyotype as being near-tetraploid, with amplification of regions of 7q including MET and 17q including ERBB2, and multiple gains, losses, and copy neutral loss of heterozygosity (CN-LOH) affecting most chromosomes. The Y chromosome was absent, consistent with the origin of the OE33 cell line from a female patient. These findings are consistent with the diagnosis of oesophageal carcinoma. A summary of relative copy number gains, losses and loss of heterozygosity identified using the array CGH is shown in Tables 5.9 and 5.10.

Table 5.9. Summary of abnormalities (copy number gains and losses) detected in both OE33P and OE33R cell lines.

(A) GAINS				
Chromosome	**Start (Mb)**	**Stop (Mb)**	**Size (Mb)**	**Cytoband**
1	59.0	161.0	102.0	1p32.2-1q23.2
2	Entire chromosome			
3	115.5	198.0	82.5	3q13.31-3qter
6	61.9	83.9	22.0	6q11.1-6q14.2
7	0.0	120.0	120.0	7pter-7q31.31
8	106.7	146.3	39.6	8q23.1-8qter
10	0.0	4.8	4.8	5pter-5p
10	42.0	135.0	93.0	10q11.1-10qter
11	55.0	108.5	53.5	11q11-1q22.3
13	31.9	32.5	0.6	13q12.3-13q13.1
16	Entire chromosome except 62.0-69.0			Except 16q21-22.1
17	25.3	38.3	13.0	17q11-17q21.1
20	Entire chromosome			
(B) LOSSES				
Chromosome	**Start (Mb)**	**Stop (Mb)**	**Size (Mb)**	**Cytoband**
1	0.0	59.0	59.0	1pter-1p32.2
3	0.0	115.5	115.5	3pter-3q13.31
4	0.0	190.5	190.5	4pter-4qter
6	39.0	171.0	132.0	6p21.2-6qter
7	122.2	159.0	36.8	7q31.32-7qter
8	0.0	106.5	106.5	8pter-8q23.1
11	108.5	115.3	6.8	11q22.3-11q23.3
13	19.5	31.8	12.3	13q11-13q12.13
13	35.4	63.0	27.6	13q13.2-q21.31
13	64.0	101.0	37.0	13q21.31-13q32.3
14	87.9	97.9	10.0	14q31.3-14q32.2
17	0.0	22.2	22.2	17pter-17p11.1
17	38.3	39.3	1.0	17q21.1-q21.2
17	40.1	40.5	0.4	17q21.2-17q21.2
18	0.0	15.1	15.1	18pter-18p11
18	22.3	78.0	55.7	18q11.2-18qter
21	Entire chromosome			
X	0.0	125.8	125.8	Xpter-Xq25

OE33P and OE33R cell lines were karyotyped using FISH and array CGH analysis. **(A)** Gains identified **(B)** Losses identified. Genome coordinates are approximated down to the megabase (Mb) level using genome build hg19. p refers to short arm; q refers to long arm; pter refers to telomere end of short arm; qter refers to telomere end of long arm.

Table 5.10. Summary of abnormalities (loss of heterozygosity) detected in both OE33P and OE33R cell lines.

LOSS OF HETEROZYGOSITY				
Chromosome	**Start (Mb)**	**Stop (Mb)**	**Size (Mb)**	**Cytoband**
1	161.0	249.0	88.0	1q23.3-1qter
3	0.0	115.5	115.5	3pter-3q13.31
4	0.0	171.5	171.5	4pter-4q33
5	3.1	181.0	177.9	5p15.33-5qter
6	Entire chromosome			
7	0.0	28.0	28.0	7pter-7p15.1
9	Entire chromosome			
11	0.0	51.5	51.5	11pter-11p11.1
11	108.5	135.0	26.5	11q22.3-11qter
12	Entire chromosome			
13	51.0	63.0	12.0	13q14.3-13q21.31
16	61.1	90.5	29.4	16q21.1-16qter
17	0.0	22.2	22.2	17pter-17p11.1
18	22.3	78.0	55.7	18q11.2-18qter
22	Entire chromosome			
X	Entire chromosome			

OE33P and OE33R cell lines were karyotyped using FISH and array CGH analysis. Genome coordinates are approximated down to the megabase (Mb) level using genome build hg19. p refers to short arm; q refers to long arm; pter refers to telomere end of short arm; qter refers to telomere end of long arm

5.4.2 Array CGH analysis identifies alterations in OE33R compared to OE33P

OE33P and OE33R cell lines were characterized using array CGH and analyzed using Affymetrix ChAs software. Differences in copy number between OE33P and OE33R are summarized in Table 5.11. Compared to OE33P, OE33R demonstrated new deletions on chromosomes 2 and 9, and low level mosaic losses on chromosomes 5, 6, 12, 14 and 19. New regions of LOH were seen on chromosomes 3, 10, 16 and 20, with increased copy number complexity on chromosomes 11, 17 and 18. New regions of loss of heterozygosity may encompass new gene mutations and there was a large deletion on chromosome nine encompassing 9p24.2-21.3.

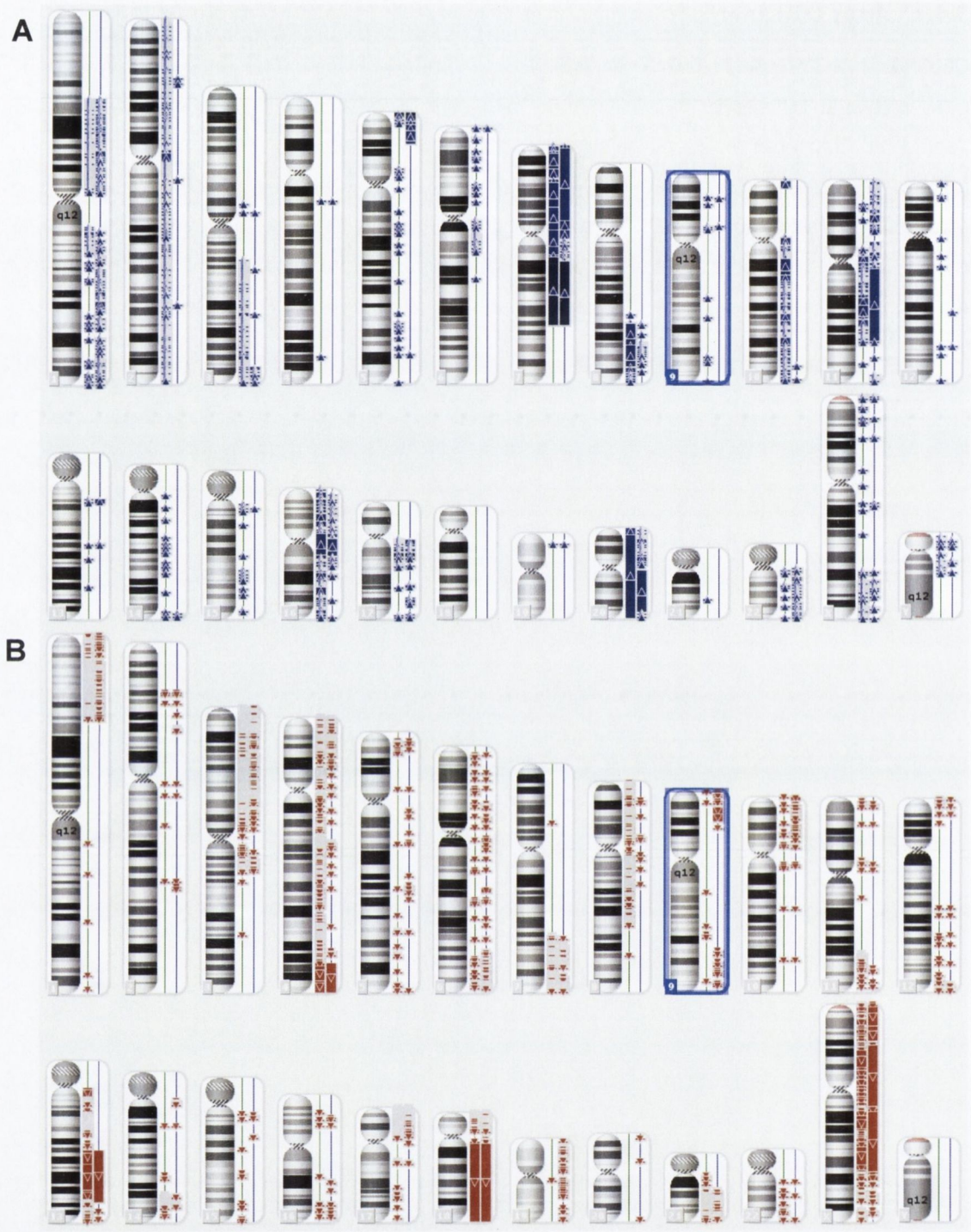


Figure 5.1. Gains and losses in OE33P compared to OE33R

This image shows the karyotype of OE33P and OE33R. OE33P is represented on the green line to the left; OE33R on the blue line to the right. **(A)** This image illustrates regions of copy number gains on OE33P and OE3R as represented by the blue symbol. **(B)** This image illustrates regions of copy number loss on OE33P and OE3R as represented by the red symbol.

Corresponds to copy number gain

Corresponds to copy number loss



Figure 5.2. Loss of heterozygosity in OE33P and OE33R

This image shows the karyotype of OE33P and OE33R. OE33P is represented on the green line to the left; OE33R on the blue line to the right. This image illustrates regions of loss of heterozygosity on OE33P and OE3R as represented by the purple symbol.

Corresponds to loss of heterozygosity

Table 5.11. Summary of differences in OE33R compared to OE33P cells identified by array CGH.

Chr	Event	Start (Mb)	Stop (Mb)	Size (Mb)	Cytoband
2	Deletion	51.0	62.0	11.0	2p16.3-2p15
2	Deletion	145.0	152.5	7.5	2q22.3-2q23.3
3	LOH	115.5	187.0	71.5	3q13.31-3q27.3
5	Low level mosaic	49.5	126-3		5q11.1-5q23.2
6	Low level mosaic	38.9	171.0	132.1	6p21.2-6qter
8	CN nearly normal instead of deletion and duplication	Entire chromosome			
9	Deletion	2.0	22.0	20.0	9p24.2-9p21.3
10	Normal CN (no duplication)	0.0	4.8	4.8	10pter-10p15.1
10	LOH	0.0	35.5	35.5	10pter-10p11.21
11	Increased CN complexity and no LOH	0.0	51.5	51.5	11pter-11p11.1
12	Low level mosaic	127.0	134.0	7.0	12q24.32-12qter
14	Low level mosaic	20.5	41.0	20.5	14q11.2-14q21.1
16	LOH	Entire chromosome instead of just 16q			
17	Increased CN complexity	17q distal to regions of amplification			
18	Increased CN complexity	18q			
19	Low level mosaic	Entire chromosome			
20	LOH	0.0	26.5	26.5	20pter-20p11.1
20	LOH	59.4	63.0	3.6	20q13.33-20qter

OE33P and OE33R cell lines were characterized using microarray and analyzed using ChAs software. Genome coordinates are approximated down to the megabase (Mb) level using genome build hg19. CN=Copy number

5.4.3 Selection of targets and validation in cell lines

Several regions of copy number variation between OE33P and OE33R were identified (Figure 5.1 and 5.2); the most significant appeared to be the 9p deletion affecting 9p24.2-21.3 (Figure 5.3 and 5.4). Over twenty genes and microRNAs (miRNAs) were present in this region, including one gene involved with regulating radioresponse, IL33 (located at 9p24.1) in addition to the microRNA miR-31 (located at 9p21.3) (Figure 5.4). IL33 was selected for measurement in OE33P and OE33R.

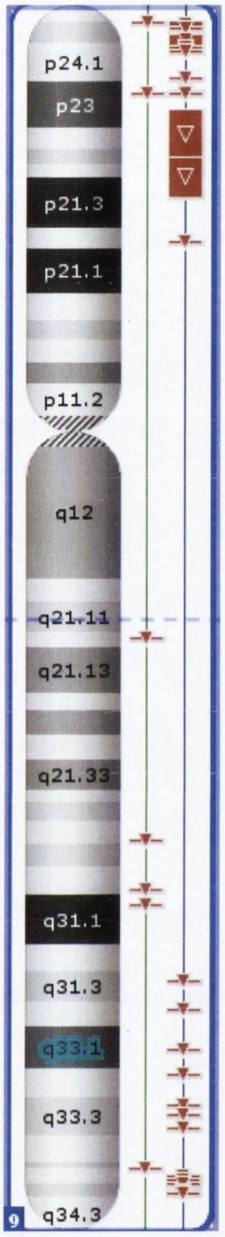


Figure 5.3. Copy number losses on chromosome 9 in OE33P compared to OE33R
This image represents chromosome 9 on OE33P and OE33R as seen on the ChAs software. The most significant genomic alteration in OE33R compared to OE33P was the deletion on chromosome 9 affecting 9p24.2-21.3. This image shows areas of copy number variation on chromosome 9 in OE33P and OE33R. OE33P is represented on the green line to the left, while OE33R is represented on the blue line to the right. In this array, the vertical direction is the genome order from 1pter to 23qter. The red colour means the log ratio for that gene/clone is negative. The OE33R allele track shows a deletion from 9p24.2-21.3, 20.0 Mb in size.
▽ Corresponds to areas of copy number loss

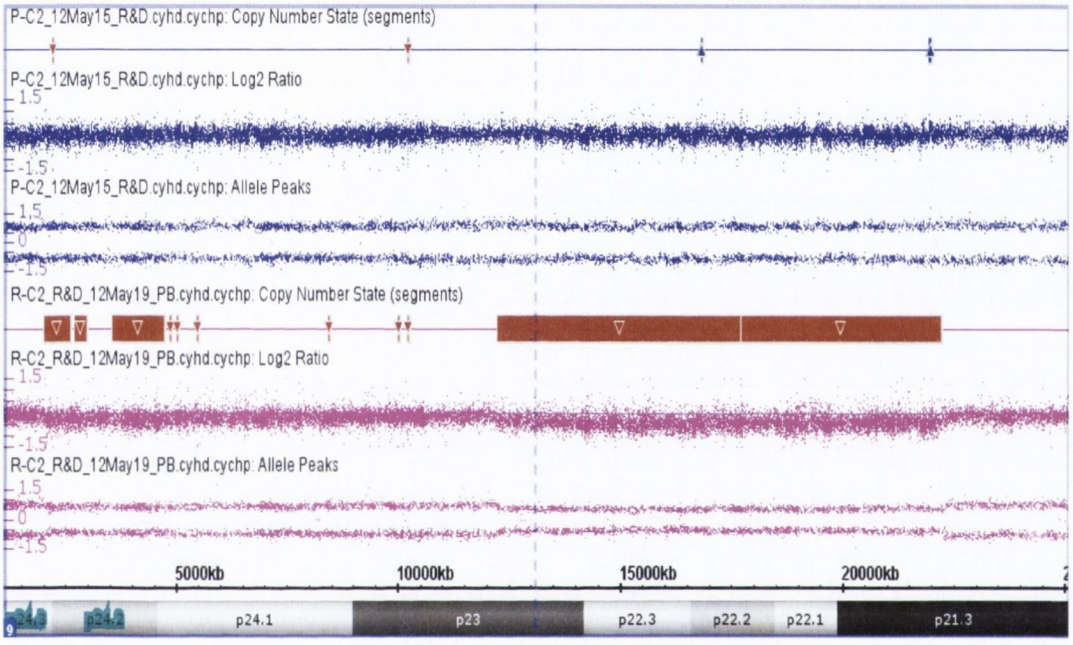


Figure 5.4. The 9p deletion in OE33R cells as seen on ChAs software encompasses 9p24.2-21.3

This image represents the 9p24.2-21.3 region of chromosome 9 on OE33P and OE33R. In this array, the horizontal direction is the genome order from 1pter to 23qter. Allele tracks from OE33P are coloured in purple; allele tracks from OE33R are coloured pink. The heights of the purple and pink lines represent the $\log_2$ ratio for the genes/probes. The red colour means the log ratio for that gene/clone is negative. The OE33R allele track shows a deletion from 9p24.2-21.3, 20.0 Mb in size.

Corresponds to areas of copy number loss

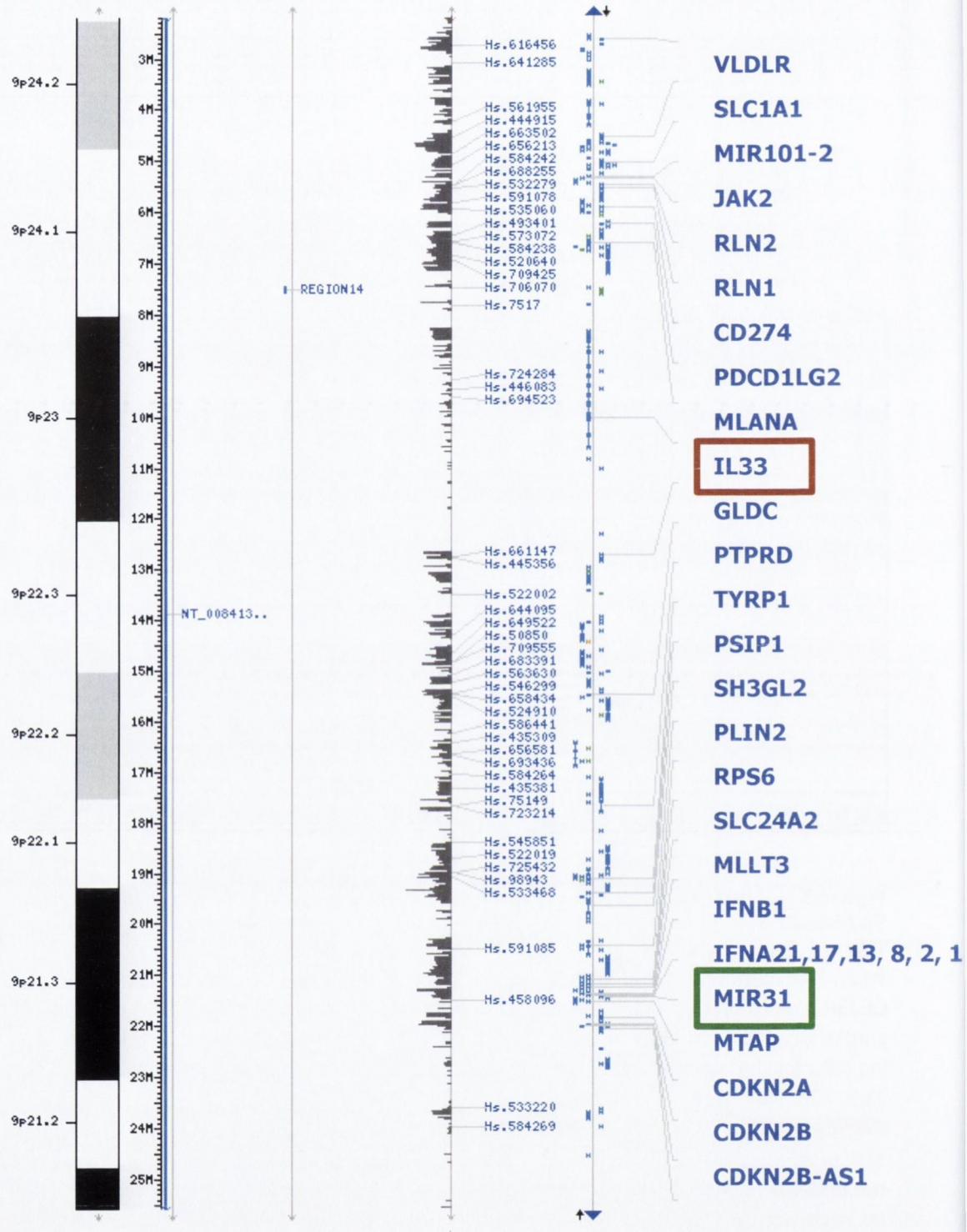


Figure 5.5. Genes located at the 9p deletion as per the National Centre for Biotechnology Information (NCBI) Map viewer: 9 2,200K-25,600K (9p24.2-21.3)
The NCBI database was interrogated to elucidate gene targets located on the region of interest on chromosome 9 (9p24.2-21.3). Thirty-one gene and microRNA targets were identified at this region. Targets known to be associated with the radioresponse were selected for validation in OE33P and OE33R cell lines (IL33).

5.4.4. Target gene expression in OE33P and OE33R

IL33 was selected as the target for validation in OE33P and OE33R cells using quantitative real-time PCR. IL33 expression was twenty-fold higher in OE33P compared to OE33R cells ($p<0.0001$) (Figure 5.6).

5.4.5 Target gene expression in responder and non-responder patient cohorts

IL33 expression was determined in oesophageal adenocarcinoma pre-treatment biopsy samples from patients who went on to have a good pathological response (TRG 1-3) and poor TRG response (TRG 4-5, non-responder) at resection (patient details are outlined in chapter two, table 2.7). There was no difference in IL33 expression between pre-treatment biopsy tissues from responder compared with non-responder patients (Figure 5.7).

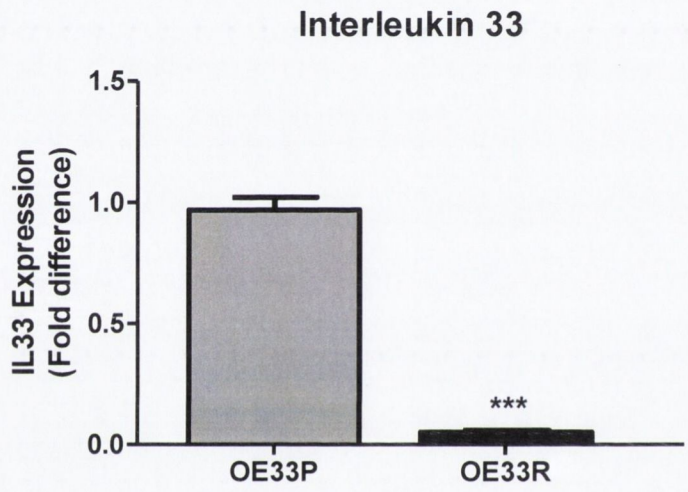


Figure 5.6. IL33 expression is higher in OE33P compared to OE33R cells
IL33 expression is twenty-fold higher in OE33P compared to OE33R cells ($p<0.001$). Data are expressed as mean RQ values ± SEM. Analysis was performed using unpaired two-tailed student's *t*-test, *$p<0.05$, **$p<0.001$, ***$p<0.0001$.

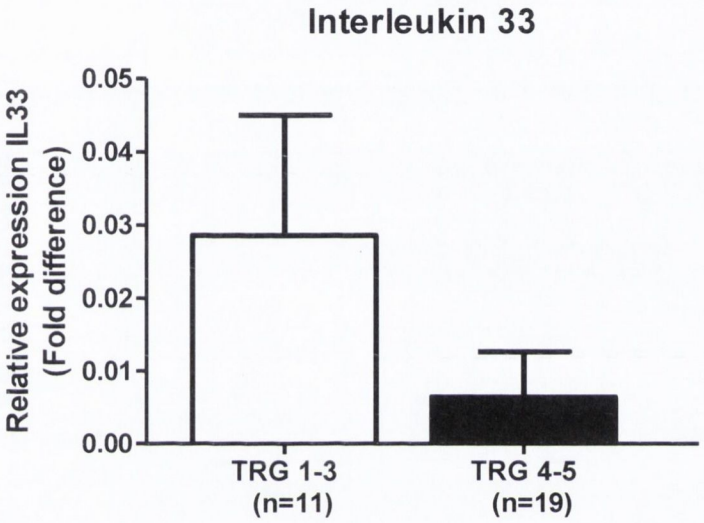


Figure 5.7. IL33 expression in oesophageal cancer patients

IL33 expression was determined in oesophageal adenocarcinoma pre-treatment tumour biopsy samples from responder and non-responder patients using quantitative real-time PCR. Data are expressed as mean RQ values ± SEM. Statistical analysis was performed using Mann Whitney U test, *$p<0.05$, **$p<0.001$, ***$p<0.0001$. There was no difference in IL33 expression in pre-treatment biopsy tumour samples from responder patients compared to biopsy samples from non-responder patients.

5.5 Discussion

Discoveries in the last several years have advanced our understanding of molecular biology underlying the radioresponse. Array-CGH permits high density, high resolution genomic scanning for losses and gains over many thousands of genomic targets. Comparative whole-exome sequencing has been reported for OAC[660,678], and DNA copy number alterations have been shown to correlate with survival in OAC[659]. However, no clear contributors to radioresponse have been identified at the gene level. Our goal was to interrogate the genome to identify specific alterations or patterns of alterations that distinguish CRT responders and non-responders. FISH was performed to confirm the karyotype. The OE33 cell line was derived from a poorly differentiated, stage IIA adenocarcinoma that arose in Barrett's oesophagus[645]. A combination of chromosome CGH and FISH was used to karyotype the radioresistant model. This was important due to the possibility that variations may have arisen due to differentiation or transformation during *in vitro* culture. The karyotype was still aneuploid, near tetraploid and consistent with the diagnosis of oesophageal adenocarcinoma.

The aim of the study was to screen and identify the chromosomal aberrations that distinguish OE33P from OE33R, and which may correlate with clinicopathological characteristics of radioresponse in OAC patients. The results showed that a deletion located on chromosome 9 in OE33R (9p24.2-21.3) was a significant area of copy number variation between the two cell lines. This region encompasses mir-31, located at 9p21. We have previously demonstrated that mir-31 is a key regulator of radioresponse in OAC patients[175]. This confirms the validity of the array data. 9p losses are a frequent event in OAC[679]. A high resolution array of 189 OAC patients reported a frequency rate of 37% for losses at 9p[679]. Previous studies with smaller cohort sizes and different hybridization techniques identified 9p losses in 18-26% of OAC samples[651,680]. Deletions of 9p24-21 are associated with resistance to therapy in glioblastoma, ovarian, and head and neck cancer patients[681–683]. Hence, detection of 9p deletions might be helpful in the prediction of clinical outcome of patients with OAC. Several targets from this chromosome were investigated in our isogenic model, and significance was detected for IL33, located at 9p24.1.

In this study, IL33 expression was significantly higher in radioresponsive compared to radioresistant cells. IL33 belongs to the IL1 family of cytokines, and was recently identified as a ligand to the previously orphan ST2 receptor[684]. IL33, through its receptor T1/ST2 (transmembrane form of ST2), is a potent inducer of Th2-type immune responses dominated by antibody production, with concomitant expression of Th2-associated cytokines such as IL4, IL5, and IL13[684]. IL33 is expressed by several cell types including epithelial and endothelial cells[685]. The IL33 receptor is expressed on mast cells and in addition to its effects on Th2 responses, IL33 has been found to activate mast cells and to stimulate the production of

numerous pro-inflammatory cytokines including TNF, IL1, IL6, and IFN-c (Interferon-c) in these cells[686–688]. IL33 and mast cells constitute a link between cell injury and the inflammatory response. Il33 is released by necrotic structural cells and recognised by mast cells via ST2[689]. Mast cells are located in all tissues and are well positioned to rapidly recognize IL33 release from damaged cells[689]. IL33 may play a role as an 'alarmin'—a signalling protein released by cells upon cell damage, and may initiate either cell survival or cell death signalling[690]. IL33 expression in the isogenic model was highest in the radioresponsive cells, however, suppression of the IL33 pathway in directly irradiated and bystander human fibroblasts, substantially increased radiation-induced or TNF-related apoptosis-inducing ligand (TRAIL)-mediated apoptosis[690]. This suggests that resistance to apoptosis depends on IGF1R-Akt-IL33-mediated protective function[690]. IL33 plays an important role in radiation-induced bystander effects via NF-κB-dependent regulation of expression of numerous genes[690]. NF-κB is the central mediator of inflammation, carcinogenesis and radioresistance[691]. Massive production and release of pro-inflammatory cytokines by directly irradiated cells, besides protective anti-apoptotic effects for these cells, initiate a strong inflammatory response of non-target cells, which may result in different final points such as resistance to radiation[692]. A trend of increased IL33 expression in responder compared to non-responders was detected in patient samples; however, the differences in expression between responders and non-responders, was not statistically significant. This may be due to the small sample size, and requires greater power. The patient cohort used for this study was the maximum number available in the departmental bioresource that met the inclusion criteria. Given the small sample size, the results warrant further investigation of this target gene as a potential in vivo biomarker to predict response in OAC in a larger cohort of patients. In any systematic approach to study the oesophageal adenocarcinoma genome within pre-treatment core biopsies (and relate these findings to radiotherapy outcome), it must be recognized that intra- and intertumoural (and indeed, intra-biopsy) heterogeneity exists and this can potentially confound the interpretation of the genomic "status" of the tumour sample[693]. This must be accounted for when validating a gene signature for use as a new prognostic or predictive factor. Furthermore, the tumour microenvironment (e.g. hypoxia; epithelial-mesenchymal interactions) may add complexity to a RNA profile for a given patient. Appropriate sample acquisition using macro- or micro-dissection in close collaboration with pathologists is required for the careful study of genetic factors. It should also be noted that certain genomic events do not directly translate into gene expression changes; RNA and subsequent protein expressions are often subjected to complex post-transcriptional regulations including effects of microRNA and non-coding RNAs[660].

A microRNA (miRNA) is a small (19–30 nucleotides), RNA species which functions in transcriptional and post-transcriptional regulation of gene expression[694]. The human genome may encode over 1000 miRNAs, which may target about 60% of mammalian genes and are

abundant in many human cell types[695,696]. It has been shown that miRNAs regulate pathways involved in the cellular response to radiation, such as cell cycle and DNA repair[697]. miRNA-101-2 has been shown to sensitise tumour cells to radiation *in vitro* and in vivo[698]. Expression of miR-101-2 regulated gene targets including mTOR (mechanistic target of rapamycin), EZH2 (enhancer of zeste 2), PRKDC (protein kinase, DNA-activated, catalytic polypeptide), PTGS2 (prostaglandin-endoperoxide synthase 2) and ATM (ataxia telangiectasia mutated) are associated with radiosensitivity status in a variety of human cancers[698–704]. To fully investigate the functional role of miR-101-2 in modulating radiosensitivity, miR-101-2 expression should be characterised in this radioresistant model.

In addition to the 9p deletion investigated in this study, other regions were identified which may potentially be biomarkers of radioresponse in OAC. The deletions identified on chromosome two of OE33R at 2p16.3-15 and 2q22.3-23.3 have been reported in multidrug resistant lung adenocarcinoma cell lines[705], and are associated with chemoresistance in lymphoma patients[706]. These two regions encompass over fifty genes. For example, MSH6 (MutS homolog 6), located at 2p16, is a gene that codes for a DNA mismatch repair protein. Defects in this gene are linked with atypical HNPCC (Hereditary non-polyposis colorectal cancer)[707], and poor outcomes in endometrial cancer patients following adjuvant CRT[708]. This array data provides a useful starting point for further assessment and validation.

Instead of focusing on specific factors, array-based gene expression profiling technology enables the simultaneous analysis of large numbers of genes, and might therefore have immense potential for predicting the response to preoperative CRT in OAC. There is a clinical need to establish molecular biomarkers that differentiate responsive and resistant tumours because such biomarkers could be used pre-therapeutically to predict the response of an individual patient's tumour to multimodal treatment. In addition, genes that are differentially expressed between resistant and responsive tumours could be used to identify novel therapeutic targets and thereby assist in implementing novel therapeutic strategies. For instance, targeted inhibition of the activities of the IL33 may be achieved through neutralization with antibodies or inactivation through soluble receptor decoys. Antibodies directed against IL-33 have proven effective for the treatment of asthma in a mouse model. While humanized antibodies for this molecule have not yet been developed, further investigations are warranted, as the targeted inhibition of IL-33 may not only have the potential to eliminate inflammation, but may also have limited systemic side effects as a result of the tissue distribution of IL-33 and the receptor ST2. This study identified IL33 as a potential biomarker of radioresponse in our isogenic model. Increasing the number of patients analysed for more accurate prediction is necessary, in addition to extensive validation of predictive classifiers in prospective clinical trials[709]. Global analysis of genetic aberrations can identify relevant therapeutic targets and genetic aberrations involved in radioresponse. It is anticipated that the advent of next

generation deep sequencing and paired-end analyses will further expand the role for DNA-associated genomic studies on the road to more personalized cancer therapies in the future.

Chapter 6 Concluding discussion

6.1 Concluding discussion

The interaction between obesity, genomic instability and the radioresponse in oesophageal adenocarcinoma (OAC) is poorly understood. The incidence of OAC is increasing more than any other cancer in the western world, paralleling the current epidemic of obesity[4,554]. There is robust epidemiological evidence linking obesity with oesophageal adenocarcinoma; in fact, OAC may be considered the exemplar model of an obesity-related cancer[26,710]. It has become evident that it is specifically visceral obesity, with its associated systemic inflammation that is pro-tumourigenic[635]. Adipose tissue, particularly viscerally located fat, is metabolically active, associated with the development of chronic inflammation, oxidative stress, adipokine production and genomic instability events[253,561].

OAC carries a dismal prognosis, with five year survival rates of 35-50%[55,61–65]. The best outcomes are seen in patients with local disease treated with curative intent using a multimodal approach comprising NA-CRT and surgery[55,61–65]. The patients who receive maximum benefit from NA-CRT are those who achieve a pCR, characterised by no residual cancer cells in the primary tumour or lymph nodes[79–83]. Unfortunately only ~30% of patients achieve a pCR[79]. Patients who do not respond to CRT are subject to toxicities without therapeutic gain and their prognosis may be worsened by the delay to surgery[79]. Thus there is an impetus to understand the mechanisms driving the malignant progression, to determine strategies to optimise outcomes in patients undergoing treatment, and to develop improved markers capable of predicting patients who will respond well to treatment.

The ability to analyse predictive markers at the level of RNA, DNA, and protein promises to revolutionize our understanding of the disease process, and it is hoped that the era of genomics, transcriptomics, and proteomics will herald new biomarkers of response. Given the epidemic of obesity in the western world, more studies are needed to precisely delineate the relationship between obesity and cancer. In this research, novel mechanisms linking visceral obesity to the radioresponse in OAC, insight into how visceral obesity drives genomic instability events in radioresistant OAC, and a potential role for telomerase inhibition to improve outcomes in OAC patients are presented.

An increasing number of studies have emerged in recent years linking excess visceral adiposity with increased risk of cancer recurrence and death following treatment[228–235,237,239,456,457]. However, there have been a number of studies that have reported no association between obesity and outcomes[240–244], and of those with significant findings, there are inconsistencies about the measurement and level of obesity, treatment modality, and the role of gender[228,229,232,245]. Although several studies have reported no difference in survival between obese and non-obese patients with OAC[246,247,252], others have reported better survival outcomes

in patients with high BMIs[248,458]. One recent study, performed by Shridhar et al., specifically examined oncological and survival outcomes in a cohort of OAC patients who received NA CRT; BMI was not associated with tumour response or survival[251]. The impact of obesity on outcomes in OAC, in particular the response to neoadjuvant chemoradiotherapy (NA CRT), is not clear. Thus the first step in this research programme was to assess response to NA therapy in OAC patients undergoing curative therapy in this institution. A retrospective analysis of a prospectively maintained database was performed on patients with OAC treated with NA radiotherapy between 1990 and 2013. This study demonstrated that BMI status influences the radioresponse in OAC. Overweight and obese OAC patients are more likely to have a good response to NA-CRT than non-obese patients. This did not translate to a survival benefit in these patients. Improved TRG outcome indicates improved locoregional control-however the effect on survival in obese patients may be offset by associated morbidities, salvage systemic therapies, early metastatic events or treatment toxicity.

There were limitations of this study. Body mass index was obtained at the time of diagnosis, which might not reflect changes in BMI that occurred before diagnosis. Weight loss is a major symptom of advanced disease, and malnourished patients (BMI<19.5 kg/m^2) were excluded from the study. In addition, we had a relatively small sample size that limited our power to stratify analyses by factors such as sex. However, this study included a homogeneous population of non-metastatic OAC patients that were all treated with NA CRT followed by resection. Although small, this study was strengthened by the focus on a homogeneous patient population that reduced the possibility of outcomes differences due to stage or treatment differences. A larger sample size in future studies will help to confirm our findings. It is becoming increasingly apparent that BMI alone is inadequate as a consistent prognostic indicator. CT measurement of VFA is the gold standard marker of obesity, and radiologic visceral fat quantification with its use of existing diagnostic imaging might ultimately represent an easily performed and more precise and reproducible instrument of clinical prognostication. Overall, we have demonstrated that there is a significant relationship between adiposity and oncologic outcomes. Even when subject to multivariate analysis, BMI was a predictor of tumour response among this group of OAC patients. This study represents an important proof of concept that adiposity is an important determinant of outcomes in patients with OAC undergoing NA CRT and resection. Data has demonstrated that NA concurrent CRT improves local control and survival compared with surgery alone and offers a modest survival benefit compared to a NA chemotherapy alone approach in patients with resectable OAC. NA CRT is the standard of care for these patients[74–76], therefore current and future research is aimed at optimizing NA therapies. Chemotherapy is a very important component of NA therapy in OAC, and it is important to acknowledge that the impact of obesity on the response to chemotherapy has not been specifically investigated in this study. Clinicians should be aware of higher BMI

status as a host factor influencing tumour response to NA CRT. This is particularly important given that patients with severe obesity-associated medical co-morbidities (including diabetes, hypertension, and coronary artery disease) are more likely to be excluded from radical curative therapies. Patients with low BMI might either not benefit from NA CRT or require a higher dosage. If further validation studies corroborate our results, the incorporation of measurement of BMI/VFA into prospective oncologic therapeutic and epidemiologic studies in OAC is warranted.

The relationship between adipose tissue and radioresponse has not been investigated at a molecular level. Mechanisms of radioresistance are still poorly understood. We and others have shown that the radioresistant phenotype is correlated with features such as altered DNA repair, cell cycle checkpoint operation, telomere biology, reactive oxygen species (ROS) biology, and induction of apoptosis[115,440,459–462]. Many of these processes may also be affected by adiposity. To investigate the interaction between obesity and genomic instability in a radioresistant model, the radioresistant OAC cell line model called OE33R was used; the age and passage-matched cell line called OE33P was used as a control. This isogenic model of radioresistance largely avoids the influence of confounding factors, facilitating the identification of specific markers or radioresponse/radioresistance. Clinical data from the retrospective study were consolidated by the in vitro work showing that ACM influences radiosensitivity in both radioresponsive OE33P and radioresistant OE33R; cells treated with ACM demonstrated decreased radioresistance. This effect was seen with ACM from three patient cohorts, including non-cancer patients, radiation naïve OAC patients and previously irradiated patients, suggesting that this outcome is not merely a bystander effect caused by previous exposure to radiation nor is it a secondary effect of malignancy. Radioresistance was lowest in cells treated with ACM from patients who had received NA CRT, suggesting that previous exposure to irradiation induced a bystander effect on the visceral fat, thus stimulating a more radioresponsive phenotype. Radioresistance was altered to a greater degree in OE33R compared to OE33P cells. Both cell lines were treated with identical patient ACM, suggesting that differences in cell line receptor expression may account for the difference in response.

ACM can promote tumourigenesis in cancer cells, by increasing cell proliferation, invasive potential, angiogenesis and induction of cross-talk between cancer cells and the surrounding extracellular matrix[254,463,466]. These actions are thought to be mediated by the production of biologically active proteins such as adiponectin, leptin, and numerous cytokines including VEGF, TNFα, IL6, IL8, IL10, and IL1 receptor agonist[255]. From this panel of ACM constituents, adiponectin, leptin and VEGF expression are associated with altered prognosis in OAC[185,262,263,267,277–281]; expression of these adipokine receptors (AR1, AR2, LepR and NRP1) was assessed in the OE33P and OE33R at baseline and following ACM treatment. AR1 and AR2

expression was higher in OE33P compared to OE33R, while LepR and NRP1 expression was lower in OE33P compared to OE33R. Adiponectin levels are inversely correlated with BMI[257], and over 90% of oesophageal and junctional adenocarcinomas express the adiponectin receptors AR1 and AR2[271]. Overexpression of AR1 and AR2 is associated with prolonged survival in lung, thyroid and gastric cancer[263,472–474]. These findings are consistent with our *in vitro* data demonstrating that AR1 and AR2 levels are higher in radioresponsive compared to radioresistant cancer. Recombinant adiponectin has antiproliferative and proapoptotic effects on OAC cell lines expressing both AR1 and AR2[523,524]; adiponectin-induced inhibition of cellular proliferation may contribute to delaying recovery from DNA damage following irradiation, enhancing radiosensitivity[258,523,524]. The pro-tumour effects of leptin are the direct opposite of those of adiponectin[711]. *In vitro* studies from this unit confirm promotion of cell proliferation, angiogenesis and matrix metalloproteinase expression in OAC cell lines[271]. In addition leptin interferes with the antiproliferative effect of 5FU, taxol and vinblastine in breast cancer cells[525], and the obese db/db mouse which lacks the LepR, demonstrates increased susceptibility to IR[529]. These studies are consistent with our results demonstrating an association of high LepR levels with a radioresistant phenotype. VEGF is currently under investigation as a therapeutic target for radiosensitization in rectal cancer[539]. The radiosensitizing effect of VEGF blockade was thought to be mediated via an anti-angiogenic effect[476]; emerging data now suggest that multiple mechanisms account for the efficacy of VEGF-targeted therapies in patients with cancer[540]. There are three main subtypes of VEGFR 1, 2 and 3, as well as co-receptors including the neuropilins[282]. The co-receptor NRP1 is upregulated in OAC and is associated with risk of invasive behaviour in Barrett's oesophagus[291]. In this study, NRP1 expression was significantly higher in OE33R compared to OE33P cells. NRP1 is undergoing investigation as a target for cancer therapy, and it is interesting to note that combined anti-VEGF and anti-NRP1 therapy with monoclonal antibodies is synergistic in mouse models of cancer[541]. This study demonstrated that low AR1 and AR2 expression, and high LepR and NRP1 expression are associated with radioresistance in this isogenic model. A larger study is required to confirm our findings in an *in vivo* setting. Adipokine receptor expression may be a potential biomarker to predict response in OAC; in addition clinical trials are already underway investigating NRP1 as a therapeutic target.

While alterations in adipokine receptor expression may account for differences in radioresponse elicited in OE33P and OE33R, heterogeneity of ACM composition may explain differences in radioresponse induced by ACM from the three patient cohorts. By replicating an obese microenvironment *in vitro* via ACM treatment of OE33P and OE33R, radiosensitivity was enhanced in both cell lines; however this effect was greatest in cells treated with ACM from patients who received NA CRT. Previous work from this unit demonstrated that ACM generated from NA CRT OAC patients contained higher levels of Leptin and IL-6 (Interleukin 6) compared

to surgery only OAC patients, and higher levels of IL6, IL8 (Interleukin 8), MCP1 (Monocyte chemoattractant protein 1), and IFNγ (Interferon-gamma), compared to ACM from non-cancer patients. In chapter two, we also demonstrated that the metabolomic milieu is different in ACM from non-cancer patients compared to surgery only OAC patients and NA CRT OAC patients, and that obesity status influences the metabolomic profile of OAC patients. The role of adipose tissue metabolites in modulating cancer risk in obese individuals requires further investigation.

In chapter two we showed that adiposity influences radioresponse in OAC patients, and in an *in vitro* model, and identified adipokine and metabolites that be implicated in this radiosensitizing effect. Subsequently we investigated potential mechanisms linking adiposity and radiosensitization. Given the complexity of the cellular response to IR, it is likely that multiple interacting processes can regulate sensitivity to radiation. We and others have shown that the radioresistant phenotype is correlated with features such as altered cell cycle checkpoint operation, reactive oxygen species biology, DNA repair and genomic instability events[115,440,459–462], which may be influenced by adiposity. OAC is a model of inflammation and tumourigenesis, as the majority present in a background of longstanding GORD and BO. vACM is a rich source of proinflammatory adipokines such as IL6 and TNFα , while high levels of activated proinflammatory CD4+ and CD8+ T cells are present in visceral adipose tissue (VAT), suggesting that VAT may fuel chronic inflammation via T cell-mediated pathways[185]. Obesity is associated with a state of chronic inflammation and the production of active mediators, chemotactic molecules, cytokines, and adipokines, results in the excessive production of ROS causing systemic oxidative stress[434,464]. The induction of oxidative stress is one of the mechanisms by which ionizing radiation damages cell components. The radioresistant phenotype has been associated with lower levels of ROS, which is likely to be due, at least in part, to enhanced ROS scavenging by antioxidant enzymes, particularly those involved in GSH processing such as GCLM (glutamate-cysteine ligase modifier subunit), GSS (glutathione synthetase) and GPX (glutathione peroxidase)[459,460]. Oxidative stress in adipose tissue over time is associated with inhibition of G_1-S phase transition, which is mediated via transcriptional repression of E2F target genes[465]. Cell cycle phase plays a role in determining cellular radiosensitivity[116]. This unit has previously shown that ACM co-culture with oesophageal cancer cells alters expression of genes involved in cell cycle control[466]. ACM treatment of OE33P and OE33R altered the cell cycle distribution, with both OE33P and OE33R cells having a significant increase of cells in S phase and OE33R cells having a decrease of cells in G_0/G_1 phase. This is not surprising given that the S phase is relatively resistant to radiation and the G_0/G_1 phase is relatively sensitive to radiation[510]. However, these differences were small (3-4% difference in phase distribution) and unlikely to be a major factor in the enhanced radiosensitivity seen in cells treated with ACM.

Genomic instability is an emerging hallmark of cancer, which is an established feature of most forms of cancer as well as pre-malignant conditions such as Barrett's Oesophagus[297,307–309,423]. Genomic instability refers to the increased tendency of the genome to acquire mutations when the various processes involved in maintaining and replicating the genome are dysfunctional. Breakage-fusion-bridge (BFB) cycles link telomere dysfunction with anaphase bridge formation, and are now generally accepted as a mechanism explaining genetic plasticity in CIN tumours[359]. Telomeres are composed of tandem repeats of TTAGGG and are associated with a wide variety of telomere binding proteins which mediate their function[315,317,359]. Telomeres shorten with every cell division, and telomere length is inversely correlated with age in humans[320–322]. Significant negative relationships exist between adiposity measures (BMI, waist circumference, hip circumference, total body fat, and visceral adipose tissue) and leukocyte telomere length[415–419]. Telomere length is inversely associated with increasing OAC risk,[423,563] and telomere shortening occurs early in the aetiology of oesophageal carcinogenesis[372]. Telomere dysfunction has been linked to radiosensitivity status *in vitro* and in animal models: telomere shortening and telomerase inactivation are associated with a radiosensitive phenotype[439,440,442,449,450,560]. The interaction between obesity, telomere dynamics and the radioresponse in OAC however, has not been investigated. In this study ACM stimulated telomere shortening and dysregulation of the shelterin complex and telomerase. ACM induced telomere shortening in OE33P and OE33R cells to an equal degree, and telomere length at baseline was not different in OE33P compared to OE33R cells, suggesting that average telomere length is not implicated in the radioresistance of this isogenic model or the radiosensitization seen with ACM treatment. ACM promoted upregulation of the telomerase components including TERC and TERT, and TERT expression was significantly higher in obese compared to non-obese OAC patients, confirming findings from the *in vitro* experiments. Our findings contradict a study reporting a significant inverse association between adiposity and telomerase activity in normal healthy cells[401], but are consistent with the findings of Rahmati-Yamchi et al. who demonstrated that increased TERT expression in breast cancer tissue is associated with high BMI[429]. TERT expression was increased in ACM-treated OE33R compared to OE33P cells. The shelterin gene TINF2 was expressed at a higher level in OE33P compared to OE33R cells at baseline; however this was reversed following ACM treatment when expression was higher in OE33R cells. TERT and TINF2 expression was investigated in pre-treatment biopsies from OAC patients who went on to have NA CRT. A trend for increased TERT gene expression in non-responders and decreased TINF2 expression in non-responders was apparent, but did not reach statistical significance. This study shows for the first time, that ACM drives telomere abnormalities in OAC, and this is the first study to investigate these processes in a radioresistant OAC model. Telomeres and the telomerase complex have been tentatively suggested as targets for anti-cancer therapies[712], and clinical trials with telomerase inhibitors are already underway (Roth 2010). This highlights the importance of validating our *in vitro* findings in a large in vivo study. Further elucidation of

the relationship between these telomere abnormalities, obesity and radioresponse, may lead to the stratification of patients based on predicted response to therapy and ultimately to the manipulation of these factors to sensitize these cells to radiation.

To further characterize if the effect of ACM on the radioresponse is mediated via upregulation of genomic instability events, anaphase bridge levels were assessed in the radioresistant model. This is the first study to demonstrate that ACM increases anaphase bridge levels in OAC. Anaphase bridges are a functional, mechanistic marker of genomic instability. Live cell imaging has demonstrated that the majority of anaphase bridges formed will break, usually unevenly, giving rise to structural chromosomal rearrangement[354,616,713]. ACM stimulated anaphase bridge formation in both OE33P and OE33R cells, but bridge levels were significantly higher in the OE33R cell line. This is the first study demonstrating that increased levels of anaphase bridges are associated with radioresistance and this anaphase bridge formation correlates with visceral obesity in radioresistant oesophageal cancer cells. A study by McCaul et al, found no relationship between anaphase bridge levels and radiosensitivity to clinically relevant doses of 2 Gy in 16 oral squamous cell carcinoma cell lines[444]. The same study found that in some cell lines, anaphase bridge levels were inversely correlated with radiosensitivity to higher 4 Gy doses of radiation[444]. The cell lines which demonstrated this relationship between high levels of bridging and radiosensitivity were cell lines with high anaphase bridge levels, indicating that a certain threshold of bridging is necessary for this association to hold true[444]. Furthermore, the cell lines used in this study also demonstrated varying degrees of telomere dysfunction[444]. Given the number of possible factors that can influence intrinsic radioresistance, it is not surprising that the relationship between anaphase bridging and radiosensitivity may differ in individual cancer types. This unit previously demonstrated that ACM generated from obese and non-obese OAC patients contains VEGF and IL-8[185], and that ACM-induced anaphase bridge formation in healthy oesophageal squamous cells is abrogated by neutralising VEGF and IL-8[296]. In chapter one, we showed that OE33R cells demonstrate higher NRP1 expression compared to OE33P. Therefore, the higher levels of anaphase bridges in OE33R may be mediated via VEGF; this possible association requires further investigation. Interestingly, emerging concepts point to a possible crosstalk between DNA repair responses and VEGF-induced angiogenesis[714]. Our group has demonstrated that the radioresistance of OE33R cells is due at least in part to alterations in DNA damage repair efficiency[174]. Anaphase bridges are associated with DNA double strand breaks (DSBs)[639]. Mammalian cells have two major double strand break (DSB) repair pathways: non homologous end joining (NHEJ) and homologous recombination (HR). While the majority of DSBs are repaired correctly, restoring the original chromosome structure, misalignment of two nonmatching ends may also occur resulting in anaphase bridges and chromosomal instability[640,641]. Non homologous end joining (NHEJ) acts to prevent anaphase bridges and in its absence the activity of homologous recombination (HR) leads to anaphase bridge formation; indeed, intrinsic NHEJ activity correlates with the induction of anaphase

bridges[639], suggesting a mechanistic link between genomic instability and radioresistance[639].

BFB cycles involve multiple DNA breakages, associated with gene amplification in cells with defective DNA damage repair or dysfunctional cell cycle checkpoint machinery[715–718]. The spindle assembly checkpoint (SAC) is a surveillance mechanism that ensures the fidelity of chromosome replication during mitosis[373]. The proteins responsible for the SAC signal include MAD2L2, BUB1b, CDC20, CENPE and ESPL1[373]. Alterations in MAD2L2 expression drive tumourigenesis in mice and aberrant MAD2L2 expression is seen in number of human epithelial cancers[357,622]. Doak et al reported both under and over expression of both MAD2L2 and BUB1b genes in Barrett's Oesophagus specimens, but SAC disruption has not previously been documented in oesophageal adenocarcinoma[637]. This study showed that ACM upregulates expression of MAD2L2 and BUB1b in radioresponsive and radioresistant OAC. Obese OAC patients demonstrate increased expression of MAD2L2 but not BUB1b in their tumour specimens. Studies identifying causal mechanisms for SAC deregulation are lacking, and obesity has never previously been linked with dysregulation of the SAC complex. However, obesity induces systemic oxidative stress; biomarkers of oxidative damage are higher in individuals with obesity and correlate directly with BMI and the percentage of body fat and oxidative stress has been linked to malfunction of the SAC in cancer cells[433].

SAC dysregulation is linked to genomic instability in a number of cancer types, but genomic instability may still occur in the presence of an intact SAC, suggesting that while both anaphase bridge formation and a compromised SAC are conducive to aneuploidy and carcinogenesis, these processes may occur independently of each other[357,623,719]. A weakened SAC may function as a facilitator rather than a driving force of tumourigenesis. Dysregulation of the SAC has been implicated in the radioresponse. Abrogation of MAD2L2 expression is associated with enhanced radiosensitivity in glioma cells through activation of apoptosis via cleavage of PARP[455], which is overexpressed in oesophageal tumour tissue of poor responders[175]. Overexpression of CENPE is associated with recurrence in patients with pituitary tumours, and with chemoresistance in ovarian cancer patients[642]. Overexpression of the ESPL1-encoded protein separase strongly correlates with high incidence of relapse and lower 5 year survival rate in breast and prostate cancer patients[643]. MAD2L2, CENPE and ESPL1 expression differed in radioresponsive compared to radioresistant cells. Interestingly, expression of CENPE and ESPL1 also correlated with anaphase bridge levels, suggesting the possibility that expression of these SAC genes may be involved in the link between the anaphase bridge formation and radiosensitivity. The cohort of oesophageal cancer patients who had a poor response to RT demonstrated higher levels of MAD2L2, CENPE and ESPL1 expression compared to patients who had a good response to treatment. Pharmacologic inhibition of the SAC has been putatively proposed as a promising strategy for anticancer treatment[644]. The indolocarbazole compound Gö6976 overrides spindle

checkpoint-mediated mitotic arrest, resulting in apoptosis in spindle checkpoint-compromised cancer cells[644]. Investigation of these gene targets in a large prospective study of OAC patients receiving NA CRT is required to identify if disruption of the SAC in OAC may represent an important target for obese patients treated with NA CRT.

Cancer progression is associated with genomic instability and an accumulation of gains and losses of DNA. The growing variety of tools for measuring genomic copy number includes array-based comparative genomic hybridization (aCGH). aCGH and gene expression microarray profiling have been used separately to identify molecular aberrations in small cohorts of OAC patients[651,652,657,658,670–674]. Goh et al integrated data from an aCGH platform with corresponding gene expression microarray profiles from 56 fresh frozen OAC resection samples to generate a potential prognostic signature for OAC[660]. Identification of the genomic alteration "signatures" in OAC CRT responders and non-responders may provide more sensitive and specific biomarkers of radioresponse. The aCGH used in this study allows monitoring of tumour genomes with unprecedented resolution (1,953,246 oligonucleotides and 743,304 SNP probes). The aCGH profile of OE33R was characterised by deletions on chromosomes two (2p16.3-2p15, 2q22.3-2q23.3) and nine (9p24.2-9p21.3). Although this was a pilot study, we then attempted to investigate whether the identified set of genetic aberrations could potentially be informative for identifying novel rational therapeutic targets, or therapies currently available or in clinical trials. For example, the deletion on chromosome nine included mir-31, located at 9p21, which we have previously demonstrated is a key regulator of radioresponse in OAC patients[175]. This confirms the validity of the array data. This study identified a promising molecular marker of radioresistance; interleukin 33 (IL33), located at 9p24.1. IL33 is a recently described cytokine belonging to the IL-1 superfamily which stimulates helper T cells, mast cells, eosinophils and basophils to produce cytokines typical of a type two immune response[688]. IL-33 mediates its biological effects by interacting with the receptors ST2 (IL1RL1) and IL-1 Receptor Accessory Protein (IL1RAP), activating intracellular molecules in the NF-κB and MAP kinase signalling pathways that drive production of type 2 cytokines from polarized Th_2 cells[684,688]. IL33 plays an important role in radiation-induced bystander effects via NF-κB-dependent regulation of expression of numerous genes[690]. Suppression of IL-33 expression results in an increase in apoptosis in both directly irradiated and bystander human skin fibroblasts[690]. In this study, IL33 expression was significantly higher in radioresponsive compared to radioresistant cells. While the same trend was seen in responder and non-responder patient samples, the difference in expression did not reach statistical significance. It must be recognized that intra- and intertumoural (and indeed, intra-biopsy) heterogeneity exists and this can potentially confound the interpretation of the genomic "status" of the tumour samples, particularly in pre-treatment biopsies[693]. This must be accounted for when validating a gene signature for use as a new prognostic or predictive factor. Investigation of IL33 expression in a large cohort of OAC patients is necessary to fully assess its role in radioresistant OAC.

As the focus on outcomes and comparative effectiveness research increases, and OAC and obesity levels continue to rise, the development of accurate and reliable risk and prognosis stratification strategies for obese OAC patients are clearly necessary to better guide patient treatment decisions. This body of work has generated a number of interesting findings relating to the treatment response in OAC. For the first time, the impact of visceral obesity and adipokine receptor expression on the radioresponse was characterised. A novel role for visceral obesity in the induction of genomic instability events (telomere dysfunction and anaphase bridge induction) in radioresistant cells was demonstrated, highlighting the complex interaction between obesity, genomic instability and radioresponse. In addition, novel genomic instability events in radioresistant OAC were identified using aCGH technology. This study has so far demonstrated that obesity influences radiosensitivity, and drives genomic instability events in OAC, particularly radioresistant OAC. Together these findings add to the knowledge base regarding the treatment response in oesophageal cancer. Additional studies that elucidate the physiologic and biologic mechanisms mediating the adiposity-radioresponse link are clearly needed. The incorporation of quantitative measures of visceral obesity and corresponding correlative molecular studies into prospective oncologic therapeutic and epidemiologic studies is also warranted. Uncovering the mechanisms of interaction of visceral obesity, genomic instability and radioresistance could identify shared pathways as potential preventative and therapeutic targets, improving outcomes in patients suffering from this aggressive malignancy.

6.2 Future directions

This research has identified a number of areas for future work. The promising findings relating to the role of obesity in regulating tumour response in OAC patients requires confirmation in a large prospective clinical trial. Whilst this study has demonstrated a role for adipose tissue in modulating the radioresponse via induction of genomic instability events, the exact mechanism(s) by which adipose tissue mediates radiosensitivity remain to be elucidated. Neutralisation and overexpression of adipokines such as adiponectin and leptin in radioresistant and radiosensitive OAC cell lines may reveal a role for these factors in the induction of chromosomal instability in radioresistant OAC. Future analysis may allow the metabolic pathways associated with adipokine receptors to be identified based on the results of metabolomics analysis. A trend for higher expression of LepR, NRP1 and TERT was noted in tumour tissue from non-responder patients compared to responder patients, while levels of AR1, AR2, MAD2L2, CENPE, ESPL1 and IL33 were higher in radioresponder compared to non-responder oesophageal cancer patients. Given the small sample size available in the bioresource, the gene targets associated with require investigation in a larger *in vivo* cohort. In addition, the alterations in mRNA expression were not validated at the protein and functional level, and this may be an important area for future investigation. In addition to the 9p deletion investigated in this study, other regions of copy number variation were identified which may potentially be biomarkers of radioresponse in OAC. This array data provides a useful starting point for further assessment and validation.

References

1. Jemal, A., Bray, F. & Ferlay, J. Global Cancer Statistics. *CA Cancer J Clin* **61,** 69–90 (2011).

2. Ferlay, J. *et al.* Estimates of worldwide burden of cancer in 2008: GLOBOCAN 2008. *Int J Cancer* **127,** 2893–2917 (2010).

3. Sweed, M. R., Edmonson, D. & Cohen, S. J. Tumors of the esophagus, gastroesophageal junction, and stomach. *Semin Oncol Nurs* **25,** 61–75 (2009).

4. DeMeester, S. R. Epidemiology and biology of esophageal cancer. *Gastrointest. cancer Res. GCR* **3,** 2–5 (2009).

5. National Cancer Registry of Ireland. at <http://www.ncri.ie>

6. Vaughan, T. L., Davis, S., Kristal, A. & Thomas, D. B. Obesity, alcohol, and tobacco as risk factors for cancers of the esophagus and gastric cardia: adenocarcinoma versus squamous cell carcinoma. *Cancer Epidemiol. Biomarkers Prev.* **4,** 85–92 (1995).

7. Kubo, A. & Corley, D. A. Marked multi-ethnic variation of esophageal and gastric cardia carcinomas within the United States. *Am. J. Gastroenterol.* **99,** 582–8 (2004).

8. Lagergren, J. Adenocarcinoma of oesophagus: what exactly is the size of the problem and who is at risk? *Gut* **54 Suppl 1,** i1–5 (2005).

9. Fléjou, J.-F. Barrett's oesophagus: from metaplasia to dysplasia and cancer. *Gut* **54 Suppl 1,** i6–12 (2005).

10. Reid, B. J. Early events during neoplastic progression in Barrett's esophagus. *Cancer Biomark.* **9,** 307–24 (2010).

11. Solaymani-Dodaran, M., Logan, R. F. A., West, J., Card, T. & Coupland, C. Risk of extra-oesophageal malignancies and colorectal cancer in Barrett's oesophagus and gastro-oesophageal reflux. *Scand. J. Gastroenterol.* **39,** 680–5 (2004).

12. Ryan, A. M. *et al.* Barrett esophagus: prevalence of central adiposity, metabolic syndrome, and a proinflammatory state. *Ann. Surg.* **247,** 909–15 (2008).

13. Farrow, D. C. *et al.* Gastroesophageal reflux disease, use of H2 receptor antagonists, and risk of esophageal and gastric cancer. *Cancer Causes Control* **11,** 231–8 (2000).

14. Lagergren, J., Bergström, R. & Nyrén, O. Association between body mass and adenocarcinoma of the esophagus and gastric cardia. *Ann. Intern. Med.* **130,** 883–90 (1999).

15. Edelstein, Z. R., Farrow, D. C., Bronner, M. P., Rosen, S. N. & Vaughan, T. L. Central adiposity and risk of Barrett's esophagus. *Gastroenterology* **133,** 403–11 (2007).

16. Jankowski, J. A. *et al.* Molecular evolution of the metaplasia-dysplasia-adenocarcinoma sequence in the esophagus. *Am. J. Pathol.* **154,** 965–73 (1999).

17. Renehan, A. G., Tyson, M., Egger, M., Heller, R. F. & Zwahlen, M. Body-mass index and incidence of cancer: a systematic review and meta-analysis of prospective observational studies. *Lancet* **371,** 569–78 (2008).

18. Calle, E. E., Rodriguez, C., Walker-Thurmond, K., Thun, M. J. & Calle, EE, R. C. Overweight, obesity, and mortality from cancer in a prospectively studied cohort of US adults. *New Engl. J. ...* **348,** 1625–1638 (2003).

19. Engel, L. S. *et al.* Population attributable risks of esophageal and gastric cancers. *J. Natl. Cancer Inst.* **95,** 1404–13 (2003).

20. Ryan, A. M., Rowley, S. P., Fitzgerald, A. P., Ravi, N. & Reynolds, J. V. Adenocarcinoma of the oesophagus and gastric cardia: male preponderance in association with obesity. *Eur. J. Cancer* **42,** 1151–8 (2006).

21. Chow, W. H. *et al.* Body mass index and risk of adenocarcinomas of the esophagus and gastric cardia. *J. Natl. Cancer Inst.* **90,** 150–5 (1998).

22. Brown, L. M. *et al.* Adenocarcinoma of the esophagus: role of obesity and diet. *J. Natl. Cancer Inst.* **87,** 104–9 (1995).

23. *Cancer Trends National Cancer Registry Ireland.* 2009–2012 (2011).

24. Bollschweiler, E., Wolfgarten, E., Gutschow, C. & Holscher, A. H. Demographic variations in the rising incidence of esophageal adenocarcinoma in white males. *Cancer* **92,** 549–555 (2001).

25. Enzinger, P. C. & Mayer, R. J. Esophageal cancer. *N. Engl. J. Med.* **349,** 2241–52 (2003).

26. Calle, E. E. & Kaaks, R. Overweight, obesity and cancer: epidemiological evidence and proposed mechanisms. *Nat. Rev. Cancer* **4,** 579–91 (2004).

27. Vainio, H., Kaaks, R. & Bianchini, F. Weight control and physical activity in cancer prevention: international evaluation of the evidence. *Eur. J. Cancer Prev.* **11 Suppl 2,** S94–100 (2002).

28. Després, J.-P. *et al.* Abdominal obesity and the metabolic syndrome: contribution to global cardiometabolic risk. *Arterioscler. Thromb. Vasc. Biol.* **28,** 1039–49 (2008).

29. Corley, D. A. Obesity and the rising incidence of oesophageal and gastric adenocarcinoma: what is the link? *Gut* **56,** 1493–4 (2007).

30. Friedenberg, F. K., Xanthopoulos, M., Foster, G. D. & Richter, J. E. The association between gastroesophageal reflux disease and obesity. *Am. J. Gastroenterol.* **103,** 2111–22 (2008).

31. Beddy, P. *et al.* Association of visceral adiposity with oesophageal and junctional adenocarcinomas. *Br. J. Surg.* **97,** 1028–34 (2010).

32. Corley, D. A., Kubo, A. & Zhao, W. Abdominal obesity and the risk of esophageal and gastric cardia carcinomas. *Cancer Epidemiol. Biomarkers Prev.* **17,** 352–8 (2008).

33. Hanahan, D., Weinberg, R. A. & Francisco, S. The Hallmarks of Cancer. *Cell* **100,** 57–70 (2000).

34. Bax, D. A., Siersema, P. D., Van Vliet, A. H. M., Kuipers, E. J. & Kusters, J. G. Molecular alterations during development of esophageal adenocarcinoma. *J. Surg. Oncol.* **92,** 89–98; discussion 99 (2005).

35. Bani-Hani, K. *et al.* Prospective study of cyclin D1 overexpression in Barrett's esophagus: association with increased risk of adenocarcinoma. *J. Natl. Cancer Inst.* **92,** 1316–21 (2000).

36. Souza, R. F., Shewmake, K., Terada, L. S. & Spechler, S. J. Acid exposure activates the mitogen-activated protein kinase pathways in Barrett's esophagus. *Gastroenterology* **122,** 299–307 (2002).

37. Garewal, H. *et al.* Biomarker studies in reversed Barrett's esophagus. *Am. J. Gastroenterol.* **94,** 2829–33 (1999).

38. Shammas, M. A. *et al.* Growth arrest, apoptosis, and telomere shortening of Barrett's-associated adenocarcinoma cells by a telomerase inhibitor. *Gastroenterology* **126,** 1337–46 (2004).

39. Lord, R. V *et al.* Telomerase reverse transcriptase expression is increased early in the Barrett's metaplasia, dysplasia, adenocarcinoma sequence. *J. Gastrointest. Surg.* **4,** 135–42 (2000).

40. Elder, D. J. E., Halton, D. E., Playle, L. C. & Paraskeva, C. The MEK/ERK pathway mediates COX-2-selective NSAID-induced apoptosis and induced COX-2 protein expression in colorectal carcinoma cells. *Int. J. Cancer* **99,** 323–7 (2002).

41. Zimmermann, K. C. *et al.* Cyclooxygenase-2 expression in human esophageal carcinoma. *Cancer Res.* **59,** 198–204 (1999).

42. Merola, E., Claudio, P. P. & Giordano, A. p53 and the malignant progression of Barrett's esophagus. *J. Cell. Physiol.* **206,** 574–7 (2006).

43. Reid, B. J. *et al.* Predictors of progression in Barrett's esophagus II: baseline 17p (p53) loss of heterozygosity identifies a patient subset at increased risk for neoplastic progression. *Am. J. Gastroenterol.* **96,** 2839–48 (2001).

44. Hughes, S. J. *et al.* Fas/APO-1 (CD95) is not translocated to the cell membrane in esophageal adenocarcinoma. *Cancer Res.* **57,** 5571–8 (1997).

45. Maley, C. C. *et al.* Selectively advantageous mutations and hitchhikers in neoplasms: p16 lesions are selected in Barrett's esophagus. *Cancer Res.* **64,** 3414–27 (2004).

46. González, M. V *et al.* Mutation analysis of the p53, APC, and p16 genes in the Barrett's oesophagus, dysplasia, and adenocarcinoma. *J. Clin. Pathol.* **50,** 212–7 (1997).

47. Wong, D. J., Barrett, M. T., Stöger, R., Emond, M. J. & Reid, B. J. p16INK4a promoter is hypermethylated at a high frequency in esophageal adenocarcinomas. *Cancer Res.* **57,** 2619–22 (1997).

48. Klump, B., Hsieh, C. J., Holzmann, K., Gregor, M. & Porschen, R. Hypermethylation of the CDKN2/p16 promoter during neoplastic progression in Barrett's esophagus. *Gastroenterology* **115,** 1381–6 (1998).

49. Möbius, C. *et al.* The "angiogenic switch" in the progression from Barrett's metaplasia to esophageal adenocarcinoma. *Eur. J. Surg. Oncol.* **29,** 890–4 (2003).

50. Brekken, R. A. & Thorpe, P. E. VEGF-VEGF receptor complexes as markers of tumor vascular endothelium. *J. Control. Release* **74,** 173–81 (2001).

51. Nelson, A. R., Fingleton, B., Rothenberg, M. L. & Matrisian, L. M. Matrix metalloproteinases: biologic activity and clinical implications. *J. Clin. Oncol.* **18,** 1135–49 (2000).

52. Reid, B. J., Li, X., Galipeau, P. C. & Vaughan, T. L. Barrett's oesophagus and oesophageal adenocarcinoma: time for a new synthesis. *Nat. Rev. Cancer* **10,** 87–101 (2010).

53. Barrett, M. T. *et al.* Evolution of neoplastic cell lineages in Barrett oesophagus. *Nat. Genet.* **22,** 106–9 (1999).

54. Daly, J. M. *et al.* Esophageal cancer: results of an American College of Surgeons Patient Care Evaluation Study. *J. Am. Coll. Surg.* **190,** 562–72; discussion 572–3 (2000).

55. Portale, G. *et al.* Modern 5-year survival of resectable esophageal adenocarcinoma: single institution experience with 263 patients. *J. Am. Coll. Surg.* **202,** 588–96; discussion 596–8 (2006).

56. Plukker, J. T. M. & van Westreenen, H. L. Staging in oesophageal cancer. *Best Pract. Res. Clin. Gastroenterol.* **20,** 877–91 (2006).

57. Kim, H.-I. *et al.* Staging of Adenocarcinoma of the Esophagogastric Junction: Comparison of AJCC 6th and 7th Gastric and 7th Esophageal Staging Systems. *Ann. Surg. Oncol.* **3,** (2013).

58. Edge, S. B. & Compton, C. C. The American Joint Committee on Cancer: the 7th edition of the AJCC cancer staging manual and the future of TNM. *Ann. Surg. Oncol.* **17,** 1471–4 (2010).

59. Pennathur, A., Gibson, M. K., Jobe, B. a & Luketich, J. D. Oesophageal carcinoma. *Lancet* **381,** 400–12 (2013).

60. Pennathur, A. *et al.* Esophagectomy for T1 esophageal cancer: outcomes in 100 patients and implications for endoscopic therapy. *Ann. Thorac. Surg.* **87,** 1048–54; discussion 1054–5 (2009).

61. Reynolds, J. V *et al.* Evolving progress in oncologic and operative outcomes for esophageal and junctional cancer: lessons from the experience of a high-volume center. *J. Thorac. Cardiovasc. Surg.* **143,** 1130–1137.e1 (2012).

62. Orringer, M. B. *et al.* Two thousand transhiatal esophagectomies: changing trends, lessons learned. *Ann. Surg.* **246,** 363–72; discussion 372–4 (2007).

63. Low, D. E. *et al.* Esophagectomy--it's not just about mortality anymore: standardized perioperative clinical pathways improve outcomes in patients with esophageal cancer. *J. Gastrointest. Surg.* **11,** 1395–402; discussion 1402 (2007).

64. Lagarde, S. M., Vrouenraets, B. C., Stassen, L. P. S. & van Lanschot, J. J. B. Evidence-based surgical treatment of esophageal cancer: overview of high-quality studies. *Ann. Thorac. Surg.* **89,** 1319–26 (2010).

65. Altorki, N., Kent, M., Ferrara, C. & Port, J. Three-field lymph node dissection for squamous cell and adenocarcinoma of the esophagus. *Ann. Surg.* **236,** 177–83 (2002).

66. Steiger, Z. *et al.* Eradication and palliation of squamous cell carcinoma of the esophagus with chemotherapy, radiotherapy, and surgical therapy. *J. Thorac. Cardiovasc. Surg.* **82,** 713–9 (1981).

67. Franklin, R. *et al.* Combined modality therapy for esophageal squamous cell carcinoma. *Cancer* **51,** 1062–71 (1983).

68. Leichman, L., Steiger, Z., Seydel, H. G. & Vaitkevicius, V. K. Combined preoperative chemotherapy and radiation therapy for cancer of the esophagus: the Wayne State University, Southwest Oncology group and Radiation Therapy Oncology Group experience. *Semin. Oncol.* **11,** 178–85 (1984).

69. Nygaard, K. *et al.* Pre-operative radiotherapy prolongs survival in operable esophageal carcinoma: a randomized, multicenter study of pre-operative radiotherapy and chemotherapy. The second Scandinavian trial in esophageal cancer. *World J. Surg.* **16,** 1104–9; discussion 1110 (1992).

70. Apinop, C., Puttisak, P. & Preecha, N. A prospective study of combined therapy in esophageal cancer. *Hepatogastroenterology.* **41,** 391–3 (1994).

71. Walsh, T. N. *et al.* A COMPARISON OF MULTIMODAL THERAPY AND SURGERY for esophageal adenocarcinoma. *N. Engl. J. Med.* **335,** 462–467 (1996).

72. Urba, S. Combined-modality treatment of esophageal cancer. *Oncology (Williston Park).* **11,** 63–7 (1997).

73. Burmeister, B. H. *et al.* Surgery alone versus chemoradiotherapy followed by surgery for resectable cancer of the oesophagus: a randomised controlled phase III trial. *Lancet Oncol.* **6,** 659–68 (2005).

74. Urschel, J. D. & Vasan, H. A meta-analysis of randomized controlled trials that compared neoadjuvant chemoradiation and surgery to surgery alone for resectable esophageal cancer. *Am. J. Surg.* **185,** 538–43 (2003).

75. Gebski, V. *et al.* Survival benefits from neoadjuvant chemoradiotherapy or chemotherapy in oesophageal carcinoma: a meta-analysis. *Lancet Oncol.* **8,** 226–34 (2007).

76. Fiorica, F. Preoperative chemoradiotherapy for oesophageal cancer: a systematic review and meta-analysis. *Gut* **53,** 925–930 (2004).

77. Reynolds, J. V. *et al.* Long-term outcomes following neoadjuvant chemoradiotherapy for esophageal cancer. *Ann. Surg.* **245,** 707–16 (2007).

78. Hur, C. *et al.* Trends in esophageal adenocarcinoma incidence and mortality. *Cancer* **119,** 1149–1158 (2013).

79. Geh, J. I., Crellin, A. M. & Glynne-Jones, R. Preoperative (neoadjuvant) chemoradiotherapy in oesophageal cancer. *Br. J. Surg.* **88,** 338–56 (2001).

80. Ancona, E. *et al.* Only pathologic complete response to neoadjuvant chemotherapy improves significantly the long term survival of patients with resectable esophageal squamous cell carcinoma: final report of a randomized, controlled trial of preoperative chemotherapy versus . *Cancer* **91,** 2165–74 (2001).

81. Forastiere, A. A., Orringer, M. B., Perez-Tamayo, C., Urba, S. G. & Zahurak, M. Preoperative chemoradiation followed by transhiatal esophagectomy for carcinoma of the esophagus: final report. *J. Clin. Oncol.* **11,** 1118–23 (1993).

82. Donington, J. S. *et al.* Tumor response to induction chemoradiation: influence on survival after esophagectomy. *Eur. J. Cardiothorac. Surg.* **24,** 631–6; discussion 636–7 (2003).

83. Swisher, S. G. *et al.* Long-term outcome of phase II trial evaluating chemotherapy, chemoradiotherapy, and surgery for locoregionally advanced esophageal cancer. *Int. J. Radiat. Oncol. Biol. Phys.* **57,** 120–7 (2003).

84. Luu, T. D. *et al.* Neoadjuvant chemoradiation versus chemotherapy for patients undergoing esophagectomy for esophageal cancer. *Ann. Thorac. Surg.* **85,** 1217–23; discussion 1223–4 (2008).

85. Ilson, D. H., Bains, M., Ginsberg, R. J. & Kelsen, D. P. Neoadjuvant therapy of esophageal cancer. *Surg. Oncol. Clin. N. Am.* **6,** 723–40 (1997).

86. Mandard, A. M. *et al.* Pathologic assessment of tumor regression after preoperative chemoradiotherapy of esophageal carcinoma. Clinicopathologic correlations. *Cancer* **73,** 2680–6 (1994).

87. Gillham, C. M., Reynolds, J. & Hollywood, D. Predicting the response of localised oesophageal cancer to neo-adjuvant chemoradiation. *World J. Surg. Oncol.* **5,** 97 (2007).

88. Campbell, N. P. & Villaflor, V. M. Neoadjuvant treatment of esophageal cancer. *World J. Gastroenterol.* **16,** 3793–803 (2010).

89. Kelsen, D. P. & Ilson, D. H. Chemotherapy and combined-modality therapy for esophageal cancer. *Chest* **107,** 224S–232S (1995).

90. Seiwert, T. Y., Salama, J. K. & Vokes, E. E. The concurrent chemoradiation paradigm--general principles. *Nat. Clin. Pract. Oncol.* **4,** 86–100 (2007).

91. Bernier, J. Alteration of radiotherapy fractionation and concurrent chemotherapy: a new frontier in head and neck oncology? *Nat. Clin. Pract. Oncol.* **2,** 305–14 (2005).

92. Jaffe, N., Paed, D., Traggis, D., Salian, S. & Cassady, J. R. Improved outlook for Ewing's sarcoma with combination chemotherapy (vincristine, actinomycin D and cyclophosphamide) and radiation therapy. *Cancer* **38,** 1925–30 (1976).

93. Nishimura, Y. Rationale for chemoradiotherapy. *Int. J. Clin. Oncol.* **9,** 414–20 (2004).

94. Eastman, A. Characterization of the adducts produced in DNA by cis-diamminedichloroplatinum(II) and cis-dichloro(ethylenediamine)platinum(II). *Biochemistry* **22,** 3927–33 (1983).

95. Jordan, P. & Carmo-Fonseca, M. Molecular mechanisms involved in cisplatin cytotoxicity. *Cell. Mol. Life Sci.* **57,** 1229–35 (2000).

96. Ciccarelli, R. B., Solomon, M. J., Varshavsky, A. & Lippard, S. J. In vivo effects of cis- and trans-diamminedichloroplatinum(II) on SV40 chromosomes: differential repair, DNA-protein cross-linking, and inhibition of replication. *Biochemistry* **24,** 7533–40 (1985).

97. Mello, J. A., Lippard, S. J. & Essigmann, J. M. DNA adducts of cis-diamminedichloroplatinum(II) and its trans isomer inhibit RNA polymerase II differentially in vivo. *Biochemistry* **34,** 14783–91 (1995).

98. Sorenson, C. M., Barry, M. A. & Eastman, A. Analysis of events associated with cell cycle arrest at G2 phase and cell death induced by cisplatin. *J. Natl. Cancer Inst.* **82,** 749–55 (1990).

99. Amorino, G. P., Freeman, M. L., Carbone, D. P., Lebwohl, D. E. & Choy, H. Radiopotentiation by the oral platinum agent, JM216: role of repair inhibition. *Int. J. Radiat. Oncol. Biol. Phys.* **44,** 399–405 (1999).

100. Wilson, G. D., Bentzen, S. M. & Harari, P. M. Biologic basis for combining drugs with radiation. *Semin. Radiat. Oncol.* **16,** 2–9 (2006).

101. McGinn, C. J. *et al.* The role of cell cycle redistribution in radiosensitization: implications regarding the mechanism of fluorodeoxyuridine radiosensitization. *Int. J. Radiat. Oncol. Biol. Phys.* **30,** 851–9 (1994).

102. McGinn, C. J. *et al.* Leucovorin modulation of 5-iododeoxyuridine radiosensitization: a phase I study. *Clin. Cancer Res.* **2,** 1299–305 (1996).

103. Bruso, C. E., Shewach, D. S. & Lawrence, T. S. Fluorodeoxyuridine-induced radiosensitization and inhibition of DNA double strand break repair in human colon cancer cells. *Int. J. Radiat. Oncol. Biol. Phys.* **19,** 1411–7 (1990).

104. Bernier, J., Hall, E. J. & Giaccia, A. Radiation oncology: a century of achievements. *Nat. Rev. Cancer* **4,** 737–47 (2004).

105. ELKIND, M. M., SUTTON-GILBERT, H., MOSES, W. B., ALESCIO, T. & SWAIN, R. W. RADIATION RESPONSE OF MAMMALIAN CELLS GROWN IN CULTURE. V. TEMPERATURE DEPENDENCE OF THE REPAIR OF X-RAY DAMAGE IN SURVIVING CELLS (AEROBIC AND HYPOXIC). *Radiat. Res.* **25,** 359–76 (1965).

106. ELKIND, M. M. Cellular aspects of tumor therapy. *Radiology* **74,** 529–41 (1960).

107. Núñez, M. I., McMillan, T. J., Valenzuela, M. T., Ruiz de Almodóvar, J. M. & Pedraza, V. Relationship between DNA damage, rejoining and cell killing by radiation in mammalian cells. *Radiother. Oncol.* **39,** 155–65 (1996).

108. Hall, E. & Giaccia, A. *Radiobiology for the Radiologist, 6e.* (2006).

109. Jeggo, P. & Lavin, M. F. Cellular radiosensitivity: how much better do we understand it? *Int. J. Radiat. Biol.* **85,** 1061–81 (2009).

110. Hennequin, C., Quero, L. & Favaudon, V. [Determinants and predictive factors of tumour radiosensitivity]. *Cancer Radiother.* **12,** 3–13 (2008).

111. Mladenov, E., Kalev, P. & Anachkova, B. The complexity of double-strand break ends is a factor in the repair pathway choice. *Radiat. Res.* **171,** 397–404 (2009).

112. Mladenov, E. & Iliakis, G. Induction and repair of DNA double strand breaks: the increasing spectrum of non-homologous end joining pathways. *Mutat. Res.* **711,** 61–72 (2011).

113. Radford, I. R. The level of induced DNA double-strand breakage correlates with cell killing after X-irradiation. *Int. J. Radiat. Biol. Relat. Stud. Phys. Chem. Med.* **48,** 45–54 (1985).

114. Wood, L. D. *et al.* Characterization of ataxia telangiectasia fibroblasts with extended life-span through telomerase expression. *Oncogene* **20,** 278–88 (2001).

115. Maity, A., Kao, G. D., Muschel, R. J. & McKenna, W. G. Potential molecular targets for manipulating the radiation response. *Int. J. Radiat. Oncol. Biol. Phys.* **37,** 639–53 (1997).

116. Hu, B. *et al.* The radioresistance to killing of A1-5 cells derives from activation of the Chk1 pathway. *J. Biol. Chem.* **276,** 17693–8 (2001).

117. Riley, P. A. Free radicals in biology: oxidative stress and the effects of ionizing radiation. *Int. J. Radiat. Biol.* **65,** 27–33 (1994).

118. Kawabe, S., Roth, J. A., Wilson, D. R. & Meyn, R. E. Adenovirus-mediated p16 INK4a gene expression radiosensitizes non-small cell lung cancer cells in a p53-dependent manner. *Oncogene* **19,** 5359–5366 (2000).

119. Rothkamm, K., Krüger, I., Thompson, L. H. & Löbrich, M. Pathways of DNA double-strand break repair during the mammalian cell cycle. *Mol. Cell. Biol.* **23,** 5706–15 (2003).

120. Valerie, K. & Povirk, L. F. Regulation and mechanisms of mammalian double-strand break repair. *Oncogene* **22,** 5792–812 (2003).

121. Branzei, D. & Foiani, M. Regulation of DNA repair throughout the cell cycle. *Nat. Rev. Mol. Cell Biol.* **9,** 297–308 (2008).

122. Walker, J. R., Corpina, R. A. & Goldberg, J. Structure of the Ku heterodimer bound to DNA and its implications for double-strand break repair. *Nature* **412,** 607–14 (2001).

123. Lees-Miller, S. P. *et al.* Absence of p350 subunit of DNA-activated protein kinase from a radiosensitive human cell line. *Science* **267,** 1183–5 (1995).

124. Tai, Y. T. *et al.* Ku86 variant expression and function in multiple myeloma cells is associated with increased sensitivity to DNA damage. *J. Immunol.* **165,** 6347–55 (2000).

125. Negroni, A. *et al.* Radioresistance in a tumour cell line correlates with radiation inducible Ku 70/80 end-binding activity. *Int. J. Radiat. Biol.* **84,** 265–76 (2008).

126. Jones, K. R. *et al.* Radiosensitization of MDA-MB-231 breast tumor cells by adenovirus-mediated overexpression of a fragment of the XRCC4 protein. *Mol. Cancer Ther.* **4,** 1541–7 (2005).

127. Chan, C. X., Beiko, R. G. & Ragan, M. A. Detecting recombination in evolving nucleotide sequences. *BMC Bioinformatics* **7,** 412 (2006).

128. Hümmerich, J. *et al.* Constitutive mRNA expression of DNA repair-related genes as a biomarker for clinical radio-resistance: A pilot study in prostate cancer patients receiving radiotherapy. *Int. J. Radiat. Biol.* **82,** 593–604 (2006).

129. Vispé, S., Cazaux, C., Lesca, C. & Defais, M. Overexpression of Rad51 protein stimulates homologous recombination and increases resistance of mammalian cells to ionizing radiation. *Nucleic Acids Res.* **26,** 2859–64 (1998).

130. Reed, E. Nucleotide excision repair and anti-cancer chemotherapy. *Cytotechnology* **27,** 187–201 (1998).

131. Smith, A. J. & Savery, N. J. Effects of the bacterial transcription-repair coupling factor during transcription of DNA containing non-bulky lesions. *DNA Repair (Amst).* **7,** 1670–9 (2008).

132. Zhang, B. *et al.* Silencing PinX1 compromises telomere length maintenance as well as tumorigenicity in telomerase-positive human cancer cells. *Cancer Res.* **69,** 75–83 (2009).

133. Song, Z. *et al.* Lifestyle impacts on the aging associated expression of biomarkers of DNA damage and telomere dysfunction in human blood. *Aging Cell* **9,** 607–615 (2011).

134. Long, X.-H. *et al.* Dose-dependent expression changes of early response genes to ionizing radiation in human lymphoblastoid cells. *Int. J. Mol. Med.* **19,** 607–15 (2007).

135. Snyder, A. R. & Morgan, W. F. Radiation-induced chromosomal instability and gene expression profiling: searching for clues to initiation and perpetuation. *Mutat. Res.* **568,** 89–96 (2004).

136. Despras, E. *et al.* Long-term XPC silencing reduces DNA double-strand break repair. *Cancer Res.* **67,** 2526–34 (2007).

137. Zhu, Z., Chung, W.-H., Shim, E. Y., Lee, S. E. & Ira, G. Sgs1 helicase and two nucleases Dna2 and Exo1 resect DNA double-strand break ends. *Cell* **134,** 981–94 (2008).

138. Robertson, K. A. *et al.* Altered expression of Ape1/ref-1 in germ cell tumors and overexpression in NT2 cells confers resistance to bleomycin and radiation. *Cancer Res.* **61,** 2220–5 (2001).

139. Vens, C. *et al.* The role of DNA polymerase beta in determining sensitivity to ionizing radiation in human tumor cells. *Nucleic Acids Res.* **30,** 2995–3004 (2002).

140. Dantzer, F. *et al.* Involvement of poly(ADP-ribose) polymerase in base excision repair. *Biochimie* **81,** 69–75 (1999).

141. Brock, W. A. *et al.* Radiosensitization of human and rodent cell lines by INO-1001, a novel inhibitor of poly(ADP-ribose) polymerase. *Cancer Lett.* **205,** 155–60 (2004).

142. Calabrese, C. R. *et al.* Anticancer chemosensitization and radiosensitization by the novel poly(ADP-ribose) polymerase-1 inhibitor AG14361. *J. Natl. Cancer Inst.* **96,** 56–67 (2004).

143. Fernandez-Capetillo, A. J. L.-C. and O. *Protein Phosphorylation in Human Health*. (InTech, 2012). doi:10.5772/2944

144. Sinclair, W. K. Cyclic x-ray responses in mammalian cells in vitro. *Radiat. Res.* **33,** 620–43 (1968).

145. Lodish, H. F. & Zinder, N. D. Semi-conservative replication of bacteriophage f2 RNA. *J. Mol. Biol.* **21,** 207–9 (1966).

146. Houtgraaf, J. H., Versmissen, J. & van der Giessen, W. J. A concise review of DNA damage checkpoints and repair in mammalian cells. *Cardiovasc. Revasc. Med.* **7,** 165–72 (2006).

147. Kruuv, J. & Sinclair, W. K. X-ray sensitivity of synchronized Chinese hamster cells irradiated during hypoxia. *Radiat. Res.* **36,** 45–54 (1968).

148. Sinclair, W. K. & Morton, R. A. X-ray sensitivity during the cell generation cycle of cultured Chinese hamster cells. *Radiat. Res.* **29,** 450–74 (1966).

149. Labib, K. & De Piccoli, G. Surviving chromosome replication: the many roles of the S-phase checkpoint pathway. *Philos. Trans. R. Soc. Lond. B. Biol. Sci.* **366,** 3554–61 (2011).

150. Hartwell, L. H. & Weinert, T. A. Checkpoints: controls that ensure the order of cell cycle events. *Science* **246,** 629–34 (1989).

151. Painter, R. B. & Young, B. R. X-ray-induced inhibition of DNA synthesis in Chinese hamster ovary, human HeLa, and Mouse L cells. *Radiat. Res.* **64,** 648–56 (1975).

152. YAMADA, M. & PUCK, T. T. Action of radiation on mammalian cells. IV. Reversible mitotic lag in the S3 HeLa cell produced by low doses of x-rays. *Proc. Natl. Acad. Sci. U. S. A.* **47,** 1181–91 (1961).

153. Su, L. N. & Little, J. B. Prolonged cell cycle delay in radioresistant human cell lines transfected with activated ras oncogene and/or simian virus 40 T-antigen. *Radiat. Res.* **133,** 73–9 (1993).

154. Tamamoto, T. *et al.* Correlation between gamma-ray-induced G2 arrest and radioresistance in two human cancer cells. *Int. J. Radiat. Oncol. Biol. Phys.* **44,** 905–9 (1999).

155. Strunz, A. M. *et al.* Preferential radiosensitization in p53-mutated human tumour cell lines by pentoxifylline-mediated disruption of the G2/M checkpoint control. *Int. J. Radiat. Biol.* **78,** 721–32 (2002).

156. Koniaras, K., Cuddihy, A. R., Christopoulos, H., Hogg, A. & O'Connell, M. J. Inhibition of Chk1-dependent G2 DNA damage checkpoint radiosensitizes p53 mutant human cells. *Oncogene* **20,** 7453–63 (2001).

157. CELL BIOLOGY. at <http://jpkc.scu.edu.cn/ywwy/zbsw(E)/edetail11.htm>

158. Fareed, K. R. *et al.* Biomarkers of response to therapy in oesophago-gastric cancer. *Gut* **58,** 127–43 (2009).

159. Chirieac, L. R. *et al.* Posttherapy pathologic stage predicts survival in patients with esophageal carcinoma receiving preoperative chemoradiation. *Cancer* **103,** 1347–55 (2005).

160. McLoughlin, J. M. *et al.* Are patients with esophageal cancer who become PET negative after neoadjuvant chemoradiation free of cancer? *J. Am. Coll. Surg.* **206,** 879–86; discussion 886–7 (2008).

161. Smithers, B. M. *et al.* Positron emission tomography and pathological evidence of response to neoadjuvant therapy in adenocarcinoma of the esophagus. *Dis. Esophagus* **21,** 151–8 (2008).

162. Flamen, P. *et al.* The utility of positron emission tomography for the diagnosis and staging of recurrent esophageal cancer. *J. Thorac. Cardiovasc. Surg.* **120,** 1085–92 (2000).

163. Gillham, C. M. *et al.* (18)FDG uptake during induction chemoradiation for oesophageal cancer fails to predict histomorphological tumour response. *Br. J. Cancer* **95,** 1174–9 (2006).

164. Brink, I. *et al.* Effects of neoadjuvant radio-chemotherapy on 18F-FDG-PET in esophageal carcinoma. *Eur. J. Surg. Oncol.* **30,** 544–50 (2004).

165. Levine, E. A. *et al.* Predictive value of 18-fluoro-deoxy-glucose-positron emission tomography (18F-FDG-PET) in the identification of responders to chemoradiation therapy for the treatment of locally advanced esophageal cancer. *Ann. Surg.* **243,** 472–8 (2006).

166. Blackstock, A. W. *et al.* A prospective evaluation of the impact of 18-F-fluoro-deoxy-D-glucose positron emission tomography staging on survival for patients with locally advanced esophageal cancer. *Int. J. Radiat. Oncol. Biol. Phys.* **64,** 455–60 (2006).

167. Rebollo Aguirre, A. C. *et al.* 18F-fluorodeoxiglucose positron emission tomography for the evaluation of neoadjuvant therapy response in esophageal cancer: systematic review of the literature. *Ann. Surg.* **250,** 247–54 (2009).

168. Swisher, S. G. *et al.* 2-Fluoro-2-deoxy-D-glucose positron emission tomography imaging is predictive of pathologic response and survival after preoperative chemoradiation in patients with esophageal carcinoma. *Cancer* **101,** 1776–85 (2004).

169. Javeri, H. *et al.* The higher the decrease in the standardized uptake value of positron emission tomography after chemoradiation, the better the survival of patients with gastroesophageal adenocarcinoma. *Cancer* **115,** 5184–92 (2009).

170. Konski, A. A. *et al.* Correlation of molecular response as measured by 18-FDG positron emission tomography with outcome after chemoradiotherapy in patients with esophageal carcinoma. *Int. J. Radiat. Oncol. Biol. Phys.* **69,** 358–63 (2007).

171. Sepesi, B. *et al.* Does the value of PET-CT extend beyond pretreatment staging? An analysis of survival in surgical patients with esophageal cancer. *J. Gastrointest. Surg.* **13,** 2121–7 (2009).

172. Yin, E., Nelson, D. O., Coleman, M. A., Peterson, L. E. & Wyrobek, A. J. Gene expression changes in mouse brain after exposure to low-dose ionizing radiation. *Int. J. Radiat. Biol.* **79,** 759–75 (2003).

173. Ogawa, K., Murayama, S. & Mori, M. Predicting the tumor response to radiotherapy using microarray analysis (Review). *Oncol. Rep.* **18,** 1243–8 (2007).

174. Lynam-Lennon, N. *et al.* Alterations in DNA repair efficiency are involved in the radioresistance of esophageal adenocarcinoma. *Radiat Res* **174,** 703–711 (2010).

175. Lynam-Lennon, N. *et al.* MicroRNA-31 modulates tumour sensitivity to radiation in oesophageal adenocarcinoma. *J. Mol. Med. (Berl).* **90,** 1449–58 (2012).

176. Maher, S. G. *et al.* Gene expression analysis of diagnostic biopsies predicts pathological response to neoadjuvant chemoradiotherapy of esophageal cancer. *Ann. Surg.* **250,** 729–37 (2009).

177. Maher, S. G. *et al.* Serum proteomic profiling reveals that pretreatment complement protein levels are predictive of esophageal cancer patient response to neoadjuvant chemoradiation. *Ann. Surg.* **254,** 809–16; discussion 816–7 (2011).

178. Obesity: preventing and managing the global epidemic. Report of a WHO consultation. *World Health Organ. Tech. Rep. Ser.* **894,** i–xii, 1–253 (2000).

179. Berghöfer, A. *et al.* Obesity prevalence from a European perspective: a systematic review. *BMC Public Health* **8,** 200 (2008).

180. Ogden, C. L. *et al.* Prevalence of overweight and obesity in the United States, 1999-2004. *JAMA* **295,** 1549–55 (2006).

181. *Irish Universities Nutrition Alliance: National Adult Nutrition Survey.* (2011).

182. Griffin, A. C., Younger, K. M. & Flynn, M. A. T. Assessment of obesity and fear of fatness among inner-city Dublin schoolchildren in a one-year follow-up study. *Public Health Nutr.* **7,** 729–35 (2004).

183. Serdula, M. K. *et al.* Prevalence of attempting weight loss and strategies for controlling weight. *JAMA* **282,** 1353–8 (1999).

184. Fox, C. S. *et al.* Abdominal visceral and subcutaneous adipose tissue compartments: association with metabolic risk factors in the Framingham Heart Study. *Circulation* **116,** 39–48 (2007).

185. Lysaght, J. *et al.* Pro-inflammatory and tumour proliferative properties of excess visceral adipose tissue. *Cancer Lett.* **312,** 62–72 (2011).

186. Vohl, M.-C. *et al.* A survey of genes differentially expressed in subcutaneous and visceral adipose tissue in men. *Obes. Res.* **12,** 1217–22 (2004).

187. Van Kruijsdijk, R. C. M., van der Wall, E. & Visseren, F. L. J. Obesity and cancer: the role of dysfunctional adipose tissue. *Cancer Epidemiol. Biomarkers Prev.* **18,** 2569–78 (2009).

188. Kershaw, E. E. & Flier, J. S. Adipose tissue as an endocrine organ. *J. Clin. Endocrinol. Metab.* **89,** 2548–56 (2004).

189. Galic, S., Oakhill, J. S. & Steinberg, G. R. Adipose tissue as an endocrine organ. *Mol. Cell. Endocrinol.* **316,** 129–39 (2010).

190. Snijder, M. B., van Dam, R. M., Visser, M. & Seidell, J. C. What aspects of body fat are particularly hazardous and how do we measure them? *Int. J. Epidemiol.* **35,** 83–92 (2006).

191. Ford, E. S., Li, C., Zhao, G., Pearson, W. S. & Mokdad, A. H. Prevalence of the metabolic syndrome among U.S. adolescents using the definition from the International Diabetes Federation. *Diabetes Care* **31,** 587–9 (2008).

192. Oka, R. *et al.* Reassessment of the cutoff values of waist circumference and visceral fat area for identifying Japanese subjects at risk for the metabolic syndrome. *Diabetes Res. Clin. Pract.* **79,** 474–81 (2008).

193. Lee, M.-J., Wu, Y. & Fried, S. K. Adipose tissue heterogeneity: mplication of depot differences in adipose tissue for obesity complications. *Mol. Aspects Med.* **34,** 1–11 (2013).

194. Hu, F. B. Obesity and mortality: watch your waist, not just your weight. *Arch. Intern. Med.* **167,** 875–6 (2007).

195. Wajchenberg, B. L. Subcutaneous and visceral adipose tissue: their relation to the metabolic syndrome. *Endocr. Rev.* **21,** 697–738 (2000).

196. Okorodudu, D. O. *et al.* Diagnostic performance of body mass index to identify obesity as defined by body adiposity: a systematic review and meta-analysis. *Int. J. Obes. (Lond).* **34,** 791–9 (2010).

197. Romero-Corral, A. *et al.* Accuracy of body mass index in diagnosing obesity in the adult general population. *Int. J. Obes. (Lond).* **32,** 959–66 (2008).

198. Balentine, C. J. *et al.* Validating quantitative obesity measurements in colorectal cancer patients. *J. Surg. Res.* **164,** 18–22 (2010).

199. Rössner, S. *et al.* Adipose tissue determinations in cadavers--a comparison between cross-sectional planimetry and computed tomography. *Int. J. Obes.* **14,** 893–902 (1990).

200. Després, J. P. & Lamarche, B. Effects of diet and physical activity on adiposity and body fat distribution: implications for the prevention of cardiovascular disease. *Nutr. Res. Rev.* **6,** 137–59 (1993).

201. Hunter, G. R., Snyder, S. W., Kekes-Szabo, T., Nicholson, C. & Berland, L. Intra-abdominal adipose tissue values associated with risk of possessing elevated blood lipids and blood pressure. *Obes. Res.* **2,** 563–8 (1994).

202. Björntorp, P. Abdominal obesity and the metabolic syndrome. *Ann. Med.* **24,** 465–8 (1992).

203. Björntorp, P. [Metabolic difference between visceral fat and subcutaneous abdominal fat]. *Diabetes Metab.* **26 Suppl 3,** 10–2 (2000).

204. Doyle, S. L. *et al.* Establishing computed tomography-defined visceral fat area thresholds for use in obesity-related cancer research. *Nutr. Res.* **33,** 171–9 (2013).

205. Rankinen, T., Kim, S. Y., Pérusse, L., Després, J. P. & Bouchard, C. The prediction of abdominal visceral fat level from body composition and anthropometry: ROC analysis. *Int. J. Obes. Relat. Metab. Disord.* **23,** 801–9 (1999).

206. Zhu, S. *et al.* Combination of BMI and Waist Circumference for Identifying Cardiovascular Risk Factors in Whites. *Obes. Res.* **12,** 633–45 (2004).

207. Kashihara, H., Lee, J. S., Kawakubo, K., Tamura, M. & Akabayashi, A. Criteria of waist circumference according to computed tomography-measured visceral fat area and the clustering of cardiovascular risk factors. *Circ. J.* **73,** 1881–6 (2009).

208. Klein, S., Wadden, T. & Sugerman, H. J. AGA technical review on obesity. *Gastroenterology* **123,** 882–932 (2002).

209. Valsamakis, G. *et al.* Association of simple anthropometric measures of obesity with visceral fat and the metabolic syndrome in male Caucasian and Indo-Asian subjects. *Diabetes* 1339–1345 (2004). doi:10.1046/j.1464-5491.2004.01361.x

210. Lemieux, S., Prud'homme, D., Bouchard, C., Tremblay, A. & Després, J. P. A single threshold value of waist girth identifies normal-weight and overweight subjects with excess visceral adipose tissue. *Am. J. Clin. Nutr.* **64,** 685–93 (1996).

211. Alberti, K. G. M. M., Zimmet, P. & Shaw, J. Metabolic syndrome--a new world-wide definition. A Consensus Statement from the International Diabetes Federation. *Diabet. Med.* **23,** 469–80 (2006).

212. Reeves, G. K. *et al.* Cancer incidence and mortality in relation to body mass index in the Million Women Study: cohort study. *BMJ* **335,** 1134 (2007).

213. Sjöström, L. *et al.* Effects of bariatric surgery on cancer incidence in obese patients in Sweden (Swedish Obese Subjects Study): a prospective, controlled intervention trial. *Lancet Oncol.* **10,** 653–62 (2009).

214. Reynolds, J. V *et al.* Neoadjuvant chemoradiation may increase the risk of respiratory complications and sepsis after transthoracic esophagectomy. *J. Thorac. Cardiovasc. Surg.* **132,** 549–55 (2006).

215. Ji, B. T. *et al.* Body mass index and the risk of cancers of the gastric cardia and distal stomach in Shanghai, China. *Cancer Epidemiol. Biomarkers Prev.* **6,** 481–5 (1997).

216. Whiteman, D. C. *et al.* Combined effects of obesity, acid reflux and smoking on the risk of adenocarcinomas of the oesophagus. *Gut* **57,** 173–80 (2008).

217. Lindblad, M., Rodríguez, L. A. G. & Lagergren, J. Body mass, tobacco and alcohol and risk of esophageal, gastric cardia, and gastric non-cardia adenocarcinoma among men and women in a nested case-control study. *Cancer Causes Control* **16,** 285–94 (2005).

218. Yancik, R. *et al.* Comorbidity and age as predictors of risk for early mortality of male and female colon carcinoma patients: a population-based study. *Cancer* **82,** 2123–34 (1998).

219. Yancik, R. & Ries, L. A. Aging and cancer in America. Demographic and epidemiologic perspectives. *Hematol. Oncol. Clin. North Am.* **14,** 17–23 (2000).

220. Extermann, M. Measurement and impact of comorbidity in older cancer patients. *Crit. Rev. Oncol. Hematol.* **35,** 181–200 (2000).

221. Fleisher, L. A. *et al.* ACC/AHA 2007 Guidelines on Perioperative Cardiovascular Evaluation and Care for Noncardiac Surgery: Executive Summary: A Report of the American College of Cardiology/American Heart Association Task Force on Practice Guidelines (Writing Committee to Revise. *Circulation* **116,** 1971–96 (2007).

222. Ahrendt, G. M. *et al.* Does breast tumor location influence success of sentinel lymph node biopsy? *J. Am. Coll. Surg.* **194,** 278–84 (2002).

223. Werner, R. S. *et al.* Arm edema in conservatively managed breast cancer: obesity is a major predictive factor. *Radiology* **180,** 177–84 (1991).

224. Banerjee, D., Williams, E. V, Ilott, J., Monypenny, I. J. & Webster, D. J. Obesity predisposes to increased drainage following axillary node clearance: a prospective audit. *Ann. R. Coll. Surg. Engl.* **83,** 268–71 (2001).

225. Pata, G., Solaini, L., Roncali, S., Pasini, M. & Ragni, F. Impact of Obesity on Early Surgical and Oncologic Outcomes after Total Gastrectomy with "Over-D1" Lymphadenectomy for Gastric Cancer. *World J. Surg.* (2013). doi:10.1007/s00268-013-1942-8

226. Millender, L. E., Aubin, M., Pouliot, J., Shinohara, K. & Roach, M. Daily electronic portal imaging for morbidly obese men undergoing radiotherapy for localized prostate cancer. *Int. J. Radiat. Oncol. Biol. Phys.* **59,** 6–10 (2004).

227. Wong, J. R. *et al.* Potential for higher treatment failure in obese patients: correlation of elevated body mass index and increased daily prostate deviations from the radiation beam isocenters in an analysis of 1,465 computed tomographic images. *Int. J. Radiat. Oncol. Biol. Phys.* **75,** 49–55 (2009).

228. Dignam, J. J. *et al.* Body mass index and outcomes in patients who receive adjuvant chemotherapy for colon cancer. *J. Natl. Cancer Inst.* **98,** 1647–54 (2006).

229. Meyerhardt, J. a *et al.* Influence of body mass index on outcomes and treatment-related toxicity in patients with colon carcinoma. *Cancer* **98,** 484–95 (2003).

230. Meyerhardt, J. A. *et al.* Impact of body mass index on outcomes and treatment-related toxicity in patients with stage II and III rectal cancer: findings from Intergroup Trial 0114. *J. Clin. Oncol.* **22,** 648–57 (2004).

231. Prizment, A. E., Flood, A., Anderson, K. E. & Folsom, A. R. Survival of women with colon cancer in relation to precancer anthropometric characteristics: the Iowa Women's Health Study. *Cancer Epidemiol. Biomarkers Prev.* **19,** 2229–37 (2010).

232. Sinicrope, F. a, Foster, N. R., Sargent, D. J., O'Connell, M. J. & Rankin, C. Obesity is an independent prognostic variable in colon cancer survivors. *Clin. Cancer Res.* **16,** 1884–93 (2010).

233. Tamakoshi, K. *et al.* A prospective study of body size and colon cancer mortality in Japan: The JACC Study. *Int. J. Obes. Relat. Metab. Disord.* **28,** 551–8 (2004).

234. Amling, C. L. *et al.* Pathologic variables and recurrence rates as related to obesity and race in men with prostate cancer undergoing radical prostatectomy. *J. Clin. Oncol.* **22,** 439–45 (2004).

235. Efstathiou, J. A., Chen, M.-H. H., Renshaw, A. A., Loffredo, M. J. & D'Amico, A. V. Influence of body mass index on prostate-specific antigen failure after androgen suppression and radiation therapy for localized prostate cancer. *Cancer* **109,** 1493–1498 (2007).

236. Palma, D., Pickles, T. & Tyldesley, S. Obesity as a predictor of biochemical recurrence and survival after radiation therapy for prostate cancer. *BJU Int* **100,** 315–319 (2007).

237. Strom, S. S. *et al.* Influence of obesity on biochemical and clinical failure after external-beam radiotherapy for localized prostate cancer. *Cancer* **107,** 631–9 (2006).

238. Stroup, S. P., Cullen, J., Auge, B. K., L'Esperance, J. O. & Kang, S. K. Effect of obesity on prostate-specific antigen recurrence after radiation therapy for localized prostate cancer as measured by the 2006 Radiation Therapy Oncology Group-American Society for Therapeutic Radiation and Oncology (RTOG-ASTRO) Phoenix consensus. *Cancer* **110,** 1003–1009 (2007).

239. Freedland, S. J. & Platz, E. A. Obesity and prostate cancer: making sense out of apparently conflicting data. *Epidemiol. Rev.* **29,** 88–97 (2007).

240. Merrick, G. S. *et al.* Obesity is not predictive of overall survival following permanent prostate brachytherapy. *Am. J. Clin. Oncol.* **30,** 588–96 (2007).

241. Haydon, A. M. M., Macinnis, R. J., English, D. R. & Giles, G. G. Effect of physical activity and body size on survival after diagnosis with colorectal cancer. *Gut* **55,** 62–7 (2006).

242. Meyerhardt, J. a *et al.* Impact of body mass index and weight change after treatment on cancer recurrence and survival in patients with stage III colon cancer: findings from Cancer and Leukemia Group B 89803. *J. Clin. Oncol.* **26,** 4109–15 (2008).

243. Morrison, D. S. *et al.* Risk factors for colonic and rectal cancer mortality: evidence from 40 years' follow-up in the Whitehall I study. *J. Epidemiol. Community Health* **65,** 1053–8 (2011).

244. Van Roermund, J. G. H. *et al.* Body mass index is not a prognostic marker for prostate-specific antigen failure and survival in Dutch men treated with brachytherapy. *BJU Int.* **105,** 42–8 (2010).

245. Cao, Y. & Ma, J. Body Mass Index, Prostate Cancer–Specific Mortality, and Biochemical Recurrence: a Systematic Review and Meta-analysis. *Cancer Prev. Res.* **4,** 486–501 (2011).

246. Healy, L. A. *et al.* Impact of obesity on outcomes in the management of localized adenocarcinoma of the esophagus and esophagogastric junction. *J Thorac Cardiovasc Surg* **134,** 1284–1291 (2007).

247. Morgan, M. a *et al.* Prognostic significance of body mass indices for patients undergoing esophagectomy for cancer. *Dis. Esophagus* **20,** 29–35 (2007).

248. Melis, M. *et al.* An elevated body mass index does not reduce survival after esophagectomy for cancer. *Ann. Surg. Oncol.* **18,** 824–31 (2011).

249. Yoon, H. H. *et al.* Prognostic impact of body mass index stratified by smoking status in patients with esophageal adenocarcinoma. *J. Clin. Oncol.* **29,** 4561–7 (2011).

250. Scarpa, M. *et al.* Overweight patients operated on for cancer of the esophagus survive longer than normal-weight patients. *J. Gastrointest. Surg.* **17,** 218–27 (2013).

251. Shridhar, R. *et al.* Body mass index and survival in esophageal adenocarcinoma treated with chemoradiotherapy followed by esophagectomy. *J. Gastrointest. Surg.* **16,** 1296–302 (2012).

252. Wang, J. *et al.* Obesity and outcomes in patients treated with chemoradiotherapy for esophageal carcinoma. *Dis. Esophagus* (2013). doi:10.1111/dote.12074

253. Donohoe, C. L., Doyle, S. L. & Reynolds, J. V. Visceral adiposity, insulin resistance and cancer risk. *Diabetol. Metab. Syndr.* **3,** 12 (2011).

254. Iyengar, P. *et al.* Adipocyte-secreted factors synergistically promote mammary tumorigenesis through induction of anti-apoptotic transcriptional programs and proto-oncogene stabilization. *Oncogene* **22,** 6408–23 (2003).

255. Tilg, H. & Moschen, A. R. Adipocytokines: mediators linking adipose tissue, inflammation and immunity. *Nat. Rev. Immunol.* **6,** 772–83 (2006).

256. Aggarwal, B. B., Vijayalekshmi, R. V & Sung, B. Targeting inflammatory pathways for prevention and therapy of cancer: short-term friend, long-term foe. *Clin. Cancer Res.* **15,** 425–30 (2009).

257. Kadowaki, T. & Yamauchi, T. Adiponectin and adiponectin receptors. *Endocr. Rev.* **26,** 439–51 (2005).

258. Rose, D. P., Komninou, D. & Stephenson, G. D. Obesity, adipocytokines, and insulin resistance in breast cancer. *Obes. Rev.* **5,** 153–65 (2004).

259. Brakenhielm, E. *et al.* Adiponectin-induced antiangiogenesis and antitumor activity involve caspase-mediated endothelial cell apoptosis. *Proc Natl Acad Sci U S A* **101,** 2476–2481 (2004).

260. Wang, Y., Lam, K. S. L. & Xu, A. Adiponectin as a negative regulator in obesity-related mammary carcinogenesis. *Cell Res.* **17,** 280–2 (2007).

261. Monickaraj, F. *et al.* Convergence of adipocyte hypertrophy, telomere shortening and hypoadiponectinemia in obese subjects and in patients with type 2 diabetes. *Clin. Biochem.* **45,** 1432–8 (2012).

262. De Oliveira, C., de Mattos, A. B. M., Silva, C. B. R., Mota, J. F. & Zemdegs, J. C. S. Nutritional and hormonal modulation of adiponectin and its receptors adipoR1 and adipoR2. *Vitam. Horm.* **90,** 57–94 (2012).

263. Abdul-Ghafar, J., Park, S. & Wairagu, P. Expression of Adiponectin Receptor 1 Is Indicative of Favorable Prognosis in Non-small Cell Lung Carcinoma. *Tohoku J. ...* 153–162 (2012). doi:10.1620/tjem.229.153.Correspondence

264. Cummings, D. E. & Foster, K. E. Ghrelin-leptin tango in body-weight regulation. *Gastroenterology* **124,** 1532–5 (2003).

265. Stattin, P. *et al.* Obesity and colon cancer: does leptin provide a link? *Int. J. Cancer* **109,** 149–52 (2004).

266. Garofalo, C. & Surmacz, E. Leptin and cancer. *J. Cell. Physiol.* **207,** 12–22 (2006).

267. Chen, X. *et al.* Leptin attenuates the anti-estrogen effect of tamoxifen in breast cancer. *Biomed. Pharmacother.* **67,** 22–30 (2013).

268. Uddin, S. *et al.* Overexpression of leptin receptor predicts an unfavorable outcome in Middle Eastern ovarian cancer. *Mol. Cancer* **8,** 74 (2009).

269. Hoon Kim, J. *et al.* Clinical significance of the leptin and leptin receptor expressions in prostate tissues. *Asian J. Androl.* **10,** 923–8 (2008).

270. Ellerhorst, J. A. *et al.* Promotion of melanoma growth by the metabolic hormone leptin. *Oncol. Rep.* **23,** 901–7 (2010).

271. Howard, J. M. *et al.* Associations between leptin and adiponectin receptor upregulation, visceral obesity and tumour stage in oesophageal and junctional adenocarcinoma. *Br. J. Surg.* **97,** 1020–7 (2010).

272. Ishikawa, M., Kitayama, J. & Nagawa, H. Enhanced expression of leptin and leptin receptor (OB-R) in human breast cancer. *Clin. Cancer Res.* **10,** 4325–31 (2004).

273. Somasundar, P., McFadden, D. W., Hileman, S. M. & Vona-Davis, L. Leptin is a growth factor in cancer. *J. Surg. Res.* **116,** 337–49 (2004).

274. Park, H. Y. *et al.* Potential role of leptin in angiogenesis: leptin induces endothelial cell proliferation and expression of matrix metalloproteinases in vivo and in vitro. *Exp. Mol. Med.* **33,** 95–102 (2001).

275. Ogunwobi, O. O. & Beales, I. L. P. Leptin stimulates the proliferation of human oesophageal adenocarcinoma cells via HB-EGF and Tgfalpha mediated transactivation of the epidermal growth factor receptor. *Br. J. Biomed. Sci.* **65,** 121–7 (2008).

276. Healy, L. a *et al.* Metabolic syndrome and leptin are associated with adverse pathological features in male colorectal cancer patients. *Colorectal Dis.* **14,** 157–65 (2012).

277. Ferrara, N. VEGF-A: a critical regulator of blood vessel growth. *Eur. Cytokine Netw.* **20,** 158–63 (2009).

278. Katoh, O., Tauchi, H., Kawaishi, K., Kimura, a & Satow, Y. Expression of the vascular endothelial growth factor (VEGF) receptor gene, KDR, in hematopoietic cells and inhibitory effect of VEGF on apoptotic cell death caused by ionizing radiation. *Cancer Res.* **55,** 5687–92 (1995).

279. Hicklin, D. J. & Ellis, L. M. Role of the vascular endothelial growth factor pathway in tumor growth and angiogenesis. *J. Clin. Oncol.* **23,** 1011–27 (2005).

280. Jakeman, L. B., Armanini, M., Phillips, H. S. & Ferrara, N. Developmental expression of binding sites and messenger ribonucleic acid for vascular endothelial growth factor suggests a role for this protein in vasculogenesis and angiogenesis. *Endocrinology* **133,** 848–59 (1993).

281. Hurwitz, H. *et al.* Bevacizumab plus irinotecan, fluorouracil, and leucovorin for metastatic colorectal cancer. *N. Engl. J. Med.* **350,** 2335–42 (2004).

282. Cao, Y. *et al.* VEGF exerts an angiogenesis-independent function in cancer cells to promote their malignant progression. *Cancer Res.* **72,** 3912–8 (2012).

283. Soker, S., Fidder, H., Neufeld, G. & Klagsbrun, M. Characterization of novel vascular endothelial growth factor (VEGF) receptors on tumor cells that bind VEGF165 via its exon 7-encoded domain. *J. Biol. Chem.* **271,** 5761–7 (1996).

284. Bagri, A., Tessier-Lavigne, M. & Watts, R. J. Neuropilins in tumor biology. *Clin. Cancer Res.* **15,** 1860–4 (2009).

285. Cao, Y. *et al.* Neuropilin-1 upholds dedifferentiation and propagation phenotypes of renal cell carcinoma cells by activating Akt and sonic hedgehog axes. *Cancer Res.* **68,** 8667–72 (2008).

286. Prud'homme, G. J. & Glinka, Y. Neuropilins are multifunctional coreceptors involved in tumor initiation, growth, metastasis and immunity. *Oncotarget* **3,** 921–939 (2012).

287. Escudero-Esparza, A., Martin, T. A., Douglas-Jones, A., Mansel, R. E. & Jiang, W. G. PGF isoforms, PLGF-1 and PGF-2 and the PGF receptor, neuropilin, in human breast cancer: prognostic significance. *Oncol. Rep.* **23,** 537–44 (2010).

288. Ghosh, S. *et al.* High levels of vascular endothelial growth factor and its receptors (VEGFR-1, VEGFR-2, neuropilin-1) are associated with worse outcome in breast cancer. *Hum. Pathol.* **39,** 1835–43 (2008).

289. Broholm, H. & Laursen, H. Vascular endothelial growth factor (VEGF) receptor neuropilin-1's distribution in astrocytic tumors. *APMIS* **112,** 257–63 (2004).

290. Stephenson, J. M., Banerjee, S., Saxena, N. K., Cherian, R. & Banerjee, S. K. Neuropilin-1 is differentially expressed in myoepithelial cells and vascular smooth muscle cells in preneoplastic and neoplastic human breast: a possible marker for the progression of breast cancer. *Int. J. Cancer* **101,** 409–14 (2002).

291. Hansel, D. E. *et al.* Expression of neuropilin-1 in high-grade dysplasia, invasive cancer, and metastases of the human gastrointestinal tract. *Am. J. Surg. Pathol.* **28,** 347–56 (2004).

292. Latil, A. *et al.* VEGF overexpression in clinically localized prostate tumors and neuropilin-1 overexpression in metastatic forms. *Int. J. Cancer* **89,** 167–71 (2000).

293. Parikh, A. A. *et al.* Neuropilin-1 in human colon cancer: expression, regulation, and role in induction of angiogenesis. *Am. J. Pathol.* **164,** 2139–51 (2004).

294. Lantuéjoul, S. *et al.* Expression of VEGF, semaphorin SEMA3F, and their common receptors neuropilins NP1 and NP2 in preinvasive bronchial lesions, lung tumours, and cell lines. *J. Pathol.* **200,** 336–47 (2003).

295. Huang, S. M., Li, J., Armstrong, E. A. & Harari, P. M. Modulation of radiation response and tumor-induced angiogenesis after epidermal growth factor receptor inhibition by ZD1839 (Iressa). *Cancer Res* **62,** 4300–4306 (2002).

296. Casey, R. Delineating the pro-Carcinogenic Pathways Activated by Obesity in Barrett's Oesophagus. (2011).

297. Hanahan, D. & Weinberg, R. A. Hallmarks of cancer: the next generation. *Cell* **144,** 646–674 (2011).

298. Esposito, K. & Giugliano, D. The metabolic syndrome and inflammation: association or causation? *Nutr. Metab. Cardiovasc. Dis.* **14,** 228–32 (2004).

299. Das, U. N. Is obesity an inflammatory condition? *Nutrition* **17,** 953–66 (2001).

300. Schäffler, A., Müller-Ladner, U., Schölmerich, J. & Büchler, C. Role of adipose tissue as an inflammatory organ in human diseases. *Endocr. Rev.* **27,** 449–67 (2006).

301. Xu, H. *et al.* Chronic inflammation in fat plays a crucial role in the development of obesity-related insulin resistance. *J. Clin. Invest.* **112,** 1821–30 (2003).

302. Weisberg, S. P. *et al.* Obesity is associated with macrophage accumulation in adipose tissue. *J Clin Invest* **112,** 1796–1808 (2003).

303. Platell, C., Cooper, D., Papadimitriou, J. M. & Hall, J. C. The omentum. *World J. Gastroenterol.* **6,** 169–176 (2000).

304. Lynch, L. *et al.* Invariant NKT cells and CD1d(+) cells amass in human omentum and are depleted in patients with cancer and obesity. *Eur. J. Immunol.* **39,** 1893–901 (2009).

305. Fenech, M. Chromosomal biomarkers of genomic instability relevant to cancer. *Drug Discov Today* **7,** 1128–1137 (2002).

306. Fenech, M. *et al.* Molecular mechanisms of micronucleus, nucleoplasmic bridge and nuclear bud formation in mammalian and human cells. *Mutagenesis* **26,** 125–132 (2011).

307. Draviam, V., Xie, S. & Sorger, P. Chromosome segregation and genomic stability. *Curr. Opin. Genet. Dev.* 120–125 (2004). doi:10.1016/j.gde.2004.02.007

308. Charames, G. S. & Bapat, B. Genomic instability and cancer. *Curr Mol Med* **3,** 589–596 (2003).

309. Pihan, G. & Doxsey, S. J. Mutations and aneuploidy : Co-conspirators in cancer ? *Cancer Cell* **4,** 89–94 (2003).

310. Acilan, C. DNA REPAIR PATHWAYS INVOLVED IN THE FORMATION OF ANAPHASE. (2006).

311. Saunders, W. S. *et al.* Chromosomal instability and cytoskeletal defects in oral cancer cells. *Proc. Natl. Acad. Sci. U. S. A.* **97,** 303–8 (2000).

312. Jallepalli, P. V & Lengauer, C. Chromosome segregation and cancer: cutting through the mystery. *Nat. Rev. Cancer* **1,** 109–17 (2001).

313. Gisselsson, D. Chromosome instability in cancer: how, when, and why? *Adv. Cancer Res.* **87,** 1–29 (2003).

314. Deng, C.-X. BRCA1: cell cycle checkpoint, genetic instability, DNA damage response and cancer evolution. *Nucleic Acids Res.* **34,** 1416–26 (2006).

315. Wai, L. K. Telomeres, telomerase, and tumorigenesis--a review. *MedGenMed* **6,** 19 (2004).

316. Bailey, S. M. & Murnane, J. P. Telomeres, chromosome instability and cancer. *Nucleic Acids Res.* **34,** 2408–17 (2006).

317. Martinez, P., Blasco, M. A. & Martínez, P. Role of shelterin in cancer and aging. *Aging Cell* **9,** 653–666 (2010).

318. Griffith, J. D. *et al.* Mammalian telomeres end in a large duplex loop. *Cell* **97,** 503–14 (1999).

319. Londoño-Vallejo, J. A. & Wellinger, R. J. Telomeres and telomerase dance to the rhythm of the cell cycle. *Trends Biochem. Sci.* **37,** 391–9 (2012).

320. Harley, C. B., Futcher, A. B. & Greider, C. W. Telomeres shorten during ageing of human fibroblasts. *Nature* **345,** 458–60 (1990).

321. Nawrot, T. S., Staessen, J. A., Gardner, J. P. & Aviv, A. Telomere length and possible link to X chromosome. *Lancet* **363,** 507–10 (2004).

322. Tümpel, S. & Rudolph, K. L. The role of telomere shortening in somatic stem cells and tissue aging: lessons from telomerase model systems. *Ann. N. Y. Acad. Sci.* **1266,** 28–39 (2012).

323. Shay, J. W. & Wright, W. E. Senescence and immortalization: role of telomeres and telomerase. *Carcinogenesis* **26,** 867–74 (2005).

324. Harley, C. B. *et al.* Telomerase, cell immortality, and cancer. *Cold Spring Harb. Symp. Quant. Biol.* **59,** 307–15 (1994).

325. Wright, W. E. & Shay, J. W. Telomere dynamics in cancer progression and prevention: fundamental differences in human and mouse telomere biology. *Nat. Med.* **6,** 849–51 (2000).

326. Artandi, S. E. & DePinho, R. A. Telomeres and telomerase in cancer. *Carcinogenesis* **31,** 9–18 (2010).

327. Lansdorp, P. M. Telomeres and disease. *EMBO J.* **28,** 2532–40 (2009).

328. Cesare, A. J. & Reddel, R. R. Alternative lengthening of telomeres: models, mechanisms and implications. *Nat. Rev. Genet.* **11,** 319–30 (2010).

329. Levy, M. Z., Allsopp, R. C., Futcher, A. B., Greider, C. W. & Harley, C. B. Telomere end-replication problem and cell aging. *J Mol Biol* **225,** 951–960 (1992).

330. Counter, C. M. *et al.* Telomere shortening associated with chromosome instability is arrested in immortal cells which express telomerase activity. *EMBO J.* **11,** 1921–9 (1992).

331. Murnane, J. P., Sabatier, L., Marder, B. A. & Morgan, W. F. Telomere dynamics in an immortal human cell line. *EMBO J.* **13,** 4953–62 (1994).

332. Dunham, M. A., Neumann, A. A., Fasching, C. L. & Reddel, R. R. Telomere maintenance by recombination in human cells. *Nat. Genet.* **26,** 447–50 (2000).

333. Zhu, H., Belcher, M. & van der Harst, P. Healthy aging and disease: role for telomere biology? *Clin. Sci.* **120,** 427–440 (2011).

334. Gilley, D., Tanaka, H. & Herbert, B.-S. Telomere dysfunction in aging and cancer. *Int. J. Biochem. Cell Biol.* **37,** 1000–13 (2005).

335. Meier, U. T. The many facets of H/ACA ribonucleoproteins. *Chromosoma* **114,** 1–14 (2005).

336. Mitchell, J. R., Cheng, J. & Collins, K. A box H/ACA small nucleolar RNA-like domain at the human telomerase RNA 3′ end. *Mol. Cell. Biol.* **19,** 567–76 (1999).

337. Greider, C. W. & Blackburn, E. H. A telomeric sequence in the RNA of Tetrahymena telomerase required for telomere repeat synthesis. *Nature* **337,** 331–7 (1989).

338. Vaziri, H. & Benchimol, S. Reconstitution of telomerase activity in normal human cells leads to elongation of telomeres and extended replicative life span. *Curr. Biol.* **8,** 279–82 (1998).

339. Bodnar, A. G. *et al.* Extension of life-span by introduction of telomerase into normal human cells. *Science* **279,** 349–52 (1998).

340. Jiang, X. R. *et al.* Telomerase expression in human somatic cells does not induce changes associated with a transformed phenotype. *Nat. Genet.* **21,** 111–4 (1999).

341. Kim, N. W. *et al.* Specific association of human telomerase activity with immortal cells and cancer. *Science* **266,** 2011–5 (1994).

342. Shay, J. W. & Bacchetti, S. A survey of telomerase activity in human cancer. *Eur. J. Cancer* **33,** 787–91 (1997).

343. Cosme-Blanco, W. & Chang, S. Dual roles of telomere dysfunction in initiation and suppression of tumorigenesis. *Exp. Cell Res.* **314,** 1973–9 (2008).

344. De Lange, T. Shelterin: the protein complex that shapes and safeguards human telomeres. *Genes Dev.* **19,** 2100–10 (2005).

345. Wong, J. M. Y. & Collins, K. Telomere maintenance and disease. *Lancet* **362,** 983–8 (2003).

346. Moon, I. K. & Jarstfer, M. B. The human telomere and its relationship to human disease, therapy, and tissue engineering. *Front. Biosci.* **12,** 4595–620 (2007).

347. McClintock, B. The Behavior in Successive Nuclear Divisions of a Chromosome Broken at Meiosis. *Proc. Natl. Acad. Sci. U. S. A.* **25,** 405–16 (1939).

348. Gisselsson, D. *et al.* Chromosomal breakage-fusion-bridge events cause genetic intratumor heterogeneity. *Proc Natl Acad Sci U S A* **97,** 5357–5362 (2000).

349. Stewenius, Y. *et al.* Structural and numerical chromosome changes in colon cancer develop through telomere-mediated anaphase bridges, not through mitotic multipolarity. *Proc Natl Acad Sci U S A* **102,** 5541–5546 (2005).

350. Montgomery, E. *et al.* Analysis of Anaphase Figures in Routine Histologic Sections Distinguishes Chromosomally Unstable from Chromosomally Stable Malignancies. *Cancer Biol. Ther.* **2,** 248–252 (2003).

351. McClintock, B. The Stability of Broken Ends of Chromosomes in Zea Mays. *Genetics* **26,** 234–282 (1941).

352. Artandi, S. E. *et al.* Telomere dysfunction promotes non-reciprocal translocations and epithelial cancers in mice. *Nature* **406,** 641–5 (2000).

353. Fouladi, B., Sabatier, L., Miller, D., Pottier, G. & Murnane, J. P. The relationship between spontaneous telomere loss and chromosome instability in a human tumor cell line. *Neoplasia* **2,** 540–554 (2000).

354. Gisselsson, D. *et al.* Telomere dysfunction triggers extensive DNA fragmentation and evolution of complex chromosome abnormalities in human malignant tumors. *Proc Natl Acad Sci U S A* **98,** 12683–12688 (2001).

355. Zhu, C. *et al.* Unrepaired DNA breaks in p53-deficient cells lead to oncogenic gene amplification subsequent to translocations. *Cell* **109,** 811–21 (2002).

356. Rudolph, K. L., Millard, M., Bosenberg, M. W. & DePinho, R. a. Telomere dysfunction and evolution of intestinal carcinoma in mice and humans. *Nat. Genet.* **28,** 155–9 (2001).

357. Prencipe, M. *et al.* Cellular senescence induced by aberrant MAD2 levels impacts on paclitaxel responsiveness in vitro. *Br. J. Cancer* **101,** 1900–8 (2009).

358. Gorman, S. *et al.* Radiation and chemotherapy bystander effects induce early genomic instability events: telomere shortening and bridge formation coupled with mitochondrial dysfunction. *Mutat. Res.* **669,** 131–8 (2009).

359. Martinez, P., Blasco, M. A. & Martínez, P. Telomeric and extra-telomeric roles for telomerase and the telomere-binding proteins. *Nat Rev Cancer* **11,** 161–176 (2011).

360. Murnane, J. P. Telomeres and chromosome instability. *DNA Repair (Amst).* **5,** 1082–92 (2006).

361. Murnane, J. P. & Sabatier, L. Chromosome rearrangements resulting from telomere dysfunction and their role in cancer. *BioEssays* **26,** 1164–1174 (2004).

362. Ford, M. & Fried, M. Large inverted duplications are associated with gene amplification. *Cell* **45,** 425–30 (1986).

363. Meltzer, P. S., Guan, X. Y. & Trent, J. M. Telomere capture stabilizes chromosome breakage. *Nat. Genet.* **4,** 252–5 (1993).

364. Ingvarsson, S. Molecular genetics of breast cancer progression. *Semin. Cancer Biol.* **9,** 277–88 (1999).

365. Campbell, P. J. *et al.* The patterns and dynamics of genomic instability in metastatic pancreatic cancer. *Nature* **467,** 1109–13 (2010).

366. Tanaka, H., Bergstrom, D. A., Yao, M.-C. & Tapscott, S. J. Widespread and nonrandom distribution of DNA palindromes in cancer cells provides a structural platform for subsequent gene amplification. *Nat. Genet.* **37,** 320–7 (2005).

367. Meeker, A. K. & Argani, P. Telomere shortening occurs early during breast tumorigenesis: a cause of chromosome destabilization underlying malignant transformation? *J Mammary Gland Biol Neoplasia* **9,** 285–296 (2004).

368. Selvarajah, S. *et al.* The breakage-fusion-bridge (BFB) cycle as a mechanism for generating genetic heterogeneity in osteosarcoma. *Chromosoma* **115,** 459–67 (2006).

369. Vukovic, B. *et al.* Correlating breakage-fusion-bridge events with the overall chromosomal instability and in vitro karyotype evolution in prostate cancer. *Cytogenet. Genome Res.* **116,** 1–11 (2007).

370. Vukovic, B. *et al.* Evidence of multifocality of telomere erosion in high-grade prostatic intraepithelial neoplasia (HPIN) and concurrent carcinoma. *Oncogene* **22,** 1978–87 (2003).

371. DePinho, R. A. & Polyak, K. Cancer chromosomes in crisis. *Nat. Genet.* **36,** 932–4 (2004).

372. Meeker, A. K. *et al.* Telomere length abnormalities occur early in the initiation of epithelial carcinogenesis. *Clin Cancer Res* **10,** 3317–3326 (2004).

373. Jr, V. D., Lawrence, T. & Rosenberg, S. *Cancer: Principles & Practice of Oncology*. 35–51 (Lippincott Williams & Wilkins, 2010).

374. Santaguida, S. & Musacchio, A. The life and miracles of kinetochores. *EMBO J.* **28,** 2511–31 (2009).

375. Chan, G. K., Liu, S.-T. & Yen, T. J. Kinetochore structure and function. *Trends Cell Biol.* **15,** 589–98 (2005).

376. Cheeseman, I. M. & Desai, A. Molecular architecture of the kinetochore-microtubule interface. *Nat. Rev. Mol. Cell Biol.* **9,** 33–46 (2008).

377. Acquaviva, C., Herzog, F., Kraft, C. & Pines, J. The anaphase promoting complex/cyclosome is recruited to centromeres by the spindle assembly checkpoint. *Nat. Cell Biol.* **6,** 892–8 (2004).

378. Chen, R.-H. BubR1 is essential for kinetochore localization of other spindle checkpoint proteins and its phosphorylation requires Mad1. *J. Cell Biol.* **158,** 487–96 (2002).

379. Fang, G., Yu, H. & Kirschner, M. W. The checkpoint protein MAD2 and the mitotic regulator CDC20 form a ternary complex with the anaphase-promoting complex to control anaphase initiation. *Genes Dev.* **12,** 1871–83 (1998).

380. Fraschini, R. *et al.* Bub3 interaction with Mad2, Mad3 and Cdc20 is mediated by WD40 repeats and does not require intact kinetochores. *EMBO J.* **20,** 6648–59 (2001).

381. Hardwick, K. G., Johnston, R. C., Smith, D. L. & Murray, A. W. MAD3 encodes a novel component of the spindle checkpoint which interacts with Bub3p, Cdc20p, and Mad2p. *J. Cell Biol.* **148,** 871–82 (2000).

382. Braunstein, I., Miniowitz, S., Moshe, Y. & Hershko, A. Inhibitory factors associated with anaphase-promoting complex/cylosome in mitotic checkpoint. *Proc. Natl. Acad. Sci. U. S. A.* **104,** 4870–5 (2007).

383. Sudakin, V., Chan, G. K. & Yen, T. J. Checkpoint inhibition of the APC/C in HeLa cells is mediated by a complex of BUBR1, BUB3, CDC20, and MAD2. *J. Cell Biol.* **154,** 925–36 (2001).

384. Tang, Z., Bharadwaj, R., Li, B. & Yu, H. Mad2-Independent inhibition of APCCdc20 by the mitotic checkpoint protein BubR1. *Dev. Cell* **1,** 227–37 (2001).

385. Yu, H. Regulation of APC-Cdc20 by the spindle checkpoint. *Curr. Opin. Cell Biol.* **14,** 706–14 (2002).

386. Abrieu, A., Kahana, J. A., Wood, K. W. & Cleveland, D. W. CENP-E as an essential component of the mitotic checkpoint in vitro. *Cell* **102,** 817–26 (2000).

387. Yu, H. *et al.* Identification of a cullin homology region in a subunit of the anaphase-promoting complex. *Science* **279,** 1219–22 (1998).

388. Harper, J. W., Burton, J. L. & Solomon, M. J. The anaphase-promoting complex: it's not just for mitosis any more. *Genes Dev.* **16,** 2179–206 (2002).

389. Peters, J.-M. The anaphase-promoting complex: proteolysis in mitosis and beyond. *Mol. Cell* **9,** 931–43 (2002).

390. Nasmyth, K., Peters, J. M. & Uhlmann, F. Splitting the chromosome: cutting the ties that bind sister chromatids. *Science* **288,** 1379–85 (2000).

391. Nasmyth, K. Segregating sister genomes: the molecular biology of chromosome separation. *Science* **297,** 559–65 (2002).

392. Kramer, E. R., Gieffers, C., Hölzl, G., Hengstschläger, M. & Peters, J. M. Activation of the human anaphase-promoting complex by proteins of the CDC20/Fizzy family. *Curr. Biol.* **8,** 1207–10 (1998).

393. Stegmeier, F. *et al.* Anaphase initiation is regulated by antagonistic ubiquitination and deubiquitination activities. *Nature* **446,** 876–81 (2007).

394. Howell, B. J., Hoffman, D. B., Fang, G., Murray, A. W. & Salmon, E. D. Visualization of Mad2 dynamics at kinetochores, along spindle fibers, and at spindle poles in living cells. *J. Cell Biol.* **150,** 1233–50 (2000).

395. Rajagopalan, H. & Lengauer, C. Aneuploidy and cancer. *Nature* **432,** 338–41 (2004).

396. Shi, Q. & King, R. W. Chromosome nondisjunction yields tetraploid rather than aneuploid cells in human cell lines. *Nature* **437,** 1038–42 (2005).

397. Fang, X. & Zhang, P. Aneuploidy and tumorigenesis. *Semin. Cell Dev. Biol.* **22,** 595–601 (2011).

398. Voet, T., Liebe, B., Labaere, C., Marynen, P. & Scherthan, H. Telomere-independent homologue pairing and checkpoint escape of accessory ring chromosomes in male mouse meiosis. *J. Cell Biol.* **162,** 795–807 (2003).

399. Mukherjee, M. *et al.* Separase loss of function cooperates with the loss of p53 in the initiation and progression of T- and B-cell lymphoma, leukemia and aneuploidy in mice. *PLoS One* **6,** e22167 (2011).

400. Li, M. & Zhang, P. Spindle assembly checkpoint, aneuploidy and tumorigenesis. *Cell Cycle* **8,** 3440 (2009).

401. Foijer, F., Draviam, V. & Sorger, P. Studying chromosome instability in the mouse. ... *Biophys. Acta (BBA)-Reviews* ... **1786,** 73–82 (2008).

402. Thirthagiri, E. *et al.* Spindle assembly checkpoint and centrosome abnormalities in oral cancer. *Cancer Lett.* **258,** 276–85 (2007).

403. Zhu, X.-L., Ai, Z.-H., Wang, J., Xu, Y.-L. & Teng, Y.-C. Weighted gene co-expression network analysis in identification of endometrial cancer prognosis markers. *Asian Pac. J. Cancer Prev.* **13,** 4607–11 (2012).

404. Yuan, B. *et al.* Increased expression of mitotic checkpoint genes in breast cancer cells with chromosomal instability. *Clin. Cancer Res.* **12,** 405–10 (2006).

405. Pinto, M. *et al.* Expression changes of the MAD mitotic checkpoint gene family in renal cell carcinomas characterized by numerical chromosome changes. *Virchows Arch.* **450,** 379–85 (2007).

406. Grabsch, H. *et al.* Overexpression of the mitotic checkpoint genes BUB1, BUBR1, and BUB3 in gastric cancer--association with tumour cell proliferation. *J. Pathol.* **200,** 16–22 (2003).

407. Kato, T. *et al.* Overexpression of CDC20 predicts poor prognosis in primary non-small cell lung cancer patients. *J. Surg. Oncol.* **106,** 423–30 (2012).

408. Ko, Y. H. *et al.* Expression of mitotic checkpoint proteins BUB1B and MAD2L1 in salivary duct carcinomas. *J. Oral Pathol. Med.* **39,** 349–55 (2010).

409. Mondal, G. *et al.* Overexpression of Cdc20 leads to impairment of the spindle assembly checkpoint and aneuploidization in oral cancer. *Carcinogenesis* **28,** 81–92 (2007).

410. Díaz-Rodríguez, E. *et al.* Deficient spindle assembly checkpoint in multiple myeloma. *PLoS One* **6,** e27583 (2011).

411. Chang, D. Z. *et al.* Increased CDC20 expression is associated with pancreatic ductal adenocarcinoma differentiation and progression. *J. Hematol. Oncol.* **5,** 15 (2012).

412. Assié, G. *et al.* The pathophysiology, diagnosis and prognosis of adrenocortical tumors revisited by transcriptome analyses. *Trends Endocrinol. Metab.* **21,** 325–34 (2010).

413. Baker, D. J., Chen, J. & van Deursen, J. M. A. The mitotic checkpoint in cancer and aging: what have mice taught us? *Curr. Opin. Cell Biol.* **17,** 583–9 (2005).

414. Kops, G. J. P. L., Weaver, B. A. A. & Cleveland, D. W. On the road to cancer: aneuploidy and the mitotic checkpoint. *Nat. Rev. Cancer* **5,** 773–85 (2005).

415. Njajou, O. T. *et al.* Shorter telomeres are associated with obesity and weight gain in the elderly. *Int. J. Obes. (Lond).* **36,** 1176–9 (2012).

416. Fitzpatrick, A. L. *et al.* Leukocyte telomere length and cardiovascular disease in the cardiovascular health study. *Am. J. Epidemiol.* **165,** 14–21 (2007).

417. Valdes, a M. *et al.* Obesity, cigarette smoking, and telomere length in women. *Lancet* **366,** 662–4 (2005).

418. Nordfjäll, K. *et al.* Telomere length is associated with obesity parameters but with a gender difference. *Obesity (Silver Spring).* **16,** 2682–9 (2008).

419. O'Donnell, C. J. *et al.* Leukocyte telomere length and carotid artery intimal medial thickness: the Framingham Heart Study. *Arterioscler. Thromb. Vasc. Biol.* **28,** 1165–71 (2008).

420. Bekaert, S. *et al.* Telomere length and cardiovascular risk factors in a middle-aged population free of overt cardiovascular disease. *Aging Cell* **6,** 639–47 (2007).

421. McGrath, M., Wong, J. Y. Y., Michaud, D., Hunter, D. J. & De Vivo, I. Telomere length, cigarette smoking, and bladder cancer risk in men and women. *Cancer Epidemiol. Biomarkers Prev.* **16,** 815–9 (2007).

422. Brouilette, S. W. *et al.* Telomere length, risk of coronary heart disease, and statin treatment in the West of Scotland Primary Prevention Study: a nested case-control study. *Lancet* **369,** 107–114 (2007).

423. Risques, R. A. *et al.* Leukocyte telomere length predicts cancer risk in Barrett's esophagus. *Cancer Epidemiol. Biomarkers Prev.* **16,** 2649–55 (2007).

424. Nettleton, J. A. *et al.* Dietary patterns, food groups, and telomere length in the Multi-Ethnic Study of Atherosclerosis (MESA). *Am J Clin Nutr* **88,** 1405–1412 (2011).

425. Moreno-Navarrete, J. M., Ortega, F., Sabater, M., Ricart, W. & Fernández-Real, J. M. Telomere length of subcutaneous adipose tissue cells is shorter in obese and formerly obese subjects. *Int. J. Obes. (Lond).* **34,** 1345–8 (2010).

426. Epel, E. S. *et al.* Cell aging in relation to stress arousal and cardiovascular disease risk factors. *Psychoneuroendocrinology* **31,** 277–87 (2006).

427. Ren, H. *et al.* Leptin upregulates telomerase activity and transcription of human telomerase reverse transcriptase in MCF-7 breast cancer cells. *Biochem. Biophys. Res. Commun.* **394,** 59–63 (2010).

428. Daubenmier, J., Lin, J. & Blackburn, E. Changes in stress, eating, and metabolic factors are related to changes in telomerase activity in a randomized mindfulness intervention pilot study. ... **37,** 917–928 (2012).

429. Rahmati-Yamchi, M., Zarghami, N., Rahbani, M. & Montazeri, A. Plasma Leptin, hTERT Gene Expression, and Anthropometric Measures in Obese and Non-Obese Women with Breast Cancer. *Breast Cancer (Auckl).* **5,** 27–35 (2011).

430. Ornish, D. *et al.* Increased telomerase activity and comprehensive lifestyle changes: a pilot study. *Lancet Oncol.* **9,** 1048–57 (2008).

431. Almén, M. S. *et al.* Genome wide analysis reveals association of a FTO gene variant with epigenetic changes. *Genomics* **99,** 132–7 (2012).

432. Kim, E. J. *et al.* Biological features of core networks that result from a high-fat diet in hepatic and pulmonary tissues in mammary tumour-bearing, obesity-resistant mice. *Br. J. Nutr.* 1–15 (2012). doi:10.1017/S0007114512004965

433. D'Angiolella, V., Santarpia, C. & Grieco, D. Oxidative stress overrides the spindle checkpoint. *Cell Cycle* **6,** 576–579 (2007).

434. Furukawa, S. *et al.* Increased oxidative stress in obesity and its impact on metabolic syndrome. *J. Clin. Invest.* **114,** 1752–61 (2004).

435. Taalman, R. D., Jaspers, N. G., Scheres, J. M., de Wit, J. & Hustinx, T. W. Hypersensitivity to ionizing radiation, in vitro, in a new chromosomal breakage disorder, the Nijmegen Breakage Syndrome. *Mutat. Res.* **112,** 23–32 (1983).

436. Lavin, M. F. & Shiloh, Y. The genetic defect in ataxia-telangiectasia. *Annu. Rev. Immunol.* **15,** 177–202 (1997).

437. Beamish, H. *et al.* Functional link between BLM defective in Bloom's syndrome and the ataxia-telangiectasia-mutated protein, ATM. *J. Biol. Chem.* **277,** 30515–23 (2002).

438. Callén, E. & Surrallés, J. Telomere dysfunction in genome instability syndromes. *Mutat. Res.* **567,** 85–104 (2004).

439. Goytisolo, F. a *et al.* Short telomeres result in organismal hypersensitivity to ionizing radiation in mammals. *J. Exp. Med.* **192,** 1625–36 (2000).

440. Mcilrath, J. *et al.* Telomere Length Abnormalities in Mammalian Radiosensitive Cells. *Cancer Res.* **61,** 912–915 (2001).

441. Rubio, M. A., Kim, S.-H. H. & Campisi, J. Reversible manipulation of telomerase expression and telomere length. Implications for the ionizing radiation response and replicative senescence of human cells. *J Biol Chem* **277,** 28609–28617 (2002).

442. Drissi, R., Wu, J., Hu, Y., Bockhold, C. & Dome, J. Telomere shortening alters the kinetics of the DNA damage response after ionizing radiation in human cells. *Cancer Prev. Res.* **4,** 1973–1981 (2011).

443. Zhong, Y.-H. *et al.* Telomere length inversely correlates with radiosensitivity in human carcinoma cells with the same tissue background. *Biochem. Biophys. Res. Commun.* **367,** 84–9 (2008).

444. McCaul, J. a, Gordon, K. E., Minty, F., Fleming, J. & Parkinson, E. K. Telomere dysfunction is related to the intrinsic radio-resistance of human oral cancer cells. *Oral Oncol.* **44,** 261–9 (2008).

445. Wesbuer, S. *et al.* Association of telomerase activity with radio- and chemosensitivity of neuroblastomas. *Radiat. Oncol.* **5,** 66 (2010).

446. Blasco, M. A. *et al.* Mouse models for the study of telomerase. *Ciba Found. Symp.* **211,** 160–70; discussion 170–6 (1997).

447. Wong, K. K. *et al.* Telomere dysfunction impairs DNA repair and enhances sensitivity to ionizing radiation. *Nat Genet* **26,** 85–88 (2000).

448. Castella, M., Puerto, S., Creus, a, Marcos, R. & Surralles, J. Telomere length modulates human radiation sensitivity in vitro. *Toxicol. Lett.* **172,** 29–36 (2007).

449. Nakamura, M. *et al.* Efficient inhibition of human telomerase reverse transcriptase expression by RNA interference sensitizes cancer cells to ionizing radiation and chemotherapy. *Hum. Gene Ther.* **16,** 859–68 (2005).

450. Masutomi, K. *et al.* The telomerase reverse transcriptase regulates chromatin state and DNA damage responses. *Proc. Natl. Acad. Sci. U. S. A.* **102,** 8222–7 (2005).

451. Rubio, M. A., Davalos, A. R. & Campisi, J. Telomere length mediates the effects of telomerase on the cellular response to genotoxic stress. *Exp. Cell Res.* **298,** 17–27 (2004).

452. Erdmann, N. & Harrington, L. A. LA. No attenuation of the ATM-dependent DNA damage response in murine telomerase-deficient cells. *DNA Repair (Amst).* **8,** 347–353 (2009).

453. Zhou, F.-X. *et al.* cDNA expression analysis of a human radiosensitive-radioresistant cell line model identifies telomere function as a hallmark of radioresistance. *Radiat. Res.* **174,** 550–7 (2010).

454. Tang, T. *et al.* Increased expression of telomere-related proteins correlates with resistance to radiation in human laryngeal cancer cell lines. *Oncol. Rep.* 1505–1509 (2009). doi:10.3892/or

455. Zhao, J. *et al.* Mitotic arrest deficient protein MAD2B is overexpressed in human glioma, with depletion enhancing sensitivity to ionizing radiation. *J. Clin. Neurosci.* **18,** 827–33 (2011).

456. Palma, D., Pickles, T. & Tyldesley, S. Obesity as a predictor of biochemical recurrence and survival after radiation therapy for prostate cancer. *BJU Int.* **100,** 315–9 (2007).

457. Stroup, S. P., Cullen, J., Auge, B. K., L'Esperance, J. O. & Kang, S. K. Effect of obesity on prostate-specific antigen recurrence after radiation therapy for localized prostate cancer as measured by the 2006 Radiation Therapy Oncology Group-American Society for Therapeutic Radiation and Oncology (RTOG-ASTRO) Phoenix consensus. *Cancer* **110,** 1003–9 (2007).

458. Hayashi, Y. *et al.* The influence of high body mass index on the prognosis of patients with esophageal cancer after surgery as primary therapy. *Cancer* **116,** 5619–27 (2010).

459. Diehn, M. *et al.* Association of reactive oxygen species levels and radioresistance in cancer stem cells. *Nature* **458,** 780–3 (2009).

460. Lee, H.-C. *et al.* Increased expression of antioxidant enzymes in radioresistant variant from U251 human glioblastoma cell line. *Int. J. Mol. Med.* **13,** 883–7 (2004).

461. Goytisolo, F. & Blasco, M. Many ways to telomere dysfunction: in vivo studies using mouse models. *Oncogene* 584–591 (2002). doi:10.1038/sj/onc/1205085

462. Karar, J. & Maity, A. Modulating the tumor microenvironment to increase radiation responsiveness. *Cancer Biol. Ther.* **8,** 1994–2001 (2009).

463. Lysaght, J. *et al.* T lymphocyte activation in visceral adipose tissue of patients with oesophageal adenocarcinoma. *Br. J. Surg.* **98,** 964–74 (2011).

464. Fyhrquist, F. & Saijonmaa, O. Telomere length and cardiovascular aging. *Ann. Med.* **44 Suppl 1,** S138–42 (2012).

465. Findeisen, H. M. *et al.* Oxidative stress accumulates in adipose tissue during aging and inhibits adipogenesis. *PLoS One* **6,** e18532 (2011).

466. Allott, E. H. *et al.* MMP9 expression in oesophageal adenocarcinoma is upregulated with visceral obesity and is associated with poor tumour differentiation. *Mol Carcinog* **52,** 144–54 (2013).

467. Yuzefovych, L. V, Musiyenko, S. I., Wilson, G. L. & Rachek, L. I. Mitochondrial DNA damage and dysfunction, and oxidative stress are associated with endoplasmic reticulum stress, protein degradation and apoptosis in high fat diet-induced insulin resistance mice. *PLoS One* **8,** e54059 (2013).

468. Barouch, L. A. *et al.* Cardiac myocyte apoptosis is associated with increased DNA damage and decreased survival in murine models of obesity. *Circ. Res.* **98,** 119–24 (2006).

469. Scarpato, R. *et al.* Nuclear damage in peripheral lymphocytes of obese and overweight Italian children as evaluated by the gamma-H2AX focus assay and micronucleus test. *FASEB J.* **25,** 685–93 (2011).

470. Allott, E. H. *et al.* Elevated Tumor Expression of PAI-1 and SNAI2 in Obese Esophageal Adenocarcinoma Patients and Impact on Prognosis. *Clin. Transl. Gastroenterol.* **3,** e12 (2012).

471. Neeland, I. J. *et al.* Associations of visceral and abdominal subcutaneous adipose tissue with markers of cardiac and metabolic risk in obese adults. *Obesity (Silver Spring).* (2012). doi:10.1002/oby.20135

472. Barresi, V., Grosso, M., Giuffrè, G., Tuccari, G. & Barresi, G. The expression of adiponectin receptors Adipo-R1 and Adipo-R2 is associated with an intestinal histotype and longer survival in gastric carcinoma. *J. Clin. Pathol.* **62,** 705–9 (2009).

473. Tsukada, T. *et al.* Adiponectin receptor-1 expression is associated with good prognosis in gastric cancer. *J. Exp. Clin. Cancer Res.* **30,** 107 (2011).

474. Cheng, S.-P. *et al.* Expression and biologic significance of adiponectin receptors in papillary thyroid carcinoma. *Cell Biochem. Biophys.* **65,** 203–10 (2013).

475. Geng, Y. *et al.* Leptin and HER-2 are associated with gastric cancer progression and prognosis of patients. *Biomed. Pharmacother.* **66,** 419–24 (2012).

476. Willett, C. G. *et al.* Direct evidence that the VEGF-specific antibody bevacizumab has antivascular effects in human rectal cancer. *Nat Med* **10,** 145–147 (2004).

477. Li, Z. *et al.* Effector genes altered in MCF-7 human breast cancer cells after exposure to fractionated ionizing radiation. *Radiat Res* **155,** 543–553 (2001).

478. Guo, G. *et al.* Manganese superoxide dismutase-mediated gene expression in radiation-induced adaptive responses. *Mol Cell Biol* **23,** 2362–2378 (2003).

479. Fukuda, K. *et al.* Differential gene expression profiles of radioresistant oesophageal cancer cell lines established by continuous fractionated irradiation. *Br J Cancer* **91,** 1543–1550 (2004).

480. Trotti, A. *et al.* Common toxicity criteria: version 2.0. an improved reference for grading the acute effects of cancer treatment: impact on radiotherapy. *Int. J. Radiat. Oncol. Biol. Phys.* **47,** 13–47 (2000).

481. Ibrahim, N. B. ACP. Best Practice No 155. Guidelines for handling oesophageal biopsies and resection specimens and their reporting. *J. Clin. Pathol.* **53,** 89–94 (2000).

482. Dindo, D., Demartines, N. & Clavien, P.-A. Classification of surgical complications: a new proposal with evaluation in a cohort of 6336 patients and results of a survey. *Ann. Surg.* **240,** 205–13 (2004).

483. Ennis, D. P., Pidgeon, G. P., Millar, N., Ravi, N. & Reynolds, J. V. Building a bioresource for esophageal research: lessons from the early experience of an academic medical center. *Dis. Esophagus* **23,** 1–7 (2010).

484. Alvarez-Llamas, G. *et al.* Characterization of the human visceral adipose tissue secretome. *Mol. Cell. Proteomics* **6,** 589–600 (2007).

485. Miller, K. D. *et al.* Visceral abdominal-fat accumulation associated with use of indinavir. *Lancet* **351,** 871–5 (1998).

486. Baumgartner, R. N., Heymsfield, S. B., Roche, A. F. & Bernardino, M. Abdominal composition quantified by computed tomography. *Am. J. Clin. Nutr.* **48,** 936–45 (1988).

487. Allott, E. H. Molecular interactions in obesity and cancer. (2010).

488. Franken, N. A. P., Rodermond, H. M., Stap, J., Haveman, J. & van Bree, C. Clonogenic assay of cells in vitro. *Nat. Protoc.* **1,** 2315–9 (2006).

489. Darzynkiewicz, Z. *et al.* Cytometry in cell necrobiology: analysis of apoptosis and accidental cell death (necrosis). *Cytometry* **27,** 1–20 (1997).

490. Klopfenstein, B. J. *et al.* Comparison of 3 T MRI and CT for the measurement of visceral and subcutaneous adipose tissue in humans. *Br. J. Radiol.* **85,** e826–30 (2012).

491. Lynam-Lennon, N. Investigation of the molecular mechanisms underlying radioresistance in oesophageal cancer. (2010).

492. Kern, P. A., Ranganathan, S., Li, C., Wood, L. & Ranganathan, G. Adipose tissue tumor necrosis factor and interleukin-6 expression in human obesity and insulin resistance. *Am J Physiol Endocrinol Metab* **280,** E745–751 (2001).

493. Hosoi, Y. *et al.* Induction of interleukin-1beta and interleukin-6 mRNA by low doses of ionizing radiation in macrophages. *Int. J. Cancer* **96,** 270–6 (2001).

494. Beetz, A. *et al.* NF-kappaB and AP-1 are responsible for inducibility of the IL-6 promoter by ionizing radiation in HeLa cells. *Int. J. Radiat. Biol.* **76,** 1443–53 (2000).

495. Chou, C.-H., Chen, S.-U. & Cheng, J. C.-H. Radiation-induced interleukin-6 expression through MAPK/p38/NF-kappaB signaling pathway and the resultant antiapoptotic effect

on endothelial cells through Mcl-1 expression with sIL6-Ralpha. *Int. J. Radiat. Oncol. Biol. Phys.* **75,** 1553–61 (2009).

496. Chen, M.-F., Hsieh, C.-C., Chen, W.-C. & Lai, C.-H. Role of interleukin-6 in the radiation response of liver tumors. *Int. J. Radiat. Oncol. Biol. Phys.* **84,** e621–30 (2012).

497. Chen, C.-C. *et al.* Significance of interleukin-6 signaling in the resistance of pharyngeal cancer to irradiation and the epidermal growth factor receptor inhibitor. *Int. J. Radiat. Oncol. Biol. Phys.* **76,** 1214–24 (2010).

498. Efimova, E. V *et al.* Radioresistance of Stat1 over-expressing tumour cells is associated with suppressed apoptotic response to cytotoxic agents and increased IL6-IL8 signalling. *Int. J. Radiat. Biol.* **85,** 421–31 (2009).

499. Tamatani, T. *et al.* Enhanced radiosensitization and chemosensitization in NF-kappaB-suppressed human oral cancer cells via the inhibition of gamma-irradiation- and 5-FU-induced production of IL-6 and IL-8. *Int. J. Cancer* **108,** 912–21 (2004).

500. Kim, C.-S. *et al.* Circulating levels of MCP-1 and IL-8 are elevated in human obese subjects and associated with obesity-related parameters. *Int. J. Obes. (Lond).* **30,** 1347–55 (2006).

501. Blirando, K. *et al.* Mast cells and ionizing radiation induce a synergistic expression of inflammatory genes in endothelial cells by a mechanism involving p38α MAP kinase and (p65) NF-κB activation. *Radiat. Res.* **178,** 556–67 (2012).

502. Schildkopf, P. *et al.* Radiation combined with hyperthermia induces HSP70-dependent maturation of dendritic cells and release of pro-inflammatory cytokines by dendritic cells and macrophages. *Radiother. Oncol.* **101,** 109–15 (2011).

503. Le, Q.-T. *et al.* Prognostic and predictive significance of plasma HGF and IL-8 in a phase III trial of chemoradiation with or without tirapazamine in locoregionally advanced head and neck cancer. *Clin. Cancer Res.* **18,** 1798–807 (2012).

504. Kim, T.-D. *et al.* Radiation-induced thymidine phosphorylase upregulation in rectal cancer is mediated by tumor-associated macrophages by monocyte chemoattractant protein-1 from cancer cells. *Int. J. Radiat. Oncol. Biol. Phys.* **73,** 853–60 (2009).

505. Nalla, A. K., Gogineni, V. R., Gupta, R., Dinh, D. H. & Rao, J. S. Suppression of uPA and uPAR blocks radiation-induced MCP-1 mediated recruitment of endothelial cells in meningioma. *Cell. Signal.* **23,** 1299–310 (2011).

506. Utsal, L. *et al.* Elevated serum IL-6, IL-8, MCP-1, CRP, and IFN-γ levels in 10- to 11-year-old boys with increased BMI. *Horm. Res. pædiatrics* **78,** 31–9 (2012).

507. De Ridder, M. *et al.* IFN-gamma+ CD8+ T lymphocytes: possible link between immune and radiation responses in tumor-relevant hypoxia. *Int. J. Radiat. Oncol. Biol. Phys.* **71,** 647–51 (2008).

508. Lindkvist, A., Ivarsson, K., Jernberg-Wiklund, H. & Paulsson-Karlsson, Y. Interferon-induced sensitization to apoptosis is associated with repressed transcriptional activity of the hTERT promoter in multiple myeloma. *Biochem. Biophys. Res. Commun.* **341,** 1141–8 (2006).

509. Tate, D. J. *et al.* Interferon-gamma-induced nitric oxide inhibits the proliferation of murine renal cell carcinoma cells. *Int. J. Biol. Sci.* **8,** 1109–20 (2012).

510. Brown, J. M. & Attardi, L. D. The role of apoptosis in cancer development and treatment response. *Nat Rev Cancer* **5,** 231–237 (2005).

511. Choy, H. *et al.* Phase I trial of outpatient weekly paclitaxel and concurrent radiation therapy for advanced non-small-cell lung cancer. *J. Clin. Oncol.* **12,** 2682–6 (1994).

512. Formenti, S. C. *et al.* Concurrent paclitaxel and radiation therapy for breast cancer. *Semin. Radiat. Oncol.* **9,** 34–42 (1999).

513. Falck, J., Mailand, N., Syljuåsen, R. G., Bartek, J. & Lukas, J. The ATM-Chk2-Cdc25A checkpoint pathway guards against radioresistant DNA synthesis. *Nature* **410,** 842–7 (2001).

514. Enns, L., Murray, D. & Mirzayans, R. Effects of the protein kinase inhibitors wortmannin and KN62 on cellular radiosensitivity and radiation-activated S phase and G1/S checkpoints in normal human fibroblasts. *Br. J. Cancer* **81,** 959–65 (1999).

515. Russell, K. J. *et al.* Preferential radiosensitization of G1 checkpoint-deficient cells by methylxanthines. *Int. J. Radiat. Oncol. Biol. Phys.* **36,** 1099–106 (1996).

516. Seker, M. *et al.* The association of serum adiponectin levels with histopathological variables in gastric cancer patients. *Med. Oncol.* **27,** 1319–23 (2010).

517. Michalakis, K. *et al.* Serum adiponectin concentrations and tissue expression of adiponectin receptors are reduced in patients with prostate cancer: a case control study. *Cancer Epidemiol. Biomarkers Prev.* **16,** 308–13 (2007).

518. Jung, T. W. *et al.* Adiponectin protects human neuroblastoma SH-SY5Y cells against acetaldehyde-induced cytotoxicity. *Biochem. Pharmacol.* **72,** 616–23 (2006).

519. Lam, K. S. L. & Xu, A. Adiponectin: protection of the endothelium. *Curr. Diab. Rep.* **5,** 254–9 (2005).

520. Li, R. *et al.* Adiponectin improves endothelial function in hyperlipidemic rats by reducing oxidative/nitrative stress and differential regulation of eNOS/iNOS activity. *Am. J. Physiol. Endocrinol. Metab.* **293,** E1703–8 (2007).

521. Gutteridge, J. M. & Halliwell, B. Free radicals and antioxidants in the year 2000. A historical look to the future. *Ann. N. Y. Acad. Sci.* **899,** 136–47 (2000).

522. Nakanishi, S. *et al.* A protective effect of adiponectin against oxidative stress in Japanese Americans: the association between adiponectin or leptin and urinary isoprostane. *Metabolism.* **54,** 194–9 (2005).

523. Konturek, P. C., Burnat, G., Rau, T., Hahn, E. G. & Konturek, S. Effect of adiponectin and ghrelin on apoptosis of Barrett adenocarcinoma cell line. *Dig. Dis. Sci.* **53,** 597–605 (2008).

524. Ogunwobi, O. O. & Beales, I. L. P. Globular adiponectin, acting via adiponectin receptor-1, inhibits leptin-stimulated oesophageal adenocarcinoma cell proliferation. *Mol. Cell. Endocrinol.* **285,** 43–50 (2008).

525. Dubois, V., Delort, L., Billard, H., Vasson, M.-P. & Caldefie-Chezet, F. Breast cancer and obesity: in vitro interferences between adipokines and proangiogenic features and/or antitumor therapies? *PLoS One* **8,** e58541 (2013).

526. Jardé, T. *et al.* Involvement of adiponectin and leptin in breast cancer: clinical and in vitro studies. *Endocr. Relat. Cancer* **16,** 1197–210 (2009).

527. Fusco, R. *et al.* Cellular and molecular crosstalk between leptin receptor and estrogen receptor-{alpha} in breast cancer: molecular basis for a novel therapeutic setting. *Endocr. Relat. Cancer* **17,** 373–82 (2010).

528. Mełeń-Mucha, G. & Lawnicka, H. Leptin promotes the growth of Colon 38 cancer cells and interferes with the cytotoxic effect of fluorouracil in vitro. *Endokrynol. Pol.* **58,** 2–6 (2007).

529. Gove, M. E., Sherry, C. L., Pini, M. & Fantuzzi, G. Generation of leptin receptor bone marrow chimeras: recovery from irradiation, immune cellularity, cytokine expression, and metabolic parameters. *Obesity (Silver Spring).* **18,** 2274–81 (2010).

530. Jiang, H., Yu, J., Guo, H., Song, H. & Chen, S. Upregulation of survivin by leptin/STAT3 signaling in MCF-7 cells. *Biochem. Biophys. Res. Commun.* **368,** 1–5 (2008).

531. Kajdaniuk, D., Marek, B., Foltyn, W. & Kos-Kudła, B. Vascular endothelial growth factor (VEGF) - part 1: in physiology and pathophysiology. *Endokrynol. Pol.* **62,** 456–64 (2011).

532. Tugues, S., Koch, S., Gualandi, L., Li, X. & Claesson-Welsh, L. Vascular endothelial growth factors and receptors: anti-angiogenic therapy in the treatment of cancer. *Mol. Aspects Med.* **32,** 88–111 (2011).

533. Kurt, A. *et al.* Low Mmp 9 and VEGF levels predict good oncologic outcome in mid and low rectal cancer patients with neoadjuvant chemoradiation. *BMC Clin. Pathol.* **12,** 27 (2012).

534. Gorski, D. H. *et al.* Blockade of the Vascular Endothelial Growth Factor Stress Response Increases the Antitumor Effects of Ionizing Radiation Advances in Brief Blockade of the Vascular Endothelial Growth Factor Stress Response Increases the Antitumor Effects of Ionizing Radia. *Cancer Res.* **59,** 3374–3378 (1999).

535. Winkler, F. *et al.* Kinetics of vascular normalization by VEGFR2 blockade governs brain tumor response to radiation: role of oxygenation, angiopoietin-1, and matrix metalloproteinases. *Cancer Cell* **6,** 553–63 (2004).

536. Vredenburgh, J. J. *et al.* Bevacizumab plus irinotecan in recurrent glioblastoma multiforme. *J. Clin. Oncol.* **25,** 4722–9 (2007).

537. Drigotas, M., Affolter, A., Mann, W. J. & Brieger, J. Reactive oxygen species activation of MAPK pathway results in VEGF upregulation as an undesired irradiation response. *J. Oral Pathol. Med.* (2013). doi:10.1111/jop.12056

538. Affolter, A. *et al.* Increased radioresistance via G12S K-Ras by compensatory upregulation of MAPK and PI3K pathways in epithelial cancer. *Head Neck* **35,** 220–8 (2013).

539. Willett, C., Duda, D. & Czito, B. Targeted therapy in rectal cancer. ... *(willist. Park. NY)* **21,** 964–970 (2007).

540. Ellis, L. M. & Hicklin, D. J. VEGF-targeted therapy: mechanisms of anti-tumour activity. *Nat. Rev. Cancer* **8,** 579–91 (2008).

541. Pan, Q. *et al.* Blocking neuropilin-1 function has an additive effect with anti-VEGF to inhibit tumor growth. *Cancer Cell* **11,** 53–67 (2007).

542. Quennet, V. *et al.* Tumor lactate content predicts for response to fractionated irradiation of human squamous cell carcinomas in nude mice. *Radiother. Oncol.* **81,** 130–5 (2006).

543. Sattler, U. G. A. *et al.* Glycolytic metabolism and tumour response to fractionated irradiation. *Radiother. Oncol.* **94,** 102–9 (2010).

544. Schwickert, G., Walenta, S., Sundfør, K., Rofstad, E. K. & Mueller-Klieser, W. Correlation of high lactate levels in human cervical cancer with incidence of metastasis. *Cancer Res.* **55,** 4757–9 (1995).

545. Cheng, L. L., Chang, I. W., Smith, B. L. & Gonzalez, R. G. Evaluating human breast ductal carcinomas with high-resolution magic-angle spinning proton magnetic resonance spectroscopy. *J. Magn. Reson.* **135,** 194–202 (1998).

546. Seymour, C. B. & Mothersill, C. The effect of lactate on the radiation response of CHO-K1 cells in culture. *Int. J. Radiat. Biol. Relat. Stud. Phys. Chem. Med.* **40,** 283–91 (1981).

547. Johnson, C. H. *et al.* Radiation metabolomics. 5. Identification of urinary biomarkers of ionizing radiation exposure in nonhuman primates by mass spectrometry-based metabolomics. *Radiat. Res.* **178,** 328–40 (2012).

548. Nicholson, J. K. *et al.* Metabolic phenotyping in clinical and surgical environments. *Nature* **491,** 384–92 (2012).

549. Kelleher C, Nic Gabhainn S, F. S. *The National Health and Lifestyle Surveys: Survery of Lifestyle, Attitudes and Nutrition (SLAN 1998) and the Irish Health Behaviours in School-Aged Children Survery (HBSC).* (1999).

550. Kelleher C, Nic Gabhainn S, Friel S, Corrigan H, Nolan G, Sixsmith J, Walsh O, C. M. *The National Health and Lifestyle Surveys: Survery of Lifestyle, Attitudes and Nutrition (SLAN 2002) and the Irish Health Behaviours in School-Aged Children Survery (HBSC).* (2003).

551. Morgan K, McGee H, Watson D, Perry I, Barry M, Shelley E, Harrington J, Molcho M, L., R, Tully N, van Lente E, Ward M, Lutomski J , Conroy R, B. R. & Morgan K, McGee H, Watson D, Perry I, Barry M, Shelley E, Harrington J, Molcho M, Layte R, Tully N, van Lente E, Ward M, Lutomski J , Conroy R, B. R. *SLÁN 2007: Survey of Lifestyle, Attitudes & Nutrition in Ireland.* (2008).

552. *International Obesity Taskforce and European Association for the Study if Obesity (2002) Obesity in Europe – The Case for Action.* (2002).

553. Devesa, S. S., Blot, W. J. & Fraumeni Jr., J. F. Changing patterns in the incidence of esophageal and gastric carcinoma in the United States. *Cancer* **83,** 2049–2053 (1998).

554. Pera, M., Manterola, C., Vidal, O. & Grande, L. Epidemiology of esophageal adenocarcinoma. *J Surg Oncol* **92,** 151–159 (2005).

555. *World Cancer Research Fund. Food, Nutrition, Physical Activity and the Prevention of Cancer: A Global Perspective (2nd edn).* (2007).

556. Renehan, A. G., Tyson, M., Egger, M., Heller, R. F. & Zwahlen, M. Body-mass index and incidence of cancer: a systematic review and meta-analysis of prospective observational studies. *Lancet* **371,** 569–578 (2008).

557. Zhong, Z., Shiue, L., Kaplan, S. & de Lange, T. A mammalian factor that binds telomeric TTAGGG repeats in vitro. *Mol Cell Biol* **12,** 4834–4843 (1992).

558. Chong, L. *et al.* A human telomeric protein. *Science (80-.).* **270,** 1663–1667 (1995).

559. Donigian, J. R. & de Lange, T. The role of the poly(ADP-ribose) polymerase tankyrase1 in telomere length control by the TRF1 component of the shelterin complex. *J Biol Chem* **282,** 22662–22667 (2007).

560. Rubio, M., Kim, S. & Campisi, J. Manipulation of Telomerase Expression and Telomere Length IMPLICATIONS FOR THE IONIZING RADIATION RESPONSE AND REPLICATIVE SENESCENCE OF. *J. Biol. Chem.* **277,** 28609–28617 (2002).

561. Tzanetakou, I. P., Katsilambros, N. L., Benetos, A., Mikhailidis, D. P. & Perrea, D. N. "Is obesity linked to aging?": adipose tissue and the role of telomeres. *Ageing Res. Rev.* **11,** 220–9 (2012).

562. Wentzensen, I. M., Mirabello, L., Pfeiffer, R. M. & Savage, S. a. The association of telomere length and cancer: a meta-analysis. *Cancer Epidemiol. Biomarkers Prev.* **20,** 1238–50 (2011).

563. Xing, J. *et al.* Constitutive short telomere length of chromosome 17p and 12q but not 11q and 2p is associated with an increased risk for esophageal cancer. *Cancer Prev. Res. (Phila).* **2,** 459–65 (2009).

564. Greil, R. & Stein, H. J. Is it time to consider neoadjuvant treatment as the standard of care in oesophageal cancer? *Lancet Oncol* **8,** 189–190 (2007).

565. Berger, B. & Belka, C. Evidence-based radiation oncology: oesophagus. *Radiother Oncol* **92,** 276–290 (2009).

566. Geh, J. I., Bond, S. J., Bentzen, S. M. & Glynne-Jones, R. Systematic overview of preoperative (neoadjuvant) chemoradiotherapy trials in oesophageal cancer: evidence of a radiation and chemotherapy dose response. *Radiother. Oncol.* **78,** 236–44 (2006).

567. Cawthon, R. M. Telomere measurement by quantitative PCR. *Nucleic Acids Res.* **30,** e47 (2002).

568. Finley, J. C. *et al.* Chromosomal instability in Barrett's esophagus is related to telomere shortening. *Cancer Epidemiol Biomarkers Prev* **15,** 1451–1457 (2006).

569. Fyhrquist, F. *et al.* Telomere length and cardiovascular risk in hypertensive patients with left ventricular hypertrophy: the LIFE study. *J Hum Hypertens* **25,** 711–718 (2011).

570. Gardner, J. P. *et al.* Rise in insulin resistance is associated with escalated telomere attrition. *Circulation* **111,** 2171–2177 (2005).

571. Demissie, S. *et al.* Insulin resistance, oxidative stress, hypertension, and leukocyte telomere length in men from the Framingham Heart Study. *Aging Cell* **5,** 325–330 (2006).

572. Sampson, M. J., Winterbone, M. S., Hughes, J. C., Dozio, N. & Hughes, D. a. Monocyte telomere shortening and oxidative DNA damage in type 2 diabetes. *Diabetes Care* **29,** 283–9 (2006).

573. Adaikalakoteswari, A., Balasubramanyam, M., Ravikumar, R., Deepa, R. & Mohan, V. Association of telomere shortening with impaired glucose tolerance and diabetic macroangiopathy. *Atherosclerosis* **195,** 83–89 (2007).

574. Yang, Z. *et al.* Short telomeres and prognosis of hypertension in a chinese population. *Hypertension* **53,** 639–645 (2009).

575. Al-Attas, O. S. *et al.* Telomere length in relation to insulin resistance, inflammation and obesity among Arab youth. *Acta Paediatr.* **99,** 896–9 (2010).

576. Von Zglinicki, T. *et al.* Short telomeres in patients with vascular dementia: an indicator of low antioxidative capacity and a possible risk factor? *Lab Invest* **80,** 1739–1747 (2000).

577. Merchant, N. B., Dutta, S. K., Girotra, M., Arora, M. & Meltzer, S. J. Evidence for Enhanced Telomerase Activity in Barrett's Esophagus with Dysplasia and Adenocarcinoma. *Asian Pac. J. Cancer Prev.* **14,** 679–83 (2013).

578. Avilion, A. A. *et al.* Human telomerase RNA and telomerase activity in immortal cell lines and tumor tissues. *Cancer Res.* **56,** 645–50 (1996).

579. Meyerson, M. *et al.* hEST2, the putative human telomerase catalytic subunit gene, is up-regulated in tumor cells and during immortalization. *Cell* **90,** 785–95 (1997).

580. Nakayama, J. *et al.* Telomerase activation by hTRT in human normal fibroblasts and hepatocellular carcinomas. *Nat. Genet.* **18,** 65–8 (1998).

581. Going, J. J. *et al.* Zoning of mucosal phenotype, dysplasia, and telomerase activity measured by telomerase repeat assay protocol in Barrett's esophagus. *Neoplasia* **6,** 85–92 (2004).

582. Clément, G., Braunschweig, R., Pasquier, N., Bosman, F. T. & Benhattar, J. Methylation of APC, TIMP3, and TERT: a new predictive marker to distinguish Barrett's oesophagus patients at risk for malignant transformation. *J. Pathol.* **208,** 100–7 (2006).

583. Shammas, M. A. & Rao, M. Y. Purification of diseased cells from Barrett's esophagus and related lesions by laser capture microdissection. *Methods Mol. Biol.* **755,** 181–7 (2011).

584. Kirkpatrick, K. L., Newbold, R. F. & Mokbel, K. The mRNA expression of hTERT in human breast carcinomas correlates with VEGF expression. *J. Carcinog.* **3,** 1 (2004).

585. Hong, D.-Y. *et al.* Expression of VEGF, HGF, IL-6, IL-8, MMP-9, Telomerase in Peripheral Blood of Patients with Head and Neck Squamous Cell Carcinoma. *Clin. Exp. Otorhinolaryngol.* **2,** 186–92 (2009).

586. Mansfield, L. *et al.* HTERT mRNA expression correlates with matrix metalloproteinase-1 and vascular endothelial growth factor expression in human breast cancer: a correlative study using RT-PCR. *Anticancer Res.* **27,** 2265–8 (2007).

587. Bermudez, Y. *et al.* VEGF- and LPA-induced telomerase in human ovarian cancer cells is Sp1-dependent. *Gynecol Oncol* **106,** 526–537 (2007).

588. Shen, X.-H. *et al.* Interleukin-8 prevents oxidative stress-induced human endothelial cell senescence via telomerase activation. *Int. Immunopharmacol.* **16,** 261–267 (2013).

589. Kojima, K. *et al.* Telomerase activation without shortening of telomeric 3'-overhang is a poor prognostic factor in human colorectal cancer. *Cancer Sci.* **102,** 330–5 (2011).

590. Oh, B.-K., Kim, Y.-J., Park, C. & Park, Y. N. Up-regulation of telomere-binding proteins, TRF1, TRF2, and TIN2 is related to telomere shortening during human multistep hepatocarcinogenesis. *Am. J. Pathol.* **166,** 73–80 (2005).

591. Cabuy, E. *et al.* Accelerated telomere shortening and telomere abnormalities in radiosensitive cell lines. *Radiat. Res.* **164,** 53–62 (2005).

592. Zongaro, S., Verri, A., Giulotto, E. & Mondello, C. Telomere length and radiosensitivity in human fibroblast clones immortalized by ectopic telomerase expression. *Oncol. Rep.* **19,** 1605–9 (2008).

593. Barwell, J. *et al.* Is telomere length in peripheral blood lymphocytes correlated with cancer susceptibility or radiosensitivity? *Br. J. Cancer* **97,** 1696–700 (2007).

594. Hemann, M. T., Strong, M. A., Hao, L. Y. & Greider, C. W. The Shortest Telomere , Not Average Telomere Length , Is Critical for Cell Viability and Chromosome Stability. *Cell* **107,** 67–77 (2001).

595. Berardinelli, F., Nieri, D., Sgura, A., Tanzarella, C. & Antoccia, A. Telomere loss, not average telomere length, confers radiosensitivity/radioresistance to tk6-irradiated cells. *Mutat. Res. ...* **740,** 13–20 (2012).

596. Hauguel, T. & Bunz, F. Haploinsufficiency of hTERT leads to telomere dysfunction and radiosensitivity in human cancer cells. *Cancer Biol. Ther.* 679–684 (2003).

597. Komuro, Y., Watanabe, T., Tsurita, G., Muto, T. & Nagawa, H. Expression pattern of telomerase reverse transcriptase in rectal carcinoma predicts tumor radiosensitivity, local recurrence and disease-free survival. *Hepatogastroenterology.* **52,** 985–9 (2005).

598. Genescà, A. *et al.* Telomere dysfunction: a new player in radiation sensitivity. *Bioessays* **28,** 1172–80 (2006).

599. Chiodi, I. & Mondello, C. Telomere-independent functions of telomerase in nuclei, cytoplasm, and mitochondria. *Front. Oncol.* **2,** 133 (2012).

600. Dudognon, C. *et al.* Death receptor signaling regulatory function for telomerase: hTERT abolishes TRAIL-induced apoptosis, independently of telomere maintenance. *Oncogene* **23,** 7469–74 (2004).

601. Del Bufalo, D. *et al.* Involvement of hTERT in apoptosis induced by interference with Bcl-2 expression and function. *Cell Death Differ.* **12,** 1429–38 (2005).

602. Lee, J. *et al.* TERT promotes cellular and organismal survival independently of telomerase activity. *Oncogene* **27,** 3754–60 (2008).

603. Ruden, M. & Puri, N. Novel anticancer therapeutics targeting telomerase. *Cancer Treat. Rev.* (2012). doi:10.1016/j.ctrv.2012.06.007

604. Zhou, F.-X. *et al.* Radiosensitization effect of zidovudine on human malignant glioma cells. *Biochem. Biophys. Res. Commun.* **354,** 351–6 (2007).

605. Kim, S. H., Kaminker, P. & Campisi, J. TIN2, a new regulator of telomere length in human cells. *Nat. Genet.* **23,** 405–12 (1999).

606. Ye, J. Z.-S. *et al.* TIN2 binds TRF1 and TRF2 simultaneously and stabilizes the TRF2 complex on telomeres. *J. Biol. Chem.* **279,** 47264–71 (2004).

607. Slijepcevic, P. Is there a link between telomere maintenance and radiosensitivity? *Radiat. Res.* **161,** 82–6 (2004).

608. Bakkenist, C. J., Drissi, R., Wu, J., Kastan, M. B. & Dome, J. S. Disappearance of the telomere dysfunction-induced stress response in fully senescent cells. *Cancer Res.* **64,** 3748–52 (2004).

609. d'Adda di Fagagna, F. *et al.* A DNA damage checkpoint response in telomere-initiated senescence. *Nature* **426,** 194–8 (2003).

610. Guiu, B. *et al.* Visceral fat area is an independent predictive biomarker of outcome after first-line bevacizumab-based treatment in metastatic colorectal cancer. *Gut* **59,** 341–347 (2010).

611. Ladoire, S. *et al.* Visceral fat area as a new independent predictive factor of survival in patients with metastatic renal cell carcinoma treated with antiangiogenic agents. *Oncologist* **16,** 71–81 (2011).

612. Tepper, J. *et al.* Phase III trial of trimodality therapy with cisplatin, fluorouracil, radiotherapy, and surgery compared with surgery alone for esophageal cancer: CALGB 9781. *J. Clin. Oncol.* **26,** 1086–92 (2008).

613. Van Hagen, P. *et al.* Preoperative chemoradiotherapy for esophageal or junctional cancer. *N. Engl. J. Med.* **366,** 2074–84 (2012).

614. O'Sullivan, J. N. *et al.* Chromosomal instability in ulcerative colitis is related to telomere shortening. *Nat Genet* **32,** 280–284 (2002).

615. Pampalona, J., Soler, D., Genesca, A. & Tusell, L. Whole chromosome loss is promoted by telomere dysfunction in primary cells. *Genes Chromosom. Cancer* **49,** 368–378 (2010).

616. Pampalona, J. *et al.* Progressive telomere dysfunction causes cytokinesis failure and leads to the accumulation of polyploid cells. *PLoS Genet* **8,** e1002679 (2012).

617. Cleveland, D. W., Mao, Y. & Sullivan, K. F. Centromeres and kinetochores: from epigenetics to mitotic checkpoint signaling. *Cell* **112,** 407–21 (2003).

618. Malmanche, N., Maia, A. & Sunkel, C. E. The spindle assembly checkpoint: preventing chromosome mis-segregation during mitosis and meiosis. *FEBS Lett* **580,** 2888–2895 (2006).

619. Musacchio, A. & Salmon, E. D. The spindle-assembly checkpoint in space and time. *Nat Rev Mol Cell Biol* **8,** 379–393 (2007).

620. Mao, Y., Desai, A. & Cleveland, D. W. Microtubule capture by CENP-E silences BubR1-dependent mitotic checkpoint signaling. *J. Cell Biol.* **170,** 873–80 (2005).

621. Martínez-a, C. & Wely, K. H. M. Van. Are aneuploidy and chromosome breakage caused by a CINgle mechanism? *Cell Cycle* 2275–2280 (2010).

622. Sotillo, R. *et al.* Mad2 overexpression promotes aneuploidy and tumorigenesis in mice. *Cancer Cell* **11,** 9–23 (2007).

623. Cahill, D. P. *et al.* Mutations of mitotic checkpoint genes in human cancers. *Nature* **392,** 300–3 (1998).

624. Geley, S. *et al.* Anaphase-promoting complex/cyclosome-dependent proteolysis of human cyclin A starts at the beginning of mitosis and is not subject to the spindle assembly checkpoint. *J. Cell Biol.* **153,** 137–48 (2001).

625. Kidokoro, T. *et al.* CDC20, a potential cancer therapeutic target, is negatively regulated by p53. *Oncogene* **27,** 1562–71 (2008).

626. Yao, X., Anderson, K. L. & Cleveland, D. W. The microtubule-dependent motor centromere-associated protein E (CENP-E) is an integral component of kinetochore corona fibers that link centromeres to spindle microtubules. *J. Cell Biol.* **139,** 435–47 (1997).

627. Weaver, B. A. A. & Cleveland, D. W. Aneuploidy: instigator and inhibitor of tumorigenesis. *Cancer Res.* **67,** 10103–5 (2007).

628. Chen, W.-S. *et al.* Depletion of securin induces senescence after irradiation and enhances radiosensitivity in human cancer cells regardless of functional p53 expression. *Int. J. Radiat. Oncol. Biol. Phys.* **77,** 566–74 (2010).

629. Lee, A. J. *et al.* Chromosomal instability confers intrinsic multidrug resistance. *Cancer Res* **71,** 1858–1870 (2011).

630. Swanton, C. *et al.* Chromosomal instability determines taxane response. *Proc Natl Acad Sci U S A* **106,** 8671–8676 (2009).

631. Rimkus, C. *et al.* Expression of the mitotic checkpoint gene MAD2L2 has prognostic significance in colon cancer. *Int. J. Cancer* **120,** 207–11 (2007).

632. Bie, L. *et al.* The accuracy of survival time prediction for patients with glioma is improved by measuring mitotic spindle checkpoint gene expression. *PLoS One* **6,** e25631 (2011).

633. Cheung, H. W. *et al.* Inactivation of human MAD2B in nasopharyngeal carcinoma cells leads to chemosensitization to DNA-damaging agents. *Cancer Res.* **66,** 4357–67 (2006).

634. Fung, M. K. L. *et al.* Role of MEK/ERK pathway in the MAD2-mediated cisplatin sensitivity in testicular germ cell tumour cells. *Br. J. Cancer* **95,** 475–84 (2006).

635. Doyle, S. L., Donohoe, C. L., Lysaght, J. & Reynolds, J. V. Visceral obesity, metabolic syndrome, insulin resistance and cancer. *Proc. Nutr. Soc.* **71,** 181–9 (2012).

636. Bulcão, C., Ferreira, S. R. G., Giuffrida, F. M. A. & Ribeiro-Filho, F. F. The new adipose tissue and adipocytokines. *Curr. Diabetes Rev.* **2,** 19–28 (2006).

637. Doak, S. H. *et al.* Differential expression of the MAD2, BUB1 and HSP27 genes in Barrett's oesophagus-their association with aneuploidy and neoplastic progression. *Mutat Res* **547,** 133–144 (2004).

638. Fernández-Sánchez, A. *et al.* Inflammation, oxidative stress, and obesity. *Int. J. Mol. Sci.* **12,** 3117–32 (2011).

639. Acilan, C., Potter, D. M. & Saunders, W. S. DNA repair pathways involved in anaphase bridge formation. *Genes Chromosom. Cancer* **46,** 522–531 (2007).

640. Rief, N. & Löbrich, M. Efficient rejoining of radiation-induced DNA double-strand breaks in centromeric DNA of human cells. *J. Biol. Chem.* **277,** 20572–82 (2002).

641. Pfeiffer, P., Goedecke, W., Kuhfittig-Kulle, S. & Obe, G. Pathways of DNA double-strand break repair and their impact on the prevention and formation of chromosomal aberrations. *Cytogenet Genome Res* **104,** 7–13 (2004).

642. Raverot, G. *et al.* Prognostic factors in prolactin pituitary tumors: clinical, histological, and molecular data from a series of 94 patients with a long postoperative follow-up. *J. Clin. Endocrinol. Metab.* **95,** 1708–16 (2010).

643. Meyer, R., Fofanov, V. & Panigrahi, A. Overexpression and mislocalization of the chromosomal segregation protein separase in multiple human cancers. *Clin. Cancer ...* **15,** 2703–2710 (2009).

644. Stolz, A. *et al.* Pharmacologic abrogation of the mitotic spindle checkpoint by an indolocarbazole discovered by cellular screening efficiently kills cancer cells. *Cancer Res.* **69,** 3874–83 (2009).

645. Rockett, J. C., Larkin, K., Darnton, S. J., Morris, A. G. & Matthews, H. R. Five newly established oesophageal carcinoma cell lines: phenotypic and immunological characterization. *Br. J. Cancer* **75,** 258–63 (1997).

646. Rosenberg, C. *et al.* Spectrum of genetic changes in gastro-esophageal cancer cell lines determined by an integrated molecular cytogenetic approach. *Cancer Genet. Cytogenet.* **135,** 35–41 (2002).

647. DeRisi, J. *et al.* Use of a cDNA microarray to analyse gene expression patterns in human cancer. *Nat. Genet.* **14,** 457–60 (1996).

648. Geigl, J. B., Obenauf, A. C., Schwarzbraun, T. & Speicher, M. R. Defining "chromosomal instability". *Trends Genet.* **24,** 64–9 (2008).

649. Ricke, R. M., van Ree, J. H., van Deursen, J. M., Ree, J. H. Van & Deursen, J. M. Van. Whole chromosome instability and cancer : a complex relationship. *Trends Genet* **24,** 457–466 (2008).

650. Falkenback, D., Johansson, J., Halvarsson, B. & Nilbert, M. Defective mismatch-repair as a minor tumorigenic pathway in Barrett esophagus-associated adenocarcinoma. *Cancer Genet. Cytogenet.* **157,** 82–6 (2005).

651. Nancarrow, D. J. *et al.* Genome-wide copy number analysis in esophageal adenocarcinoma using high-density single-nucleotide polymorphism arrays. *Cancer Res.* **68,** 4163–72 (2008).

652. Li, X. *et al.* Single nucleotide polymorphism-based genome-wide chromosome copy change, loss of heterozygosity, and aneuploidy in Barrett's esophagus neoplastic progression. *Cancer Prev. Res. (Phila).* **1,** 413–23 (2008).

653. Jenkins, R. B. *et al.* A cytogenetic study of 53 human gliomas. *Cancer Genet. Cytogenet.* **39,** 253–79 (1989).

654. Paulson, T. G. *et al.* Chromosomal instability and copy number alterations in Barrett's esophagus and esophageal adenocarcinoma. *Clin Cancer Res* **15,** 3305–3314 (2009).

655. Lai, L. a *et al.* Deletion at fragile sites is a common and early event in Barrett's esophagus. *Mol. Cancer Res.* **8,** 1084–94 (2010).

656. Wijnhoven, B. P., Tilanus, H. W. & Dinjens, W. N. Molecular biology of Barrett's adenocarcinoma. *Ann. Surg.* **233,** 322–37 (2001).

657. Wiech, T. *et al.* Genome-wide analysis of genetic alterations in Barrett's adenocarcinoma using single nucleotide polymorphism arrays. *Lab. Invest.* **89,** 385–97 (2009).

658. Isinger-Ekstrand, A. *et al.* Genetic profiles of gastroesophageal cancer: combined analysis using expression array and tiling array--comparative genomic hybridization. *Cancer Genet. Cytogenet.* **200,** 120–6 (2010).

659. Pasello, G. *et al.* DNA copy number alterations correlate with survival of esophageal adenocarcinoma patients. *Mod. Pathol.* **22,** 58–65 (2009).

660. Goh, X. Y. *et al.* Integrative analysis of array-comparative genomic hybridisation and matched gene expression profiling data reveals novel genes with prognostic significance in oesophageal adenocarcinoma. *Gut* **60,** 1317–26 (2011).

661. Pegram, M. D., Konecny, G. & Slamon, D. J. The molecular and cellular biology of HER2/neu gene amplification/overexpression and the clinical development of herceptin (trastuzumab) therapy for breast cancer. *Cancer Treat. Res.* **103,** 57–75 (2000).

662. Shigematsu, H. & Gazdar, A. F. Somatic mutations of epidermal growth factor receptor signaling pathway in lung cancers. *Int. J. Cancer* **118,** 257–62 (2006).

663. Bang, Y.-J. *et al.* Trastuzumab in combination with chemotherapy versus chemotherapy alone for treatment of HER2-positive advanced gastric or gastro-oesophageal junction cancer (ToGA): a phase 3, open-label, randomised controlled trial. *Lancet* **376,** 687–97 (2010).

664. Lee, J.-S. *et al.* A novel prognostic subtype of human hepatocellular carcinoma derived from hepatic progenitor cells. *Nat. Med.* **12,** 410–6 (2006).

665. Lee, J.-S. *et al.* Classification and prediction of survival in hepatocellular carcinoma by gene expression profiling. *Hepatology* **40,** 667–76 (2004).

666. Lee, J.-S. *et al.* Application of comparative functional genomics to identify best-fit mouse models to study human cancer. *Nat. Genet.* **36,** 1306–11 (2004).

667. Van de Vijver, M. J. *et al.* A gene-expression signature as a predictor of survival in breast cancer. *N. Engl. J. Med.* **347,** 1999–2009 (2002).

668. Alizadeh, A. A. *et al.* Distinct types of diffuse large B-cell lymphoma identified by gene expression profiling. *Nature* **403,** 503–11 (2000).

669. Van 't Veer, L. J. *et al.* Gene expression profiling predicts clinical outcome of breast cancer. *Nature* **415,** 530–6 (2002).

670. Riegman, P. H. *et al.* Genomic alterations in malignant transformation of Barrett's esophagus. *Cancer Res.* **61,** 3164–70 (2001).

671. Varis, A. *et al.* DNA copy number profiling in esophageal Barrett adenocarcinoma: comparison with gastric adenocarcinoma and esophageal squamous cell carcinoma. *Cancer Genet. Cytogenet.* **127,** 53–8 (2001).

672. Albrecht, B. *et al.* Array-based comparative genomic hybridization for the detection of DNA sequence copy number changes in Barrett's adenocarcinoma. *J. Pathol.* **203,** 780–8 (2004).

673. Gu, J. *et al.* Genome-wide catalogue of chromosomal aberrations in barrett's esophagus and esophageal adenocarcinoma: a high-density single nucleotide polymorphism array analysis. *Cancer Prev. Res. (Phila).* **3,** 1176–86 (2010).

674. Beroukhim, R. *et al.* The landscape of somatic copy-number alteration across human cancers. *Nature* **463,** 899–905 (2010).

675. Lockwood, W. W. *et al.* Integrative genomics identified RFC3 as an amplified candidate oncogene in esophageal adenocarcinoma. *Clin. Cancer Res.* **18,** 1936–46 (2012).

676. Catenacci, D. V. T. *et al.* RON (MST1R) is a novel prognostic marker and therapeutic target for gastroesophageal adenocarcinoma. *Cancer Biol. Ther.* **12,** 9–46 (2011).

677. Chen, Z. *et al.* Chromosomal copy number alterations are associated with tumor response to chemoradiation in locally advanced rectal cancer. *Genes. Chromosomes Cancer* **50,** 689–99 (2011).

678. Dulak, A. M. *et al.* Exome and whole-genome sequencing of esophageal adenocarcinoma identifies recurrent driver events and mutational complexity. *Nat. Genet.* **45,** 478–86 (2013).

679. Bandla, S., Pennathur, A. & Luketich, J. Comparative genomics of esophageal adenocarcinoma and squamous cell carcinoma. *Ann. Thorac. ...* **93,** 1101–1106 (2012).

680. Rumiato, E. *et al.* DNA copy number profile discriminates between esophageal adenocarcinoma and squamous cell carcinoma and represents an independent prognostic parameter in esophageal adenocarcinoma. *Cancer Lett.* **310,** 84–93 (2011).

681. Blons, H. *et al.* Microsatellite analysis and response to chemotherapy in head-and-neck squamous-cell carcinoma. *Int. J. Cancer* **84,** 410–5 (1999).

682. Osterberg, L. *et al.* Potential predictive markers of chemotherapy resistance in stage III ovarian serous carcinomas. *BMC Cancer* **9,** 368 (2009).

683. Ducray, F. *et al.* An ANOCEF genomic and transcriptomic microarray study of the response to radiotherapy or to alkylating first-line chemotherapy in glioblastoma patients. *Mol. Cancer* **9,** 234 (2010).

684. Chackerian, A. A. *et al.* IL-1 Receptor Accessory Protein and ST2 Comprise the IL-33 Receptor Complex. *J. Immunol.* **179,** 2551–2555 (2007).

685. Liew, F. Y., Pitman, N. I. & McInnes, I. B. Disease-associated functions of IL-33: the new kid in the IL-1 family. *Nat. Rev. Immunol.* **10,** 103–10 (2010).

686. Moulin, D. *et al.* Interleukin (IL)-33 induces the release of pro-inflammatory mediators by mast cells. *Cytokine* **40,** 216–25 (2007).

687. Smithgall, M. D. *et al.* IL-33 amplifies both Th1- and Th2-type responses through its activity on human basophils, allergen-reactive Th2 cells, iNKT and NK cells. *Int. Immunol.* **20,** 1019–30 (2008).

688. Schmitz, J. *et al.* IL-33, an interleukin-1-like cytokine that signals via the IL-1 receptor-related protein ST2 and induces T helper type 2-associated cytokines. *Immunity* **23,** 479–90 (2005).

689. Lunderius-Andersson, C., Enoksson, M. & Nilsson, G. Mast Cells Respond to Cell Injury through the Recognition of IL-33. *Front. Immunol.* **3,** 82 (2012).

690. Ivanov, V. N. *et al.* Radiation-induced bystander signaling pathways in human fibroblasts : a role for interleukin-33 in the signal transmission. *Cell Signal* **22,** 1076–1087 (2011).

691. Deorukhkar, A. & Krishnan, S. Targeting inflammatory pathways for tumor radiosensitization. *Biochem. Pharmacol.* **80,** 1904–14 (2010).

692. Hei, T. K., Zhou, H., Chai, Y., Ponnaiya, B. & Ivanov, V. N. Radiation induced non-targeted response: mechanism and potential clinical implications. *Curr. Mol. Pharmacol.* **4,** 96–105 (2011).

693. Ishkanian, A. S., Zafarana, G., Thoms, J. & Bristow, R. G. Array CGH as a potential predictor of radiocurability in intermediate risk prostate cancer. *Acta Oncol.* **49,** 888–94 (2010).

694. Lynam-Lennon, N., Maher, S. G. & Reynolds, J. V. The roles of microRNA in cancer and apoptosis. *Biol. Rev. Camb. Philos. Soc.* **84,** 55–71 (2009).

695. Bentwich, I. *et al.* Identification of hundreds of conserved and nonconserved human microRNAs. *Nat. Genet.* **37,** 766–70 (2005).

696. Friedman, R. C., Farh, K. K.-H., Burge, C. B. & Bartel, D. P. Most mammalian mRNAs are conserved targets of microRNAs. *Genome Res.* **19,** 92–105 (2009).

697. Linsley, P. S. *et al.* Transcripts targeted by the microRNA-16 family cooperatively regulate cell cycle progression. *Mol. Cell. Biol.* **27,** 2240–52 (2007).

698. Yan, D. *et al.* Targeting DNA-PKcs and ATM with miR-101 sensitizes tumors to radiation. *PLoS One* **5,** e11397 (2010).

699. Schiewer, M. J. *et al.* mTOR is a selective effector of the radiation therapy response in androgen receptor-positive prostate cancer. *Endocr. Relat. Cancer* **19,** 1–12 (2012).

700. Someya, M. *et al.* The association of DNA-dependent protein kinase activity of peripheral blood lymphocytes with prognosis of cancer. *Br. J. Cancer* **104,** 1724–9 (2011).

701. Zeidler, M. *et al.* The Polycomb Group Protein EZH2 Impairs DNA Repair in Breast Epithelial Cells. *Neoplasia* **7,** 1011–1019 (2005).

702. Varambally, S. *et al.* Genomic Loss of microRNA-101 Leads to Overexpression of Histone Methyltransferase EZH2 in Cancer. *Science (80-.).* **322,** 1695–1699 (2009).

703. Hao, Y. *et al.* Enforced expression of miR-101 inhibits prostate cancer cell growth by modulating the COX-2 pathway in vivo. *Cancer Prev. Res. (Phila).* **4,** 1073–83 (2011).

704. Loong, S. L. E. *et al.* Weak expression of cyclooxygenase-2 is associated with poorer outcome in endemic nasopharyngeal carcinoma: analysis of data from randomized trial between radiation alone versus concurrent chemo-radiation (SQNP-01). *Radiat. Oncol.* **4,** 23 (2009).

705. Struski, S. *et al.* Identification of chromosomal loci associated with non-P-glycoprotein-mediated multidrug resistance to topoisomerase II inhibitor in lung adenocarcinoma cell line by comparative genomic hybridization. *Genes. Chromosomes Cancer* **30,** 136–42 (2001).

706. Robledo, C. *et al.* Array comparative genomic hybridization identifies genetic regions associated with outcome in aggressive diffuse large B-cell lymphomas. *Cancer* **115,** 3728–37 (2009).

707. Wagner, A. *et al.* Atypical HNPCC owing to MSH6 germline mutations: analysis of a large Dutch pedigree. *J. Med. Genet.* **38,** 318–22 (2001).

708. Resnick, K. E. *et al.* Mismatch repair status and outcomes after adjuvant therapy in patients with surgically staged endometrial cancer. *Gynecol. Oncol.* **117,** 234–8 (2010).

709. Akiyoshi, T., Kobunai, T. & Watanabe, T. Predicting the response to preoperative radiation or chemoradiation by a microarray analysis of the gene expression profiles in rectal cancer. *Surg. Today* **42,** 713–9 (2012).

710. Ryan, A. M. *et al.* Obesity, metabolic syndrome and esophageal adenocarcinoma: epidemiology, etiology and new targets. *Cancer Epidemiol.* **35,** 309–19 (2011).

711. Roberts, D. L., Dive, C. & Renehan, A. G. Biological mechanisms linking obesity and cancer risk: new perspectives. *Annu. Rev. Med.* **61,** 301–16 (2010).

712. Bilsland, A. E., Cairney, C. J. & Keith, W. N. Targeting the telomere and shelterin complex for cancer therapy: current views and future perspectives. *J Cell Mol Med* **15,** 179–186 (2011).

713. Hoffelder, D. R. *et al.* Resolution of anaphase bridges in cancer cells. *Chromosoma* **112,** 389–397 (2004).

714. Chavakis, T., Orlova, V. V & Langer, H. F. A possible crosstalk between DNA repair pathways and angiogenesis. *Cell Cycle* **8,** 3438–9 (2009).

715. Livingstone, L. R. *et al.* Altered cell cycle arrest and gene amplification potential accompany loss of wild-type p53. *Cell* **70,** 923–935 (1992).

716. Yin, Y., Tainsky, M. A., Bischoff, F. Z., Strong, L. C. & Wahl, G. M. Wild-type p53 restores cell cycle control and inhibits gene amplification in cells with mutant p53 alleles. *Cell* **70,** 937–948 (1992).

717. Paulson, T. G., Almasan, A., Brody, L. L. & Wahl, G. M. Gene amplification in a p53-deficient cell line requires cell cycle progression under conditions that generate DNA breakage. *Mol Cell Biol* **18,** 3089–3100 (1998).

718. El-Hizawi, S., Lagowski, J. P., Kulesz-Martin, M. & Albor, A. Induction of gene amplification as a gain-of-function phenotype of mutant p53 proteins. *Cancer Res* **62,** 3264–3270 (2002).

719. Yoon, D. S. *et al.* Variable levels of chromosomal instability and mitotic spindle checkpoint defects in breast cancer. *Am J Pathol* **161,** 391–397 (2002).